Nonlinear Control of an Exoskeleton Seven Degrees of Freedom Robot to Realize an Active and Passive Rehabilitation Tasks

by

Brahim BRAHMI

MANUSCRIPT-BASED THESIS PRESENTED TO ÉCOLE DE TECHNOLOGIE SUPÉRIEURE IN PARTIAL FULFILLMENT OF THE REQUIREMENTS FOR THE DEGREE OF DOCTOR OF PHILOSOPHY
Ph.D.

MONTREAL, MAY 14, 2019

ÉCOLE DE TECHNOLOGIE SUPÉRIEURE
UNIVERSITÉ DU QUÉBEC

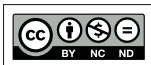

BOARD OF EXAMINERS

THIS THESIS HAS BEEN EVALUATED

BY THE FOLLOWING BOARD OF EXAMINERS:

Mr. Maarouf Saad, Thesis Supervisor
Department of Electrical Engineering, École de technologie supèrieure

Mr. Mohammad Habibur Rahman, Co-supervisor
Department of Mechanical/Biomedical Engineering, University of Wisconsin-Milwaukee

Mr. Guy Gauthier, President of the Board of Examiners
Department of System Engineering, École de technologie supèrieure

Mr. Vahé Nerguizian , Member of the jury
Department of Electrical Engineering, École de technologie supèrieure

Mr. Guchuan Zhu, External Independent Examiner
Department of Electrical Engineering at Polytechnique Montréal

THIS THESIS WAS PRESENTED AND DEFENDED

IN THE PRESENCE OF A BOARD OF EXAMINERS AND THE PUBLIC

ON "MAY 7, 2019"

AT ÉCOLE DE TECHNOLOGIE SUPÉRIEURE

ACKNOWLEDGEMENTS

My first thanks go to my thesis supervisor, Professor Maarouf Saad, who accompanied and directed me along this work. I am grateful for his availability, his enthusiasm, his confidence and his generous help in all time. Without his support, the achievement of the present work would have not been possible.

I want to thank as well my co-supervisor, Professor Mohammed Habibur Rahman for his availability, his daily monitoring of my work and his valuable advice. I thank him very much.

I want to thank as well all my laboratory colleagues: Dr. Cristobal Ochoa Luna, Dr. Abdelkrim Brahmi and Abdelhak Badi for their important contributions to this research.
I am honoured by the presence of all the members of the committee who provided useful advice that helped me to structure my study during my thesis. I wish to express my gratitude to Dr. Maarouf Saad, Dr. Mohammed Habibur Rahman, Dr. Guy Gauthier, Dr. Vahé Nerguizian, and Dr. Guchuan Zhu for being part of the committee who agreed to review and evaluate this research.

Moreover, my thanks would be incomplete, if I do not mention my parents, my brothers, my wife, my uncle Zahazah Brahmi and all my family, for their unconditional love and support in all possible ways.
Finally, My most sincere thanks to my friends and colleagues who have helped me, from near or far, directly or indirectly in the development of this work.

Contrôle non linéaire d'un robot exosquelette sept degrés de liberté pour réaliser des tâches de réhabilitation active et passive

Brahim BRAHMI

RÉSUMÉ

Cette thèse de doctorat propose le développement d'un robot exosquelette appelé robot ETS-MARSE, utilisé pour réhabiliter les patients ayant une déficience à un membre supérieur. Les développements, inclus dans ce travail, sont la conception et la validation expérimentale d'une solution de cinématique inverse de robot et de contrôle non-linéaire pour le robot ETS-MARSE. Ces approches garantissent une bonne performance de l'exosquelette en mouvement de réhabilitation passive et active en présence d'incertitudes dynamiques et cinématiques et de perturbations indésirables.

Considérant la population croissante de personnes atteintes par ce genre de déficience, il est nécessaire d'améliorer l'accessibilité à la physiothérapie en utilisant une technologie robotique pour la réadaptation. Récemment, la robotique de réadaptation a attiré beaucoup d'attention de la communauté scientifique, car elle est capable de surmonter les limites de la thérapie physique conventionnelle. L'importance du robot de réadaptation réside dans sa capacité à assurer une physiothérapie intensive pendant une longue période. Les données mesurées du robot permettent au physiothérapeute d'évaluer avec précision les performances du patient. Cependant, ces dispositifs font toujours partie d'un domaine émergent et présentent de nombreux défis par rapport aux manipulateurs classiques, tels que la non-linéarité élevée, la dimension élevée (un nombre élevé de degrés de liberté) et la dynamique inconnue (incertitudes). Ces limitations sont provoquées par la structure mécanique complexe conçue pour un usage humain, les types de mouvement d'assistance et la sensibilité de l'interaction avec une grande diversité d'usagers (différentes conditions physiologiques des sujets). En conséquence, ces conditions rendent le système vulnérable aux incertitudes dynamiques et aux perturbations externes. Ces uncertainties et les forces externes peuvent se transformer en une fonction inconnue pouvant affecter les performances du robot exosquelette.

Les principaux défis abordés dans cette thèse consistent tout d'abord à concevoir une solution de cinématique inverse humaine permettant d'effectuer un mouvement fluide similaire au mouvement naturel de l'humaine (mouvement humain). Deuxièmement, à développer des contrôleurs robustes caractérisés par un haut niveau de robustesse et de précision, sans aucune sensibilité aux dynamiques non-linéaires incertaines et aux perturbations inattendues. Cela donnera au système de contrôle plus de flexibilité pour gérer les incertitudes et les variations de paramètres dans les différents modes de mouvement de réhabilitation (passif et actif).

Mots-clés: Cinématique inverse humaine, contrôle adaptatif, les robots de réadaptation

NONLINEAR CONTROL OF AN EXOSKELETON SEVEN DEGREES OF FREEDOM ROBOT TO REALIZE AN ACTIVE AND PASSIVE REHABILITATION TASKS

Brahim BRAHMI

ABSTRACT

This doctoral thesis proposes the developments of an exoskeleton robot used to rehabilitate patients with upper-limb impairment, named ETS-MARSE robot. The developments included in this work are the design, and validation of a kinematic inverse solution and nonlinear control strategy for an upper limb exoskeleton robot. These approaches are used in passive and active rehabilitation motion in presence of dynamics and kinematics uncertainties and unexpected disturbances.

Considering the growing population of post-stroke victims, there is a need to improve accessibility to physiotherapy by using the modern robotic rehabilitation technology. Recently, rehabilitation robotics attracted a lot of attention from the scientific community since it is able to overcome the limitations of conventional physical therapy. The importance of the rehabilitation robot lies in its ability to provide intensive physiotherapy for a long period time. The measured data of the robot allows the physiotherapist to accurately evaluate the patient's performance. However, these devices are still part of an emerging area and present many challenges compared to the conventional robotic manipulators, such as the high nonlinearity, dimensional (high number of DOFs) and unknown dynamics (uncertainties). These limitations are provoked due to their complex mechanical structure designed for human use, the types of assistive motion, and the sensitivity of the interaction with a large diversity of human wearers. As a result, these conditions make the robot system vulnerable to dynamic uncertainties and external disturbances such as saturation, friction forces, backlash, and payload. Likewise, the interaction between human and the exoskeleton make the system subjected to external disturbances due to different physiological conditions of the subjects like the different weight of the upper limb for each subject. During a rehabilitation movement, the nonlinear uncertain dynamic model and external forces can turn into unknown function that can affect the performance of the exoskeleton robot.

The main challenges addressed in this thesis are firstly to design a human inverse kinematics solution to perform a smooth movement similar to natural human movement (human-like motion). Secondly, to develop controllers characterized by a high-level of robustness and accuracy without any sensitivity to uncertain nonlinear dynamics and unexpected disturbances. This will give the control system more flexibility to handle the uncertainties and parameters' variation in different modes of rehabilitation motion (passive and active).

Keywords: Human inverse kinematics, adaptive control, rehabilitation robots.

TABLE OF CONTENTS

Page

LIST OF TABLES

Page

LIST OF FIGURES

LIST OF ABBREVIATION

ETS	École de Technologie Supérieure
MARSE	Motion Assistive Robotic-exoskeleton for Superior Extremity
GREPCI	Groupe de Recherche en Électronique de Puissance et Commande Industrielle
DC	Direct Current
VDC	Virtual Decomposition Control
DoF	Degree of Freedom
DH	Denavit-Hartenberg parameters
PD	Proportional-Derivative
PI	Proportional-Integral
PID	Proportional-Integral-Derivative
CTC	Computed Torque Control
DMI	Desired Motion Intention
TDE	Time Delay Estimation
SMC	Sliding Mode Control
RMS	Root-Mean-Square
FPGA	Field Programmable Gate Array
EMG	Electromyographic
HIV	Human Inverse Kinematics
DLS	Damped Least Square

LISTE OF SYMBOLS AND UNITS OF MEASUREMENTS

UNITS OF MEASUREMENT

m	meter
cm	centimeter
rad	radian
Nm	Newton meter
s or sec	second
μs	microsecond
$\circ$ or deg	degree
N	Newton
kg	Kilogram
g	gram

SYMBOLS

XYZ	Cartesian coordinate system main axes
α_{i-1}	angle from Z_{i-1} to Z_i measured about X_{i-1}
a_{i-1}	length from Z_{i-1} to Z_i measured along X_{i-1}
d_i	distance from X_{i-1} to X_i measured along Z_i
θ_i	angle from X_{i-1} to X_i measured about Z_i
$\dot{\theta}_i, \ddot{\theta}_i$	joint's velocity and acceleration, respectively
$x\, \dot{x}, \ddot{x}$	Cartesian position, velocity and acceleration, respectively

V_i	Lyapunov function candidate
J	Jacobian Matrix
${}^{i}_{i+1}T$	transformation matrix
τ	control torque
$\tau_{ex},\ f_{ex}$	external disturbances
F_m	measured force vector
M	inertia matrix
C	Coriolis and centrifugal matrix terms
G	gravitational vector terms
Q	regressor matrix
$\hat{f}_e$	estimated force vector
$\hat{H}$	estimated uncertain vector
$\hat{\varepsilon}$	estimated time delay error vector

INTRODUCTION

Nowadays, the technological revolution is growing by a fantastical speed. Starting from the first industrial revolution where water and steam were used to mechanize the production to the third one where information technologies are used to automate the production. Today, we stand on the bridge of a new revolution that will change fundamentally our way of working, living and communicating with each other. This revolution known as Industry 4.0 (Xu *et al.*, 2018) will bring changes that humans have never seen before. Robotics is one of the most important manifestations of this revolution (Atkeson *et al.*, 2018). These technologies are used to improve the industrial production by integrating new systems that can replace humans and replicate human activities (Bautista and Wane, 2018). However, to make this revolution succeed, several challenges must be met, among them; technological challenges such as controlling these new nonlinear systems (Atkeson *et al.*, 2018).

Currently, robotics can be used in many fields and for many purposes, for example, military (Liu *et al.*, 2018), manufacturing processes especially in dangerous environment where humans cannot intervene (Clancy *et al.*, 2018), in the medical domain (Ferguson *et al.*, 2018), and so on. Laterally, new robot systems have been introduced to improve the rehabilitation treatment known as ”rehabilitation robots” or exoskeleton robots (Xie *et al.*, 2016). The use of rehabilitation robots in the medical rehabilitation field has proved to be of great ability to improve the quality of life of the patient, enhancing its practical motions, and assisting him in daily exercises. The exoskeleton robot is an articulated mechanical structure with several degrees of freedom (DOFs) having the same anatomy of the human arm or leg. Unlike prostheses that replace a limb of the body, the exoskeleton robot clings to it externally and acts in parallel. This fixation allows robot's wearer to move his/her arm in the workspace. The reachable workspace envelope depends on the number of degrees of freedom (DOFs) available of the exoskeleton robot. It can be dedicated to a specific part of the body such as the hand, arm, leg or several limbs at the same time. Equipped with sensors and actuators, it measures

the movements and forces of the user that allow to the physiotherapist to accurately evaluate the patient's performance.

This thesis exhibits the development of an exoskeleton robot used to rehabilitate patients with upper-limb impairment, named ETS-MARSE robot (Motion Assistive Robotic-exoskeleton for Superior Extremity). In fact, this thesis presents a continuity of works presented in (Ochoa Luna, 2016; Rahman, 2012). The design of the ETS-MARSE is based on the anatomy of the human upper limb and has been developed to faithfully represent the joints and movements of the upper limb movements, in order to be worn comfortably with the robot's user during the rehabilitation tasks. The shoulder part is described by three joints: the first two joints are created to produce the vertical and horizontal extension/flexion movement of the shoulder, while the third joint is intented to perform the internal and external rotation of the shoulder. The elbow part is composed of one joint to complete the flexion/extension motion of the elbow. The wrist part is composed of three joints: the first joint is designed to perform pronation and supination motion of the forearm, the second and third joints are dedicated to offer respectively ulnar/radial deviation, and flexion/extension motions. ETS- MARSE is able to provide the different levels of robotic assistance strategies used after neurological accidents. The most urgent, usually the first six weeks after the accident, is passive physical therapy (Sidney *et al.*, 2013; Xie *et al.*, 2016). In this type of therapy, the exoskeleton brings the patient's limb, which is completely passive, to realize a therapy task. Its advantage lies in the robot's ability to provide intensive therapy over a long period of time (Brahim *et al.*, 2016b,a). The next types of therapy, active-assisted and active modes, allow the patient to voluntarily initiate movement. Then, the exoskeleton's wearer can perform a free motion (active mode), or an active-assisted movement where the robot corrects or guides this movement. In the latter case, the robot limits the tremors or corrects the trajectory. After detecting the initiation of a motion, usually voluntary, the exoskleton will guide the achievement of the activity, often using an impedance and/or admittance control (Li *et al.*, 2017a; Ochoa Luna *et al.*, 2015). Additionally, these strategies can be used

for evaluating or studying subject movements and performance improvement. In these modes, theoretically, the patient should not feel the presence of the exoskeleton robot. Therefore, the subject is completely active and the exoskeleton robot should not affect the movement.

The aim of this thesis is to design and validate experimentally a solution of inverse kinematics and nonlinear control strategy for an upper limb exoskeleton robot to achieve a passive and active rehabilitation purposes. The idea is that improved the performance of the exoskeleton robot, and a new solution of the control system may be realized by maintaining the whole nonlinear dynamics model of the robot system in its design. This strategy presents considerable challenges due to: firstly, the unavailability of an analytical solution of nonlinear equations of the robot motion. Secondly, kinematic and dynamic models may be imperfect because of the many difficulties encountered in modeling certain phenomena such as nonlinear friction, kinematics uncertainty caused by visual devices like camera, Kinect..., etc. Dynamic uncertainty or unavailability of feedback signals, necessary to compute the dynamic parameters of the robot system.

The organization of this thesis is given as follows: Chapter 1 describes the research problem, gives the literature review, state the objectives, gives the methodology and claims the originality of the work. Since this document is papers-based thesis, consequently, Chapters 2, 3, 4, 5, and 6 present the main results of the work in the form of published papers. The main contributions of this thesis are summarized as follows:

The first chapter of this thesis presents the problem of research. The identification and justification of the research problem are given in this chapter, as well as the motivation of the current work. A state-of-the-art of the existing literature in this area of research is presented. Then the global and specific objectives of this work are stated. Finally, an overview of the methodology used is provided.

Chapter 2 presents an experimental validation of a new solution of inverse kinematic for 7-DOFs exoskeleton robot (Brahmi *et al.*, 2017c). In this work, we propose a new solution to the inverse kinematic problem, considering human upper limb movement and arm configuration. The philosophy of this approach is to develop a mathematical model based on geometric and analytic solutions of human upper limb motion in order to imitate its movement.

Chapter 3 presents an experimental validation of a new compliant control based on a second-order sliding mode with adaptive-gain incorporating time delay estimation (Brahmi *et al.*, 2018a). In this work, the dynamic parameters of the system were considered uncertain and were estimated by time delay estimation. The main challenge addressed in this research is to ensure that the exoskeleton robot provides an appropriate compliance control that allows it to interact perfectly with humans. In this chapter, the proposed controller uses the human inverse kinematics presented in chapter 2 to complete the active rehabilitation motion.

Chapter 4 presents an experimental validation using backstepping approach integrated with modified time-delay estimation to provide an accurate estimation of unknown dynamics of the exoskeleton robot and to compensate for external bounded disturbances (Brahmi *et al.*, 2018d). The stability of the control system and the convergence of its state errors are established and proved based on Lyapunov–Krasovskii functional theory.

Chapter 5 investigates the passive and active control strategies to provide a physical assistance and rehabilitation by a 7-DOF exoskeleton robot with nonlinear uncertain dynamics and unknown bounded external disturbances due to the robot user's physiological characteristics (Brahmi *et al.*, 2018c). Besides, The Damped Least Square method is introduced to estimate the desired movement intention of the subject with the objective to provide active rehabilitation motion. The design, stability and convergence analysis are formulated and proven based on the Lyapunov–Krasovskii functional theory.

Chapter 6 presents a new adaptive visual tracking control approach based on sliding mode control in Cartesian space applied in real time to an exoskeleton robot with uncertain kinematics and dynamics, taking into account uncertainties in visual system (camera) parameters (Brahmi *et al.*, 2018b). In this work, the adaptation of kinematic uncertainties is based on a filtered regressor kinematic matrix, whereas, the adaptation of dynamic uncertainties is based on a modified time delay estimation approach. The updated laws are designed using Lyapunov theory to solve the adaptation problem methodically and to show the stability of the robot system.

CHAPTER 1

RESEARCH PROBLEM

Without a doubt, neurological diseases are becoming a challenging problem to the scientific community. According to recent statistics, as many as 15 million people in the world suffer from neurological diseases such as stroke, 6 million people die and 5 million live with persistent disability (Sidney *et al.*, 2013). In Canada, at least 16000 Canadians each year die from a stroke (Sidney *et al.*, 2013). Survivors of a stroke typically don't have the potential to perform daily activities of their own, such as eating, dressing, and bathing because of the permanent disability often present on one side of the body (De Morand, 2014). This weakness can create many physical and psychological problems related to the bevavior of the victim. The rehabilitation program is an effective treatment designed to help the stroke victims recover their lost functional ability, acquire new skills and improve their quality of life (De Morand, 2014). However, this treatment still suffers from several shortcomings, such as the accessibility and fatigue of the therapist (Xie *et al.*, 2016).

Given the growing population of post-stroke victims, there is a need to improve accessibility to physiotherapy. Modern robotic technology can help in many fields even to accomplish the medical tasks such physiotherapy. Recently, rehabilitation robotics has attracted a lot of attention from the scientific community to overcome the limitations of conventional physical therapy (Xie *et al.*, 2016). The importance of the rehabilitation robot lies in its ability to provide intensive physiotherapy for a long period time (Xie *et al.*, 2016). The measured data of the robot allows the physiotherapist to accurately assess the patient's performance. However, these devices are still part of an emerging area and present many challenges. In fact, these robots have an additional complexity compared to conventional robotic manipulators due to their complex mechanical structure designed for human use, types of assistive motion, and the sensitivity of the interaction with a large diversity of human wearers. As a result, these conditions make the robot system vulnerable to dynamic uncertainties and external disturbances such as saturation, friction forces, backlash, and payload. Likewise, the interaction between

human and the exoskeleton make the system subjected to external disturbances due to different physiological conditions of the subjects like the different weight of upper limb for each patient (Brahmi *et al.*, 2018d,c). During a rehabilitation movement, the nonlinear uncertain dynamic model and external forces can turn into an unknown function that can affect the performance of the exoskeleton robot.

Another problem can be raised with a redundant (in our case 7-DOFs) is the high number of inverse kinematic solutions. That is, the exoskeleton robot can reach some points of its workspace in more than one configuration of its links (redundancy). Finding a solution to the inverse kinematics problem, compatible with human upper limb movement and valid for human arm configuration will help to perform the human-like motion avoiding singularity problems.

Based on above-mentioned problems, the main challenges in this work can be summarized as follows:

- High non-linearity of the system;
- System redundancy (a lot of degree of freedom, in our case 7-DOFs);
- Unknown dynamics, or part of the system is uncertain;
- Uncertain kinematics (when the camera is used to obtain the Cartesian measurement).

The main challenges addressed of this thesis consist first of all in designing an inverse kinematics solution able making the exoskeleton ETS-MARSE robot to perform a smooth movement similar to natural human movement (human-like motion). Secondly, to design robust controllers characterized by a high-level of robustness and accuracy without any sensitivity to uncertain nonlinear dynamics and unexpected disturbances. This will give the control system more flexibility to handle the uncertainties and parameters' variation in different modes of rehabilitation motion (passive and active).

1.1 Literature review

Most research work in this type of robotic system has so far focused on the following three points: The mechanism of the exoskeleton robot, inverse kinematic solution, and control strategies to achieve different modes of rehabilitation motion.

1.1.1 Rehabilitation robot

In this section, only advanced exoskeleton robots that have demonstrated their clinical efficacy are presented.

InMotion: ”InMotion” robot is certainly the most successful rehabilitation robot so far and the most clinically tested. It is a commercialized system. It contains 2 degrees of freedom dedicated to the upper limb. It allows the patient to perform movements in the transverse plane. Most controls that have been developed for this robot are based on the impedance control. This robot also integrated therapeutic games. It demonstrates its effectiveness by its applications in clinical rehabilitation area (Hogan *et al.*, 1992, 1993).

This product delivers several versions of InMotion to different objectives as shown in Fig 1.1:

Figure 1.1 InMotion Arm Robot, InMotion Hand Robot, InMotion Wrist Robot (from the left of the figure to the right, respectively)
Taken from (Hogan *et al.*, 1992, 1993)

InMotion Arm Robot: the robot has 2-DOF developed by MIT-Manus. It allows 2D movements in the transverse plane. It is integrated with a therapeutic game that helps in the rehabilitation treatment.

InMotion Robot Hand: it is specifically dedicated to the hand. It allows to make gripping movements and relaxation.

InMotion Wrist Robot: the robot has 3-DOF designed to the wrist. It allows realizing the movements of pronation and supination, flexion / extension and abduction / adduction. This type of robot also contains therapeutic game interface.

ARM Guide robot: The ARM Guide robot (see Figure 1.2) was created by "the Rehabilitation Institute of Chicago and the University of California," and the robot is dedicated to the hand. It contains a splint to fix the patient's forearm. There are also other passive 2-DOF, equipped with electromagnetic brakes and allow performing pre-defined pointing movements in space. There are several studies (Kahn *et al.*, 2001) demonstrating its effectiveness in the area of traditional therapies. The robot also includes a visual interface that will help in the rehabilitation period.

ARMin robot: This robot was developed by Sensory-Motor Systems Lab ETH Zurich (Nef *et al.*, 2007) It is considered one of the most advanced exoskeletons today through clinical validation. ETH began developing this robot in 2005. ARMin I is the first version, it contains 4 DOFs. The latest version of this robot is ARMin IV, with 7 DOFs: 3 DOFs at shoulder joint, 2 DOF for elbow joint and 2 DOFs for wrist joint (see Figure 1.3). The lengths and weights of different parts of the robot are adjustable to suit the patient's morphology. A spring connected to the upper part of the robot compensates the mechanical gravity of the robot if or when the robot lost the power of actuation. The robot is equipped with position sensors and torque force to measure the interaction between the patient and the robot. Its integration with the environment provides feedback multi-model and different visions for making well-defined movements (Nef *et al.*, 2007).

Figure 1.2 ARM Guide robot
Taken from (Kahn *et al.*, 2001)

Several controls techniques have been developed for manipulating this robot to provide different modes of rehabilitation (passive and active). These techniques have been clinically validated on patients using the practice of daily living (Guidali *et al.*, 2011) and therapeutic games with visual feedback. Among the controls approaches applied on the robot, we find the switch to the position control that has been tested on a hemiparesis patient to try to correct pathological synergies arms.

ABLE robot: ABLE is an exoskeleton robot developed by CEA-LIST systems, located in the Institute of Intelligent Systems and Robotics in France (Crocher, 2012). It is designed to provide rehabilitation of the upper limb as shown in Figure 1.4. It is characterized by its lightness and mechanical reversibility. The complete system is a structure consisting of a main kinematics parts which has four active DOF, and two secondary kinematics parts; each with four passive DOF (Crocher, 2012). Several controls were applied on this system; among them: proportional-derivative (PD) position control, friction and gravity compensation control to make it as transparent as possible as (Crocher, 2012).

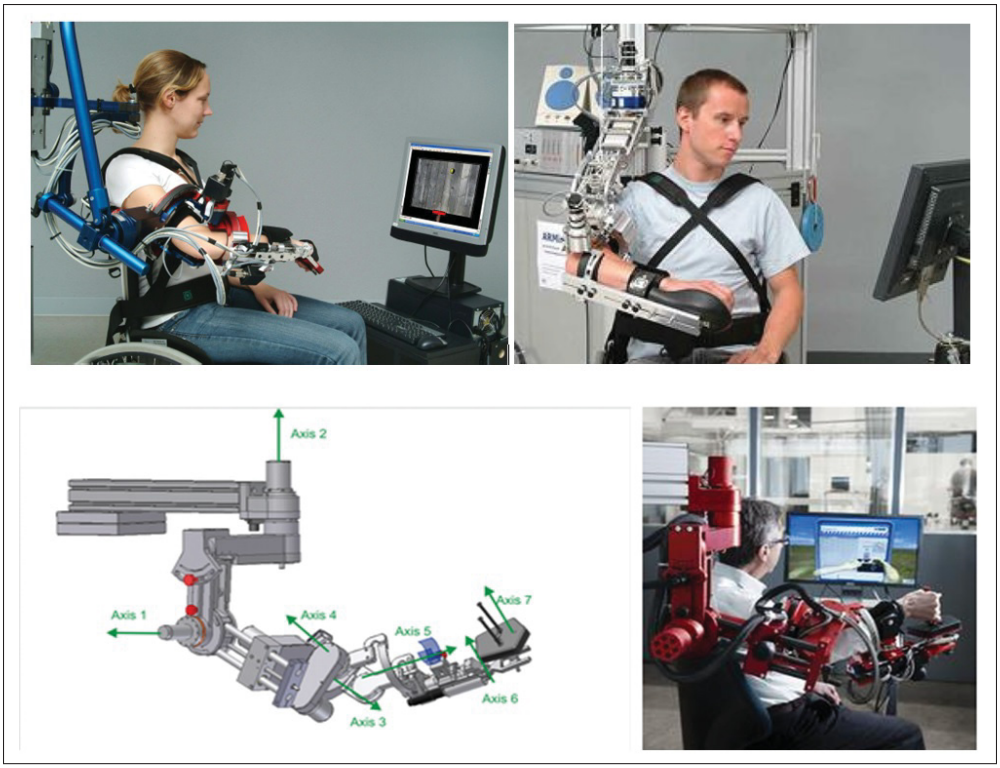

Figure 1.3 The versions of ARMin from left to right and from top to bottom: ARMin I ARMin II, ARMin III and ARMin IV Taken from (Nef *et al.*, 2007)

MGA robot: MGA is an exoskeleton robot given in Figure 1.5, it was developed by Georgetown University (Carignan *et al.*, 2007) for the shoulder and elbow joints, this robot has 5 DOF, allowing the patient to exercise flexion/extension, abduction/adduction and internal/external rotation of the shoulder joint, flexion/extension of the elbow joint, and pronation/supination of the forearm joint (Carignan *et al.*, 2007).

SAM robot: SAM is an exoskeleton robot developed by the European Space Agency (ESA). It has 7 degrees of freedom with force feedback and with a mass of 7.4 Kg. It has compact joints with local DC actuation, sensor integration, and virtual reality interface. It is dedicated to complete teleoperation applications. Several controls were applied on the robot; the most important controls are force-position and admittance control (Letier and Preumont, 2010).

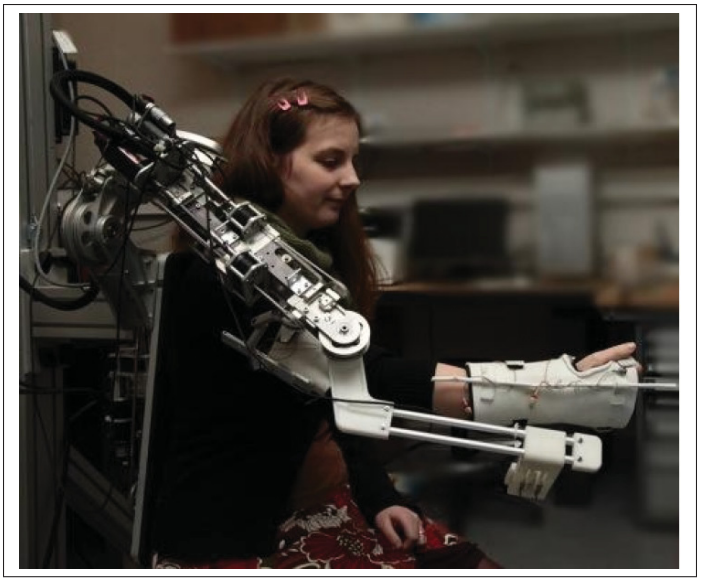

Figure 1.4 ABLE robot
Taken from (Crocher, 2012)

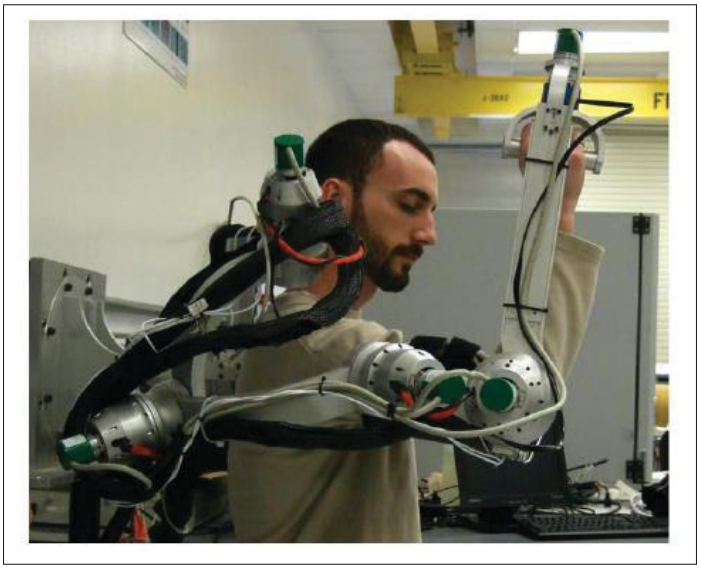

Figure 1.5 MGA Exoskeleton
Taken from (Carignan *et al.*, 2007)

1.1.2 Inverse Kinematics

Generally, in most applications using non-redundant exoskeleton robots, the desired trajectories and/or therapeutic tasks are expressed in Cartesian space particularly in active rehabiliation

motion. However, operators prefer to control redundant exoskeleton robots in joint space in order to manage their redundancy (Crocher, 2012). Numerous methods, including numerical (Tolani and Badler, 1996), analytical (Bin *et al.*, 2011), (Tolani *et al.*, 2000), optimization (Xia and Wang, 2001), (Khoogar *et al.*, 2011), vision (Jiang *et al.*, 2014),(Zhang *et al.*, 2014), (Chan *et al.*, 2014), and geometric methods (Tolani and Badler, 1996), (Loh and Rosen, 2013), (Kim *et al.*, 2011a), (Asfour and Dillmann, 2003) have been developed to solve the problem of inverse kinematics. The most frequently and most widely applied solutions for redundant robots are the inverse Jacobian and the Jacobian pseudo-inverse methods (Craig, 2005), (Kelly *et al.*, 2006), (Klein and Huang, 1983). However, these approaches provide multiple solutions in Cartesian space. Moreover, the methods present many downsides, such as singularity problems. Further, in rehabilitation applications, the objective is not only to reach the desired goal; it is also imperative to reach an optimal solution corresponding to a human movement.

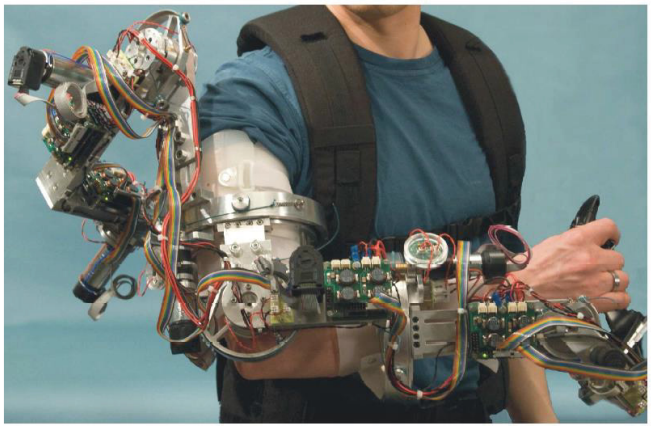

Figure 1.6 SAM Exoskeleton robot
Taken from (Letier and Preumont, 2010)

1.1.3 Uncertain nonlinear control

The control of uncertain nonlinear dynamics is one of the challenging topics of nonlinear control engineering problems. In particular, a control system should be developed to ensure the stability of the system. In addition, its performance should not be affected by the disturbances

generated from the variation of internal parameters of the system, unmodeled dynamics stimulation, and external disturbances (Slotine *et al.*, 1991; Khalil and Grizzle, 1996). Many studies discussing the problem of modeling and control of exoskeleton robot manipulator based on centralized approaches have been given in (Rahman *et al.*, 2013; Ueda *et al.*, 2010; Lee *et al.*, 2012). Nevertheless, in the previously cited studies, the control design is model-based, in which the control law requires the full dynamic model of the exoskeleton robot. The estimation of the dynamic parameters is one of the open problems in exoskeleton manipulators, notably, with high degrees of freedom (DOFs) (Krstic *et al.*, 1995), and in the presence of human-robot interaction. Conventional control approaches consider that the dynamic model of the upper arm manipulator is known. However, in practice, it becomes very difficult to get the exact model and uncertain may still exist. To overcome this problem, robust control approaches based on the Lyapunov theory are developed to ensure the stability of the full system (Khan *et al.*, 2017, 2016a,b; Huang and Chien, 2010; Luna *et al.*, 2016). However, these controllers are very complicated due to the complexity of the regression matrix (Huang and Chien, 2010). As solution, a time delay estimation (TDE) is proposed (Youcef-Toumi and Shortlidge, 1991; Youcef-Toumi and Ito, 1990; Brahmi *et al.*, 2017a). By this method, it is sufficient to delay the output-input of the system only one step to provide a good approximation of the unknown uncertainties dynamic model of the exoskeleton robot. Nevertheless, TDE approach suffers from the Time Delay Error (TDR) caused by the noisy measurements and hard nonlinear function of the robot model during delay constant, which would degrade the approximation performance.

On the other hand, many other works have used decentralized control for this type of robotic systems as in (Luna *et al.*, 2016; Ochoa Luna *et al.*, 2015). A decentralized adaptive control, based on the virtual decomposition approach, was proposed, where the whole system was decomposed virtually into several individual subsystems. This decomposition makes the parameters, adaptation and the control law very easy. As an example of these works that applied on other type of robots, an adaptive tracking control design for an uncertain mobile manipulator dynamics based on appropriate reduced dynamic model was suggested in (Aviles *et al.*, 2012). An adaptive controller based on the backstepping technique (Brahmi *et al.*, 2016)

was implemented to the trajectory tracking of the wheeled mobile manipulator. Recently, approximation-based control strategies like fuzzy logic and neural networks have been used to learn the exoskeleton dynamic model (Chen *et al.*, 2015; Li *et al.*, 2015a). However, through these approaches only uniformly ultimate boundedness of the tracking errors was achieved. Meanwhile, the estimated weights were not reached to their actual values. This might reduce convergence speed during weights training operation, which stops the approximation-based control for real-time implementation.

It is remarkable from a natural human movement (since the human upper limb is attached with the exoskeleton robot) that the human does not need accurate information about kinematics and dynamics of the arm (or any object carried by upper extremity) to reach an object in space. Due to that, many control strategies have been designed to solve the problem of kinematic and dynamic uncertainties (Arimoto, 1999; Cheah, 2006; Yazarel and Cheah, 2002; Huang and Chien, 2010; Cheah *et al.*, 2005; Hutchinson *et al.*, 1996). The main innovative point of these controllers is that the adaptation of the both kinematic/dynamic uncertainties has been provided, which allows the exoskeleton robot to perform the human-like motion and supplies to the control system more flexibility to handle the uncertainties and parameters variation. However, the above controllers are based on the classical regressor matrix. These types of controllers assume that the robot is linear in a set of physical parameters and find a control law able to ensure the stability of this linear system only around its operating points (Yao, 1996). In fact, the manipulator is highly nonlinear. So, the integration of this adaptation law may affect the stability of the system in the presence of even small disturbances (Yao, 1996). Adaptive visual or image-based tracking control (Hutchinson *et al.*, 1996; Deng *et al.*, 2002; Espiau *et al.*, 1992; Gans *et al.*, 2003; Malis and Chaumette, 2002; Liu *et al.*, 2006) is one of the powerful approaches that has been developed to transact with the kinematic/dynamic uncertainties. This is due to their robustness practically to modeling and calibration errors (Deng *et al.*, 2002). However, these controllers are concentrated on uncertainties in nonlinear transformation functions or image Jacobian matrix but they ignored the uncertain kinematic/dynamic effects. Additionally, few stability analysis are provided in the literature for visual tracking control with the uncer-

tainties of kinematics/dynamics and in the presence of uncertainties in visual system (camera) parameters (Cheah *et al.*, 2006).

1.2 Research objectives and methodology

The main objective of this work is to develop and improve the ETS-MARSE exoskeleton arm to perfectly achieve the passive and active rehabilitation motion to physically disabled people, with full shoulder, elbow and wrist rehabilitation capacities. As discussed above, with the high dimensional of the robot system (7-DOFs), the exoskeleton robot may face a problem to achieve some trajectories in Cartesian space particularly, in active mode or free motion due to the multi-solution or singularity problem provided by the conventional methods of robot inverse kinematics. So, to find an optimal solution of the robot inverse kinematics corresponds to the human arm configuration is a mandatory step to make the exoskeleton mimics the human natural motion.

As mentioned above, these robots are distinguished by a highly nonlinear dynamics because of their complex mechanical design and arduous nonlinearities, such as nonlinear friction forces, backlash, etc. Besides, the collaboration between the human and the robot makes the robot system subject to unknown and external disturbances because of different physiological conditions of each subject. These conditions involve non-linear bio-mechanical properties of the musculoskeletal system, its payload, and the possibility of the existence of spasticity,...etc. It is consequently imperative to design an adaptive controllers that approximates the dynamic model of the exoskeleton robot and minimizes the non-smooth nonlinear constraints effects, while maintaining the stability of the exoskeleton robot at the same time with different mode of rehabilitation motion (passive and active). The methodology described below were applied during this research to achieve these objectives:

1.2.1 Human inverse kinematics

In order to perform rehabilitation tasks, some trajectories must be given in Cartesian space. Because the redundancy problem was not solved, a new approach was designed and implemented to make the exoskeleton robot perform Cartesian trajectories as human-like motion without singularity problem (chapter 2).

1.2.2 Development of the nonlinear control laws

Different adaptive control strategies were investigated. The unknown dynamics or uncertainties dynamics/kinematics, the massive non-linearity, and the high dimensional characterizing such systems considerably complicate the control problem and make it difficult to solve using the conventional approaches cited previously. As a solution to these serious problems, many adaptive control laws were proposed and validated in real time in different mode of rehabilitation motions (passive and active). These techniques can be summarized as follows:

a. A new compliant control based on a second-order sliding mode with adaptive-gain incorporating time delay estimation. In this work, the dynamic parameters of the system were considered uncertain and were estimated by time delay estimation (chapter 3). it is worth mentioning that in this work, the human inverse kinematics solution proposed in chapter 2 is used to complete the active rehabilitation motion;

b. Adaptive backstepping approach integrated with modified time-delay estimation to provide an accurate estimation of unknown dynamics of the exoskeleton robot and to compensate for external bounded disturbances (chapter 4);

c. The passive and active control strategies based on integral backstepping approach to provide a physical assistance and rehabilitation by a 7-DOF exoskeleton robot with nonlinear uncertain dynamics and unknown bounded external disturbances due to the robot user's physiological characteristics. Besides, The Damped Least Square method is introduced to estimate the desired movement intention of the subject with the objective to provide active rehabilitation motion (chapter 5);

d. Finally, a new adaptive visual tracking control approach based on sliding mode control in Cartesian space applied to an exoskeleton robot with uncertain kinematics and dynamics, taking into account uncertainties in visual system (camera) parameters (chapter 6).

1.2.3 Implementation and experimentation

Besides design and simulation with a diversity of tools (MATLAB, and LabVIEW), all the control strategies and methods investigated in this work were implemented and validated on the ETS-MARSE robot.

Figure 1.7 outlines the methodology explained above and summarizes the structure of this work.

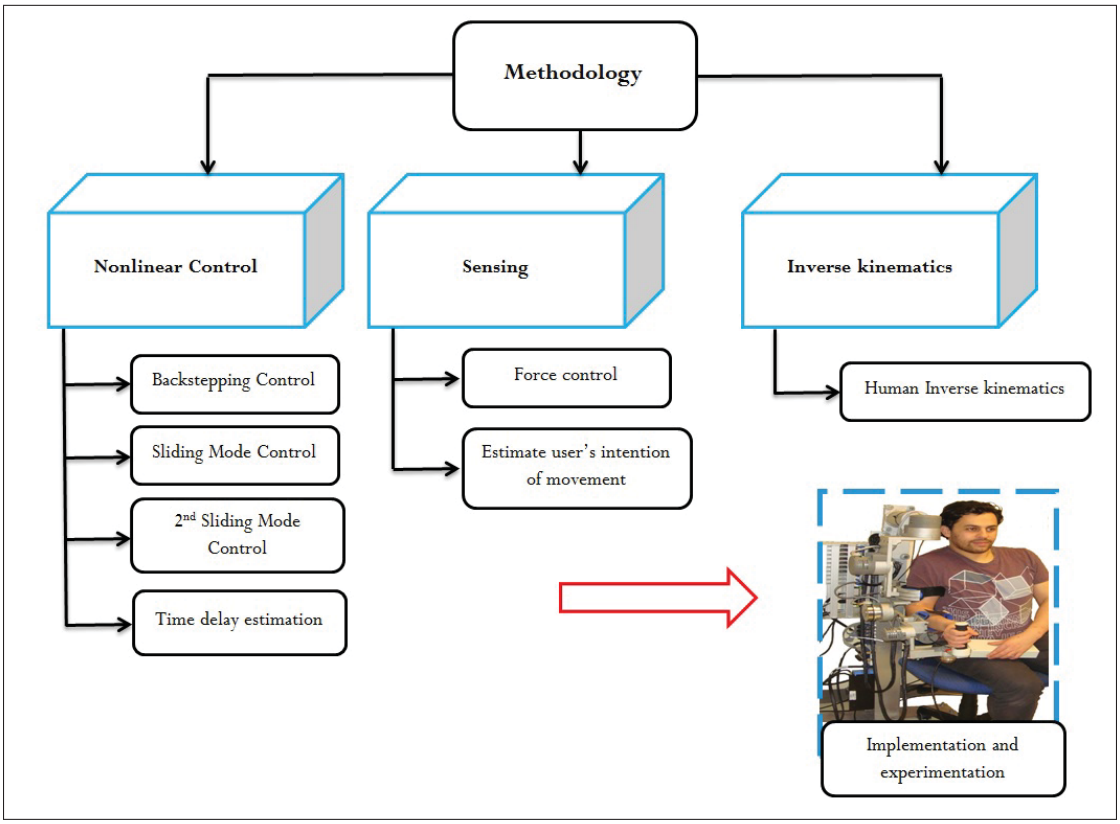

Figure 1.7 Methodology of the improvement ETS-MARSE rehabilitation system

1.3 Originality of the research and contribution

This research focuses on the development of a redundant exoskeleton robot named ETS-MARSE to provide a suitable passive and active rehabilitation motion to physically disabled people, with full shoulder, elbow and wrist rehabilitation capacities. Therefore, the development is focused on two points. The first one is to solve the inverse kinematic problem that allows the exoskeleton robot to perform a human-like motion. The second one is the development of robust nonlinear control laws that allow the exoskeleton robot to achieve the desired physiotherapy treatment, even if the exoskeleton is subject to the dynamic/kinematic uncertainties and external disturbances. Following the literature review, although numerous researches deal with the control of these kinds of robots, few of them are concerned with high nonlinearity and dynamic/kinematic uncertainties where the majority of them consider that the dynamic model of the exoskeleton is fully known. Unfortunately, it is impossible to determine exactly the overall dynamic model of the exoskeleton robot due to its complex mechanical structure and hard nonlinearities that negatively affect the performance of the exoskeleton robot. To solve uncertainty problem, some researchers have proposed an adaptive control approach based on conventional adaptive techniques. In this work, we propose different adaptive strategies. Contrary to what appears in the cited researches, this thesis has the following contributions:

a. Unlike convention inverse kinematics solutions, the proposed solution provides an optimal Cartesian solution resembling the movement of the human upper limb and always presents a valid human arm configuration. In addition, the proposed inverse kinematic algorithm provides a solution that does not pose a singularity problem and characterized by a high level of precision and rapidity of response;

b. The delay time estimation (TDE) strategy is considered to be one of the important contributions employed in this work to account for the unknown uncertainty of the dynamic model of the exoskeleton due to: firstly, its easiness to implement it in real time application. Secondly, TDE is one of the approaches that are not influenced by the size of the estimated dynamics parameters in the case of high DOFs. Nevertheless, TDE approach suffers from the Time Delay Error (TDR) caused by the noisy measurements and hard

nonlinear function of the robot model during delay constant, which would degrade the approximation performance;

c. Using a new recursive control to estimate and reduce the effect of the Time Delay Error (TDR) and improve the robustness of the control system. Usually, this error limits the performance of TDE approach;

d. Considering the unknown kinematics and dynamics with unknown external disturbances (different weight of the arm of each subject), adaptive visual controller incorporating with recursive control is developed to estimate the nonlinear kinematic and dynamic uncertainties with unknown disturbances and to drive the robot to follow the desired functional therapy activity and provide a smooth exoskeleton-aided passive activity;

e. The stability of the system and the convergence of its errors are formulated and demonstrated based on Lyapunov–Krasovskii functional theory to prove the stability of the system in each delayed interval;

f. A new compliant control is developed based on human inverse kinematics. This control ensures an accurate relation between the desired force and the desired position and produces human-like motion;

g. Adaptive gains are incorporated with a second-order sliding mode control to provide an adaptation of the switching gains and to avoid the undesired chattering;

h. Using Damped Least Squares (DLS) technique to easily estimate the user's intention of movement.

1.4 List of publications

In this section, we present only the published papers related to this thesis:

- Brahmi, Brahim, Maarouf Saad, Mohammad H. Rahman, and Cristobal Ochoa-Luna. "Cartesian trajectory tracking of a 7-DOF exoskeleton robot based on human inverse kinematics." published in IEEE Transactions on Systems, Man, and Cybernetics: Systems 99 (2017): 1-12;

- Brahmi, Brahim, Maarouf Saad, Abdelkrim Brahmi, Cristobal Ochoa Luna, and Mohammad Habibur Rahman. "Compliant control for wearable exoskeleton robot based on human inverse kinematics." published in International Journal of Advanced Robotic Systems 15, no. 6 (2018): 1729881418812133;
- Brahmi, Brahim, Maarouf Saad, Cristobal Ochoa-Luna, Mohammad Habibur Rahman, and Abdelkrim Brahmi. "Adaptive tracking control of an exoskeleton robot with uncertain dynamics based on estimated time-delay control." published in IEEE/ASME Transactions on Mechatronics 23, no. 2 (2018): 575-585;
- Brahmi, Brahim, Maarouf Saad, Cristobal Ochoa Luna, Philippe S. Archambault, and Mohammad H. Rahman. "Passive and active rehabilitation control of human upper-limb exoskeleton robot with dynamic uncertainties." published in Robotica 36, no. 11 (2018): 1757-1779;
- Brahmi, Brahim, Maarouf Saad, Jacqueline Tu Anh Thu Lam, Cristobal Ochoa Luna, Philippe S. Archambault, and Mohammad H. Rahman. "Adaptive control of a 7-DOF exoskeleton robot with uncertainties on kinematics and dynamics." published in European Journal of Control 42 (2018): 77-87;

CHAPTER 2

CARTESIAN TRAJECTORY TRACKING OF A 7-DOF EXOSKELETON ROBOT BASED ON HUMAN INVERSE KINEMATICS

Brahim Brahmi[1], Maarouf Saad[1], Mohammad H. Rahman [2]
and Cristobal Ochoa Luna[1]

[1] Département of Electrical Engineering, École de Technologie Supérieure,
1100 Notre-Dame Ouest, Montréal, Québec, Canada H3C 1K3
[2] Mechanical/Biomedical Engineering Department,University of Wisconsin-Milwaukee,
3200 N. Cramer Street, Milwaukee, WI 53211,

Paper published in *IEEE Transaction on System, Man, and Cybernetics: Systems*, April 2017

Abstract

Exoskeleton robots have become an important tool to provide rehabilitation therapy to stroke victims because of their ability to allow rehabilitation exercises, ranging from passive to active-assisted movement, for extended time periods. To generate the desired rehabilitation trajectories and ensure an optimal Cartesian solution, we propose a new solution to the inverse kinematics problem, which is compatible with human upper limb movement and is valid for human arm configuration. In addition, in order to provide passive rehabilitation therapy to the upper extremity of disabled individuals, we implement a robust nonlinear control based on the backstepping technique on the seven-degrees-of-freedom ETS-MARSE robot. The controller was designed to reject the user's force caused by the subject's muscular activity. Experimental results validate the stability, robustness, and exactness of the proposed method with the designed tests performed by healthy subjects.

Keywords: Backstepping controller, Exoskeleton robots, Inverse kinematics, Lyapunov function, Robotic rehabilitation.

2.1 Introduction

Neurological diseases have become a challenging problem for the scientific community. According to recent statistics, every year at least 15 million people worldwide suffer neurological diseases such as stroke. Six million of these people die and five million more are living with a persistent disability (Sidney *et al.*, 2013). In Canada each year at least 16,000 Canadians die because of a stroke incident (De Morand, 2014). The survivors from strokes generally do not have the means to perform daily activities such as eating, dressing, and bathing by themselves due to permanent disability, often on one side of the body (De Morand, 2014). The current treatment to aid stroke victims to regain their missing functional capacity, gain new skills, and enhance their quality of life is rehabilitation. However, rehabilitation treatments require intensive and fatiguing work by the therapist (De Morand, 2014), (Brahim *et al.*, 2016a). Modern robotic technology has become an important component in many medical specialization, even to accomplish rehabilitation tasks such as physiotherapy. Recently, robotics rehabilitation has gained attention from the scientific community because robots are able to supplement the treatments provided by conventional physical therapy (de Santé, 2012). The importance of rehabilitation robots lies in their ability to provide intensive physiotherapy for a long period of time (Brahim *et al.*, 2016a), (de Santé, 2012). The measured data of the robot permits the physiotherapist to accurately evaluate the patient's performance.

Current robotics technologies present us with new devices known as rehabilitation robots, which are used to overcome the limitations of classical physiotherapy approaches and create new methods of rehabilitation treatment (Xie *et al.*, 2016). The most valuable role played by these robots is to help both the therapist and stroke victims improve treatment with rehabilitation therapy. To rehabilitate patients with upper-limb impairment, these exoskeletons habitually are worn on the lateral side of the patients' upper-limb (Nef *et al.*, 2007). Various research groups have designed this type of manipulator like ARMin IV robot (Nef *et al.*, 2007) designed with (6-DOFs), RUPERT robot (Balasubramanian *et al.*, 2008), (Huang *et al.*, 2016) with (5- DOFs) and (SUEFUL-7) robot (Gopura *et al.*, 2009) consist of (7-DOFs). In order to provide a modern rehabilitation approach for the upper-limb, we have developed a 7- DOFs

exoskeleton robot named ETS-MARSE (Rahman *et al.*, 2015). The seven degrees of freedom (DOFs) of the manipulator makes it a redundant robot capable of reaching several arm configurations in its workspace and providing task-oriented exercises in joint space, Cartesian space and free motion (Rahman *et al.*, 2015).

The goal of the assistive automatic control is to assist patients to complete physical therapy. A passive assistive movement is an indispensable thing to do following a stroke accident. In this scenario, the exoskeleton robot carries the dysfunction upper limb of the subject to achieve a passive physical activity (Brahim *et al.*, 2016a); the user's force is thus considered as an external disturbance. Multiple control strategies have been designed to handle the exoskeleton system in order to provide an assistive passive therapy: such a PID control (Yu and Rosen, 2010), a neural PID controller (Yu and Rosen, 2013), and a nonlinear modified computed torque control (Rahman *et al.*, 2011a). Furthermore, a sliding mode controller combined with exponential reaching law was proposed in (Rahman *et al.*, 2012c) to limit the chattering problem caused by the large control gains. While the above control schemes make use of the dynamic model of the robots, the accuracy of the model, however, directly affects the controller performance. Various nonlinear control strategies developed, which do not need an exact dynamic model of the robot system, like a fuzzy sliding mode adaptive controller proposed in (Sun *et al.*, 1999), and neural sliding mode control (Ciliz, 2005), where both controllers are aimed to overcome the effect of the uncertain nonlinear dynamics and the unexpected external disturbances, which influence the robot performance. However, these methods require heavy computations, making the implementation very difficult (Li *et al.*, 2015a).

Generally, the exoskeleton manipulators originally have a highly nonlinear dynamic model. Unfortunately, it is impossible to determine exactly the overall dynamic model of the exoskeleton robot due to its complex mechanical structure and hard nonlinearities in its parameters, (Li *et al.*, 2016) such as nonlinear friction forces, backlash, etc... . In addition, the subjects exhibit different physiological conditions, such as non-linear bio-mechanical characteristics of the musculoskeletal system, the different weight of the upper-limb for each patient, the presence of spasticity in neurological patients (Brahim *et al.*, 2016b). During a physical move-

ment, the external forces can turn into an unknown function that can affect the exoskeleton performance (Brahim *et al.*, 2016b). In order to address the mentioned problems, we have implemented an adaptive nonlinear control based on the backstepping approach. A robust force observer is implemented to estimate the user's force. A powerful Lyapunov function is offered to solve the adaptation problem systematically, proving the closed-loop stability and ensuring the asymptotic convergence of the output errors (Li *et al.*, 2015a), (Brahim *et al.*, 2016b), (Jin and Xu, 2013). The principal benefit of the designed control is that an accurate knowledge of the external disturbances is not needed. In addition, it gives outstanding tracking performance similar to the natural human movement despite the presence of external perturbations (Brahim *et al.*, 2016b).

Practically, in most applications using non-redundant exoskeleton robots, the desired trajectories and/or therapeutic tasks are expressed in Cartesian space. However, operators prefer to control redundant exoskeleton robots in joint space in order to manage their redundancy (Crocher, 2012). Numerous methods, including numerical (Tolani and Badler, 1996), analytical (Bin *et al.*, 2011), (Tolani *et al.*, 2000), optimization (Xia and Wang, 2001), (Khoogar *et al.*, 2011), vision (Jiang *et al.*, 2014),(Zhang *et al.*, 2014), (Chan *et al.*, 2014), and geometric methods (Tolani and Badler, 1996), (Loh and Rosen, 2013), (Kim *et al.*, 2011a), (Asfour and Dillmann, 2003), have been developed to solve the problem of inverse kinematics. The most frequently and most widely applied solutions for redundant robots are the inverse Jacobian and the Jacobian pseudo-inverse methods (Craig, 2005), (Kelly *et al.*, 2006), (Klein and Huang, 1983). However, these approaches provide multiple solutions in Cartesian space. Moreover, the methods present many downsides, such as singularity problems. Further, in rehabilitation applications, the objective is not only to reach the desired goal; achieving an optimal solution corresponding to a human movement is also mandatory.

In this paper, a new inverse kinematics solution is proposed to provide Cartesian passive rehabilitation exercises. The philosophy of this approach is to develop a mathematical model based on geometric and analytic solutions of human upper limb motion in order to imitate its movement. To ensure the robustness of this method, we integrate new geometric solutions

consistent with the mechanical design of the ETS-MARSE exoskeleton. The main advantage of this approach is that it provides an optimal Cartesian solution resembling the human upper limb movement and always presents a valid human arm configuration. In addition, the proposed inverse kinematics algorithm provides a solution not having a singularity problem and characterized by a high level of precision and rapidity of response. The controller used to demonstrate the validity of the approach shows that it is capable of following the commanded trajectories due to the smooth output of the inverse kinematics algorithm. The precision and the durability of the control scheme and the algorithm of inverse kinematics was appraised by the implementation of designed exercises conforming to a passive physiotherapy. All therapy tasks were performed with healthy subjects.

The rest of the paper is organized as follows: section 2.2 gives a brief description of the ETS-MARSE and describes the inverse kinematics algorithm. Section 2.3 describes the control strategy. Experiments results and discussion are presented in section 2.4. Finally, the conclusion and future work are presented in section 2.4.

2.2 ETS-MARSE wearable robot

2.2.1 Description of ETS-MARSE robot

The ETS-MARSE is a redundant robot with 7-DOFs, designed to rehabilitate the impaired human upper limb, as shown in Figure 2.1. The designing of the manipulator robot ETSMARSE was originally inspired by the joints and anatomy of the human upper limb in order to be comfortable with the robot users during the rehabilitation tasks. The shoulder part is represented by three joints. The first two joints are designed to perform the horizontal and vertical extension/flexion motion, while the third joint of the shoulder conducts the external/internal rotation of the shoulder movement. The elbow part is formed by one joint to perform flexion/extension movement of the elbow. The last part of the upper limb is the wrist part that consists of three joints. The first joint is designed to achieve pronation/supination movement of the forearm; the second joints and the third joint are designed to perform radial and ulnar deviation and flexion

and extension of the wrist part, respectively (Brahim *et al.*, 2016a), (Rahman *et al.*, 2015). Table 2.1 presents the workspace of the designed robot.

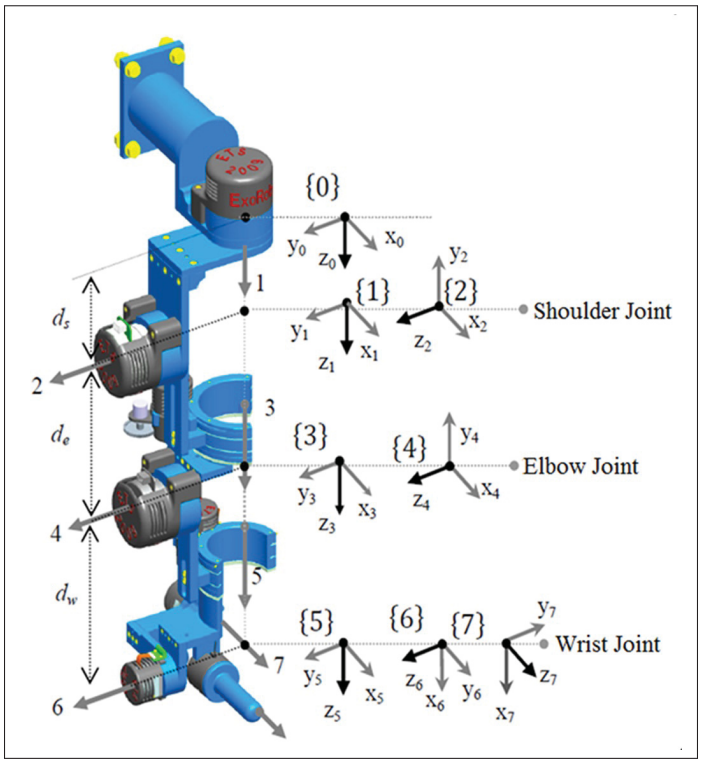

Figure 2.1 ETS-MARSE with link frame

The modified Denavit–Hartenberg (DH) parameters are given in Table 2.2. These parameters are obtained from the frame reference shown in Figure 2.1 and are used to obtain the homogeneous transformation matrices (Craig, 2005).

Table 2.1 Workspace ETS-MARSE

joint (i)	Motion	Workspace
1	Shoulder joint horizontal flexion/extension	$0°/140°$
2	Shoulder joint vertical flexion/extension	$140°/0°$
3	Shoulder joint internal/external rotation	$-85°/75°$
4	Elbow joint flexion/extension	$120°/0°$
5	Forearm joint pronation/supination	$-85°/85°$
6	Wrist joint ulnar/radial deviation	$-30°/20°$
7	Wrist joint flexion/extension	$-50°/60°$

Table 2.2 Modified DH parameters

joint (i)	α_{i-1}	a_{i-1}	d_i	θ_i
1	0	0	d_s	θ_1
2	$\frac{-\pi}{2}$	0	0	θ_2
3	$\frac{\pi}{2}$	0	d_e	θ_3
4	$\frac{-\pi}{2}$	0	0	θ_4
5	$\frac{\pi}{2}$	0	d_w	θ_5
6	$\frac{-\pi}{2}$	0	0	$\theta_6 - \frac{\pi}{2}$
7	$\frac{-\pi}{2}$	0	0	θ_7

The homogenous transformation matrix that associates frames $\{7\}$ to $\{0\}$ can be obtained by multiplying transformation matrices:

$$ {}^{0}_{7}T = \begin{bmatrix} {}^{0}_{1}T\ {}^{1}_{2}T\ {}^{2}_{3}T\ {}^{3}_{4}T\ {}^{4}_{5}T\ {}^{5}_{6}T\ {}^{6}_{7}T \end{bmatrix} \tag{2.1} $$

2.2.2 Inverse kinematics solution

The design of an exoskeleton like the ETS-MARS robot is inspired by the human arm. As the human extremity has redundant kinematics, exoskeleton redundancy permits it to perform a large number of human movements. However, due to the redundancy, there are infinite solutions to the inverse kinematics problem for any given end-effector position. The main objective of the proposed algorithm is to limit these solutions to an optimal (or unique) solution able to imitate the human motion and to correspond to the human arm configuration. It is interesting to remark that a human uses the minimum joints of the arm with its optimal configuration when he reaches for an object in 3-D space ((De Morand, 2014)). It is significant also that the first three (shoulder) joints of the ETS-MARSE are responsible for the elbow pose. The elbow position and its joint angle value are responsible for the end-effector position. The last (wrist) joints are responsible for the end-effector rotation only. The proposed inverse kinematics solution is inspired directly from the human arm movement. From a known end-effector pose, it is

possible to define the elbow joint (θ_4) geometrically and independently using Figure 2.2 (a):

$$\theta_4 = \pi \pm acos\left(\frac{d_w^2 + d_e^2 - \|w-s\|^2}{2d_e d_w}\right) \tag{2.2}$$

Without a doubt, joint θ_4 has a unique solution; with the help of a geometric relation, we can define the elbow pose. This position is determined by defining the distance (R) and the angle (α) that is located between the distance de and the virtual axis that links between the end-effector position and the fixed shoulder position. From the elbow position, the three joints of the shoulder (θ_1, θ_2, θ_3) can be derived analytically with a unique solution. Thus, the inverse kinematics problem now includes obtaining the configuration of a nonredundant structure where θ_1, θ_2, θ_3, and θ_4 joints have a unique solution (geometric and/or analytical solution). From the known (desired) end-effector rotation and the above angles (θ_1, θ_2, θ_3, and θ_4), the solution of θ_5, θ_6, and θ_7 angles can be derived by the comparison as we will see in the last part. The detail of the solution will be given later. In special positions, when the position of the wrist is fixed with particular constraints, the redundancy of the arm can be parameterized by observing that the elbow is still free to swivel about an axis from the swivel angle (ϕ) to the shoulder. The axes of this circle are perpendicular to the vector pointing from the shoulder joint to the wrist joint. The swivel angle (ϕ) is the rotation angle of the elbow around a virtual axis that connects the shoulder and wrist joints. As the swivel angle varies, the elbow traces the arc of a circle on a plane whose normal is parallel to the shoulder-to-wrist axis (Tolani and Badler, 1996), as shown in Figure 2.2 (b). The swivel angle is not a joint of the robot; it is not directly controllable, but a measurable parameter result of the kinematics of the robot, based on the constraints on the wrist orientation. It is important to notice that for a sample or basic rehabilitation motion, the swivel angle is fixed to zero (not influenced the solution of inverse kinematics solution). A simple movement does not contain any constraints on the wrist position and this fixation does not influence the redundancy of the exoskeleton robot.

In order to be able to describe the circle mathematically, the normal vector of the plane is defined as:

$$\hat{n} = \frac{w-s}{\|w-s\|} \tag{2.3}$$

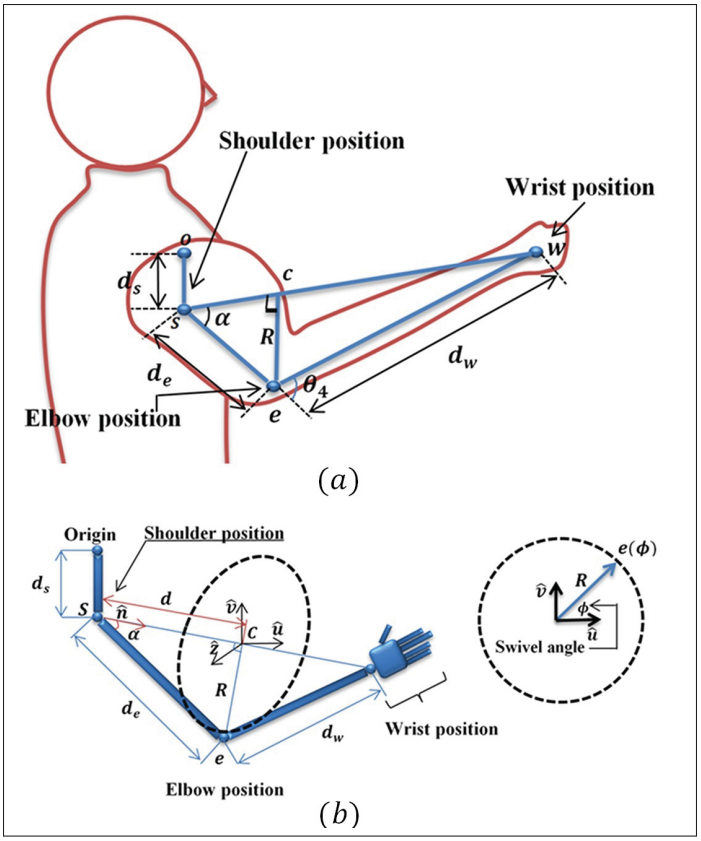

Figure 2.2 (a) Description of human movement in 3D space. (b) Representation of swivel angle (ϕ)

Then, $\hat{u}$ is set to be a projection of an axis $\hat{z}$ chosen arbitrarily on the circle:

$$\hat{z} = [0 \quad 0 \quad 1]^T \tag{2.4}$$

$$\hat{u} = \frac{\hat{z} - (\hat{z}\,\hat{n})\,\hat{n}}{\|\hat{z} - (\hat{z}\,\hat{n})\,\hat{n}\|} \tag{2.5}$$

and $\hat{\upsilon}$ is the last component of the orthonormal base:

$$\hat{\upsilon} = \hat{n} \times \hat{u} \tag{2.6}$$

R and c are the radius and center of the circle, respectively. The radius R is found with simple trigonometric relationships. Let us start by defining the distance d or center of circle c as

follows (see Figure 2.2 (b)):

$$d = Cos(\alpha)\, d_e \hat{n} \tag{2.7}$$

with:

$$Cos(\alpha) = \frac{d_w^2 - d_e^2 - \|w-s\|^2}{-2d_e\|w-s\|} \tag{2.8}$$

and:

$$R = Sin(\alpha)\, d_e \tag{2.9}$$

Finally, the elbow position can be parameterized as a function of the swivel angle (ϕ) about axis $\hat{u}$:

$$e(\phi) = d + R[Cos(\phi)\hat{u} + Sin(\phi)\hat{v}] + s \tag{2.10}$$

where s is the vector shoulder coordinate define such that: $s_{shoulder} = [0\ \ 0\ \ d_s]^T$; (see Equation (2.14)).

We see that the elbow position depends on the value of the swivel angle (ϕ) and radius R. If the value of the swivel angle (ϕ) is defined, we can subsequently solve the problem of inverse kinematics analytically. Finding a value of the swivel angle (ϕ) with a small error is very difficult even if it is restricted to the case of one specific and well-defined task (a specific reaching or grasping exercise, for instance), and for the general case, it is impossible to obtain an exact estimation of the swivel angle. Various research works, proposed in (Kim *et al.*, 2011a), (Kim *et al.*, 2011b), (Chua *et al.*, 2013), used estimation methods such as cost functions optimization and a prediction algorithm based on data acquisition to determine the value of the swivel angle for certain specific reaching activities corresponding to rehabilitation exercises. In our case, the elbow cannot rotate along the aforementioned shoulder-wrist circle due to mechanical design limitations of the ETS-MARSE robot. This indicates that even if it were possible to compute a swivel angle from the robot end-effector position, the robot would not be able to achieve it always. However, as we have mentioned, it is very difficult to have the swivel angle computed accurately in direct relation from the manipulator's end-effector position. It is then not a restriction in terms of inverse kinematics, but it is in terms of the robot working space, which lacks some shared space with a human arm. Thus, the robot lacks

the ability to perform some human motions (these motions consist of a varying swivel angle, outside the robot's envelope). As we mentioned above, there is no clear method to estimate the swivel angle exactly when we have constraints on the wrist position. However, for the mechanical design of the ETS-MARSE robot, we proposed a solution to solve this problem. Practically, we found that variation of the joint θ_6 provokes a limit variation of swivel angle. This variation is calculated geometrically (see Figure 2.3). In this case, no numerical estimation is needed, and the inverse kinematics solution will remain purely analytical. Therefore, if we have constraints on the wrist, we have a virtual axis that connects between the hand center point (d_h) and the new elbow position as shown in Figure 2.3. The variation (V) is assumed approximately equal ($V^{'}$). This variation (V) is caused by the constraint that is provoked by joint θ_6. Geometrically, the angle (ϑ) is an equal angle ($\vartheta^{'}$). Hence, according to cosines law, it is possible to define angles (ϑ) and angle ($\vartheta^{'}$) such that:

$$\begin{cases} V^2 = a_1^2 + p_1^2 - 2a_1 p_1 Cos(\vartheta) \\ V'^2 = a_2^2 + p_2^2 - 2a_2 p_2 Cos(\vartheta^{'}) \end{cases} \tag{2.11}$$

If $V = V^{'}$ we can define $Cos(\vartheta)$ as follow:

$$Cos(\vartheta) = Cos(\vartheta^{'}) = \frac{a_1^2 + p_1^2 - a_2^2 - p_2^2}{2(a_1 p_1 - a_2 p_2)} \tag{2.12}$$

Now $V^{'}$ is available from equation (2.11). Let us now to define the variation of swivel angle (ϕ) from triangle ($cee^{'}$) such that:

$$\phi = \frac{2R^2 - V'^2}{2R^2} \tag{2.13}$$

The shoulder is translated by a distance d_s on the z-axis as regard to the origin (frame $\{0\}$ in Figure 2.1).

$$P_{shoulder} = {}^{0}_{1}T\,[0\ \ 0\ \ 0\ \ 1]^T = [0\ \ 0\ \ d_s\ \ 1]^T \tag{2.14}$$

where ${}^{0}_{1}T$ is the first homogenous transformation matrix calculated by using Table 2.1. The position of the elbow is determined only by the three shoulder joints θ_1, θ_2 and θ_3:

$$P_{elbow} = {}^{0}_{1}T\ {}^{1}_{2}T\ {}^{2}_{3}T\ [0\ \ 0\ \ 0\ \ 1]^T = [e_x\ \ e_y\ \ e_z\ \ 1]^T \tag{2.15}$$

so,

$$P_{elbow} = \begin{bmatrix} e_x \\ e_y \\ e_z \end{bmatrix} = \begin{bmatrix} d_e C_1 S_2 \\ d_e S_1 S_2 \\ d_s + d_e C_2 \end{bmatrix} \tag{2.16}$$

here, C_i denotes $Cos(\theta_i)$ and S_i denotes $Sin(\theta_i)$.

The wrist joint position depends on θ_1, θ_2, θ_3 and θ_4. The last three joints θ_5, θ_6 and θ_7 intervene just to determine the wrist orientation.

$$\begin{aligned} P_{elbow} &= {}^{0}_{1}T\ {}^{1}_{2}T\ {}^{2}_{3}T\ {}^{3}_{4}T\ {}^{4}_{5}T\ [0\ \ 0\ \ 0\ \ 1]^T = [w_x\ \ w_y\ \ w_z\ \ 1]^T \\ &= \begin{bmatrix} d_e C_1 S_2 - d_w \left(S_4 \left(S_1 S_3 - C_1\right) C_2 C_3\right) - C_1 C_4 S_2 \\ d_w \left(S_4 \left(C_1 S_3 + C_2 C_3 S_1\right) + C_4 S_1 S_2\right) + d_e S_1 S_2 \\ d_s + d_w \left(C_2 C_4 - C_3 S_2 S_4\right) + d_e C_2 \end{bmatrix} \end{aligned} \tag{2.17}$$

2.2.2.1 Solving θ_1 and θ_2

Obtained directly from equation (2.16), the elbow position is known. Then:

$$\frac{e_y}{e_x} = \frac{d_e S_1 S_2}{d_e C_1 S_2} \Rightarrow \theta_1 = atan2(e_y, e_x) \tag{2.18}$$

For θ_2 we have two solutions, i.e., an analytic solution and a geometric solution, from equation (2.16):

$$Cos(\theta_2) = \frac{e_z - d_s}{d_e} \tag{2.19}$$

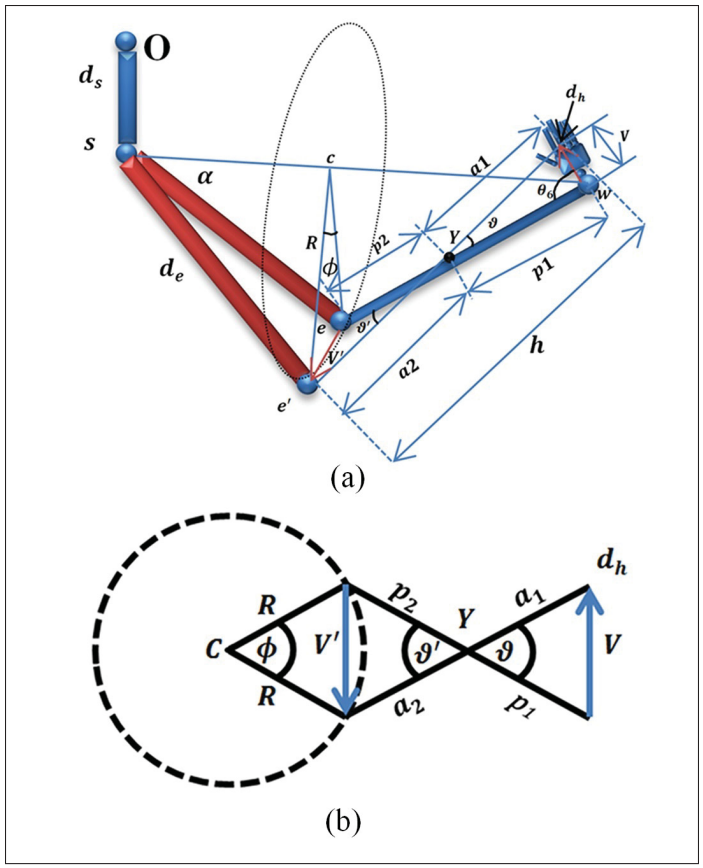

Figure 2.3 (a) Geometrical solution of swivel angle (ϕ) 3D view. (b) Geometrical solution of swivel angle 2D view

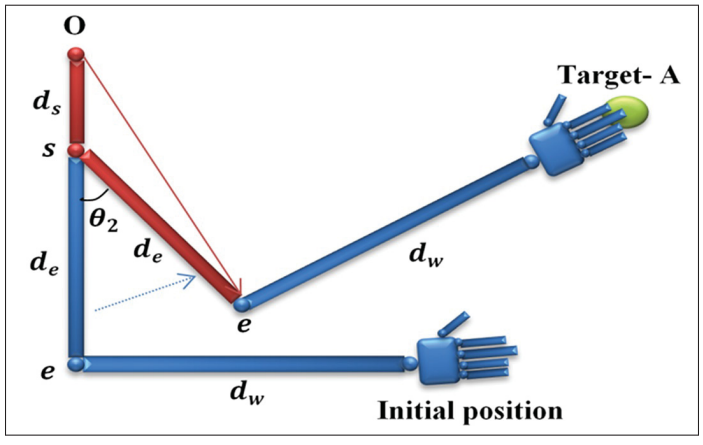

Figure 2.4 Geometrical representation of joint θ_2

In addition:

$$\begin{cases} Sin(\theta_2) = \dfrac{e_x}{d_e C_1} & if \;\; C_1 \neq 0 \\ Sin(\theta_2) = \dfrac{e_y}{d_e S_1} & Otherwise \end{cases} \tag{2.20}$$

So,

$$\theta_2 = atan2\left(Sin(\theta_2), \frac{e_z - d_s}{d_e}\right) \tag{2.21}$$

Since joint 2 is located at the shoulder in Figure 2.4, the coordinate of the origin (joint 1 in Figure 2.2) is $[0 \;\; 0 \;\; 0]$, the elbow position is defined by equation (2.16), and the distance between the shoulder and elbow d_e is constant. We can use the law of cosines to compute θ_2:

$$\theta_2^* = \pi \pm acos\left(\frac{\|e - O\|^2 - d_e^2 - d_s^2}{-2 d_e d_s}\right) \tag{2.22}$$

where θ_2^* is the geometric solution.

2.2.2.2 Solving θ_3

For joint 3 (θ_3), we have two solutions as well, analytic and geometric. To find θ_3 analytically, we multiply both sides of equation (2.17) by $\left({}^0_1T \; {}^1_2T\right)^{-1}$:

$$\left({}^0_1T \; {}^1_2T\right)^{-1} \left({}^0_1T \; {}^1_2T \; {}^2_3T \; {}^3_4T \; {}^4_5T\right) [0 \;\; 0 \;\; 0 \;\; 1]^T = \left({}^0_1T \; {}^1_2T\right)^{-1} [w_x \;\; w_y \;\; w_z \;\; 1]^T \tag{2.23}$$

This leads to:

$$\begin{bmatrix} d_w S_4 C_3 \\ -d_w C_4 - d_e \\ d_w S_4 S_3 \\ 1 \end{bmatrix} = \begin{bmatrix} d_s S_2 - w_z S_2 + w_x C_1 C_2 + w_y C_2 S_1 \\ w_x C_1 S_2 - w_y S_1 S_2 + d_s C_2 - w_z C_2 \\ w_y C_1 - w_x S_1 \\ 1 \end{bmatrix}$$

$$\theta_3 = atan2\left(w_y C_1 - w_x S_1, \; d_s S_2 - w_z S_2 + w_x C_1 C_2 + w_y C_2 S_1\right) \tag{2.24}$$

Using the law of cosines (see Figure 2.5, we can obtain the geometric solution:

$$\theta_3^* = \pi \pm acos\left(\frac{\|w - w^*\|^2 - 2d_w^2}{-2d_w^2}\right) \tag{2.25}$$

where θ_3^* is the geometric solution.

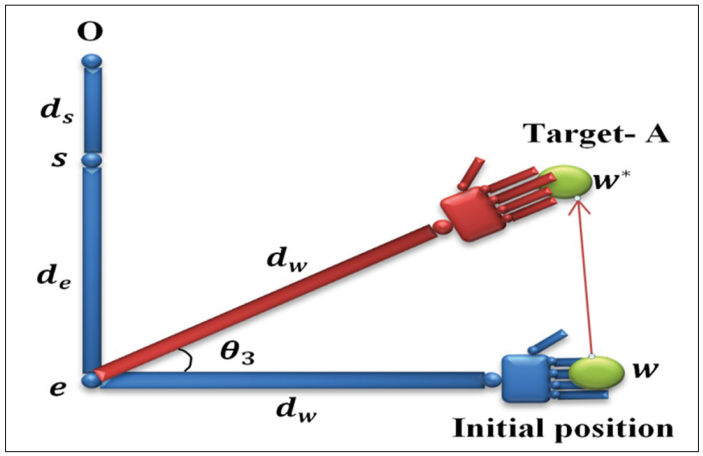

Figure 2.5 Geometrical representation of joint θ_3

Now, we have two solutions (analytic and geometric) for each joint (joints 2 and 3). The importance of these solutions is that they provide different results for the inverse kinematics, particularly in the case of singularity. These solutions are always valid for human arm movement.

2.2.2.3 Solving θ_5, θ_6 and θ_7

The orientation of the end-effector is given by:

$$R_{end-effector} = R_1R_2R_3R_4R_5R_6R_7 = \begin{bmatrix} r_{11} & r_{12} & r_{13} \\ r_{21} & r_{22} & r_{23} \\ r_{31} & r_{32} & r_{33} \end{bmatrix} \tag{2.26}$$

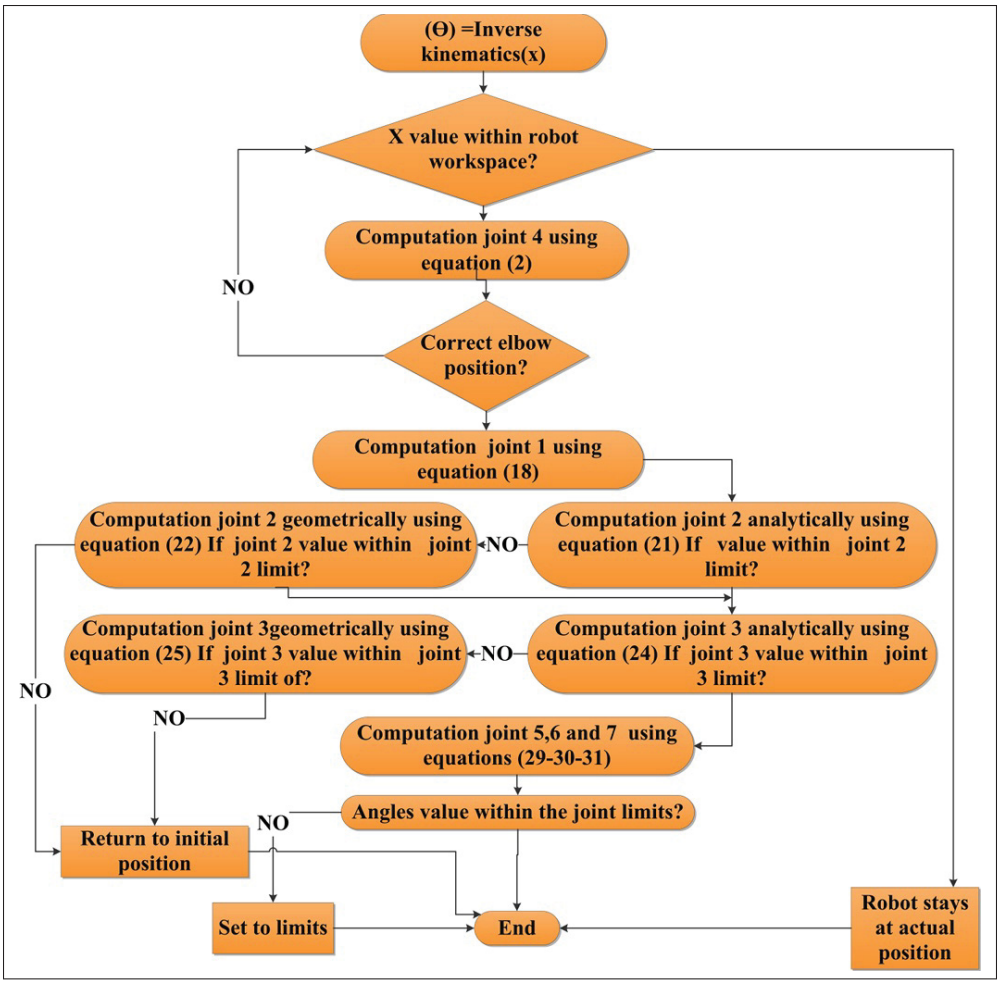

Figure 2.6 Inverse kinematics algorithm

Consider that $R_w = R_5 R_6 R_7$:

$$R_w = \begin{bmatrix} S_5S_7 + C_5C_6C_7 & C_7S_5 - C_5C_6S_7 & C_5S_6 \\ C_7S_6 & -S_6S_7 & C_6 \\ C_6C_7S_5 - C_5S_7 & C_5C_7 - C_6S_5S_7 & -S_5S_6 \end{bmatrix} \tag{2.27}$$

Substituting equation (2.27) in equation (2.26):

$$R_w = R_4^T R_3^T R_2^T R_1^T R_{end-effector} \tag{2.28}$$

where the $R_{end-effector}$ matrix defines the desired end-effector orientation with respect to the origin. In this case, we use standard matrix rotation and Euler angles.

To find the wrist angles, we apply equation (2.27) and equation (2.28) to do the comparison between them:

$$\theta_6 = \begin{cases} acos(r_{23}) \\ -[2\pi + acos(r_{23})] \end{cases} \tag{2.29}$$

If $S_6 \neq 0$

$$\begin{cases} tan(\theta_5) = \dfrac{r_{33}}{r_{13}} \Longrightarrow \theta_5 = atan2\left(\dfrac{r_{33}}{S_6}, \dfrac{r_{13}}{S_6}\right) \\ \dfrac{r_{22}}{r_{21}} = \dfrac{-S_6 S_7}{C_7 S_6} \Longrightarrow \theta_7 = atan2\left(\dfrac{-r_{22}}{S_6}, \dfrac{r_{21}}{S_6}\right) \end{cases} \tag{2.30}$$

If $S_6 = 0$

$$\begin{cases} \theta_5 = atan2\left(r_{31},\ r_{11}\right) \\ \theta_7 = 0 \end{cases} \tag{2.31}$$

In summary, the inverse kinematics algorithm of the ETSMARSE is shown in Figure 2.6. The algorithm consists of several steps. First, the desired position must be checked to determine whether or not it is within the robot workspace. If it is in the robot workspace area, the value of joint $\theta 4$ can then be extracted. The position of the elbow is determined by the values of the first four joints of the arm (three joints of the shoulder and one joint of the elbow) with the help of the value of the swivel angle (ϕ). If the elbow position is within the workspace of the shoulder joint, all the values of the remaining angles can be solved analytically. We can compute joint angle $\theta 2$ analytically; if the solution of this computation is outside $\theta 2$limits, we use its geometrical solution. Then the value of joint angle $\theta 3$ will be computed in the same manner; if no solution exists, the robot returns to its initial position. If the above angles are available, the algorithm continues to calculate the orientation of the end-effector joints ($\theta 5$, $\theta 6$

and $\theta 7$). Finally, if the angle values are outside the joint angle limits, we will set them at the mechanical limit.

2.3 Control design

The dynamics behavior of ETS-MARSE manipulator is given by the following expression by using the Lagrangian method:

$$M(\theta)\ddot{\theta} + C(\theta,\dot{\theta}) + G(\theta) + F(\theta,\dot{\theta}) = \tau + \tau_{ex} \tag{2.32}$$

$$\tau_{ex} = J^T F_{ex} \tag{2.33}$$

where θ, $\dot{\theta}$ and $\ddot{\theta} \in \mathbb{R}^7$ are, respectively, the joint's position, velocity, and acceleration vectors, $M(\theta) \in \mathbb{R}^{7\times 7}$ is the symmetric and positive definite inertia matrix, $C(\theta,\dot{\theta}) \in \mathbb{R}^{7\times 7}$ is the Coriolis and centrifugal vector, $G(\theta) \in \mathbb{R}^7$ is the gravitational vector, $\tau \in \mathbb{R}^7$ is the torque vector, and $\tau_{ex} \in \mathbb{R}^7$ is the external disturbances vector.$F(\theta,\dot{\theta}) \in \mathbb{R}^7$ is the friction vector considered in this paper and can be written as:

$$F(\theta,\dot{\theta}) = \tau_{friction} = cf\ sign(\dot{\theta}) \tag{2.34}$$

where cf is the friction constant. The stability of the overall system represented by equation (2.32) is confirmed under the following properties and assumptions.

Property 2.1: The inertia matrix $M(\theta)$ is symmetric and positive definite for all $\theta \in \mathbb{R}^n$ (Craig, 2005).

Property 2.2: $\dot{M}(\theta) - 2C(\theta,\dot{\theta})$is a skew symmetric matrix,such that: $y^T\left[\dot{M}(\theta) - 2C(\theta,\dot{\theta})\right]y = 0, \forall y,\ \theta,\ \dot{\theta} \in \mathbb{R}^n$ (Kelly *et al.*, 2006), (Dawson *et al.*, 2003).

Assumption 2.1: For all $t > 0$, there exist constants $\rho_1 > 0$, $\rho_2 > 0$ and $\rho_3 > 0$ where $\|\theta_d(t)\| \leq \rho_1$, $\|\dot{\theta}_d(t)\| \leq \rho_2$ and $\|\ddot{\theta}_d(t)\| \leq \rho_3$. These constants depend on the boundedness of all desired Cartesian trajectory (see Figure 2.11).

Equation (2.32) can be expressed as:

$$\ddot{\theta} = M(\theta)^{-1}(\tau + \tau_{ex}) - M(\theta)^{-1}\left(C(\theta,\dot{\theta})\dot{\theta} + G(\theta) + F(\theta,\dot{\theta})\right) \tag{2.35}$$

The goal of the control scheme is to ensure that the measured joint positions θ of the robot track the desired trajectory θ_d, and to limit the effect of the external perturbation by introducing a force observer.

The first step in this approach is to select the errors of the system using the position and velocity of the system, i.e., the state variables. We can define the errors as follows:

$$e_1 = \theta - \theta_d \tag{2.36}$$

$$e_2 = \dot{\theta} - \gamma \tag{2.37}$$

where $\theta \in \mathbb{R}^7$ is the measured trajectory, $\theta_d \in \mathbb{R}^7$ is the desired trajectory, and γ is a virtual control input. The derivative of equation (2.36) with respect to time is given such:

$$\dot{e}_1 = \dot{\theta} - \dot{\theta}_d \tag{2.38}$$

Substituting equation (2.37) into equation (2.38), we find:

$$\dot{e}_1 = e_2 + \gamma - \dot{\theta}_d \tag{2.39}$$

The derivative of equation (2.37) with respect to time such that:

$$\dot{e}_2 = \ddot{\theta} - \dot{\gamma} \tag{2.40}$$

The virtual control can be defined as follows:

$$\gamma = \dot{\theta}_d - k_1 e_1 \tag{2.41}$$

where $k_1 \in \mathbb{R}^{7\times 7}$ is diagonal positive definite matrix. The one time derivative of the virtual input is: $\dot{\gamma} = \ddot{\theta}_d - k_1 \dot{e}_1$.
Consider the first Lyapunov function candidate as follows:

$$V_1 = \frac{1}{2} e_1^T e_1 + \frac{1}{2} e_2^T M(\theta) e_2 \tag{2.42}$$

The derivative of V_1 is written as:

$$\begin{aligned}
\dot{V}_1 &= e_1^T \dot{e}_1 + e_2^T M(\theta)\dot{e}_2 + \frac{1}{2} e_2^T \dot{M}(\theta) e_2 \\
&= e_1^T (e_2 + \gamma - \dot{\theta}_d) + e_2^T M(\theta)(\ddot{\theta} - \dot{\gamma}) + \frac{1}{2} e_2^T \dot{M}(\theta) e_2 \\
&= -e_1^T k_1 e_1 + e_1^T e_2 + e_2^T M(\theta) \left(M(\theta)^{-1} (\tau + \tau_{ex}) - M(\theta)^{-1} \left(C(\theta,\dot{\theta})\dot{\theta} + G(\theta) + F(\theta,\dot{\theta}) \right) \right) \\
&\quad -e_2^T M(\theta)\dot{\gamma} + \frac{1}{2} e_2^T \dot{M}(\theta) e_2 \\
&= -e_1^T k_1 e_1 + e_1^T e_2 + e_2^T \left(\tau + J^T F_{ex} - C(\theta,\dot{\theta})\dot{\theta} - G(\theta) - F(\theta,\dot{\theta}) - M(\theta)\dot{\gamma} \right) \\
&\quad + \frac{1}{2} e_2^T \dot{M}(\theta) e_2
\end{aligned} \tag{2.43}$$

From equation (2.37), we can obtain: $\dot{\theta} = e_2 + \gamma$

$$\begin{aligned}
\dot{V}_1 &= -e_1^T k_1 e_1 + e_1^T e_2 \\
&+ e_2^T \left(\tau + J^T F_{ex} - C(\theta,\dot{\theta}) e_2 - C(\theta,\dot{\theta})\gamma - G(\theta) - F(\theta,\dot{\theta}) - M(\theta)\dot{\gamma} + \frac{1}{2}\dot{M}(\theta) e_2 \right)
\end{aligned} \tag{2.44}$$

Using **Property 2.2**, we obtain:

$$\dot{V}_1 = -e_1^T k_1 e_1 + e_1^T e_2 + e_2^T \left(\tau + J^T F_{ex} - C(\theta,\dot{\theta})\gamma - G(\theta) - F(\theta,\dot{\theta}) - M(\theta)\dot{\gamma}\right) \tag{2.45}$$

Let the control input that maintains the stability of the robot system as follows:

$$\tau = -k_2 e_2 - e_1 - J^T F_{ex} + C(\theta,\dot{\theta})\gamma + G(\theta) + F(\theta,\dot{\theta}) + M(\theta)\dot{\gamma} \tag{2.46}$$

where $k_2 \in \mathbb{R}^{7\times 7}$ is diagonal positive definite matrix. Substituting the control input (2.46) into equation (2.45), we obtain $\dot{V}_1 \leq -e_1^T k_1 e_1 - e_2^T k_2 e_2$. However, F_{ex} is unknown; hence, the control input (2.46) is not suitable. An observer law will be integrated into the control input to estimate the external perturbation.

Theorem 2.1: Consider the robot system described by the (2.32). Where, the control law (2.47) and the adaptation law (2.48) ensure: 1) the global asymptotic stability of the system; 2) the convergence of tracking error to zero; and 3) the boundedness of the external force error.

$$\hat{\tau} = -k_2 e_2 - e_1 - J^T \hat{f}_e + C(\theta,\dot{\theta})\gamma + G(\theta) + F(\theta,\dot{\theta}) + M(\theta)\dot{\gamma} \tag{2.47}$$

The adaptation laws are updated by:

$$\dot{\hat{f}}_e = -k_3^{-T} J e_2 \tag{2.48}$$

where $k_3 \in \mathbb{R}^{6\times 6}$ is diagonal positive definite matrix.

Proof 2.1: In the beginning, let us start by defining the estimation error of disturbance as follows:

$$\tilde{f}_e = F_{ex} - \hat{f}_e \tag{2.49}$$

Consider the second Lyapunov function candidate as follows:

$$V_2 = \frac{1}{2}e_1^T e_1 + \frac{1}{2}e_2^T M(\theta)e_2 + \frac{1}{2}\tilde{f}_e^T k_3 \tilde{f}_e \tag{2.50}$$

The derivative of V_2 with respect to time yields:

$$\begin{aligned}\dot{V}_2 = &-e_1^T k_1 e_1 + e_1^T e_2 + e_2^T \left(\tau + J^T F_{ex} - C(\theta,\dot{\theta})\gamma - G(\theta) - F(\theta,\dot{\theta}) - M(\theta)\dot{\gamma}\right) \\ &+ \tilde{f}_e^T k_3 \dot{\tilde{f}}_e\end{aligned} \tag{2.51}$$

Applying the control law (2.47) to equation (2.51) yields:

$$\dot{V}_2 = -e_1^T k_1 e_1 + e_2^T \left(-k_2 e_2 + J^T \tilde{f}_e\right) + \tilde{f}_e^T k_3 \dot{\tilde{f}}_e \tag{2.52}$$

We can rewrite equation (2.52) as follows:

$$\dot{V}_2 = -e_1^T k_1 e_1 - e_2^T k_2 e_2 + \left(\dot{\tilde{f}}_e^T k_3 + e_2^T J^T\right)\tilde{f}_e \tag{2.53}$$

Substituting equation (2.48) in equation (2.53), we obtain:

$$\dot{V}_2 \leq -e_1^T k_1 e_1 - e_2^T k_2 e_2 + \left(-k_3^{-1} k_3 J e_2 + e_2^T J^T\right)\tilde{f}_e \tag{2.54}$$

We obtain:

$$\dot{V}_2 \leq -e_1^T k_1 e_1 - e_2^T k_2 e_2 \tag{2.55}$$

with k_1 and k_2 being positive gains. Let us take the second derivative of $\dot{V}_2$ as follows:

$$\ddot{V}_2 \leq -2e_1^T k_1 \dot{e}_1 - 2e_2^T k_2 \dot{e}_2 \tag{2.56}$$

Since $\dot{\theta}$ and $\ddot{\theta}$ are bounded, this means e_1, $\dot{e}_1$, e_2 and $\dot{e}_2$ are bounded. This proves that $\ddot{V}_2$ is bounded since e_1, $\dot{e}_1$, e_2 and $\dot{e}_2$ are all bounded. So, $\dot{V}$ is continuous and negative semi-definite; according to Barbalat's lemma. We have $e_1 \to 0$, $\dot{e}_1 \to 0$, $e_2 \to 0$ and $\dot{e}_2 \to 0$ as $t \to \infty$, which mean that the system is asymptotic stable. The closed-loop system of the designed control technique is illustrated in Figure 2.7.

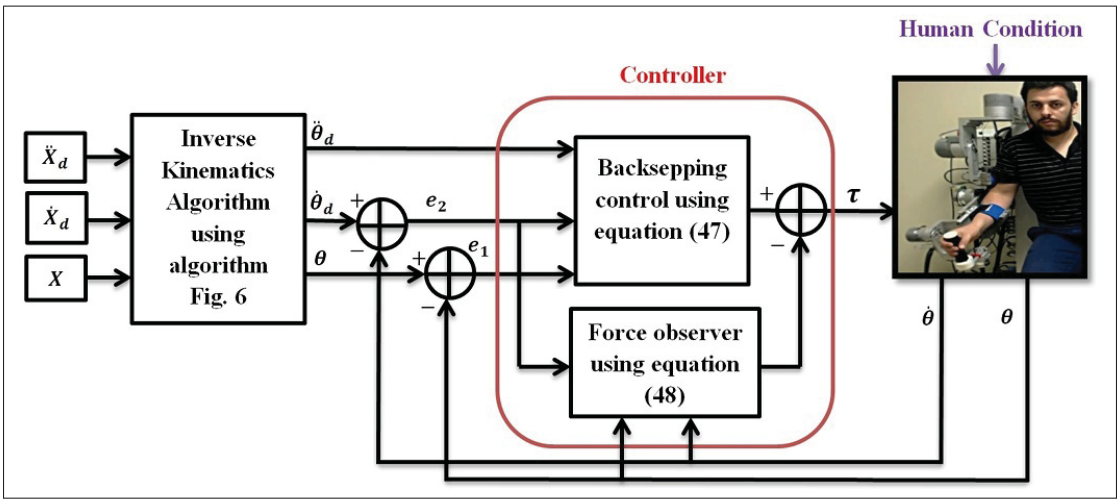

Figure 2.7 General schematic of the proposed control

2.4 Experiments and results

The architecture of the rehabilitation exoskeleton system is presented in Figure 2.8. The LabView (National Instruments) PXI system is the environment where the proposed controller of the system robot was realized. Three blocks are designed to complete the experimental setup. The first one is the user interface, used to select, determine the controller parameters, and define the specification of the rehabilitation exercise. In addition, it provides the measured data of the robot that permits the operator to evaluate accurately the performance of the human exoskeleton system. The second one is a PXI-8108 card, where the control scheme was implemented with a sampling time (1.25 μs). The robot operating system also runs in the PXI processor (Intel Core 2 Duo). The controller output is the torque to the joints; this torque was transformed to current and then to desired voltages to command the motor drivers.

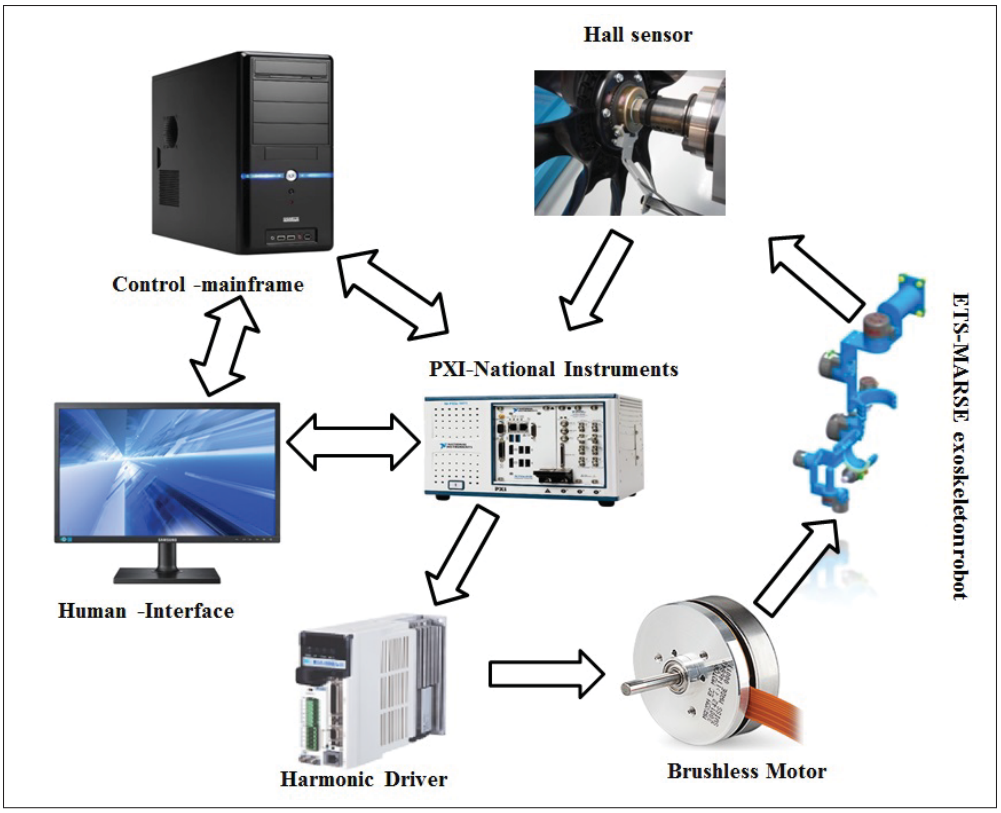

Figure 2.8 Control set-up

Finally, the last block, a field programmable gate array runs with a sampling time (50 μs). It is slated to execute two loops concurrently. The first loop holds a simple proportional-integral action for controlling the motor's current, as a function of the calculated reference current. The second loop is designed to obtain the measured data (position angles). For more details see (Rahman *et al.*, 2015), and (Ochoa Luna *et al.*, 2015).

The inverse kinematics algorithm is added to the LabView code, which controls the robot. The inverse kinematics code is inserted into a MATLAB script module of LabView, which simplifies the process since few changes have to be made to the code to fit the new environment. This module allows MATLAB code to be written directly into LabView, with some restrictions.

In this paper, we implemented a passive rehabilitation protocol with two healthy subjects (age: 27–30 years; height: 170–177 cm; and weight: 75–79 kg). Passive rehabilitation therapy com-

prises a set of exercises given by a physiotherapist or clinician to increase muscle power and joint range of movement to the physically disabled individual with impaired upper limb motion. In passive rehabilitation therapy, the subject sits relaxed, and the physiotherapist moves the subject's arm slowly, usually starting with a small range of movement, and then continuously increasing the joint range. It should be mentioned that in all our experiments, the ETS-MARSE initiated its motion with the elbow joint at 90° as can be seen in Figure 2.9. Note that the control gains used for the tests were found experimentally, and are as follows:

$$\begin{cases} k_1 = \begin{bmatrix} 18, & 16, & 18, & 18, & 18, & 18, & 18 \end{bmatrix} \\ k_2 = \begin{bmatrix} 80, & 80, & 64, & 62, & 80, & 80, & 80 \end{bmatrix} \\ k_3 = \begin{bmatrix} 0.5, & 0.5, & 0.5, & 0.5, & 0.5, & 0.5 \end{bmatrix} \end{cases}$$

In order to validate the human inverse kinematics, the healthy subjects repeated the designed tasks with the standard solution of a redundant robot called pseudo-inverse Jacobian matrix (Rahman *et al.*, 2015), (Rahman *et al.*, 2012a). It is important to notice that for the implementation of a pseudo-inverse Jacobian matrix, we used a point to point technique (Spong *et al.*, 2006a) to avoid the singularity problem. In this case, we compared the performance of the proposed controller and the human inverse kinematic algorithm (PB-HIK) and the proposed controller with the pseudo-inverse Jacobian (B-PIK). The comparison is done by using the average RMS values of the position errors and rotation errors of the end-effector and the execution time of each approach.

In the first trial, the trajectory tracking performance of the PB-HIK in Cartesian space was evaluated. The first exercise starts at the initial position with the elbow joint angle at 90°. Then, the end-effector follows a path to reach target A; next, it follows path A to B to reach target B, after which it returns to the initial position. The desired rotation of the end-effector here is used. That means the redundancy of the ETS-MARS is employed to perform the rehabilitation activity. The speed of the movement used here is $30\,deg/s$. Therefore, the objective of this task was first to assess the performance of the inverse kinematics algorithm in reaching different

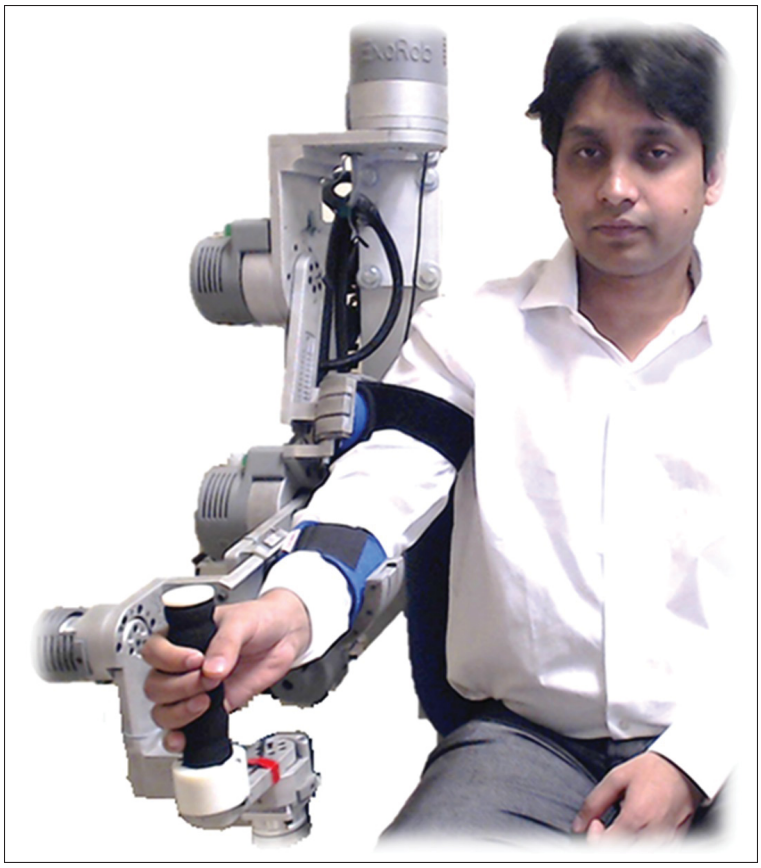

Figure 2.9 Overview of the ETS-MARSE with a human subject

targets at different locations, such as transferring objects on the surface of a table. Second, it validates the performance of the proposed control in a Cartesian trajectory.

The experimental results for the passive 3D Cartesian trajectory achieved with subject A (age: 28 years; height: 173 cm; and weight: 78.5 kg) are shown in Figure 2.10. From the plot of Figure 2.10(a), we can see that the desired Cartesian trajectory overlaps with the measured Cartesian trajectory. The plot of Figure 2.10(b) compares the desired Cartesian trajectory with the measured Cartesian one. It is clear from Figure 2.10(B) that the designed control presents an excellent trajectory tracking despite the presence of small end-effector errors. Figure 2.11(a) presents the tracking performance of ETS-MARSE in joint space (the outputs of the inverse kinematics algorithm) and it is obvious from the figure that the desired angles are smooth.

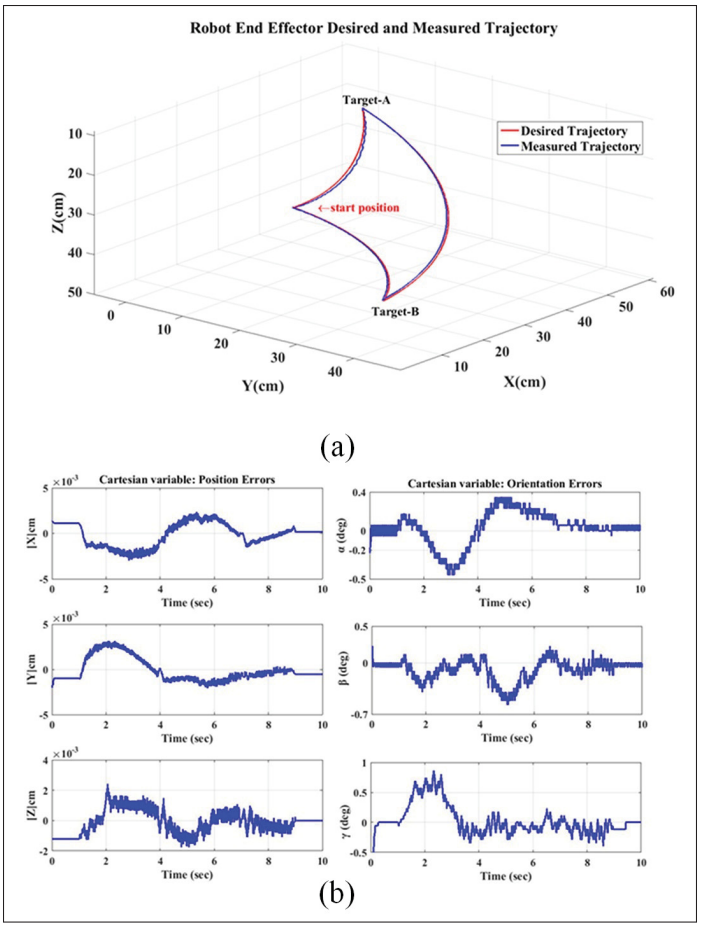

Figure 2.10 Tracking (a) performance of ETS-MARSE in 3-D Cartesian space using proposed inverse kinematics and (b) error in Cartesian co-ordinates (X-Y-Z axes)

We can say that the inverse kinematics algorithm converts trajectories from task space to joint space effectively and precisely. That conversion helps the controller to provide good results as we see in Figure 2.11(b). Figure 2.12 presents the convergence of the user's force parameters during the therapeutic task that proves the potentiality of the designed controller.

Figure 2.13 shows the experimental results for the same [Figure 2.10(a)] passive 3-D Cartesian trajectory performed with the same subject-A (age: 28 years; height: 173 cm; and weight:78.5 kg) using the B-PIK. The performed trajectory is very good due to the efficiency of the proposed controller, the trajectory obtained by the proposed inverse kinematics [Figure 2.10(a)]

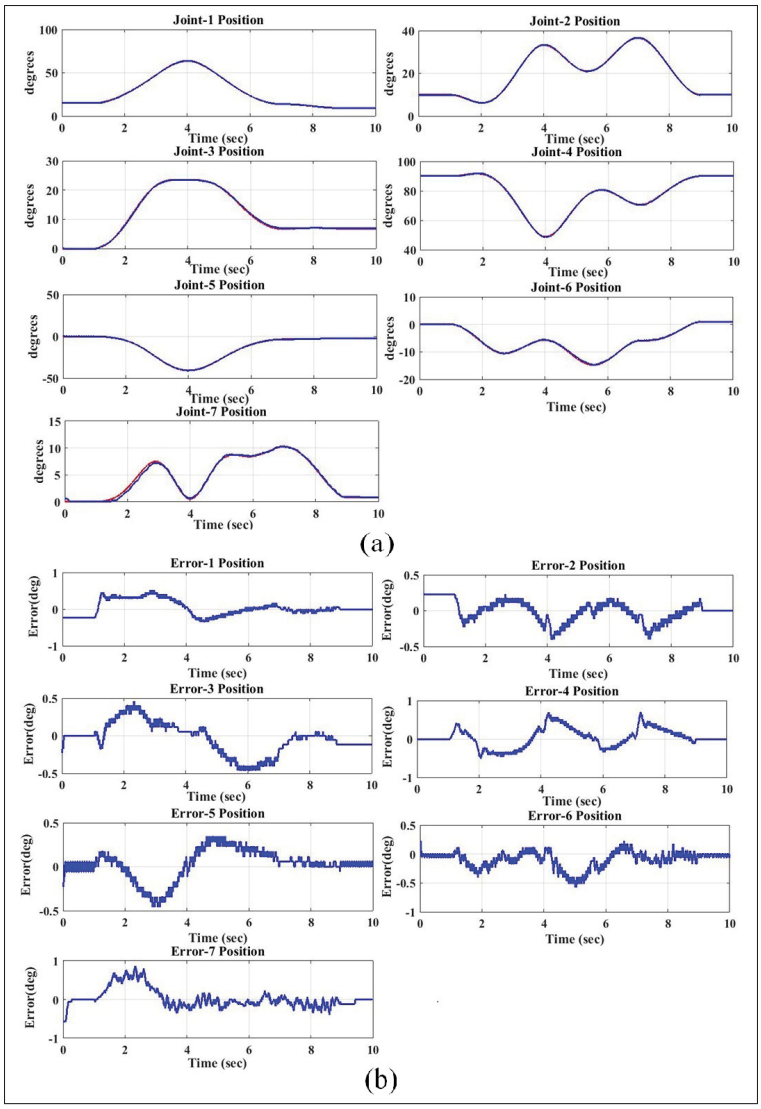

Figure 2.11 Tracking performance of ETS-MARSE in joint space (the inputs of the control joint-based) corresponding to Figure 2.10(a). (b) Tracking error in jointsspace

is more similar and more flexible to the natural movement than the trajectory obtained by pseudo-inverse kinematics (Figure 2.13). This latter is straight while the natural movement is characterized by the flexibility of the motion. We can conclude that the proposed inverse kinematics provides a good result similar to human movement.

The workspace envelope of the ETS-MARSE with the performed trajectory [illustrated in Figure 2.10(a)] is shown in Figure 2.14. It is manifest from Figure 2.14 that the proposed inverse kinematics provides a good solution with respect to the workspace limits of the ETS-MARSE exoskeleton. The variation of the elbow position is also presented to demonstrate that the variation of the swivel angle provides a good solution. This solution has always belonged to the workspace of the robot. The plot illustrating the variation of the swivel angel is presented in Figure 2.15. As mentioned above, due to the mechanical design of the ETS-MARSE, the elbow cannot rotate along the aforementioned shoulder-wrist circle. For that, we observe a small variation of the swivel angle, not more than 10°.

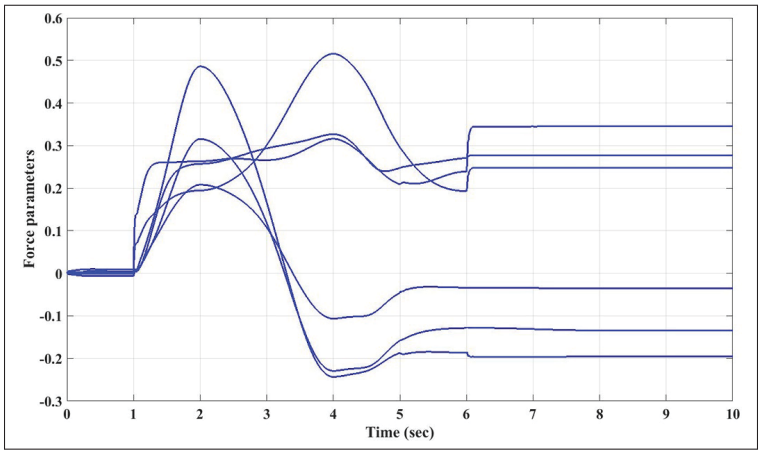

Figure 2.12 Force parameters convergence of the robot

Let us now confirm the proposed solution by comparing the human inverse kinematics and the pseudo-inverse Jacobian matrix. Table (2.3) summarizes the average RMS errors of the end-effector and time execution of each approach along the 3-D desired trajectory. Where δ°, β° and γ° are the desired rotation of the end-effector of the robot.

The comparison between the proposed controller with the human inverse algorithm (PB-HIK) and the B-PIK is illustrated in Figure 2.16. It is clear from Fig. 16 that the proposed algorithm gives excellent results for the two subjects notably at the level of the rotation of the end-effector. The execution time of the proposed approach is reduced by more than 50%.

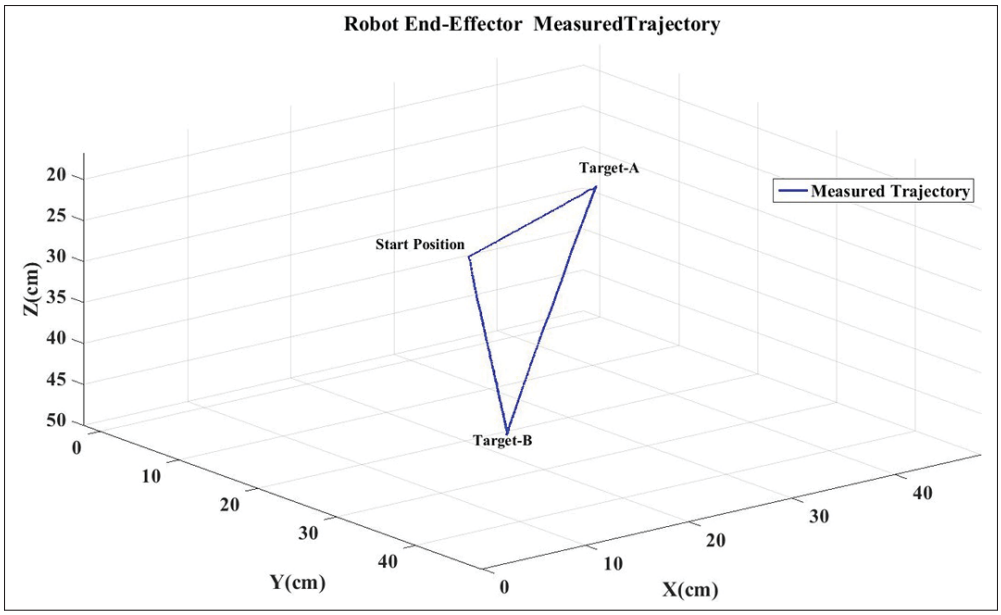

Figure 2.13 Tracking performance of ETS-MARSE in 3-D Cartesian space using proposed inverse kinematics using the B-PIK

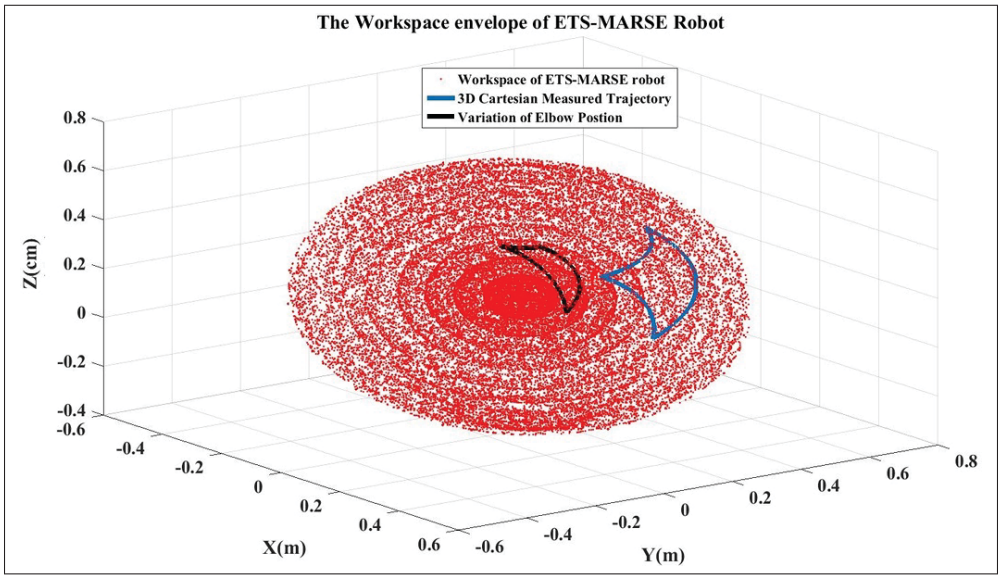

Figure 2.14 Workspace of the ETS-MARSE with performed trajectory corresponding to Fig. 11(a)

We can infer that the proposed inverse kinematics solution gives an excellent solution compared with the conventional approach. The implementation of this approach with healthy subjects confirms that the proposed algorithm provides a solution similar to the human upper limb

Table 2.3 Statistical analysis of controllers performance in cartesian space

RMS errors	PB with Human-IK		B with Pseudo-IK	
	Subject-A	Subject-B	Subject-A	Subject-B
$e_x\ (cm)$	0.0019	0.0022	0.0032	0.015
$e_y\ (cm)$	0.0028	$6.2433\ 10^{-4}$	0.0141	0.0105
$e_z\ (cm)$	0.0014	0.0016	0.0090	0.0257
$\alpha\ (deg)$	0.0080	0.0111	0.0110	0.0370
$\beta\ (deg)$	0.0130	0.0206	0.0480	0.1310
$\gamma\ (deg)$	0.0207	0.0050	0.2960	0.2945
execution time	0.0106789		0.0258761	

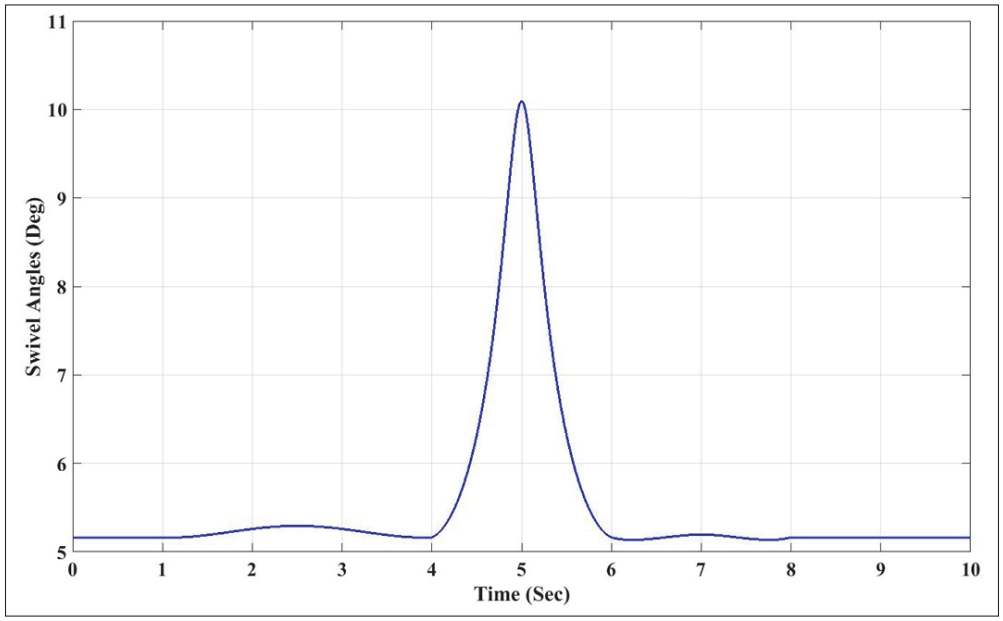

Figure 2.15 Variation of swivel angles of the performed trajectory illustrated in Fig. 11(a)

movement in 3-D space, and that is valid for the human arm configuration in all situations. Additionally, the proposed controller (PB-HIK) provides a good tracking performance even if the dynamic model is affected by different human conditions.

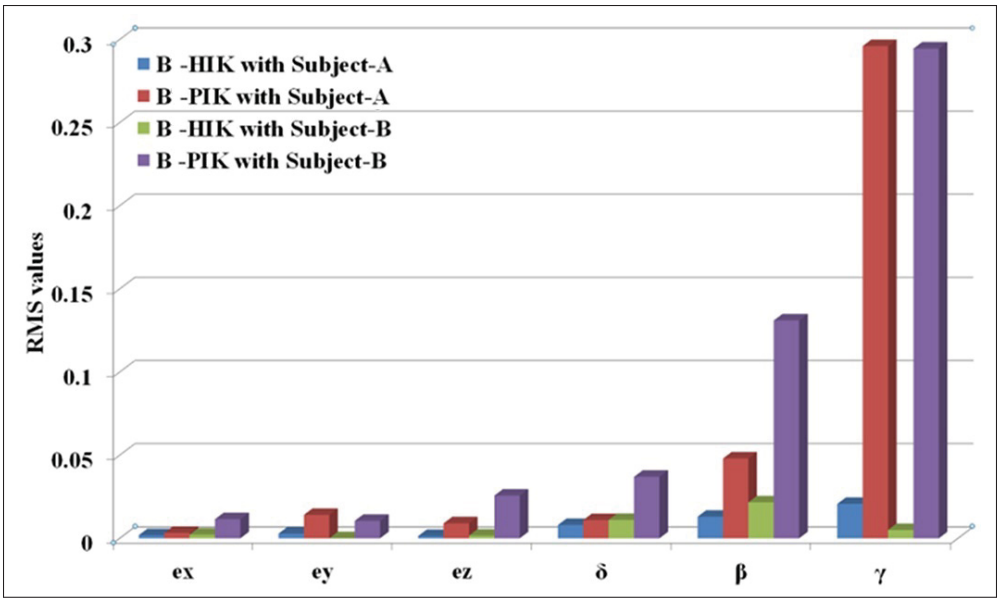

Figure 2.16 Comparison of controllers' performance based on RMS error for first 3-D Cartesian trajectory

2.5 Conclusion

In this paper, a new inverse kinematics solution was described to manage the redundancy of a 7-DOF exoskeleton robot and provide a passive rehabilitation trajectory imitating the human motion. The proposed algorithm of the inverse kinematics solution is inspired directly from the human arm movement. Therefore, this approach can be extrapolated for all upper limb rehabilitation robots. In addition, the proposed algorithm can be used to limit the multi-solution of the redundancy of this kind of robot. A robust control design, with the adaptation of external force based on backstepping control, is developed by integrating a force observer to estimate the user's force. The control achieved stability and robustness of the ETS-MARSE exoskeleton robot system with passive Cartesian trajectories. A comparison between the solution obtained by the proposed algorithm and the solution provided by a pseudo-inverse Jacobian matrix is presented to validate the advantages of the proposed human inverse kinematics algorithm. The experimental results have validated the effectiveness and practicability of the proposed algorithm. In future work, we will seek to replace the geometric solution with a visual solution using a visual system such Kinect and/or camera devices.

CHAPTER 3

COMPLIANT CONTROL FOR WEARABLE EXOSKELETON ROBOT BASED ON HUMAN INVERSE KINEMATICS

Brahim Brahmi[1], Maarouf Saad[1], Abdelkrim Brahmi[1], Cristobal Ochoa Luna [1]
and Mohammad H. Rahman[2]

[1] Département of Electrical Engineering, École de Technologie Supérieure,
1100 Notre-Dame Ouest, Montréal, Québec, Canada H3C 1K3
[2] Mechanical/Biomedical Engineering Department,University of Wisconsin-Milwaukee,
3200 N. Cramer Street, Milwaukee, WI 53211,

Paper published in *International Journal of Advanced Robotic Systems*, October, 2018

Abstract

Rehabilitation robots are a new technology dedicated to the physiotherapy and assistance motion and has aroused great interest in the scientific community. These kinds of robots have shown a high potential in limiting the patient's disability, increasing its functional movements and helping him/her in daily living activities. This technology is still an emerging area and suffers from many challenges like compliance control and human–robot collaboration. The main challenge addressed in this research is to ensure that the exoskeleton robot provides an appropriate compliance control that allows it to interact perfectly with humans. This article investigates a new compliant control based on a second-order sliding mode with adaptive-gain incorporating time delay estimation. The control uses human inverse kinematics to complete active rehabilitation protocols for an exoskeleton robot with unknown dynamics and unforeseen disturbances. The stability analysis is formulated and demonstrated based on Lyapunov function. An experimental physiotherapy session with three healthy subjects was set up to test the effectiveness of the proposed control, using virtual reality environment.

Keywords: Rehabilitation robots, human inverse kinematics, time delay estimation, second-order sliding mode control, passive and active assistive motion, virtual reality.

3.1 Introduction

Many types of injury such structural defects, cerebral palsy, brain tumors, spinal injury, multiple sclerosis or other neurological diseases can damage the human nervous system, which means loss of the functional capacity (Sidney *et al.*, 2013; Lundström *et al.*, 2008; Nichols-Larsen *et al.*, 2005). In paralyzed patients, maximum capacity can be restored through physical therapy applications and robotic devices (Sidney *et al.*, 2013; Lundström *et al.*, 2008; Nichols-Larsen *et al.*, 2005; Keller *et al.*, 2015; Xie *et al.*, 2016). The purpose of the physical therapy and the neural rehabilitation program is to help the patient achieve the best possible condition and to gain independence of his functions in order to minimize or to eventually eliminate the problems that might arise from the disease. The employment of robotic devices, known as rehabilitation robots, in assistive domains has demonstrated a high potential to improve the functional movements, and to assist her/him in daily living activities such as self-care skills (Keller *et al.*, 2015). A rehabilitation exoskeleton robot is an articulated mechanical structure with several degrees of freedom (DOFs) having the same anatomy of the human arm (Keller *et al.*, 2015; Xie *et al.*, 2016; Balasubramanian *et al.*, 2008; Gopura *et al.*, 2009; Rahman *et al.*, 2015). Unlike prostheses that replace a limb of the body, the exoskeleton robot clings to it externally and acts in parallel. It can be dedicated to a specific part of the body such as the hand, arm, leg or several limbs at the same time. Equipped with sensors and actuators, it measures the movements and forces of the user and it produces a force to interact dynamically with its wearer.

There are different levels of robotic assistance strategies used after the neurological accidents to provide suitable physical therapy. The most urgent, usually the first six weeks after the accident, is passive physical therapy (Sidney *et al.*, 2013; Xie *et al.*, 2016). In this type of therapy, the exoskeleton brings the patient's limb, which is completely passive, to realize a therapy task. Its advantage is based on the robot's ability to provide intensive therapy over a long period of time (Brahim *et al.*, 2016b,a). The next types of therapy, active-assisted and active modes, allow the patient to voluntarily initiate movement. Then, the exoskeleton's wearer can perform a free motion (active mode), the robot corrects or guides this movement (active-assisted mode).

In the latter case, the robot limits the tremors or corrects the trajectory. After detecting the initiation of a motion, usually predetermined, the robot will guide the achievement of the activity, often using an impedance and/or admittance control (Li *et al.*, 2017a; Ochoa Luna *et al.*, 2015). Additionally, these strategies can be utilized for the evaluation or the study of subject movements. In these modes, theoretically, the patient should not feel the presence of the exoskeleton robot. This is known as robot transparency. Therefore, the subject is completely active and the exoskeleton robot should not affect the movement.

In this research, we focus on active motion control. This type of control is particularly suited to rehabilitation phases where the patient has partially recovered his mobility abilities. The goal is then to improve these abilities by encouraging him to use them. Usually, we focus to interpret the intention of the subject and the abilities that already recovered. A compliant control or indirect force control is an effective approach to accomplish this level of motion assistance. Its successful application appears when the exoskeleton is in free space, and when it is in contact with the known or unknown environment. Admittance control is a typical choice for the rehabilitation application of compliance control (Ochoa Luna *et al.*, 2015; Culmer *et al.*, 2010; Ozkul and Barkana, 2013; Choi *et al.*, 2009; Zanchettin *et al.*, 2016). This control structure aims to create a dynamic relationship between a measured position (and its derivative) and the user's force. The admittance scheme is implemented by two loops. The first one is the outer force that is responsible for creating the force-position relationship; it usually uses a first order transfer function to define this relation. The second one is the inner position loop which must be as fast as possible (Calanca *et al.*, 2016). Although this control is characterized by its robustness thanks to the existing advanced tracking control (inner position loop), it also suffers from several drawbacks, such as imprecision of the desired performance of the control system or inaccuracy of conversion of the desired force to desired position dynamics (Calanca *et al.*, 2016). The inaccuracy of the performance here is caused by the gain parameters of the first order transfer function which is responsible for establishing a desired force-position relationship as given in (Calanca *et al.*, 2016; Adams and Hannaford, 1999). Many admittance controls have been developed by estimating the user force directly from his biological signals

(Khan *et al.*, 2016b; Jamwal *et al.*, 2016; Li *et al.*, 2017b). The most commonly used is electromyography (EMG) signals, which are considered important signals to describe the user's intention of motion (Khan *et al.*, 2016b; Jamwal *et al.*, 2016; Li *et al.*, 2017b). However, the sensor positioning to obtain the EMG signals is very sensitive, where the thickness of the skin, tiredness and stress of the subject, even the temperature of the body has a big influence on the performance of an EMG-based control (Huang *et al.*, 2015). More than that, the quantity of information from physiological signals and its non-linearity is so large that it takes expensive calculations to process signals, which must be clear input signals for the control (Huang *et al.*, 2015).

The inner position loop may be responsible for the inaccurate performance of the admittance control due to the limitation of the applied control tracking approach (Calanca *et al.*, 2016). This limitation is related to the complicated design of this type of robots and their high number of DOF, where the dynamics of these robots is generally uncertain (Brahim *et al.*, 2016b,a). Furthermore, the contact dynamics of the robot and its wearer increases the unknown nonlinear-uncertainties function. A sliding mode approach is one of the strategies that are widely applied on robotics systems thanks to its attractive characteristics of robustness to nonlinear-uncertainties and external disturbances (Slotine *et al.*, 1991; Utkin *et al.*, 2009). The price to achieve this robustness is to control the undesirable chattering problem (Fridman, 1999). Many conventional approaches were developed to avoid this problem by replacing the discontinuous function by a continuous function (as a saturation function or sigmoid function) to ensure a continuous control (Slotine *et al.*, 1991; Rahman *et al.*, 2013). But in this case, the sliding mode control loses its robustness to disturbances; here the controller forces the sliding trajectories of the system to be close to the sliding surface, not on the sliding surface itself. New approaches have been developed to address the chattering dilemma such high order sliding mode controller (Levant, 2003; Ling *et al.*, 2012) and a second-order sliding mode controller (Bartolini *et al.*, 2001). This latter allows a sliding surface and its derivative to get to zero and to maintain the discontinuous control under an integral function, which can attenuate the undesirable chattering (Bartolini *et al.*, 1998). This approach presents two advantages: the

first one is to keep the robustness characteristic of standard sliding mode control, and the second one is to improve the accuracy of the control performance by attenuating the chattering problem. Nevertheless, the second time-derivative of the sliding surface might amplify the instability of the system, a risk that the nonlinear uncertainties and external disturbances present. Additionally, in physical therapy, usually the exoskeleton robot would perform with different subjects with different levels of neurological injuries. In this case, the control system would be influenced by the variation of parameters of the robot and change of subjects' characteristics.

3.1.1 Main contribution

Motivated by the previous analysis, we propose new adaptive-gains second-order sliding mode control combined with time delay estimation (TDE) (Youcef-Toumi and Ito, 1990; Jin *et al.*, 2015; Brahmi *et al.*, 2017a,b). This controller deals mainly with the accuracy/robustness problem of a compliant control applied to an exoskeleton robot with a high number (seven) of DOFs. The accuracy of the performance can be decreased within the outer loop (the force loop) due to the admittance function and/or sensibility of biological sensors signals, e.g. EMG. To overcome these drawbacks, the paper proposes a simple force loop based on human inverse kinematics (Brahmi *et al.*, 2017c). Therefore, according to the force applied at the wrist joint by the subject, the force control loop produces a Cartesian displacement with respect to a constant proportional gain. In our case, the required position is the sum of this displacement and the actual Cartesian position. Unlike the existing methods, we use the human inverse kinematics algorithm developed in our previous work (Brahmi *et al.*, 2017c), which is characterized by its accuracy and rapidity of response while avoiding singularities. This makes it possible to provide an accurate relation between desired force and desired position. On the other hand, the robustness of the performance can be negatively influenced within the inner loop (or tracking control loop) thanks to the applied control strategy. Despite the accuracy and robustness of second-order sliding mode control due to its potential to attenuate the undesired chattering dilemma (Bartolini *et al.*, 1998). However, the complicated mechanical structure of the robot and the variation of its parameters (due to the uncertainties function and unforeseen external

forces due to the different subject's characteristics) require a large switching gain to maintain the stability of the robot system, which again causes the chattering problem. To overcome these limitations, we incorporate the second-order sliding mode control with TDE to achieve an accurate performance of the exoskeleton robot with unknown dynamics and external disturbances. TDE can easily estimate the unknown dynamics and external disturbances with a simple control scheme without being affected by the size of the estimated parameters (high degree of freedom) (Brahim *et al.*, 2016a). It only employs one step time-delayed knowledge about the previous state-response of the system and the previous control input to provide an accurate estimation of unknown dynamics and external perturbations. More than that, TDE is an easy approach in the real-time implementation. In addition, to cope with the variation of the characteristics of the subjects and to avoid the problem of undesirable chattering, a new adaptation law of the commutation gains is proposed. The stability of the robot system and the convergence of its errors are formulated and demonstrated based on Lyapunov function. The contribution of this paper can be summarized in three points:

- A new compliant control is developed based on human inverse kinematics. This control ensures an accurate relation between the desired force and the desired position and produces human-like arm motion. (Outer control loop);
- TDE is used for the evaluation of the unknown dynamics and external disturbances (Inner control loop);
- Adaptive gains are incorporated with a second-order sliding mode control to provide an adaptation of the switching gains and to avoid the undesired chattering (Inner control loop).

The proposed control is evaluated experimentally with healthy subjects using a virtual environment (VE) (Ferrer *et al.*, 2013). This VE is a very attractive tool bringing many benefits (Weiss *et al.*, 2014). It allows the creation of immersive and interactive scenes where the oriented task can be introduced in the form of serious games. This interface also helps in stimulating the subjects by viewing the tasks performed. Finally, we present a comparative study with a conventional control approach that shows the accuracy, robustness and flexibility of the proposed controller dealing with unknown dynamics, external disturbances and parameters variations.

The remainder of the paper is organized as follows. The human inverse kinematics and dynamics of the exoskeleton are presented in the next section. The control scheme is described in section 3.3. Experimental and comparison results are shown in section 3.4; finally, the conclusion is presented in section 3.5.

3.2 Characterization kinematics and dynamics of ETS-MARSE robot

3.2.1 Modeling of ETS-MARSE robot

To make the rehabilitation robot suitable for performing of a wide variety of daily-life activities with the ease of human–robot interaction, it must be designed to be in harmony with the human arm configuration. The ETSMARSE is a redundant robot with 7-DOFs, as shown in Figure 3.1. It is designed to assist the impaired human rightupper limb. The structure idea of the ETS-MARSE was extracted from the anatomy of the human arm to be in concordance with exoskeleton wearers along the physical therapy activities. The shoulder portion is described by three joints: The first two joints are created to produce the vertical and horizontal extension/flexion movement of the shoulder, while the third joint is aimed to conduct the internal and external rotation of the shoulder. The elbow portion is composed of one joint to complete the flexion/extension motion of the elbow. The wrist portion is composed of three joints: The first joint is shaped to perform pronation and supination motion of the forearm, the second joint and the third joint are dedicated to offering, respectively, ulnar/ radial deviation and flexion/extension motions (Rahman *et al.*, 2015, 2013). The robot system is implemented with a virtual interface in which the subject and the therapist can follow the motion of the rehabilitation tasks (Ferrer *et al.*, 2013). Virtual reality is a software environment created to simulate the subject and allow him to perform different physical therapy exercises. This virtual interface can also provide task-oriented activities in task space, Cartesian space, and free motion.

Table (3.1) presents the modified Denavit–Hartenberg (DH) of the exoskeleton robot. Figure 3.1 shows the reference frame attached to the robot which permits to acquire the mentioned

(DH) parameters (Craig, 2005). The workspace of the designed exoskeleton robot is summarized in Table (3.2).

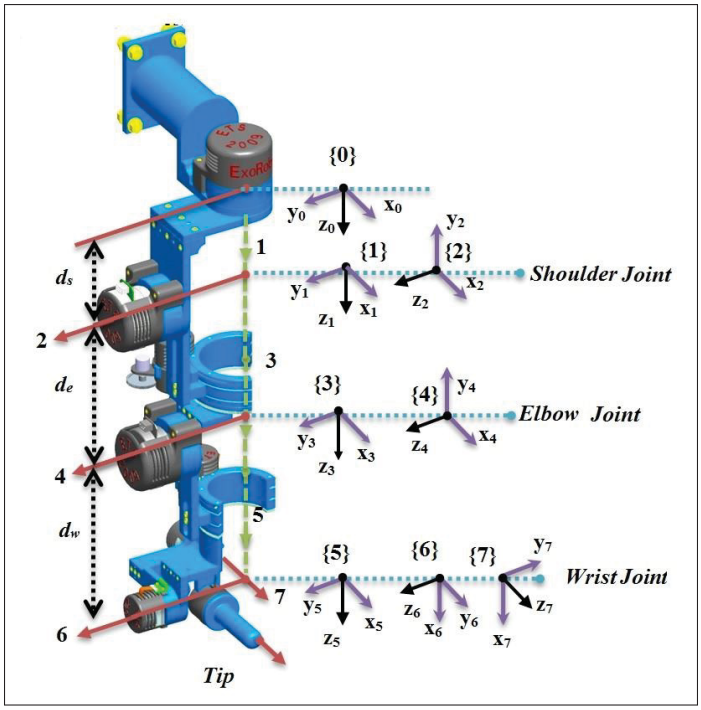

Figure 3.1 Reference frames of ETS-MARSE

3.2.2 Human inverse kinematics solution

In most applications of assistive robots, the required trajectory is given in Cartesian space. The standard transformation from Cartesian space to joint space is done by a non-linear function named Jacobian matrix. Due to the geometry of the robot, the inverse of a Jacobian matrix is not always available. In our case, the exoskeleton robot is redundant with 7 DOFs. The Jacobian pseudo-inverse solution widely used in robotics to solve this invertibility problem can be written as:

$$\dot{\theta}_d = \left(J^T (JJ^T)^{-1}\right) \dot{x}_d \tag{3.1}$$

where $\dot{x}_d \in \mathbb{R}^{6\times1}$ is the desired Cartesian velocity, $\dot{\theta}_d \in \mathbb{R}^{7\times1}$ is the calculated joint velocity and $J \in \mathbb{R}^{6\times7}$ is the Jacobian matrix of the robot. In addition to the singularity problem, the pseudo-inverse kinematic solution provides a non-unique solution. In general, it implies that it is hard to guarantee a human-like motion. In our previous work (Brahmi *et al.*, 2017c), a new solution of inverse kinematics was developed based on the analysis of human arm motion. This algorithm provides a human-like arm motion without any singularity configuration and it is characterized by its accuracy and rapidity of response. The main purpose of the human inverse kinematics is to limit solutions of the inverse kinematics to an optimal solution capable to mimic the human movement which corresponds to the human arm structure. It is remarkable that the human employs a minimum of arm joints for its optimal shape during him performs a motion in 3D space. It is remarkable also that the first three (shoulder) joints are in charge of the elbow position.

Table 3.1 Modified DH parameters

joint (i)	α_{i-1}	a_{i-1}	d_i	θ_i
1	0	0	d_s	θ_1
2	$\frac{-\pi}{2}$	0	0	θ_2
3	$\frac{\pi}{2}$	0	d_e	θ_3
4	$\frac{-\pi}{2}$	0	0	θ_4
5	$\frac{\pi}{2}$	0	d_w	θ_5
6	$\frac{-\pi}{2}$	0	0	$\theta_6 - \frac{\pi}{2}$
7	$\frac{-\pi}{2}$	0	0	θ_7

Table 3.2 Workspace ETS-MARSE

joint (i)	Motion	Workspace
1	Shoulder joint horizontal flexion/extension	$0^\circ/140^\circ$
2	Shoulder joint vertical flexion/extension	$140^\circ/0^\circ$
3	Shoulder joint internal/external rotation	$-85^\circ/75^\circ$
4	Elbow joint flexion/extension	$120^\circ/0^\circ$
5	Forearm joint pronation/supination	$-85^\circ/85^\circ$
6	Wrist joint ulnar/radial deviation	$-30^\circ/20^\circ$
7	Wrist joint flexion/extension	$-50^\circ/60^\circ$

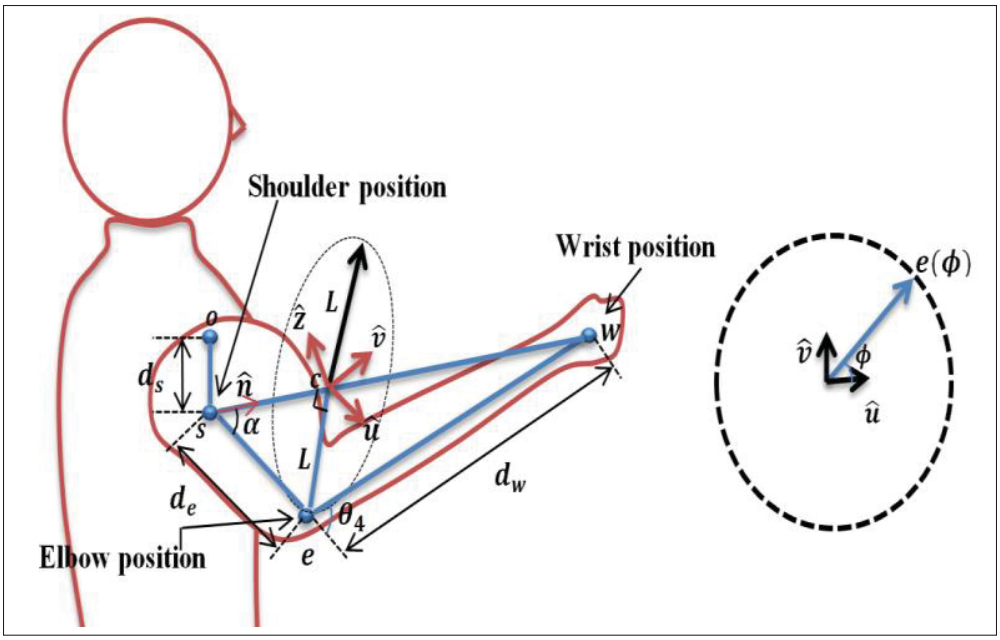

Figure 3.2 Representation of human motion in 3D space and swivel angle(ϕ)

The end-effector position is determined from the elbow pose and its joint angle amplitude, while the end-effector rotation is achieved by the last (wrist) joints. From known end-effector pose, the elbow joint (θ_4) can be calculated geometrically and separately, as we see in Figure 3.2. Based on geometric relationships, we can determine the elbow position easily. This latter is defined by obtaining the distance (L) and the angle (α) which is situated between the link d_e and the virtual axis that connects between the end-effector position and the shoulder position. While the elbow position is achieved, a unique analytic solution of three joints of the shoulder (θ_1, θ_2 and θ_3) can easily be obtained. Therefore, the inverse kinematic dilemma presently involves getting the arrangement of a non-redundant structure with uniqueness solution of θ_1, θ_2 θ_3, and θ_4 joints. Meanwhile, the solution of θ_5, θ_6 and θ_7 can be acquired by the identification based on the known end-effector rotation (reference trajectory) and the calculated joints (Brahmi *et al.*, 2017b).

In particular situations, when the position of the wrist is positioned with specific restrictions, the redundancy of the manipulator can be parameterized by remarking that the elbow is yet

free to swivel about an axis from the swivel angle (ϕ) to the shoulder. The axes of this circle are vertical to the vector guiding from the wrist joint to the shoulder. The swivel angle (ϕ) is the rotation angle of the elbow around a virtual axis that links wrist joint and the shoulder. The elbow pose draws the arc of a circle on a plane whose usual is parallel to the shoulder-to-wrist axis during the swivel angle changes. It is important to clarify that the swivel angle is not a joint, it is not straight controllable, however a measurable parameter outcome of the kinematics of the exoskeleton, based on the restrictions on the wrist rotation. Another significant point that in primary physical therapy task, the swivel angle is equal to zero, without any impact on the inverse kinematics solution dilemma. A physical therapy motion does not include any restrictions on the wrist posture and this fixation does not affect the redundancy of ETS-MARSE robot. The details can be found in (Brahmi *et al.*, 2017c).

3.2.2.1 Dynamics of ETS-MARSE robot

The dynamic model of ETS-MARSE robot in joint space ($\theta \in \mathbb{R}^{7\times 1}$) can be described as (Craig, 2005):

$$M(\theta)\ddot{\theta} + C(\theta,\dot{\theta}) + G(\theta) + F(\theta,\dot{\theta}) = \tau + \tau_{ex} \tag{3.2}$$

where θ, $\dot{\theta}$ and $\ddot{\theta} \in \mathbb{R}^7$ are, respectively, the joint's position, velocity, and acceleration vectors, $M(\theta) \in \mathbb{R}^{7\times 7}$ is the symmetric and positive definite inertia matrix, $C(\theta,\dot{\theta}) \in \mathbb{R}^{7\times 7}$ is the Coriolis and centrifugal vector, $G(\theta) \in \mathbb{R}^7$ is the gravitational vector, $\tau \in \mathbb{R}^7$ is the applied joint torque to the exoskeleton robot, and $\tau_{ex} \in \mathbb{R}^7$ is the external disturbances vector. Without loss of generality, the matrices of dynamic model (3.2) can be written as follows:

$$\begin{cases} M(\theta) = M_0(\theta) + \Delta M(\theta) \\ C(\theta,\dot{\theta}) = C_0(\theta,\dot{\theta}) + \Delta C(\theta,\dot{\theta}) \\ G(\theta) = G_0(\theta) + \Delta G(\theta) \end{cases} \tag{3.3}$$

where $M_0(\theta)$, $C_0\left(\theta,\dot{\theta}\right)$ and $G_0(\theta)$ are respectively the known inertia matrix, the Coriolis centrifugal matrix, and the gravity vector. $\Delta M(\theta)$, $\Delta C(\theta)$ and $\Delta G(\theta)$ are the uncertain parts. Let us introduce a new variable such that: $\eta_1 = \theta$ and $\eta_2 = \dot{\theta}$; hence, the dynamic model expressed in (3.2) can be rewritten as follows:

$$\begin{cases} \dot{\eta}_1 = \eta_2 \\ \dot{\eta}_2 = U(t) + f(t) + H(t) \end{cases} \tag{3.4}$$

with:

- $U(t) = M_0^{-1}(\theta)\,\tau$
- $f(t) = M_0^{-1}(\theta)\left[-C_0\left(\theta,\dot{\theta}\right) - G_0(\theta)\right]$
- $H(t) = H\left(\theta,\dot{\theta},\ddot{\theta}\right) = M_0^{-1}(\theta)\left[\tau_{ex} - \Delta M(\theta)\,\ddot{\theta} - \Delta C\left(\theta,\dot{\theta}\right)\dot{\theta} - \Delta G(\theta)\right]$

3.2.2.2 Problem formulation

The problem is the accuracy/robustness dilemma of a compliant control or indirect force control. In this paper, we focus on the implementation of a robust new controller that gives the exoskeleton system a high-level of accuracy of trajectory tracking, and more flexibility and robustness to deal with the unknown nonlinear dynamics, unstructured modeling errors and unknown bounded disturbances. It is important to mention that the controller is formulated and proved based on Lyapunov function using the following Property and Assumptions:

Property 3.1: The inertia matrix $M_0(\theta)$ is symmetric and positive definite for all $\theta \in \mathbb{R}^n$ (Craig, 2005).

Assumption 3.1: The joint position and joint velocity are measured.

Assumption 3.2: All kinematic singularities are avoided.

Assumption 3.3: Since the dynamic model of the manipulator is continuous, differentiable and bounded, the function $H(t)$ and its time derivative $\dfrac{d}{dt}[H(t)]$ are locally Lipschitz functions.

Assumption 3.4: The desired trajectory is bounded.

Assumption 3.5: The external disturbance τ_{ex} is supposed to be continuous, has finite energy and satisfies $\|\tau_{ex}\| \leq \omega$, with an unknown positive disturbance boundary ω.

3.3 Control design and its stability

The compliance control objective is to achieve force control via motion control (outer control loop). Therefore, the compliance force is to achieve the required position based on the external force or free trajectory. In such case, the required position is the sum of the current Cartesian position and a certain Cartesian displacement with respect to the gain matrix. This gain matrix consists of proportional gains. The Second-Order Sliding Mode control combined with Time Delay Estimation (inner control loop) objective is to achieve the accuracy/robustness performance of the exoskeleton system. The proposed scheme is illustrated in Figure 3.3, and corresponds to a compliance control strategy; a subcategory of indirect force control as illustrated in Figure 3.4. The desired trajectory in proposed compliance control can be given by the following relation:

$$x_d = x_a + \delta_x \tag{3.5}$$

where $x_a \in \mathbb{R}^6$ is the measured actual Cartesian position, and $\delta_x \in \mathbb{R}^6$ is the displacement causing by the user's force. This displacement can be interpreted as the estimate of Desired Movement Intention (DMI) of the subject. If $\delta_x \longrightarrow 0$ this means the exoskeleton's wearer stops to exert forces on the force sensor, so that the exoskeleton robot decreases its motion, when $x_d = x_a$, the exoskeleton rests in its most recent position. In the proposed controller, the exoskeleton changes its position depending on the user's DMI that is obtained from the user's measured force. Let us now firstly determine displacement δ_x from the user's force as follows (Craig, 2005):

$$\delta_x = k_f F \tag{3.6}$$

where $k_f \in \mathbb{R}^{6\times6}$ is a diagonal positive-definite gain matrix, and $F \in \mathbb{R}^6$ is the measured force vector of the 6-axes force sensor.

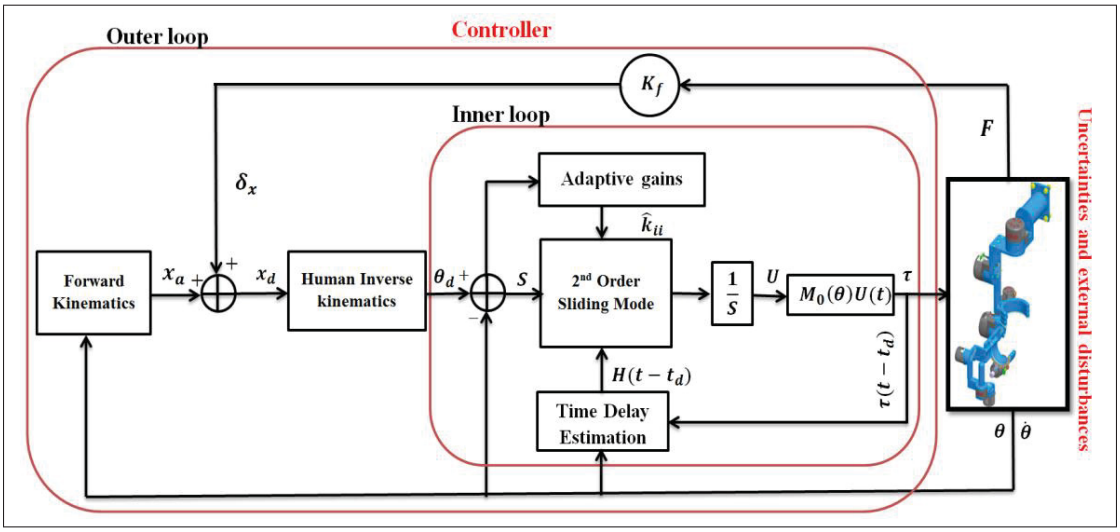

Figure 3.3 Diagram of the compliant control scheme

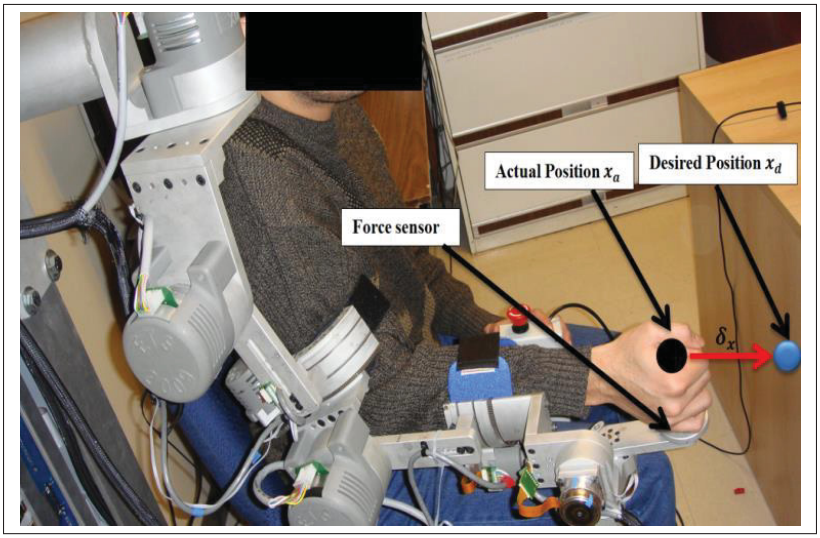

Figure 3.4 Compliance control strategy

For accurate force transmission, forces and moments expressed in the force sensor frame must be transformed into the robot's base-frame reference using well-known transformation matrix given in (Craig, 2005).

Now let us develop the control tracking of the inner loop. The new approach proposed in this research combines an adaptive-gain second-order sliding mode control and TDE, applied on the dynamic model of the exoskeleton robot presented in equation (3.2). The sliding set of $n-th$ linked to the surface or equivalent surface is determined by:

$$S = \dot{S} = \ddot{S} = \ldots = S^{(n-1)} = 0 \tag{3.7}$$

Equation (3.7) shows an n-dimensional condition of the parameter system. In our case, it's sufficient to differentiate the sliding surface once to obtain the desired control input. Let us choose the switching function or selected surface such that:

$$S = \dot{e} + \Lambda\, e \tag{3.8}$$

where $e = \eta_1 - \eta_{1d} \in \mathbb{R}^7$ and $\dot{e} = \eta_2 - \eta_{2d} \in \mathbb{R}^7$ are the position and velocity errors respectively, and $\eta_{1d},\ \eta_{2d} \in \mathbb{R}^7$ are respectively the reference position and velocity, $\Lambda = \mathbf{diag}(\lambda_{ii})$ for $i = 1,\ldots,7$ is a diagonal positive matrix. Taking the first derivative of selected surface S we obtain:

$$\begin{aligned} \dot{S} &= \ddot{e} + \Lambda\dot{e} = \dot{\eta}_2 - \dot{\eta}_{2d} + \Lambda\,\dot{e} \\ &= U(t) + f(t) + H(t) - \dot{\eta}_{2d} + \Lambda\,\dot{e} \end{aligned} \tag{3.9}$$

In this research, we seek to reduce the chattering phenomena using second-order sliding mode to transform the discontinuous control to continuous signal using integral action. So, the second

derivative of surface S is given by:

$$\begin{aligned}\ddot{S} &= \dddot{e} + \Lambda\ddot{e} = \ddot{\eta}_2 - \ddot{\eta}_{2d} + \Lambda\,\ddot{e} \\ &= \frac{d}{dt}[U(t)] + \frac{d}{dt}[f(t)] + \frac{d}{dt}[H(t)] - \ddot{\eta}_{2d} + \Lambda\,\ddot{e}\end{aligned} \tag{3.10}$$

The first and second derivative of S leads us to create a new system. Let us before that insert two new variables $\mu_1 = S$, and $\mu_2 = \dot{S}$, hence the new state-space equation is given such that:

$$\begin{cases}\dot{\mu}_1 &= \mu_2 \\ \dot{\mu}_2 &= \dfrac{d}{dt}[U(t)] + \dfrac{d}{dt}[f(t)] + \dfrac{d}{dt}[H(t)] - \ddot{\eta}_{2d} + \Lambda\,\ddot{e}\end{cases} \tag{3.11}$$

As we note, the time derivative of the control input $\dfrac{d}{dt}[U(t)]$ is responsible for handling the second-order sliding mode system presented by equation (3.11). This controller must be developed to contain a discontinuous term. However, to perfectly control the robot system (3.4), we must integrate once $\dfrac{d}{dt}[U(t)]$ to obtain the control input $U(t)$ with the desired torque $\tau = M_0(\theta)U(t)$. The integration is responsible for transforming the discontinuous control action to a continuous one which helps attenuating the undesirable chattering problem.

To complete the proposed controller procedure, let us introduce a new selected surface for the state-space equation present by (3.11) such that:

$$\rho = \mu_2 + \varphi\mu_1 \tag{3.12}$$

where $\varphi = \mathbf{diag}(\varphi_{ii})$ for $i = 1,\ldots,7$ is a diagonal positive definite matrix, and:

$$\dot{\rho} = Ksign(\rho) \tag{3.13}$$

where $K = \mathbf{diag}(k_{ii})$ for $i = 1,\ldots,7$is a switching positive gain diagonal matrix, and function $sign(\rho) = [sign(\rho_1),\ldots,sign(\rho_7)]^T$ is determined such that:

$$sign(\rho_i) = \begin{cases} 1 \;\; for \;\; \rho_i = 0 \\ 0 \;\; for \;\; \rho_i > 0 \\ -1 \;\; for \;\; \rho_i < 0 \end{cases} \tag{3.14}$$

Taking the time derivative of equation (3.12), we find:

$$\begin{aligned} \dot{\rho} &= \dot{\mu}_2 + \varphi\mu_2 \\ &= \frac{d}{dt}[U(t)] + \frac{d}{dt}[f(t)] + \frac{d}{dt}[H(t)] - \ddot{\eta}_{2d} + \Lambda\,\ddot{e} + \varphi\mu_2 \end{aligned} \tag{3.15}$$

From equation (3.13) and equation (3.15), we can conclude the time derivative of the control input such that:

$$\frac{d}{dt}[U(t)] = -\frac{d}{dt}[f(t)] - \frac{d}{dt}[H(t)] + \ddot{\eta}_{2d} - \Lambda\,\ddot{e} - \varphi\mu_2 - Ksign(\rho) \tag{3.16}$$

Since $H(t)$ and $\frac{d}{dt}[H(t)]$ are uncertain and they may influence the control purpose. In such case, the control law (3.16) is not feasible. To overcome this problem, TDE approach (Youcef-Toumi and Ito, 1990) is used to estimate the uncertainties of the nonlinear robot's dynamics. So, if **Assumption 3.3** is verified, $\frac{d}{dt}[H(t)]$ can be estimated such that:

$$\frac{d}{dt}\left[\hat{H}(t)\right] \simeq \frac{d}{dt}[H(t-t_d)] = \ddot{\eta}_2(t-t_d) - \frac{d}{dt}[f(t-t_d)] - \frac{d}{dt}[U(t-t_d)] \tag{3.17}$$

where t_d is very small time-delay constant. Practically, the smallest constant that can be used in real time is the sampling-time period.

As we discussed above, the second-order sliding mode is qualified to attenuate the undesirable chattering. However, the double time derivative of the sliding surface can magnify the risk of the nonlinear uncertainties function that can cause instability of the system. Additionally, in a

rehabilitation protocol, we deal with different subjects which mean different body characteristics. In this case, we still need large switching gains to preserve the stability and the robustness of the robot system, which generates again the chattering problem. In the paper, a solution is proposed to avoid the chattering problem and to provide a smooth human-like motion. In this solution, we tuned the switching gain K adaptively, where the adaptive gains update law is given as follows:

$$\dot{\hat{k}}_{ii} = \beta_{ii}^{-1}\left(|\rho_i| - \nu_i \hat{k}_{ii}\right) \tag{3.18}$$

where the sub-indexes i and ii denote the $i-th$ element of a vector and the $ii-th$ diagonal element of a diagonal matrix, respectively. $\beta_{ii} > 0$ is the adaptation gain. $\hat{k}_{ii}$ is the adapted value of k_{ii} taking into consideration its initial condition.

Finally, ν_i is determined as $\lim_{t\to\infty} \nu_i = 0$, $\int_0^t \nu_i(w) = Q_i < \infty$. In real time, we choose $\nu_i = \dfrac{1}{1+t^2}$. Let us now define the time delay error such that:

$$\varepsilon_i = \frac{d}{dt}\left[H_i(t)\right] - \frac{d}{dt}\left[\hat{H}_i(t)\right] = \frac{d}{dt}\left[H_i(t)\right] - \frac{d}{dt}\left[H_i(t-t_d)\right] \leq \delta_i |t-(t-t_d)| \leq \delta_i t_d \tag{3.19}$$

where δ_i for $i = 1,\ldots,7$ is a positive constant known as Lipschitz constant that satisfies the Lipschitz condition in **Assumption 3.3**.

By substituting the estimated $\dfrac{d}{dt}[H(t)]$ from equation (3.17) and introduce the adapted $\hat{k}_{ii}$ from equation (3.18) the time derivative of the control input $\dfrac{d}{dt}[U(t)]$, Equation (3.16) is rewritten such that:

$$\frac{d}{dt}\left[U(t)\right] = -\frac{d}{dt}\left[f(t)\right] - \frac{d}{dt}\left[\hat{H}(t)\right] + \ddot{\eta}_{2d} - \Lambda\,\ddot{e} - \varphi\mu_2 - \hat{K}sign(\rho) \tag{3.20}$$

The proposed joint torque law is described in **Theorem 3.1**.

Theorem 3.1: Consider the exoskeleton system presented as the state-space equation (3.4), the proposed joint torque (3.20) ensures the stability of the adaptive gains of the second-order

sliding mode with TDE if the following condition is verified:

$$k_{ii} > \delta t_d \;\; for \;\; i = 1, \ldots, 7. \tag{3.21}$$

with

$$\tau = M_0(\theta)U(t) \tag{3.22}$$

where $\int(\frac{d}{dt}[U(t)]) = U(t)$;

Proof 3.1: The proposed Lyapunov function candidate to show the stability of the robot is:

$$V = \frac{1}{2}\rho^T\rho + \sum_{i=1}^{7} \tilde{k}_{ii}^T \beta_{ii} \tilde{k}_{ii} \tag{3.23}$$

where $\tilde{k}_{ii} = \hat{k}_{ii} - k_{ii}$, The time derivative of equation (3.23) is given by:

$$\begin{aligned} \dot{V} &= \rho^T \dot{\rho} + \sum_{i=1}^{7} \tilde{k}_{ii}^T \beta_{ii} \dot{\tilde{k}}_{ii} \\ &= \rho^T \left(\frac{d}{dt}[U(t)] + \frac{d}{dt}[f(t)] + \frac{d}{dt}[H(t)] - \ddot{\eta}_{2d} + \Lambda\, \ddot{e} + \varphi\mu_2 \right) + \sum_{i=1}^{7} \tilde{k}_{ii}^T \beta_{ii} \dot{\tilde{k}}_{ii} \end{aligned} \tag{3.24}$$

Substituting $\frac{d}{dt}[U(t)]$ from equation (3.20) and $\dot{\tilde{k}}_{ii}$ from equation (3.18) into equation (3.24), the derivative of the Lyapunov function (3.24) becomes such that:

$$\begin{aligned} \dot{V} &= \rho^T \left(\left(\frac{d}{dt}[H(t)] - \frac{d}{dt}\left[\hat{H}(t)\right] \right) - \hat{K} sign(\rho) \right) + \sum_{i=1}^{7} \tilde{k}_{ii}^T |\rho_i| - \nu_i \tilde{k}_{ii}^T \hat{k}_{ii} \\ &= \sum_{i=1}^{7} \rho_i \left(\left(\frac{d}{dt}[H_i(t)] - \frac{d}{dt}\left[\hat{H}_i(t)\right] \right) - \hat{k}_{ii} sign(\rho_i) \right) + \tilde{k}_{ii}^T |\rho_i| - \nu_i \tilde{k}_{ii}^T \hat{k}_{ii} \end{aligned} \tag{3.25}$$

Using Young's inequality such that:

$$\tilde{k}_{ii}\hat{k}_{ii} \geq \frac{1}{2}\tilde{k}_{ii}^T\tilde{k}_{ii} - \frac{1}{2}k_{ii}^2 \tag{3.26}$$

where $\tilde{k}_{ii}^T = \tilde{k}_{ii}$. Substituting equation (3.25) into equation (3.26), we find:

$$\begin{aligned}
\dot{V} &\leq \sum_{i=1}^{7} \rho_i \left(\varepsilon_i - \hat{k}_{ii} sign(\rho_i)\right) + \tilde{k}_{ii}|\rho_i| - \frac{1}{2}\nu_i \tilde{k}_{ii}^T \tilde{k}_{ii} + \frac{1}{2}\nu_i k_{ii}^2 \\
&\leq \sum_{i=1}^{7} \rho_i \left(\varepsilon_i - \hat{k}_{ii} sign(\rho_i)\right) + \left(\hat{k}_{ii} - k_{ii}\right)|\rho_i| - \frac{1}{2}\nu_i \tilde{k}_{ii}^T \tilde{k}_{ii} + \frac{1}{2}\nu_i k_{ii}^2 \\
&\leq \sum_{i=1}^{7} -\left(|\rho_i|\left(k_{ii} - |\varepsilon_i|\right)\right) - \frac{1}{2}\nu_i \tilde{k}_{ii}^T \tilde{k}_{ii} + \frac{1}{2}\nu_i k_{ii}^2 \\
&\leq \sum_{i=1}^{7} -|\rho_i|\left(k_{ii} - \delta_i t_d\right) - \frac{1}{2}\nu_i \tilde{k}_{ii}^T \tilde{k}_{ii} + \frac{1}{2}\nu_i k_{ii}^2
\end{aligned} \tag{3.27}$$

Since $\sum_{i=1}^{7} \frac{1}{2}\nu_i k_{ii}^2 \longrightarrow 0$ due to the definition of ν in equation (3.18), and by verified the following condition:

$$k_{ii} > \delta t_d \;\; for \;\; i = 1, \ldots, 7. \tag{3.28}$$

The Lyapunov function $\dot{V}$ is semi-negative definite. To prove the asymptotic stability of the system. Let us integrate both sides of the equation (3.27) gives:

$$V(t) - V(0) \leq -\int_0^t \left(\sum_{i=1}^{7} -|\rho_i|\left(k_{ii} - \delta_i t_d\right) + \frac{1}{2}\nu_i \tilde{k}_{ii}^T \tilde{k}_{ii} \right) dw + \int_0^t \left(\frac{1}{2}\nu_i k_{ii}^2\right) dw \tag{3.29}$$

Since k_{ii} is constant and $\int_0^t \nu_i(w) = Q_i < \infty$ due to the definition of ν in equation (3.18), one can rewrite equation (3.29) as:

$$V(t) - V(0) \leq -\int_0^t \left(\sum_{i=1}^{7} -|\rho_i|\left(k_{ii} - \delta_i t_d\right) + \frac{1}{2}\nu_i \tilde{k}_{ii}^T \tilde{k}_{ii} \right) dw + \int_0^t \left(\frac{1}{2}\nu_i k_{ii}^2\right) dw < \infty \tag{3.30}$$

Therefore, V is bounded which implies that $\rho \in L_\infty$ and $\eta_1, \;\; \eta_2 \in L_\infty$ from boundedness of $\eta_{1d}, \; \eta_{2d}$ (**Assumption 3.4**). With k_{ii} is constant, we know that $\hat{k}_{ii}$ is also bounded. Thus, all signals in closed loop are bounded. Thus, the surface ρ_i and its derivative converge to the origin as $t \longrightarrow \infty$. Hence, the system is stable.

3.4 Experimental and comparative study

3.4.1 Experiment setup

The robot system consists of three processing units, the first is a PC where the top-level commands are sent to the robot using LabVIEW [version 2018] interface namely, the control scheme selection, joint or Cartesian space trajectory, and so on. This PC also receives the data after the robot task is executed to analyze its performance. The other two processing units are part of a National Instruments PXI platform. Firstly, a NI-PXI 8081 controller card with an Intel Core Duo processor. In this card, the main operating system of the robot and the top-level control scheme are executed. In our case, the adaptive-gains second-order sliding mode-based controller as well as the estimation based on time delay approach had a sampling time of 500 ms. The human inverse kinematics algorithm is executed in a MATLAB script module of LabVIEW which can run inside this control loop easily. Finally, at input/output level, a NI PXI-7813 R remote input/output card with a field programmable gate array (FPGA) executes the low-level control, that is, a proportional–integral (PI) current control loop (sampling time of 50 μs) to maintain the current of the motors required by the main controller.

Note that the PI controller runs 10 times faster than the proposed control loop and is executed in the FPGA. Also, in this FPGA, the position feedback via Hall-sensors (joint position) and basic input/output tasks are executed. The force sensor feedback is important to accurately control the movement of the exoskeleton. A high linearity six-axis force sensor (NANO17-R-1.8-M2-M1PCI, ATI industrial Automation, Apex, NC, USA) is chosen to obtain accurate real-time force measurements. This sensor is mounted on the tip of the robot. The joints of the ETS-MARSE are powered by brushless direct current (DC) motors (Maxon EC-45 and Maxon EC-90) combined with harmonic drives (gear ratio 120:1 for motor-1 and motor-2, and gear ratio 100:1 for motors 3–7). Let us summarize the experiments setup by presenting the architecture for the ETS-MARSE system in Figure 3.5. The output of the controller is the joints torque commands. However, the torque commands are converted to motor currents and finally to reference voltage as the voltage value is the drive command for motor drivers. Furthermore, to

realize the RT control of the ETS-MARSE and to ensure that the right control torque command is sent to the joints (as well as the reference voltage commands for the drivers), we also added a PI controller to minimize differences between desired and measured currents (i.e. the error command to PI controller).

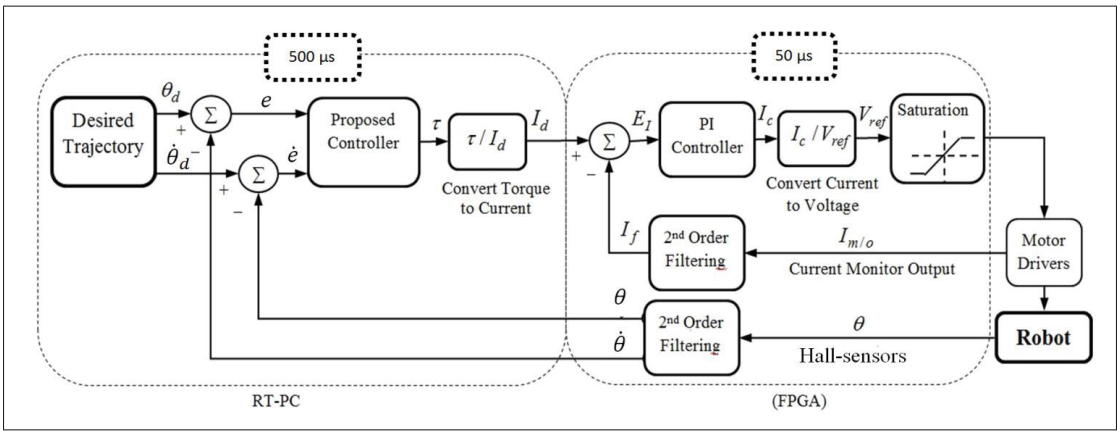

Figure 3.5 Experiments platform ETS-MARSE robot

The physical parameters of ETS-MARSE relative to the base reference frame are given in Table (3.3). The parameters of the proposed control are illustrated in Table (3.4).

Table 3.3 Physical parameters of ETS-MARSE

Joints (i)	Mass (kg)	Centre of mass (m)	Link length (m)
1	3.475	0.0984	0.145
2	3.737	0.1959	0
3	0	0	0.25
4	2.066	0.163	0
5	0	0	0.267
6	0.779	0.121	0
7	0.496	0.0622	0

A VE (HELIOS) is created in open source *Unity 3-D* platform (see Figure 3.4). This interface consists of a set of functional movement tasks defined by a therapist. There are two types of communication with the ETS-MARSE system (LabVIEW). A user datagram protocol (UDP)

protocol for transferring position data and a TCP/IP protocol for transferring the operator's commands (e.g. star/stop the execution of the task) (Ferrer *et al.*, 2013). The choice of these protocols is based on reliability and the speed of transmission of data for each one. Our platform is divided into two profiles: user profile and admin profile. The user profile is under the supervision of a therapist and a biomedical engineer. The latter is responsible for preparing the rehabilitation session (such as customized task, as per the patient's need). The admin profile is responsible to manage the database of the patient (such as Add/Edit/Delete a patient) and he/she has access to the list of all patients and information concerning the rehabilitation session (Ferrer *et al.*, 2013).

Table 3.4 Controller parameters

Gains	Value ($i = 1:7$)
φ_i	15.7
Λ_i	42.2
k_{fi}	0.05 ($i = 1:6$)
β_{ii}	2.82
β_{ii}	0.01 (initial condition of gains)

3.4.2 Experiments' results

An experimental physiotherapy session was created to show the effectiveness of the proposed control system. The physical therapy tasks are performed by three different healthy subjects (mean age: $27+4.6$ years; mean height: $170+8.75$ cm; mean weight: $75+18$ kg). Each subject participated in a full physiotherapy session, under the supervision of a therapist and control engineer. The therapist defined the range of motion of each subject and attributed suitable exercise. Within the session, the subject was comfortably seated in a chair (with height adjustment depend to size to each subject) in front of the virtual interface as shown in Figure 3.7. Experimental physiotherapy session was devised to three scenarios. In the first scenario, subject 1 performed a designed task (forearm pronation/ supination) for two repetitions using the proposed controller. The same subject repeated the same tasks using conventional second-order

sliding mode control (constant switching gains) for two consecutive times. The objective of this experiment is to show the accuracy of the proposed controller compared with conventional second-order sliding mode controller (Bartolini *et al.*, 2001). In the second scenario, subject 2 has interacted with the VE trying to follow a proposed trajectory. In the third scenario, subject 3 performed a free motion during 2 min or more. It consisted of reaching an object or perform a daily activity such as eating, and the purpose of the last two experiments is to examine the transparency of the robot with each subject and how the control system permits the robot perform a smooth motion using human inverse kinematics. It is important to mention that each subject was repeatedly asked if he was sensing tired (bored) of the VE and the exoskeleton device and if for any cause intended to pause the trial session. Also, that all the experiments started from the initial position where elbow joint is at 90° and all the other joints at 0°.

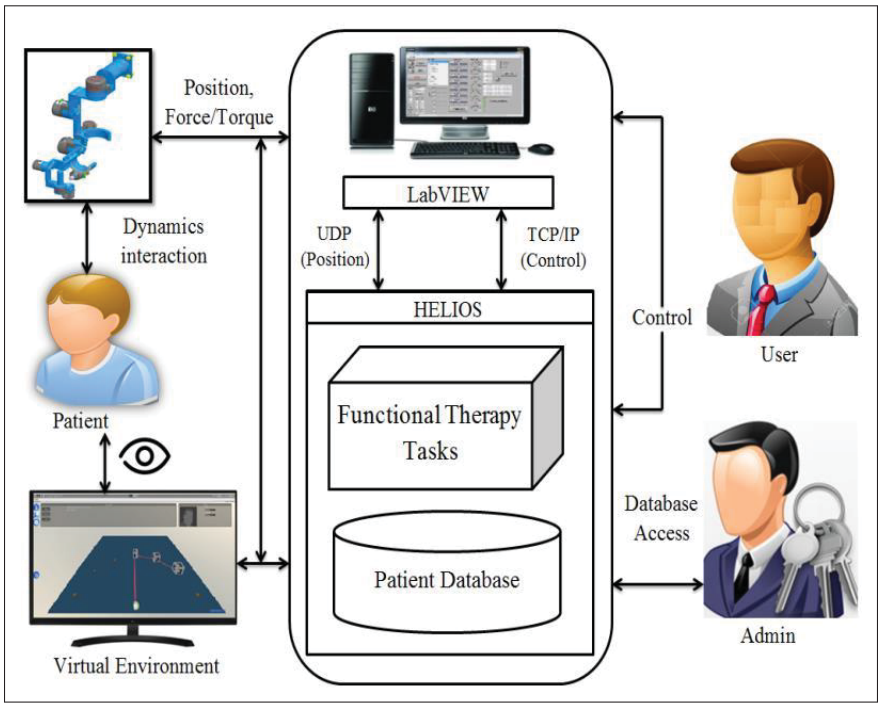

Figure 3.6 Virtual interface (HELIOS) diagram and its communication layout with ETS-MARSE robotic system

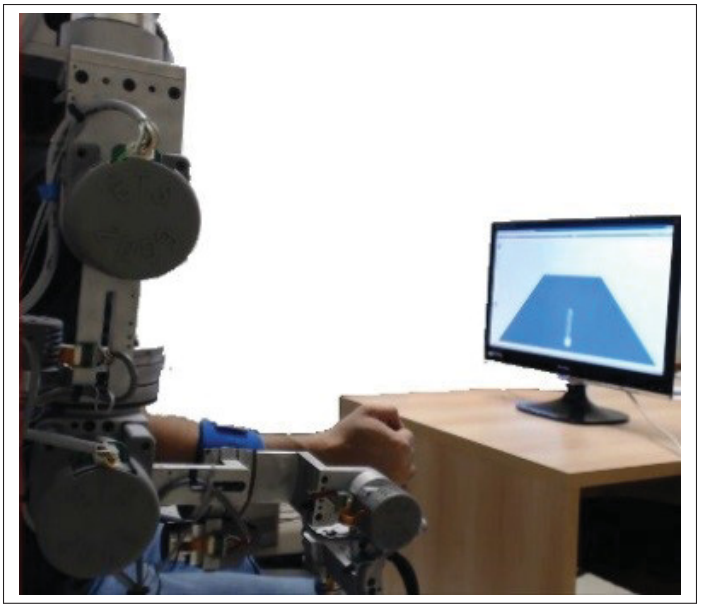

Figure 3.7 The subject on front of the virtual interface

3.4.2.1 Scenario 1

Discussion 1: Figure 3.8 presents the workspace of the performance tracking of ETS-MARSE performed by subject 1. It is clear that the proposed controller presents a good result where it keeps the stability of the robot system, small error not more than 2°, and smooth sliding surface. It is remarkable that the applied joint torque input is very smooth and the updated gains converge to a finite value as time going to infinity. Figure 3.9 presents the performance of the robot with the conventional approach. It is obvious that the conventional approach also gives good results, compared with the results (Figure 3.8) that is presented by the proposed control. The designed controller improves the performance of the second-order sliding mode control, where the error position, the sliding surface, and the control input that are provided by the proposed controller are relatively small and smooth than the results (Figure 3.9) provided by the conventional approach.

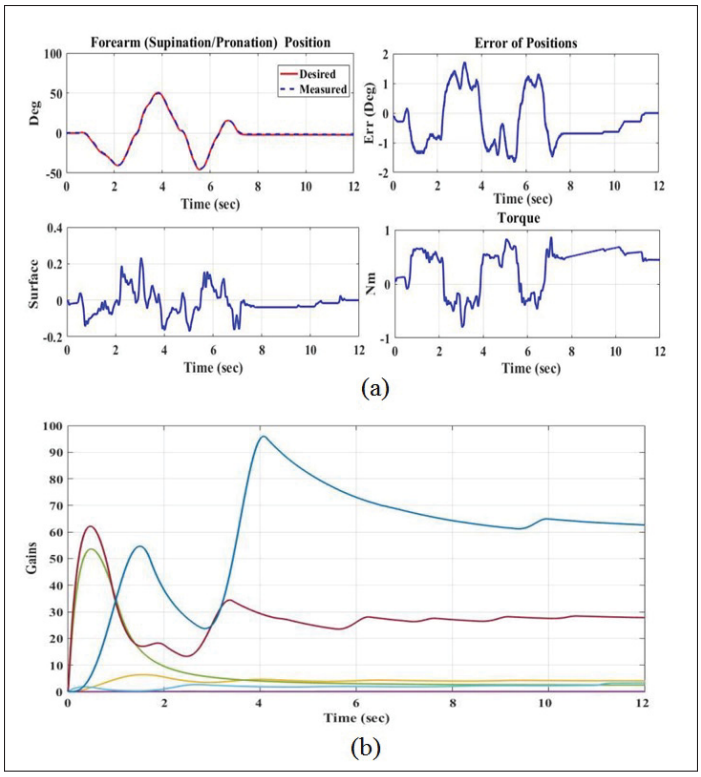

Figure 3.8 Workspace tracking of the robot performed a forearm pronation/supination by subject 1: (a) (age: 29 years; height: 178 cm; weight: 81 kg) using the proposed controller; and (b) Estimated gains

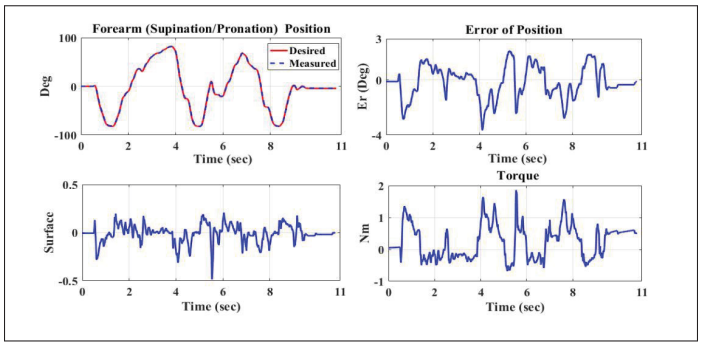

Figure 3.9 Workspace tracking of the robot performed a forearm pronation/supination by subject 1: (age: 29 years; height: 178 cm; weight: 81 kg) using the conventional controller

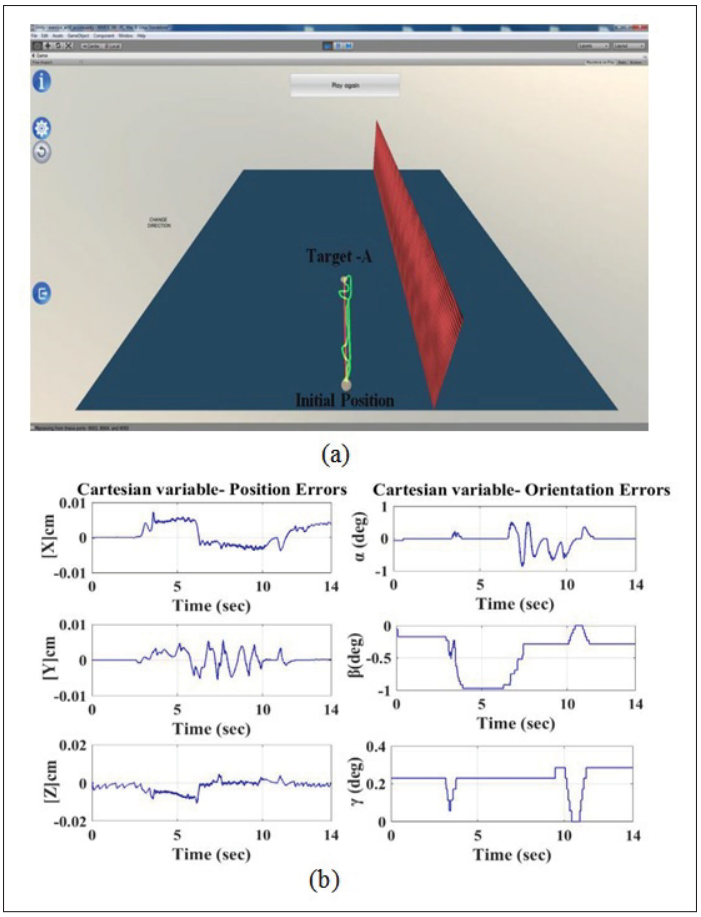

Figure 3.10 Workspace tracking of the robot using the proposed controller performed by subject 2: (a) (age: 31 years; height: 183 cm; weight: 83.5 kg; view on Unity platform); (b) Cartesian errors

3.4.2.2 Scenario 2

Discussion 2: Figure 3.10 presents the performance of subject 2 (age: 31 years; height: 183 cm; weight: 83.5 kg) in the virtual interface with the help of ETS-MARSE exoskeleton robot (red line is desired and the green line is the achieved trajectory). Figures 3.10 (b), (3.11), and (3.12) present the workspace of error tracking of the robot in Cartesian space, the estimated gains, and the control input. It is clear from these plots (Figures 3.10 to 3.12) that the control strategy achieved the desired performance with small tracking errors and acceptable control input.

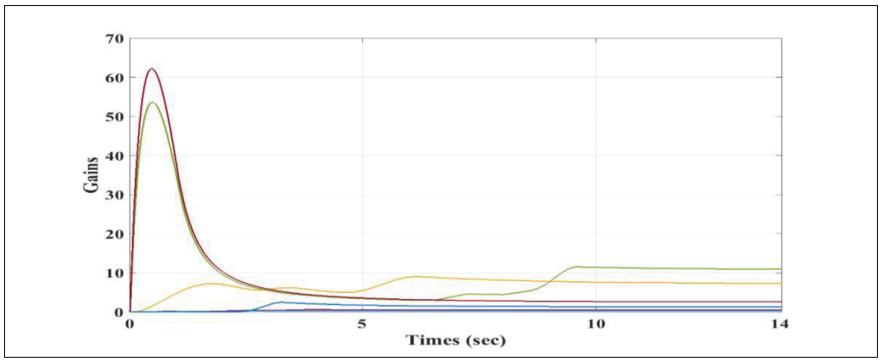

Figure 3.11 Estimated gains

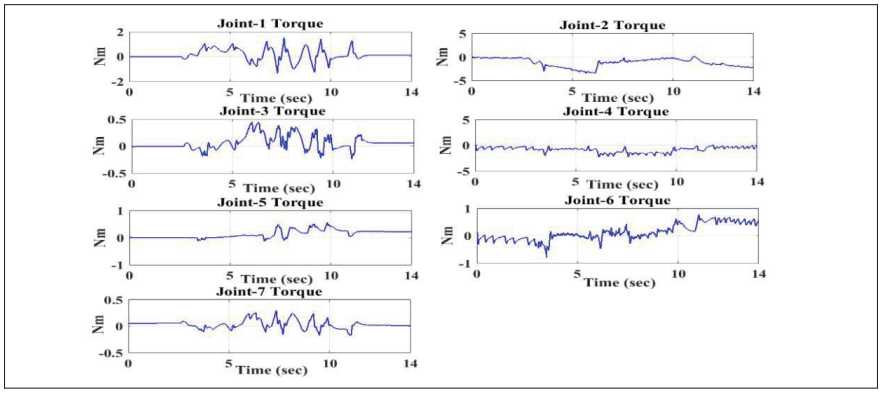

Figure 3.12 Torques input of active rehabilitation task

3.4.2.3 Scenario 3

Discussion 3: Figures 3.13 to 3.16 present the performance of free motion by subject 3 (age: 27 years; height: 168 cm; weight: 70 kg) with the help of ETS-MARSE exoskeleton robot. Figures 3.13 (b), 3.14, (3.15), and (3.16) present the workspace of error tracking of the robot in Cartesian space, the workspace of the tracking trajectory in joint space, the torque input, and updated gains. It is easy to conclude, from these plots (Figures 3.13 to 3.16) two points. The first one is that the proposed control approach achieved the desired performance with high characteristics (small tracking errors and acceptable control input and convergence of estimated gains). The second one is the algorithm of human inverse kinematics. It provides a good solution and permits to transform the Cartesian task to the joints task by a unique and accurate solution.

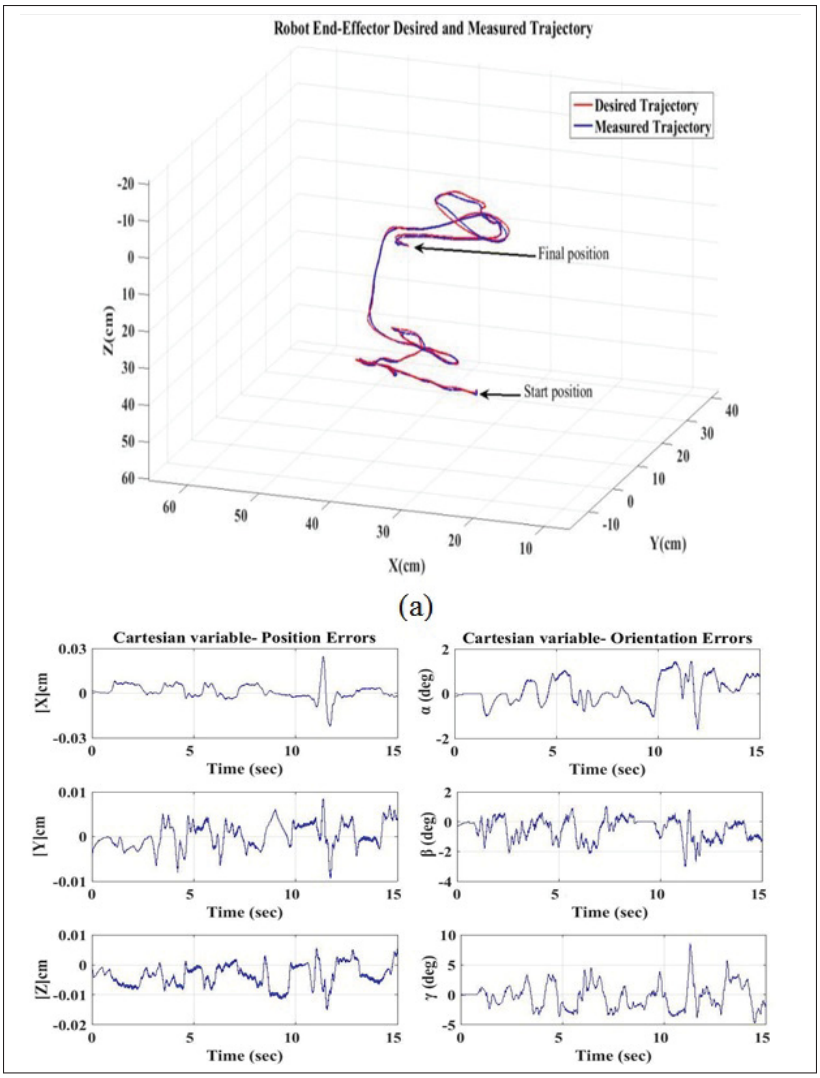

Figure 3.13 Workspace tracking of the robot performed a free motion by subject 3: (age: 27 years; height: 168 cm; weight: 70 kg). (b) Cartesian errors

3.5 Conclusion

In this article, we investigated active rehabilitation protocol by presenting a new compliant control based on secondorder sliding mode with adaptive gains incorporating TDE. The control is based on human inverse kinematics to complete active rehabilitation protocols for an exoskeleton robot with unknown dynamics and unforeseen disturbances. The proposed control

is principally aimed to deal with the accuracy/robustness problem of an admittance control. Second-order sliding mode has shown attractive characteristics of accuracy and attenuation of chattering. However, its problem is that the unknown dynamic of the exoskeleton robot and external disturbances can be amplified by the second derivative of sliding surface, which leads to instability of the robot system. Applying a large switching gain is needed to maintain the stability of the robot, which in turn makes the chattering problem existing yet again. Then, employing adaptive gains and TDE will improve the robustness of the second-order sliding mode control while overcoming its main limitation.

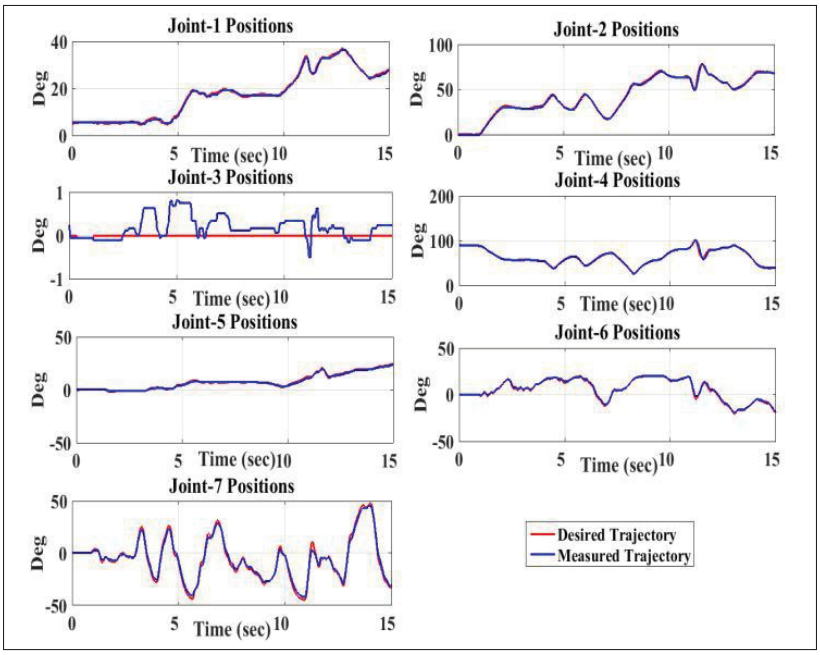

Figure 3.14 Tracking trajectory of the robot in joint space corresponding to the free motion performed by subject 3: (age: 27 years; height: 168 cm; weight: 70 kg)

The stability analysis is formulated and demonstrated based on Lyapunov function. An experimental physiotherapy session with healthy subjects using virtual reality was created to test the effectiveness and feasibility of the proposed control.

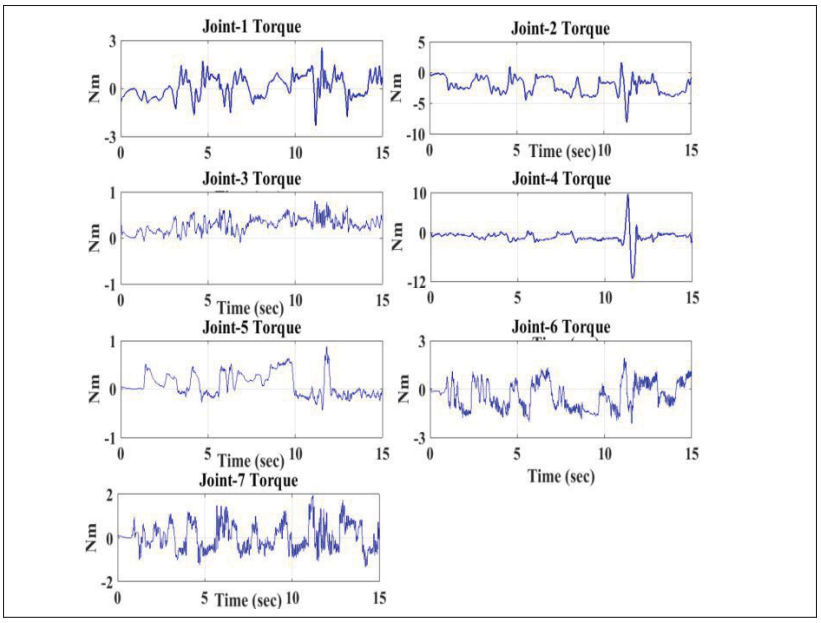

Figure 3.15 Forces and torques input of active rehabilitation

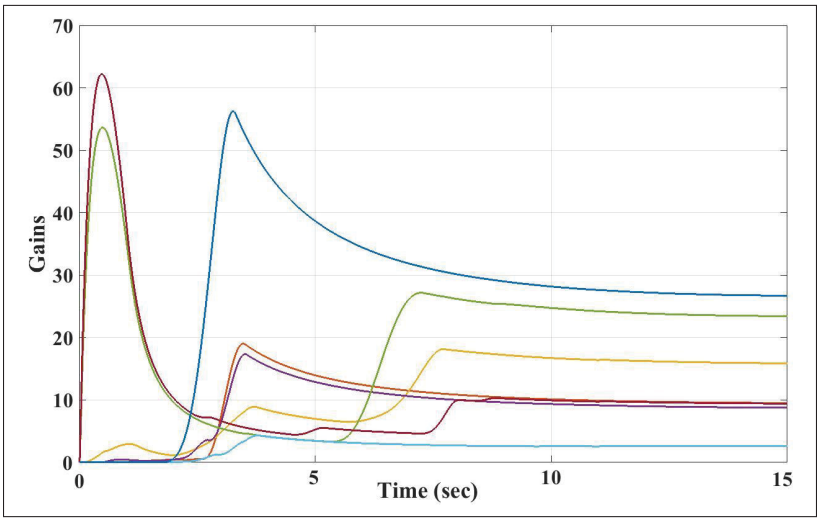

Figure 3.16 Estimated gains

In the light of these satisfactory results obtained with healthy subjects, we are looking forward to implementing the proposed control strategy with real unhealthy subjects as stroke victims in future work, which permits to evaluate the controller with true case of disturbances such as spasticity/dystonia and muscle weakness in neurological patients.

CHAPTER 4

ADAPTIVE TRACKING CONTROL OF AN EXOSKELETON ROBOT WITH UNCERTAIN DYNAMICS BASED ON ESTIMATED TIME DELAY CONTROL

Brahim Brahmi[1], Maarouf Saad[1], Cristobal Ochoa Luna [1] Mohammad H. Rahman[2] and Abdelkrim Brahmi[1]

[1] Département of Electrical Engineering, École de Technologie Supérieure, 1100 Notre-Dame Ouest, Montréal, Québec, Canada H3C 1K3
[2] Mechanical/Biomedical Engineering Department,University of Wisconsin-Milwaukee, 3200 N. Cramer Street, Milwaukee, WI 53211,

Paper published in *IEEE/ASME Transaction on Mechatronics*, April 2018

Abstract

In this paper, we present a backstepping approach integrated with time-delay estimation to provide an accurate estimation of unknown dynamics and to compensate for external bounded disturbances. The control was implemented to perform passive rehabilitation movements with a 7-DOF exoskeleton robot named ETS-Motion Assistive Robotic-Exoskeleton for Superior Extremity. The unknown dynamics and external bounded disturbances can affect the robotic system in the form of input saturation, time delay errors, friction forces, backlash, and different upper-limb's mass of each subject. The output of the time delay estimator is coupled directly to the control input of the proposed adaptive tracking control through a feed-forward loop. In this case, the control system ensures a highly accurate tracking of the desired trajectory, while being robust to the uncertainties and unforeseen external forces, and flexible with variation of parameters. Due to the proposed strategy, the designed control approach does not require accurate knowledge of the dynamic parameters of the exoskeleton robot to achieve the desired performance. The stability of the exoskeleton robot and the convergence of its state errors are established and proved based on Lyapunov–Krasovskii functional theory. Experimental results and a comparative study are presented to validate the advantages of the proposed strategy.

Keywords: Backstepping control, rehabilitation robots, time-delay control, time-delay error (TDR).

4.1 Introduction

Neurological diseases have become a growing challenge and a difficult reality for the medical and scientific community, as confirmed by the statistics of the World Health Organization. Each year, at least 15 million people worldwide suffer neurological diseases, such as stroke (Sidney *et al.*, 2013). From them, six million die and five million more are living with a persistent disability (Sidney *et al.*, 2013). At all times, human activities of everyday life, such as balance of legs and arms to move, walk, stand, sit or even relax, take objects, eat, brushing teeth, or cleaning face, depend on a healthy nervous system. Damage caused by nerve cells causes a disruption of communication between the nervous system and the rest of the body, resulting in the inability of the nervous system to function adequately. This condition causes symptoms that can include numbness, pain, balance disorders, etc. Recently, the use of robotic devices known as rehabilitation robots in physiotherapy assistive domains has demonstrated a high potential in preventing the worsening of the subject's disability, improving its functional movements, ensuring its return to normal life, and helping the subject in daily living activities, such as self-care skills and pick-and-place exercises (Hughes *et al.*, 2016; Keller *et al.*, 2016; Philips *et al.*, 2017; Volpini *et al.*, 2017). The robot's significance is due to its attractive characteristics such as its ability to provide intensive rehabilitation and its easiness to design a physical therapy activity fitted to the needs of the subject (Xie *et al.*, 2016).

The control of these kinds of robots presents additional complexity over the control of conventional robotic manipulators due to their complex mechanical structure designed for human use, the type of desired tasks, and the sensibility of the interaction with a great diversity of human wearers (Chen *et al.*, 2017; Du and Zhang, 2015; Zhao *et al.*, 2015). To address these problems, different control strategies have been developed for rehabilitation robots. Among them, a simple PID control implemented in (Yu and Rosen, 2013); a nonlinear modified computed torque control that requires a good knowledge of dynamic parameters, implemented in (Rah-

man *et al.*, 2015)) and ((Rahman *et al.*, 2011a). A robust sliding-mode control with exponential reaching law was proposed in (Rahman *et al.*, 2013) to improve the performance of the robot and to limit the chattering problem generated by the high-frequency activity of the control signal. As well, a force controller was proposed in (Ueda *et al.*, 2010) for an exoskeleton that permits to the wearer to achieve motor tasks based on muscle activity data. We can also mention a backstepping control combined with human inverse kinematics (Brahmi *et al.*, 2017c) to provide a human-like motion. Nevertheless, in the previous cited papers, the control scheme is the named model-based controller, in which the control loop requires a dynamic model of the exoskeleton.

In reality, the dynamics of these types of robots is typically uncertain due to their complex and sensitive structure Particularly, when the number of degrees of freedom (DOFs) of the robot increases, it is not straightforward to find the accurate parameters of the exoskeleton robot; e.g., the parameters' vector of the robot can be greater than 100 if the number of DOFs of the robot is greater than 4 (Brahim *et al.*, 2016a). Usually, these robots operate under input saturation constraints to ensure the safety to the robot's user. This latter is one of the most serious nonlinearities of the robotic system (Li *et al.*, 2015b). The effect of the constraint appears when the exoskeleton actuators are unable to provide the required energy to perform a rehabilitation motion, which causes tracking errors. Additionally, a repeating motion can cause the fatigue of the motors (Brahim *et al.*, 2016a), (Brahim *et al.*, 2016b), which provokes many problems, such as a dead zone (Li *et al.*, 2014), friction forces, etc. Moreover, the synergy between the subject and the exoskeleton robot forces the system to operate under unforeseen external forces as the payload caused by the attached upper limb of the subject.

Hence, the estimation of the uncertainties of the nonlinear dynamic parameters of these robots is one of the most challenging problems in the control of high-DOFs robotics exoskeleton systems. Numerous control strategies have been developed to approximate the dynamic parameters.Within these approaches, the linear parameterization of the dynamic equation of motion is used in order to obtain the regressor matrix (Cheah, 2006), (Yazarel and Cheah, 2002). This matrix is required in the design of the updated control law. However, it is not straightforward

to find the parameters of the exoskeleton robot, if it has a high number of DOFs (more than four). Additionally, the integral action of the designed updated law can cause the instability of the robot system in the presence of disturbances, even if it is small. Recently, the approach by fuzzy logic and neural networks presented a significant solution due to their attractive characteristics of the robot's unknown nonlinear dynamics estimation with minimum feedback from the robotic system (Li *et al.*, 2015b), (Chen *et al.*, 2015; Li *et al.*, 2017a, 2015a). However, these strategies demand a heavy computation cost, which makes their implementation very hard. Adaptive learning control is a robust approach designed to adapt the time-varying uncertainties and disturbances in order to reject them from the rigid body robot (Brahim *et al.*, 2016a), (Jin and Xu, 2013). In this approach, the authors have proposed that the robot performs the same exercises over a fixed period, making this approach limited to repetitive tasks only and actuators fatigue. However, in this paper, a time-delay estimation (TDE) approach (Youcef-Toumi and Ito, 1990; Youcef-Toumi and Shortlidge, 1991; Brahmi *et al.*, 2017a,b) is used to estimate the unknown uncertain parameters of the exoskeleton's dynamic. The TDE has been implemented in many robotic systems with consistently good performances (Brahmi *et al.*, 2017a), (Jin *et al.*, 2015; Kim *et al.*, 2016; Chen *et al.*, 2016). The choice of use of TDE is that one can easily estimate the unknown dynamics with a simple control scheme. In addition, TDE is one of the strategies that is not affected by the size of the estimated parameters (high DOFs). It can only be employed in time-delayed knowledge from the previous state response of the system and its control input to provide an accurate estimation of unknown dynamics. However, due to noisy measurements and nonlinearity of signals along the sampling time, a time-delay error (TDR) exists, which would deteriorate the robustness and the accuracy of the exoskeleton robot.

The cited constraints (mainly dynamic uncertainties, joint conjunction, friction forces, backlash, mass changing, and TDR), that limit the functionality of the exoskeleton robots, motivate us to design a controller able to provide a highly accurate tracking of the desired trajectory, to be robust to the uncertainties and unforeseen external forces, and to be flexible with the parameters' variation. In this paper, we present a new adaptive backstepping controller based

on TDE, applied on an upper-limb exoskeleton robot. The backstepping is employed to estimate the unknown uncertainties, unforeseen disturbances, and compensate for the TDR and unexpected disturbances. Furthermore, the theoretical development is complemented by its implementation on an exoskeleton robot. The output of the time-delay estimator is added directly to the control input of the proposed adaptive tracking control via feed-forward loops, which makes the control system more powerful and faster to estimate and compensate for unknown dynamics and external disturbances.

Summarizing, through the proposed strategy, the control approach does not require any accurate knowledge of the dynamic parameters of the exoskeleton robot to reach the desired performance. This controller is designed to be robust and more flexible to deal with the dynamic uncertainties taking into consideration the TDR, and to be more robust to the parameter variations. Moreover, the proposed strategy is not restricted by the repetitive task or periodic desired trajectory. The stability of the exoskeleton system and the convergence of its errors are formulated and demonstrated based on the Lyapunov–Krasovskii functional theory. The validation of the control platform is done by creating a rehabilitation session performed with healthy human subjects. A comparative study is provided and is compared against the conventional approach to show the advantages, feasibility, and the robustness of the proposed approach.

The remainder of the paper is organized as follows. The exoskeleton robot, its kinematics and dynamics are presented in the following section. The control scheme is described in Section 4.3. Experimental and comparison results are shown in Section 4.4. Finally, the conclusion and future work are presented in Section 4.5.

4.2 Characterization of system rehabilitation

4.2.1 Exoskeleton robot development

The developed exoskeleton robot ETS-Motion Assistive Robotic-Exoskeleton for Superior Extremity (ETS-MARSE) is a redundant robot consisting of 7 DOFs, as shown in Figure 4.1. It

was created to provide physical therapy and assisted motion to the injured upper limb. The idea of the designed exoskeleton is basically extracted from the anatomy of the upper limb of the human, to be ergonomic for the user along with the physical therapy session. The shoulder part consists of three joints; the elbow part comprises one joint, and the wrist part consists of three joints. Each part is responsible for performing a variety of upper-limb motions, as shown in Table (4.2). The design of the ETS-MARSE has special features compared with the existing exoskeleton robots. Among them, it has a comparatively low weight, an excellent power/weight ratio, can be easily fitted or removed, and is capable of adequately compensating for gravity.

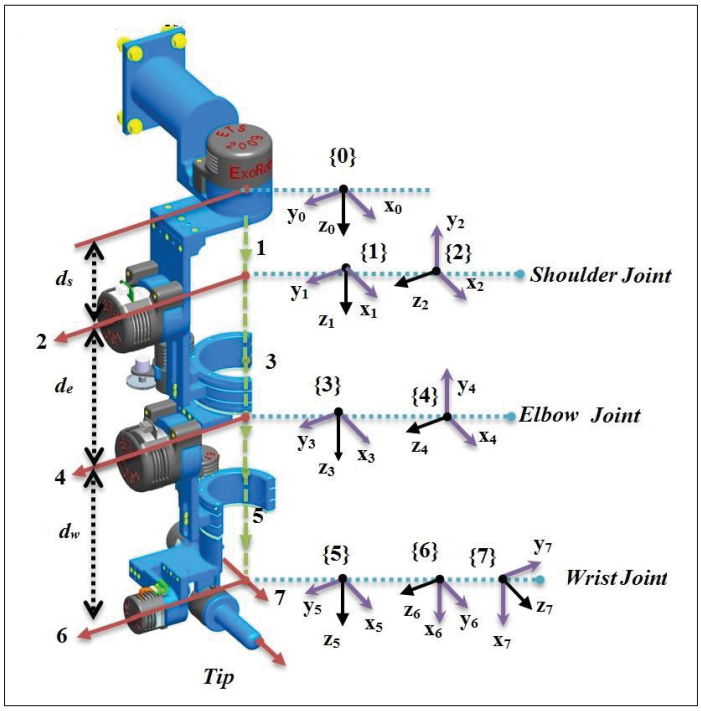

Figure 4.1 Reference frames of ETS-MARSE

A new power carrying mechanism was included for supporting the shoulder joint internal/external rotation and for forearm pronation/supination. This robot can be used with a wide range of subjects, due to the length of its adjustable links. This exoskeleton can perform passive (completely support and perform the motion on the subjects' upper limb) and active assistive

motion (respond to force, electromyography, and /or be compliant with the subject to accompany and assist him/her in the intended motion). All special characteristics of the ETS-MARSE and comparison with similar existing exoskeleton robots are summarized in (Ochoa Luna *et al.*, 2015; Rahman *et al.*, 2014, 2012b; Luna *et al.*, 2016).

Table 4.1 Modified Denavit-Hartenberg parameters

joint (i)	α_{i-1}	a_{i-1}	d_i	θ_i
1	0	0	d_s	θ_1
2	$\frac{-\pi}{2}$	0	0	θ_2
3	$\frac{\pi}{2}$	0	d_e	θ_3
4	$\frac{-\pi}{2}$	0	0	θ_4
5	$\frac{\pi}{2}$	0	d_w	θ_5
6	$\frac{-\pi}{2}$	0	0	$\theta_6 - \frac{\pi}{2}$
7	$\frac{-\pi}{2}$	0	0	θ_7

Table 4.2 Workspace ETS-MARSE

joint (i)	Motion	Workspace
1	Shoulder joint horizontal flexion/extension	$0^\circ/140^\circ$
2	Shoulder joint vertical flexion/extension	$140^\circ/0^\circ$
3	Shoulder joint internal/external rotation	$-85^\circ/75^\circ$
4	Elbow joint flexion/extension	$120^\circ/0^\circ$
5	Forearm joint pronation/supination	$-85^\circ/85^\circ$
6	Wrist joint ulnar/radial deviation	$-30^\circ/20^\circ$
7	Wrist joint flexion/extension	$-50^\circ/60^\circ$

4.2.2 Kinematics of ETS-MARSE Robot

The transformation from Cartesian space to joint space is done by a nonlinear function named the Jacobian matrix. In order to maneuver the exoskeleton in Cartesian space, we used the inverse Jacobian matrix method, since the control is executed in the joint space. Due to the redundant nature of the ETSMARSE robot, the inverse kinematics can be achieved using the

pseudoinverse of the Jacobian, which can be expressed as follows:

$$\dot{\theta} = \left(J^T (JJ^T)^{-1}\right) \dot{x}_d \tag{4.1}$$

where $\dot{x}_d \in \mathbb{R}^{6\times 1}$ is the desired Cartesian velocity, $\dot{\theta} \in \mathbb{R}^{7\times 1}$ is the calculated joint velocity and $J \in \mathbb{R}^{6\times 7}$ is the Jacobian matrix of the robot.

The modified Denavit–Hartenberg (DH) parameters (**?**) are given in Table (4.1). These parameters are obtained from the reference frames shown in Figure 4.1 and are used to obtain the homogeneous transformation matrices.

The workspace of the designed robot is given in Table (4.2). Further detailed information of the parameters and design of ETS-MARSE can be found in (Rahman *et al.*, 2015).

4.2.2.1 Dynamics of the ETS-MARSE Robot

The dynamic equation of the ETS-MARSE is expressed in joint space as follow:

$$M(\theta)\ddot{\theta} + C(\theta,\dot{\theta}) + G(\theta) + F(\theta,\dot{\theta}) + f_{dis} = \tau \tag{4.2}$$

where $\theta \in \mathbb{R}^7$, $\dot{\theta} \in \mathbb{R}^7$ and $\ddot{\theta} \in \mathbb{R}^7$ are, respectively, the joint's position, velocity, and acceleration vectors, $M(\theta) \in \mathbb{R}^{7\times 7}$ is the symmetric and positive definite inertia matrix, $C(\theta,\dot{\theta}) \in \mathbb{R}^{7\times 7}$ is the Coriolis and centrifugal vector, $G(\theta) \in \mathbb{R}^7$ is the gravitational vector, $\tau \in \mathbb{R}^7$ is the applied joint torque to the exoskeleton robot, and $f_{ex} \in \mathbb{R}^7$ is the external disturbances vector. Without loss of generality, the matrices of dynamic model (4.2) can be written as follows:

$$\begin{cases} M(\theta) = M_0(\theta) + \Delta M(\theta) \\ C\left(\theta,\dot{\theta}\right) = C_0\left(\theta,\dot{\theta}\right) + \Delta C\left(\theta,\dot{\theta}\right) \\ G(\theta) = G_0(\theta) + \Delta G(\theta) \end{cases} \tag{4.3}$$

where $M_0(\theta)$, $C_0\left(\theta,\dot{\theta}\right)$ and $G_0(\theta)$ are respectively the known inertia matrix, the Coriolis centrifugal matrix, and the gravity vector. $\Delta M(\theta)$, $\Delta C(\theta)$ and $\Delta G(\theta)$ are the uncertain parts.

Let us introduce a new variable such that: $\eta_1 = \theta$ and $\eta_2 = \dot{\theta}$; hence, the dynamic model expressed in (4.2) can be rewritten as follows:

$$\begin{cases} \dot{\eta}_1 = \eta_2 \\ \dot{\eta}_2 = U(t) + f(t) + H(t) \end{cases} \tag{4.4}$$

where, $U(t) = U(\eta_1)$, $H(t) = H(\eta_1, \eta_2, \dot{\eta}_2)$ and $f(t) = d\eta_1, \eta_2)$. This notation is employed to facilitate handling the control methodology with:

- $U(t) = M_0^{-1}(\theta)\,\tau$;
- $f(t) = -M_0^{-1}(\theta)\left[C_0\left(\theta,\dot{\theta}\right) + G_0(\theta)\right]$;
- $H(t) = H\left(\theta,\dot{\theta},\ddot{\theta}\right) = -M_0^{-1}(\theta)\left[f_{ex} + \Delta M(\theta)\,\ddot{\theta} + \Delta C\left(\theta,\dot{\theta}\right)\dot{\theta} + \Delta G(\theta)\right]$.

4.2.2.2 Problem formulation

From (4.2) and (4.4), it is difficult to obtain $H(t)$ due to the uncertainties of the dynamic model of the exoskeleton robot and the aforementioned unknown external effects. Consequently, to solve this dilemma, the proposition of this paper is to obtain a control input able to force the measured trajectory $\eta_d \in \mathbb{R}^7$ to track the desired trajectory even if the exoskeleton robot is under the effect of uncertain and unforeseen external disturbances. In this paper, the aforementioned desired trajectories correspond to those of passive rehabilitation protocol investigated under adaptive control. Before stating the control methodology, the properties and the assumptions that are used in this paper are given as follows:

Property 4.1: The inertia matrix $M_0(\theta)$ is symmetric and positive definite for all $\theta \in \mathbb{R}^7$ and satisfying: $\gamma_{min}(M_0(\theta))\,I_{7\times7} \leq M_0(\theta) \leq \gamma_{max}(M_0(\theta))\,I_{7\times7}$, where γ_{min} and γ_{max} are minimum and maximum eigenvalues, respectively, of the known inertia matrix and $I_{7\times7}$ is the 7×7 identity matrix. (see (Craig, 2005)).

Assumption 4.1: The joint position and joint velocity are measured.

Assumption 4.2: The desired trajectory is bounded.

Assumption 4.3: The external disturbance f_{ex} is supposed to be continuous, has finite energy and satisfies $\|f_{ex}\| \leq \vartheta$, with an unknown positive disturbance boundary ϑ.

Assumption 4.4: The variation of the unknown parameters model $H(t)$ in time is continuous with known delay t_d and globally Lipschitz function. It can be expressed as:

$$H(t) = H(t - t_d) + \varepsilon(t_d) \tag{4.5}$$

where $\varepsilon(t_d) \in \mathbb{R}^7$ is the TDR vector and t_d is a very-small time-delay constant.

4.3 Adaptive control design

In this section, the design of a tracking control that can estimate the uncertainties and unexpected disturbances and decrease its effects to achieve the desired tracking performance is described. Let us assume first that $H(t)$ is known. Let us define the position error and velocity error as follows:

$$e_1 = \eta_1 - \eta_d \tag{4.6}$$

$$e_2 = \eta_2 - \xi \tag{4.7}$$

where $\eta_d \in \mathbb{R}^7$ and $\eta_1 \in \mathbb{R}^7$ are the desired trajectory and measured trajectory, respectively. and ξ is a virtual control input to e_1.

Step 1: The time derivative of equation (4.6) is given by:

$$\dot{e}_1 = \eta_2 - \dot{\eta}_d = e_1 + \xi - \dot{\eta}_d \tag{4.8}$$

Consider the first Lyapunov function candidate as follow:

$$V_1 = \frac{1}{2} e_1^T e_1 \tag{4.9}$$

Taking time derivative of V_1 as follows:

$$\dot{V}_1 = e_1^T \dot{e}_1 = e_1^T \left(e_1 + \xi - \dot{\eta}_d \right) \tag{4.10}$$

Let $\xi = \dot{\eta}_d - k_1 e_1$, with $k_1 \in \mathbb{R}^{7\times 7}$ being a diagonal positive-definite matrix. Equation (4.10) becomes:

$$\dot{V}_1 = -e_1^T k_1 e_1 + e_1^T e_2 \tag{4.11}$$

The first term of (4.11) is stabilizing and the second term will be addressed in the next step.

Step 2: Differentiating (4.7), using (4.4), with respect to time yields:

$$\dot{e}_2 = U(t) - f(t) - H(t) - \dot{\xi} \tag{4.12}$$

where $\dot{\xi} = \ddot{\eta}_d - k_1 \dot{e}_1$. Therefore, the proposed model-based control can be given as follows:

$$\begin{aligned} U(t) &= -k_2 e_2 - e_1 + f(t) + H(t) + \dot{\xi} \\ with \;\; \tau &= M_0(\theta)\, U(t) \end{aligned} \tag{4.13}$$

with $k_2 \in \mathbb{R}^{7\times 7}$ being a diagonal positive-definite matrix.

Consider the second Lyapunov function candidate as:

$$V_2 = V_1 + \frac{1}{2} e_2^T e_2 \tag{4.14}$$

The time derivative of V_2 is given by:

$$\begin{aligned}\dot{V}_2 &= \dot{V}_1 + e_2^T \dot{e}_2 \\ &= \dot{V}_1 + e_2^T \left(U(t) - f(t) - H(t) - \dot{\xi} \right)\end{aligned} \tag{4.15}$$

Considering the model-based control law (4.13), the above equation can be written as follows:

$$\dot{V}_2 = -e_1^T k_1 e_1 - e_2^T k_2 e_2 \tag{4.16}$$

Having the following condition: $k_1 > 0$ and $k_2 > 0$, this implies that $\dot{V}_2 \leq 0$, which means that the robot system is stable.

Practically, as established, all dynamics parameters of the exoskeleton robot are not easy obtained due to the uncertainties and their variation during the robot's performance. Since $H(t)$ is uncertain, it might influence the control proposition. For now on, we will consider $H(t)$ uncertain. In such case, the model based control law (4.13) is not feasible. To overcome this problem, a new adaptive time-delay controller is proposed as:

$$\begin{aligned}U(t) &= -k_2 e_2 - e_1 + f(t) + \hat{H}(t) + \dot{\xi} \\ with \;\; \tau &= M_0(\theta)\, U(t)\end{aligned} \tag{4.17}$$

where $\hat{H}(t)$ is the estimated value of $H(t)$ obtained by the TDE approach (Youcef-Toumi and Ito, 1990).However, due to noisy measurements and nonlinearity of signals along the sampling time, a TDR, $\varepsilon(t_d)$, exists. This TDR would deteriorate the robustness and the accuracy of the robot. To overcome this problem, we proposed the following estimator:

$$\begin{aligned}\hat{H}(t) &= \hat{H}(t - t_d) + \varepsilon(t_d) - k_3 e_2 \\ \hat{H}(t) &= 0, \; \forall\, t \in [-t,\, 0]; \;\; k_3 = k\, I_{7\times 7}\end{aligned} \tag{4.18}$$

where k is a positive scalar constant and $I_{7\times7}$ is the 7×7 identity matrix. The proof of (4.18) is given in Appendix I (1). So, if **Assumptions 4.4** is verified, $\hat{H}(t-t_d)$ can be calculated using (4.4) such that (Youcef-Toumi and Ito, 1990):

$$\hat{H}(t-t_d) = U(t-t_d) - f(t-t_d) - \dot{\eta}_2(t-t_d) \tag{4.19}$$

where t_d is a very small time-delay constant. Practically, the smallest constant that can be achieved in real time is the sampling period. According to the Lipschitz condition (**Assumptions 4.4**), $\varepsilon(t_d)$ can be calculated as follows:

$$\varepsilon(t_d) = H(t) - H(t-t_d) \leq \rho t_d \tag{4.20}$$

where $\rho > 0$ is Lipschitz constant. To facilitate the proof of stability, we can write $\frac{d}{dt}\int_{t-t_d}^{t}\tilde{H}^T(w)\tilde{H}(w)dw$ as follows:

$$\frac{d}{dt}\int_{t-t_d}^{t}\tilde{H}(w)^T\tilde{H}(w)dw = \tilde{H}^T(t)\tilde{H}(t) - \tilde{H}^T(t-t_d)\tilde{H}(t-t_d) \tag{4.21}$$

where $\tilde{H}(w)$ is the estimation error of the uncertainties that will be defined latter. Additionally:

$$\frac{1}{2k}\tilde{H}(t)^T\tilde{H}(t) - \frac{1}{2k}\tilde{H}(t-t_d)^T\tilde{H}(t-t_d) = \tilde{H}^T(t)e_2 - e_2^T\frac{k_3^T}{2}e_2 \tag{4.22}$$

where $k_3^T = k_3$. The details of (4.21) and (4.22) are given in Appendix I (1).

Theorem 4.1: Consider the exoskeleton robot system (4.4)that satisfies **Assumptions (4.2–4.4)**, with the proposed adaptive TDE (4.17). If the previous conditions are verified with a bounded initial condition, the robot system (4.4) is stable and its errors e_1, e_2, and $\tilde{H}$ are bounded.

Proof: Consider the following Lyapunov function candidate:

$$V_3 = \frac{1}{2}e_1^T e_1 + \frac{1}{2}e_2^T e_2 + \frac{1}{2k}\int_{t-t_d}^{t}\tilde{H}^T(w)\tilde{H}(w)dw \tag{4.23}$$

with $\tilde{H}(t) = H(t) - \hat{H}$. The derivative of the proposed Lyapunov function with respect to time, using (4.21), is obtained as:

$$\dot{V}_3 = -e_1 k_1 e_1 + e_2^T \left(U(t) - f(t) - H(t) - \dot{\xi} \right) + \frac{1}{2k} \tilde{H}(t)^T \tilde{H}(t) - \frac{1}{2k} \tilde{H}(t - t_d)^T \tilde{H}(t - t_d) \tag{4.24}$$

Substituting the adaptive time-delay contol input (4.17) into (4.24) and using (4.22), we find:

$$\dot{V}_3 = -e_1^T k_1 e_1 - e_2^T k_2 e_2 - e_2^T \tilde{H}(t) + \tilde{H}^T(t) e_2 - e_2^T \frac{k_3^T}{2} e_2 \tag{4.25}$$

Finally, we obtain:

$$\dot{V}_3 = -e_1^T k_1 e_1 - e_2^T k_2 e_2 - e_2^T \frac{k_3^T}{2} e_2 \tag{4.26}$$

Since $k_1 > 0$, $k_2 > 0$ and $k_3 = k_3^T > 0$, this implies that $\dot{V}_3 \leq 0$, which means that the robot system is stable.

Remark 4.1: We observe that $\dot{V}_3$ is seminegative in the interval $[t - t_d, t]$, which means that V_3 is stable, but outside this interval, the stability of V_3 cannot be ensured. To guarantee the stability of V_3 in the interval $[0, \infty)$, we use the functional Lyapunov-Krasovskii theorem (Fridman, 2014).

To guarantee the asymptotic stability of the delayed system in the interval $[0, \infty)$, we propose the following Lyapunov–Krasovskii function:

$$V_4 = V_2 + \begin{cases} \sum_{i=1}^{n} \frac{1}{2k_{3i}} \int_0^t \tilde{H}_i^2(w) dw, \; t \in [0, t_{d1}) ; \\ \frac{1}{2k_{3i}} \int_{t-t_{d1}}^t \tilde{H}_i^2(w) dw + \sum_{i=2}^{n} \frac{1}{2k_{3i}} \int_0^t \tilde{H}_i^2(w) dw, \; t \in [t_{d1}, t_{d2}) ; \\ \vdots \\ \sum_{i=1}^{n-1} \frac{1}{2k_{3i}} \int_{t-t_{di}}^t \tilde{H}_i^2(w) dw + \frac{1}{2k_{3n}} \int_0^t \tilde{H}_n^2(w) dw, \; t \in [t_{dn-1}, t_{dn}) ; \\ \sum_{i=1}^{n} \frac{1}{2k_{3i}} \int_{t-t_{di}}^t \tilde{H}_i^2(w) dw, \; t \in [t_{dn}, \infty) ; \end{cases} \tag{4.27}$$

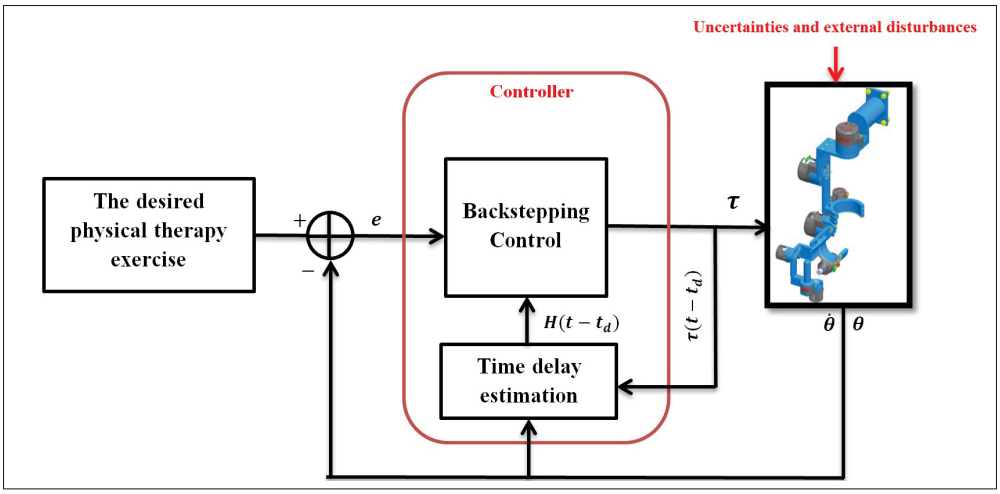

Figure 4.2 General schematic of proposed control

with:

$$V_2 = \frac{1}{2}e_1^T e_1 + \frac{1}{2}e_2^T e_2 \tag{4.28}$$

and $n = 7$. The derivative of the proposed Lyapunov–Krasovskii function with respect to time is obtained as follows:

$$\dot{V}_4 = -e_1^T k_1 e_1 - e_2^T k_2 e_2 - \frac{1}{2}\sum_{i=1}^{n} k_{3i} e_{2i}^2 \tag{4.29}$$

It is clear from (29) that $\dot{V}_4 \leq 0$, where all gains k_1, k_2, and k_3 are positive. The proof of the stability is detailed in Appendix I (2). The structure of the control scheme is shown in Figure 4.2.

4.4 Experimental and comparative study

4.4.1 Experiment Setup

Implementation was carried out on the ETS-MARSE system described in the following. The system consists of three processing units; the first is a PC, where the top-level commands are

sent to the robot using LabVIEW interface, i.e., the control scheme selection, joint or Cartesian space trajectory, gain adjustments, etc. This PC also receives the data after the robot task is executed to analyze its performance. The other two processing units are part of a National Instruments PXI platform. First is an NI-PXI 8081 controller card with an Intel Core Duo processor; in this card, the main operating system of the robot and the top-level control scheme are executed, in our case, the backstepping based controller as well as the estimation based on TDE approach, at a sampling time of 500 μs. The inverse kinematics algorithm also runs inside this control loop. Finally, at input–output level, an NI PXI-7813R remote input–output card with a field programmable gate array (FPGA) executes the low-level control; i.e., a PI current control loop (sampling time of 50 μs) to maintain the current of the motors required by the main controller. Also, in this FPGA, the position feedback via Hall-sensors (joint position), and basic input output tasks are executed. Force sensor feedback is important to accurately control the movement of the exoskeleton. A high linearity six axis force sensor [NANO17-R-1.8-M2-M1PCI, ATI industrial automation] was chosen to obtain accurate real-time force measurements for the ETS-MARSE. This sensor is mounted on the tip of the robot. The joints of the ETS-MARSE are powered by brushless dc motors (Maxon EC-45, EC-90) combined with harmonic drives [gear ratio 120:1 for motor-1, motor-2, and motor-4, and gear ratio 100:1 for motor-3 and motors (5–7)]. The diagram of the architecture of the ETS-MARSE with a healthy subject is shown in Figure 4.3.

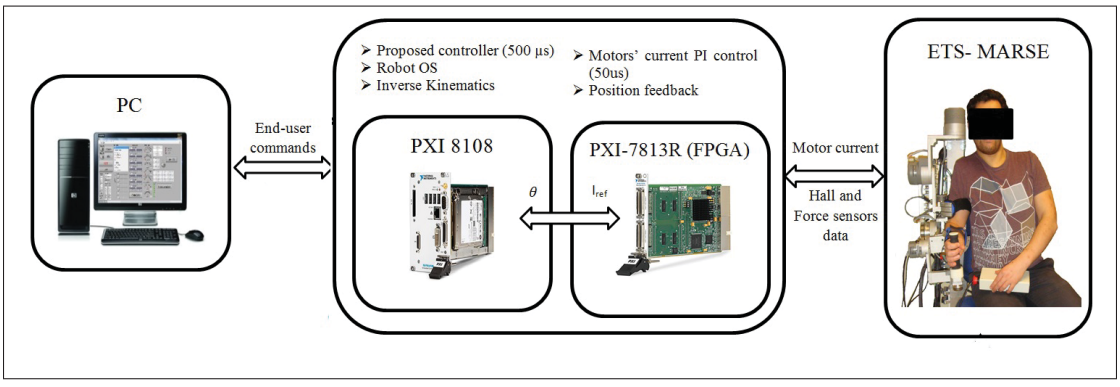

Figure 4.3 General General schematic of experiment architecture (the subject wear the ETS-MARSE robot)

The physical parameters of ETS-MARSE relative to the base reference frame are given in Table 4.3.

Table 4.3 Physical parameters of ETS-MARSE

Joints (i)	Mass (kg)	Centre of mass (m)	Link length (m)
1	3.475	0.0984	0.145
2	3.737	0.1959	0
3	0	0	0.25
4	2.066	0.163	0
5	0	0	0.267
6	0.779	0.121	0
7	0.496	0.0622	0

An experimental session was created to validate the proposed control strategy. The physical therapy tasks are performed by two different healthy subjects (mean age: 27 ± 4.6 years; mean height: 170 ± 8.75 cm; mean weight: 75 ± 18 kg). Each subject participated in a full session, under the supervision of a therapist and a control engineer. The role of the therapist is to define the range of motion of each subject and to determine a suitable exercise. During the session, the subject was ergonomically seated in a chair (height of the chair is adjustable according to the size of each subject) as shown in Figure 4.3. The experimental session was conceived in two scenarios. In the first scenario, each subject performed a basic joint physical therapy task consisting of elbow joint flexion/extension and forearm supination/pronation simultaneously, using the designed control. In this scenario, the subjects repeat the same task with a conventional approach (Khan *et al.*, 2016b) to show the feasibility of the proposed controller. In the second scenario, the proposed controller was tested using a Cartesian task described in the following section. The objective of this task is to show the tracking of the 7-DOFs of the robot in a Cartesian task. In this part, the subject also repeated the same Cartesian trajectory using the conventional controller. It is important to mention that the initial position of the robot is with the elbow joint position at 90° for all experiments, and the external disturbances here are concordantly represented by different physiological conditions of the subjects, the varying mass

of the upper limb with each subject and the TDR. The control gains were chosen arbitrarily as shown in Table (4.4).

Table 4.4 Controller parameters

Gains	Value ($i = 1:7$)
k_{1i}	15
k_{2i}	150
k_{3i}	0.12

Remark 4.2: The conventional controller (Khan *et al.*, 2016b) is characterized by its complex implementation due to the complex regressor dynamic matrix, while the robot has a high degree-of-freedom (7-DOFs).

4.4.2 Joint space tests

The experimental results of the proposed controller are illustrated in Figure 4.4. This exercise was performed with subject-1 (age: 30 years; height: 177 cm; weight: 75 kg). In this case, the speed of motion is constant ($48\circ/s$) for the two joints. We can easily see in Figure 4.4 that for the movement of all joints, the desired trajectory, represented by the red line, practically overlaps the measured trajectory, represented by the solid blue line. It is clear from the plots in Figure 4.4 that the proposed controller provides an excellent performance, where the controller has the potential to maintain stability of the system along the designed trajectory with a position error (second column of Figure 4.4) less than $1.5\circ$ for elbow joint and less than $2.0\circ$ for forearm joint. The last column of Figure 4.4 shows the control input, which is clearly smooth and without any chattering effect.

The test result of the conventional controller is given in Figure 4.5. The same subject (subject-1) repeated the task. The conventional controller has good tracking performance, where the controller preserves the stability of the robotic system. However, the proposed controller exhibits a better performance than the conventional controller does. That appears at the level of

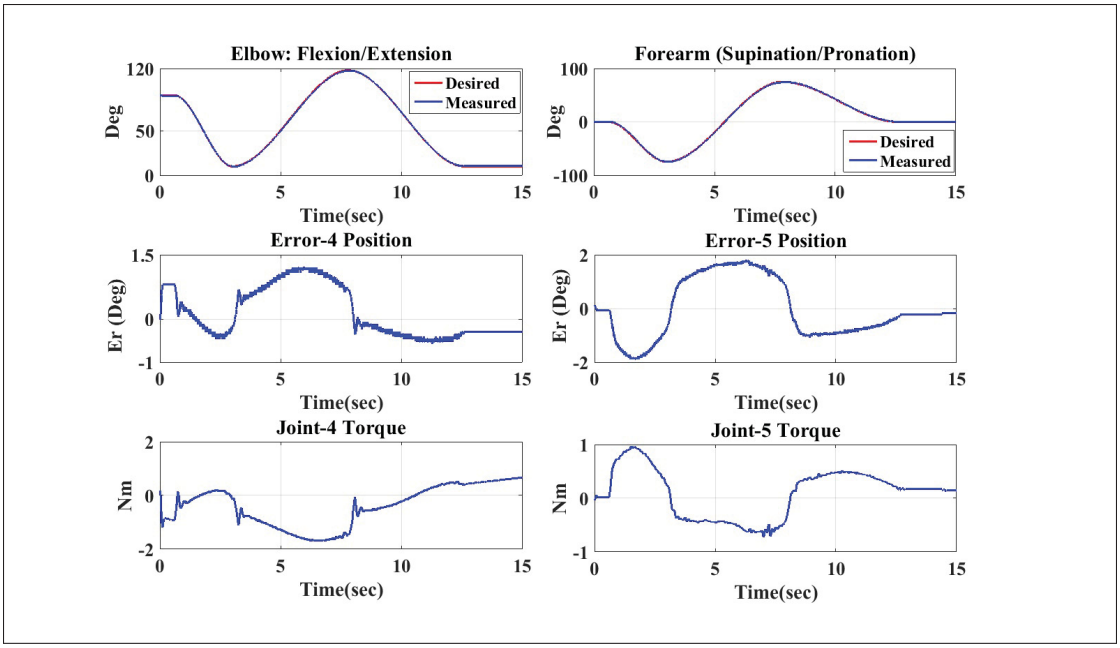

Figure 4.4 General Elbow and forearm motion, trajectory tracking in joint space using the proposed controller. Experiment was conducted with subject-1 (age: 30 years; height: 177 cm; weight: 75 kg)

tracking errors where the proposed strategy provides tracking errors smaller than the tracking errors given by the conventional approach, especially for the forearm joint.

4.4.3 Cartesian space tests

The experimental results with the ETS-MARSE robot in the Cartesian space performed by subject-2 (age: 28 years; height: 173 cm; weight: 72 kg) using the designed controller are shown in Figures 4.6–4.8; as shown in Figures 4.6(a) and (4.7), the desired trajectory (red line) nearly overlapped with the measured trajectory (green line). It can be noted that these results are very satisfactory. Figure 4.6(b) presents the Cartesian errors as functions of time.

From this figure, it is obvious that the Cartesian errors are getting smaller along the desired trajectory. Figure 4.8 shows that the control inputs are bounded without any noticeable control chattering. So, these results confirm that the control strategy is able to achieve the desired robot's performance even if the nonlinear dynamics of the exoskeleton robot is uncertain.

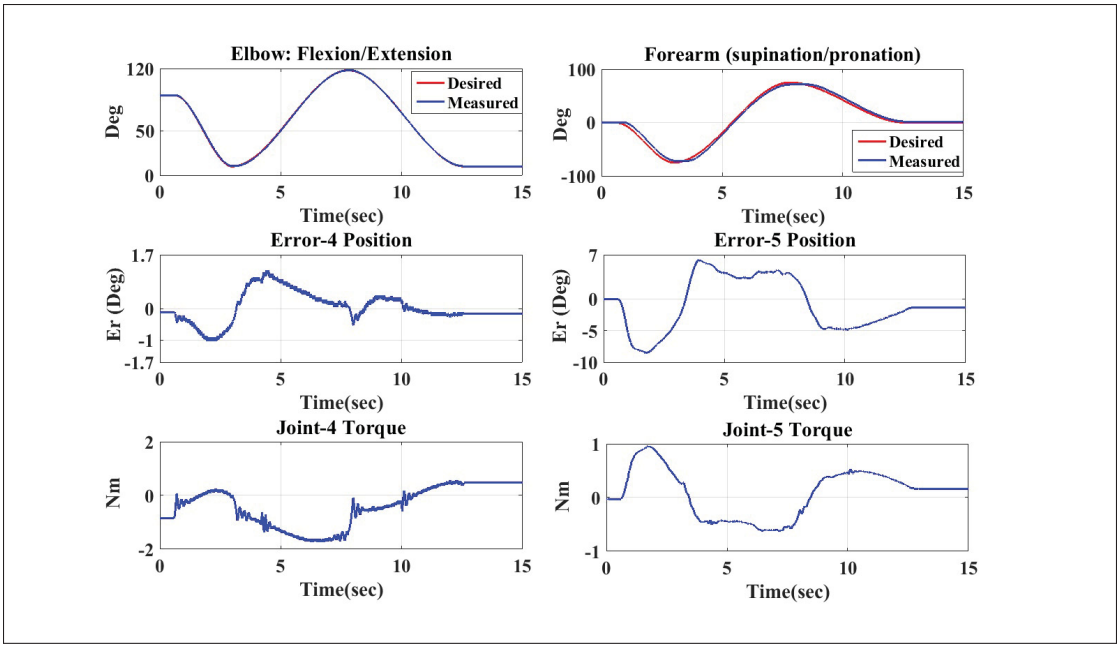

Figure 4.5 Elbow and forearm motion, trajectory tracking in joint space using the conventional approach. Experiment was conducted with subject-1 (age: 30 years; height: 177 cm; weight: 75 kg)

Figure 4.9 presents the workspace performance of the robot in the Cartesian space (red is the desired trajectory, green is the real trajectory) performed by the same subject-2 using the conventional controller.

In fact, we note from Figures 4.9 and 4.10 that the proposed controller shows a good performance where the Cartesian error [see Figure 4.9(b)] becomes smaller with time. However, the proposed strategy presents an excellent performance compared with the performance presented by the conventional approach where the tacking errors of the proposed approach seen in Figure 4.6(b) are smaller than the tracking errors provided by the classical approach [see Figure 4.9(b)].

Additionally, the control input (see Figure 4.11) presented by the conventional approach is noisier than the control input (see Figure 4.8) presented by the proposed approach. These noises may damage the motors of the robot. From the comparison of the two experimental

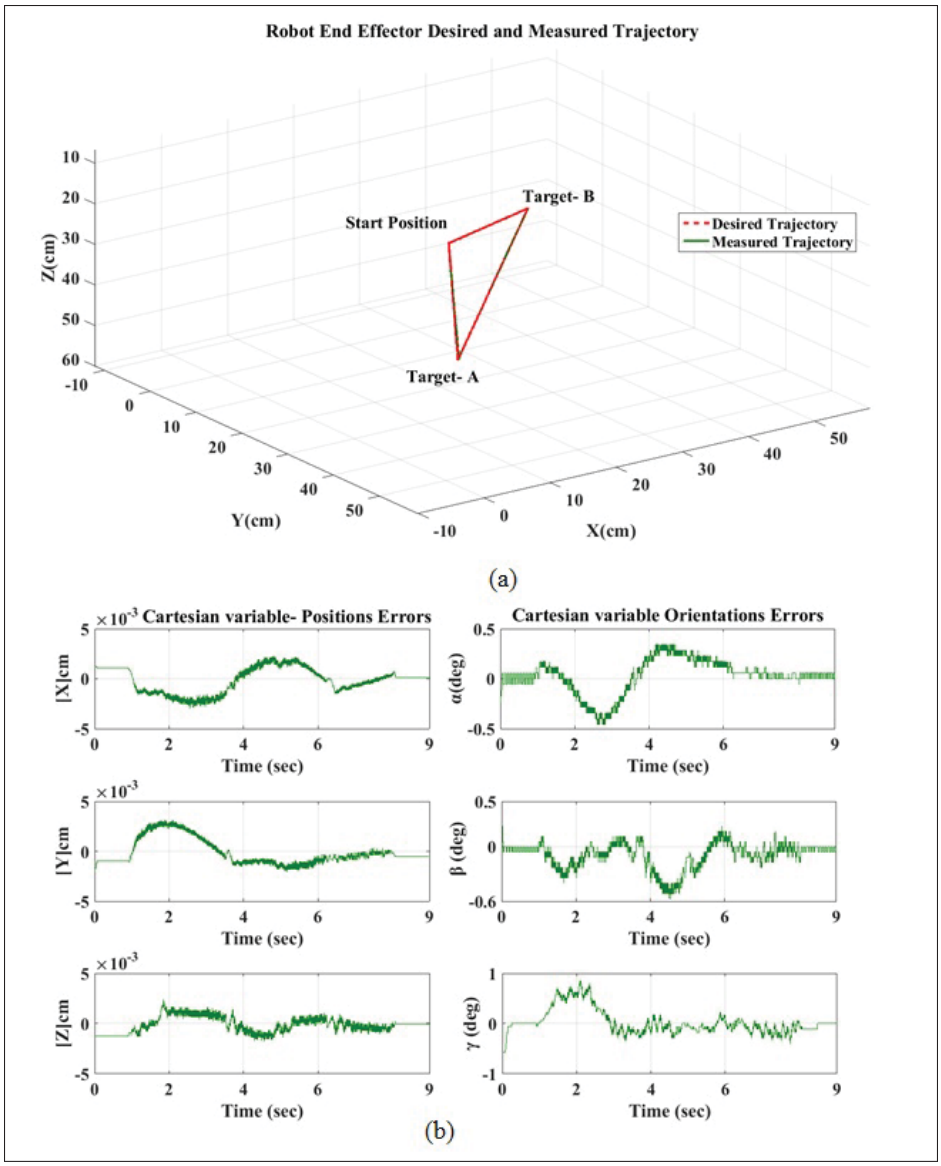

Figure 4.6 (a) Reaching movement exercise, Cartesian trajectory tracking in three-dimensional (3-D) space using the proposed controller. (b) Cartesian trajectory tracking error along X-axis, Y-axis, and Zaxis. Experiments was conducted with subject-2 (age: 28 years; height: 173 cm; weight: 72 kg)

scenarios, we can conclude that the proposed strategy provides a high level of precision and robustness against the nonlinear dynamic uncertainties and unknown disturbances.

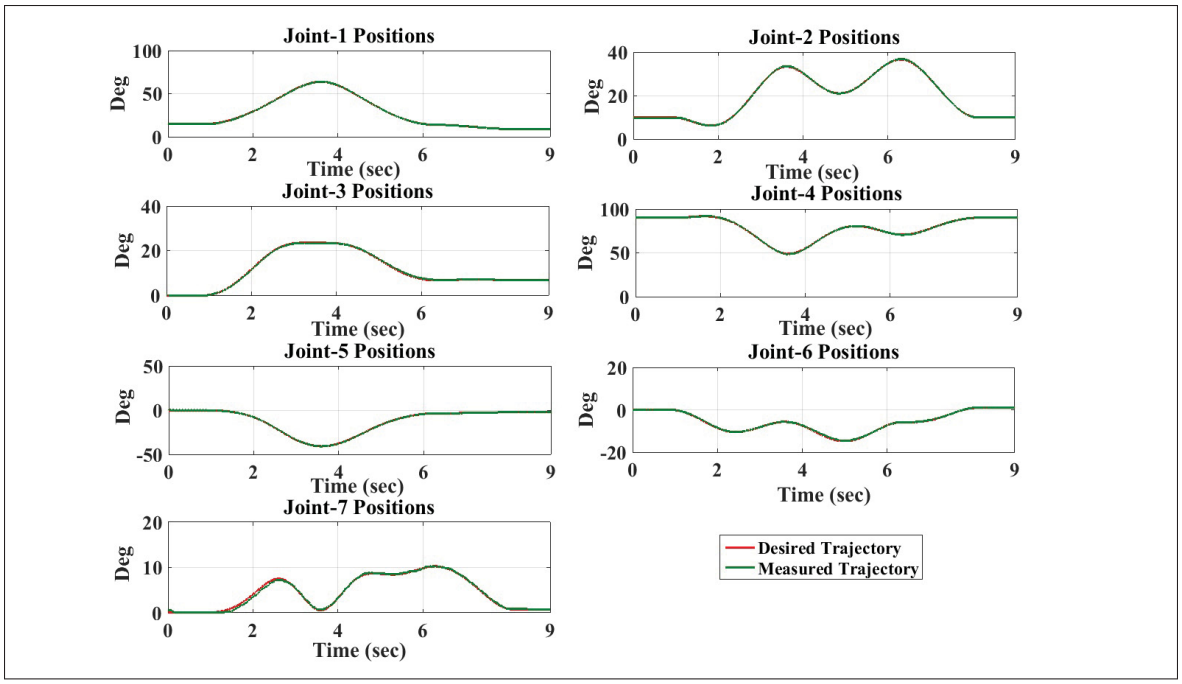

Figure 4.7 Tracking performance of ETS-MARSE in joint space corresponds to Cartesian tasks using the proposed controller

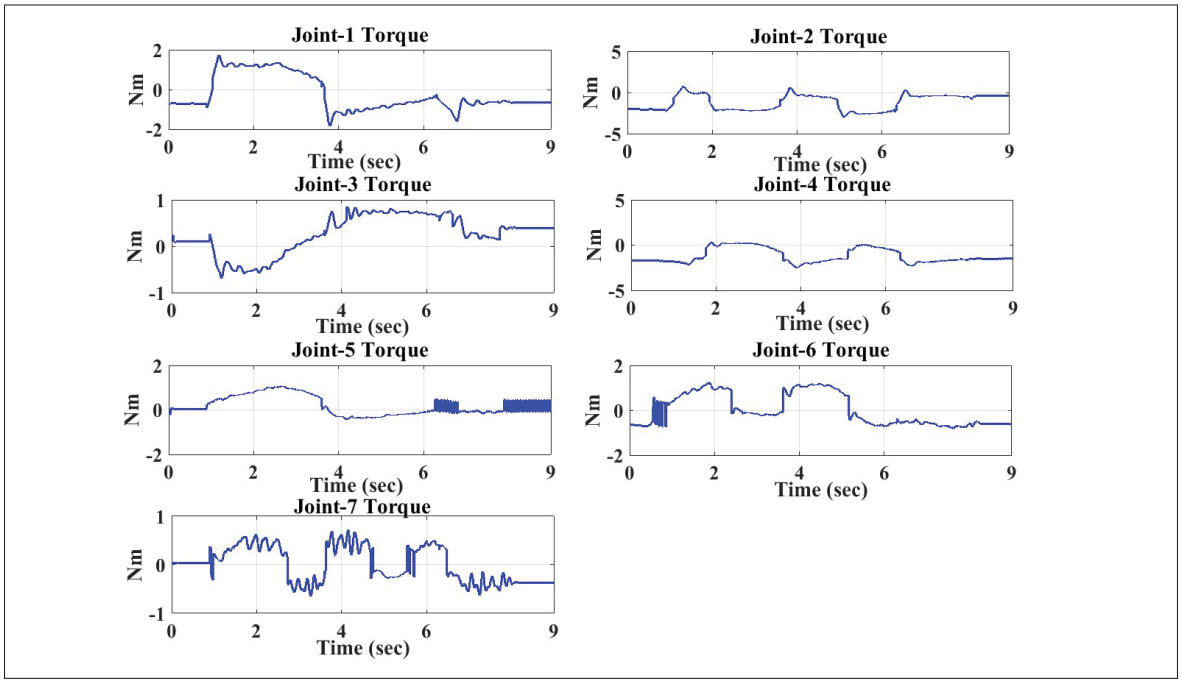

Figure 4.8 Control input the proposed controller

4.5 Conclusion

In this paper, we have proposed an adaptive control of exoskeleton robots with an unknown parameters model based on a backstepping controller. A new time-delay approach is proposed to estimate the uncertain part of the exoskeleton robot and bounded external disturbances where the TDR, friction forces, backlash, and different upper-limb's mass of each subject are taken into consideration to improve the robot performance. The main advantage of the proposed adaptive control law is that accurate estimation of robots' dynamic model is not needed. The output of the time-delay estimator is added directly to the control input through a feed-forward loop, whereby the control scheme provides a highly accurate tracking of the desired performance, robust to the uncertainties and unexpected bounded external forces, and flexible with variations in parameters.

The stability analysis of the proposed control technique with a Lyapunov–Krasovskii function was presented. The robustness of the proposed controller was realized by maneuvering the ETS-MARSE to provide both joint-based and end-effector based rehabilitation exercise to the different subjects. The experimental results demonstrate the excellent performance of the proposed controller compared with the conventional controller.

In future work, we seek to overcome the limitations of this approach, in particular, the value of delayed acceleration for the controller, where the estimation of this variable may deteriorate the accuracy of the controller.

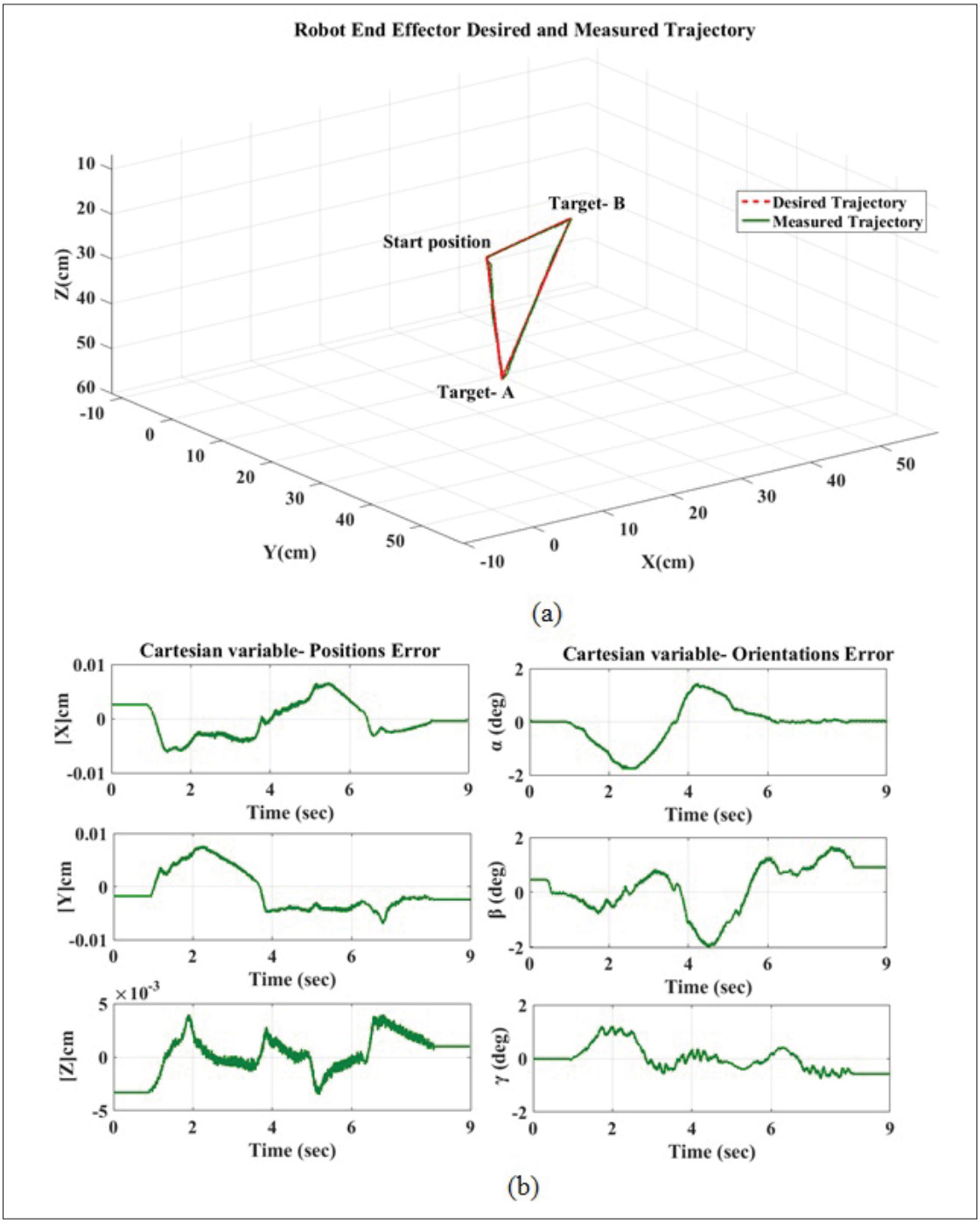

Figure 4.9 (a) Reaching movement exercise, Cartesian trajectory tracking in 3-D space using the conventional controller. (b) Cartesian trajectory tracking error along X-axis, Y-axis, and Z-axis. Experiments was conducted with subject-2 (age: 28 years; height: 173 cm; weight: 72 kg)

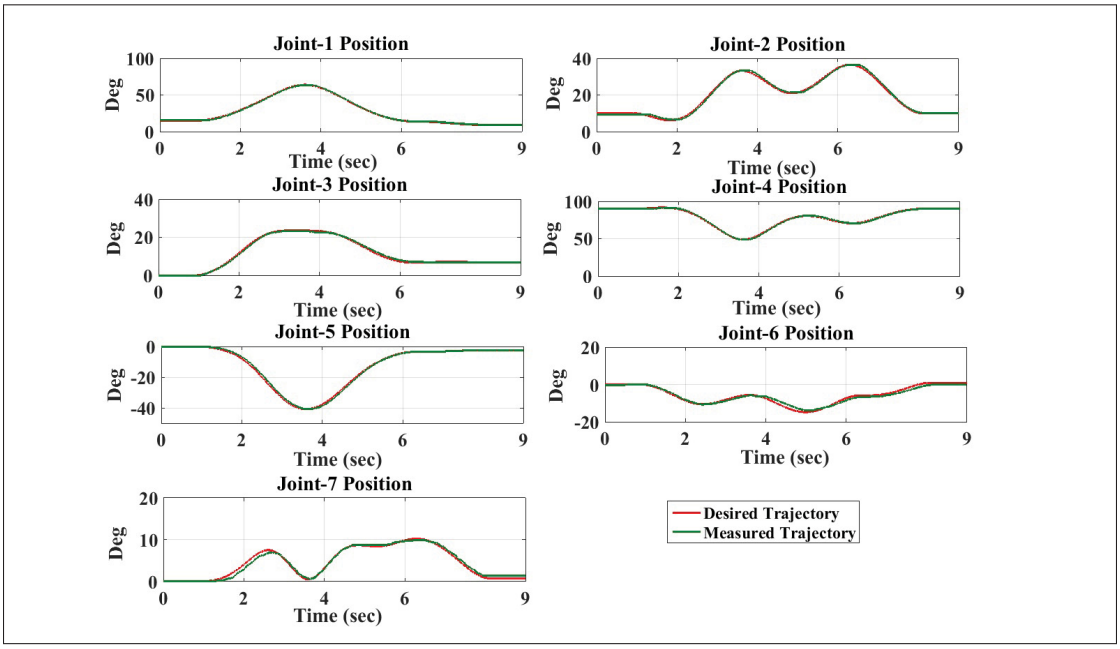

Figure 4.10 Tracking performance of ETS-MARSE in joint space corresponds to Cartesian tasks using the conventional controller

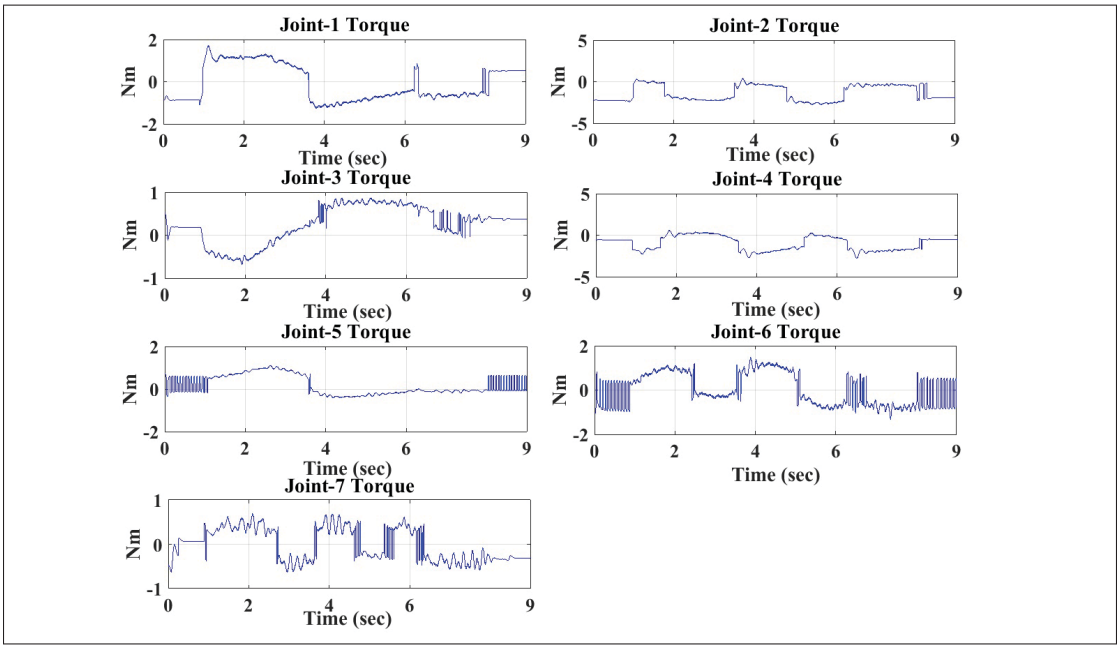

Figure 4.11 Control inputs corresponds to Cartesian tasks using the conventional controller

CHAPTER 5

PASSIVE AND ACTIVE REHABILITATION CONTROL OF HUMAN UPPER-LIMB EXOSKELETON ROBOT WITH DYNAMIC UNCERTAINTIES

Brahim Brahmi[1], Maarouf Saad[1], Cristobal Ochoa Luna [1] Mohammad H. Rahman[2] and Philippe S. Archambault[3]

[1] Département of Electrical Engineering, École de Technologie Supérieure, 1100 Notre-Dame Ouest, Montréal, Québec, Canada H3C 1K3
[2] Mechanical/Biomedical Engineering Department,University of Wisconsin-Milwaukee, 3200 N. Cramer Street, Milwaukee, WI 53211,
[3] School of Physical and Occupational Therapy, McGill University; Centre for Interdisciplinary Research in Rehabilitation of Greater Montreal, Montréal, Québec, Canada,

Paper published in *Robotica*, August 2018

Abstract

This paper investigates the passive and active control strategies to provide a physical assistance and rehabilitation by a 7-DOF exoskeleton robot with nonlinear uncertain dynamics and unknown bounded external disturbances due to the robot user's physiological characteristics. An Integral backstepping controller incorporated with Time Delay Estimation (BITDE) is used, which permits the exoskeleton robot to achieve the desired performance of working under the mentioned uncertainties constraints. The Time Delay Estimation (TDE) is employed to estimate the nonlinear uncertain dynamics of the robot and the unknown disturbances. To overcome the limitation of the time delay error inherent of the TDE approach, a recursive algorithm is used to further reduce its effect. The integral action is employed to decrease the impact of the unmodeled dynamics. Besides, The Damped Least Square method is introduced to estimate the desired movement intention of the subject with the objective to provide active rehabilitation. The controller scheme is to ensure that the robot system performs passive and active rehabilitation exercises with a high level of tracking accuracy and robustness, despite the unknown dynamics of the exoskeleton robot and the presence of unknown bounded disturbances. The design, stability and convergence analysis are formulated and proven based on

the Lyapunov–Krasovskii functional theory. Experimental results with healthy subjects, using a virtual environment, show the feasibility and ease of implementation of the control scheme. Its robustness and flexibility to deal with parameter variations due to the unknown external disturbances are also shown.

Keywords: Backstepping integral control, Time delay Estimation, Passive and active rehabilitation; Time Delay Error.

5.1 Introduction

Neurological diseases have become a challenging problem for the scientific community, as confirmed by the statistics of World Health Organization (WHO). Each year, at least 15 million people worldwide suffer from neurological diseases such as strokes (Sidney *et al.*, 2013). Among them, six million die and five million more are living with a permanent disability (Sidney *et al.*, 2013). The consequences of a stroke can vary from mild to very severe depending on the nature of the stroke, the injured region of the brain, and the degree of damage (De Morand, 2014). Usually, the stroke survivors do not have the means of performing daily-life activities independently, such as eating or dressing, due to permanent disability, frequently on one side of the body (De Morand, 2014). This weakness can generate various physical and psychological problems for the stroke victims.

Rehabilitation programs have proven clinically effective. This treatment is able to support people with stroke to recover their inadequate functional capacity, benefit from the acquisition of new skills, and improve their quality of life. However, these programs need intensive and heavy effort by the therapist (Xie *et al.*, 2016). New devices such as exoskeleton robots, help overcome the limitations of conventional physiotherapy, attracting much attention from the scientific community (Xie *et al.*, 2016). The main benefit of the rehabilitation robots is their ability to provide intensive physiotherapy for the required periods. Another important point is that these robots provide numerous data that allow the physiotherapist to accurately assess the subject's performance (Xie *et al.*, 2016). However, a major aspect is that the design of

this kind of robot must be harmonious with the human anatomy biomechanics. For this reason and to provide a modern rehabilitation treatment for the upper limb, we have developed an exoskeleton robot named ETS-MARSE (Motion Assistive Robotic-Exoskeleton for Superior Extremity) (Brahim *et al.*, 2016a,b; Rahman *et al.*, 2015, 2013). This robot is compatible with the human arm configuration and can perform various rehabilitation movements and assistive tasks. All the originality of the designed robot is summarized in (Rahman *et al.*, 2015, 2013).

One of the main goals of the control system applied to these robots is to make the exoskeleton robot perform the human-like motion. However, these robots are characterized by highly nonlinear dynamics due to their complicated mechanical construction and hard nonlinearities (Brahim *et al.*, 2017) (such as nonlinear friction forces, backlash, etc.). Furthermore, the synergy between the human and the exoskeleton makes the robot subject to external and unknown disturbances due to different physiological conditions of the subjects. These conditions include non-linear biomechanical characteristics of the musculoskeletal system, the varying weights of the upper-limb for each subject, the presence of spasticity in neurological subjects, etc (Brahim *et al.*, 2017). During a rehabilitation session, the uncertain nonlinear dynamic model and the external disturbances can turn into an unknown function that can deteriorate the robot's performance (Brahim *et al.*, 2016a,b). In such a case, we need to design a robust controller that provides the system with more flexibility and robustness to deal with these problematic characteristics.

Numerous nonlinear control systems have been designed to overcome the effect of the uncertain nonlinear dynamics and unexpected external disturbances, which influence the robot performance, e.g. conventional adaptive control (Slotine *et al.*, 1991), H_∞ control (Rigatos *et al.*, 2018) and sliding mode control (Slotine *et al.*, 1991; Khalil and Grizzle, 1996; Young *et al.*, 1999). Actually, sliding mode control (SMC) is considered one of the most robust nonlinear controllers developed to control uncertain dynamics. This control is fundamentally based on a larger high-gain switching controller which pushes the system trajectory to converge to the selected sliding surface (Fridman, 1999). Nevertheless, the high-activity switching gain causes a "chattering" problem (Fridman, 1999) which can damage the actuators of the robot. Another

successful nonlinear technique, which has been used to control a robot system with a complex dynamic model, is backstepping control (Slotine *et al.*, 1991; Khalil and Grizzle, 1996; Brahmi *et al.*, 2017c). Backstepping control is characterized by a recursive Lyapunov scheme and a virtual control input, which ensures the stability of the control system. Despite the highly accurate trajectory tracking provided by this approach, backstepping control is very sensitive to the uncertain dynamics and unknown external disturbances (Slotine *et al.*, 1991; Khalil and Grizzle, 1996). Various strategies have been combined with backstepping to improve its robustness against the effect of the nonlinear uncertain dynamics and external disturbances. For example, a conventional adaptive backstepping control was developed in (Zhou and Wen, 2008), assuming that the dynamic model of the manipulator is linear in a set of physical parameters. However, the hard nonlinearities of the manipulator's dynamic model make the system sensitive to even small disturbances. To overcome this problem, numerous approaches combine backstepping control with fuzzy logic, neural networks, or both (Chen *et al.*, 2015; Li *et al.*, 2017a, 2015a; Yoo and Ham, 2000). However, these strategies need heavy computations that make the implementation very complex. Time delay estimation (TDE) approach may be considered to compensate the uncertainties (Youcef-Toumi and Ito, 1990; Brahmi *et al.*, 2017a,b). The TDE has been implemented in many robotic systems with consistently good performance (Youcef-Toumi and Ito, 1990; Jin *et al.*, 2015; Kim *et al.*, 2016; Karafyllis *et al.*, 2016). TDE utilizes the previous response of the robot system and the previous control input to provide new control actions. However, due to noisy measurements and nonlinearity of signals along the sampling time, a time delay error (TDR) exists, which would deteriorate the robustness and the accuracy of the robot. To the best of our knowledge, no one has proposed a methodic solution to eliminate the influence of this error.

In order to address the mentioned problems, a solution is proposed in this paper by combining a nonlinear integral backstepping control (BI) (Skjetne and Fossen, 2004; Tan *et al.*, 2000) and a time delay estimation (TDE) to estimate the hard nonlinearity of the system introduced by the uncertain nonlinear dynamics and unknown disturbances. TDR is taken into consideration by estimating its value with a recursive estimator. This latter is an intensive or repeating

action used to turn down the influence of this error on the accuracy of the estimation. The integral control provides a progressive change to reduce the unmodeled error and improve the robustness of the proposed control against the dynamic uncertainties. The structure of the designed nonlinear Backstepping Integral control based on Time Delay Control (BITDC) aims to provide a high-level of robustness and accuracy without any sensitivity to uncertain nonlinear dynamics and unexpected disturbances. This will make the exoskeleton robot perform a smooth movement, similar to the natural human movement, and will supply the control system more flexibility to handle the uncertainties and parameters' variation. The stability of the robot system and the convergence of its errors are formulated and demonstrated based on Lyapunov–Krasovskii functional theory. Moreover, the proposed strategy is characterized as an easy implementation. The efficiency and the robustness of the proposed approach are validated with Cartesian trajectory tracking corresponding to passive physical therapy tasks.

The proposed strategy is not limited to perform the passive rehabilitation but also qualified to perform the active rehabilitation. To complete this protocol, we necessarily rely on the estimation of the Desired Movement Intention (DMI) of the subject using indirect force control. This latter is done by Damped Least Square method (DLS), which has been successfully used in multiple applications (Luo *et al.*, 2013; Liu *et al.*, 2015; Gauthier *et al.*, 2016). The DLS approach aims to provide a compromise between robustness of the solution and accuracy of the robot's performance. Besides, the proposed control is evaluated with healthy subjects using the virtual environment as an interface (Levant, 2003). This latter is a highly attractive tool, contributing numerous benefits. It authorized the creation of immersive and interactive scenes where the oriented task can be introduced in the form of earnest games (Weiss *et al.*, 2014). This interface also helps in stimulation of the subjects and visualizes the performed tasks. This interface permits us to record the performance data of the patient to evaluate accurately his improvement and benefit from its flexibility to adjust the designed functional movement to the requirement of the patient (Weiss *et al.*, 2014). The comparative study with the conventional approach shows the accuracy, robustness and flexibility of the proposed controller to deal with unknown dynamics, external disturbances, and parameters variations.

The outline of the paper is organized as follows. The kinematics and dynamics of the robot are presented in the next section. The control scheme is described in section 5.3. Experimental and comparison results are shown in section 5.4. Finally, the conclusion is presented in section 5.5.

5.2 Description of kinematics and dynamics of ETS-MARSE robot

5.2.1 Exoskeleton robot development

The developed exoskeleton robot ETS-MARSE is a redundant robot consisting of seven DOFs, as shown in Figure 5.1. It was created to provide physical therapy and assisted motion to the injured upper limb. The idea of the designed exoskeleton is basically extracted from the anatomy of the upper limb of the human, to be ergonomic for the user along with the physical therapy session. The shoulder part consists of three joints; the elbow part comprises one joint, and the wrist part consists of three joints. Each part is responsible for performing a variety of upper-limb motions, as shown in Table (5.2). The design of the ETS-MARSE has special features compared with the existing exoskeleton robots. Among them, it has a comparatively low weight, an excellent power/weight ratio, can be easily fitted or removed, and is capable of adequately compensating for gravity. A new power carrying mechanism was included for supporting the shoulder joint internal/external rotation and for forearm pronation/supination. This robot can be used with a wide range of subjects, due to the length of its adjustable links. This exoskeleton can perform passive (completely support and perform the motion on the subjects' upper limb) and active assistive motion (respond to force, electromyography, and /or be compliant with the subject to accompany and assist him/her in the intended motion). All special characteristics and contribution features of the ETS-MARSE and comparison with similar existing exoskeleton robots are summarized in (Rahman *et al.*, 2015, 2013; Luna *et al.*, 2016; Rahman *et al.*, 2011b).

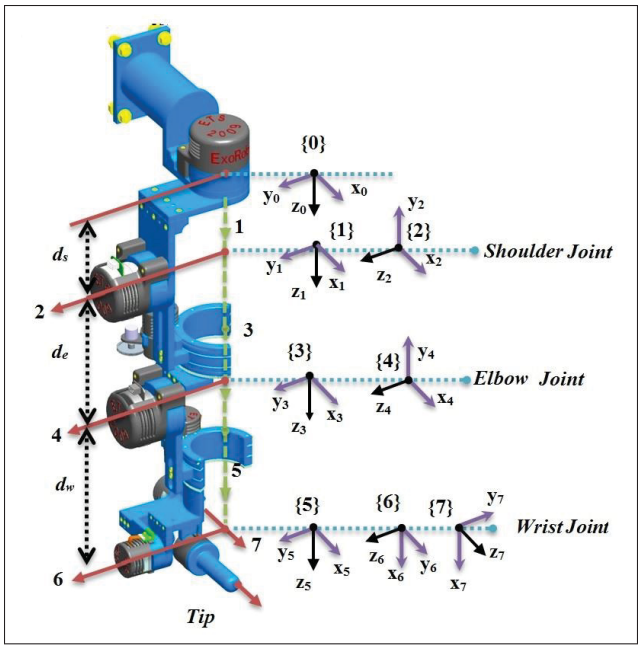

Figure 5.1 Reference frames of ETS-MARSE

5.2.2 Kinematics of ETS-MARSE Robot

The transformation from Cartesian space to joint space is done by a non-linear function named the Jacobian matrix ($J(\theta) \in \mathbb{R}^{6\times7}$ which links the end-effector Cartesian velocities to the joints angular velocity vector $J(\theta)\dot{\theta}$ 35, 36. In order to maneuver the exoskeleton in Cartesian space, we used the inverse Jacobian matrix method, since the proposed control is executed in the joint space. Due to the redundant nature of the ETS-MARSE robot where its Jacobian matrix is not quadratic, the inverse kinematics can be solved using the pseudo-inverse of the Jacobian, which can be expressed as follows (Siciliano *et al.*, 2009):

$$\begin{cases} \ddot{\theta}_d = J^{+}\ddot{x}_d - J^{+}\dot{J}J^{+}\dot{x}_d \\ \dot{\theta}_d = J^{+}\dot{x}_d \end{cases} \tag{5.1}$$

where $x_d \in \mathbb{R}^{6\times1}$, $\dot{x}_d \in \mathbb{R}^{6\times1}$ and $\ddot{x}_d \in \mathbb{R}^{6\times1}$ are the desired Cartesian position/orientation, velocity and acceleration vectors, respectively. $\ddot{\theta}_d$, $\dot{\theta}_d \in \mathbb{R}^{7\times1}$ are the calculated joint acceleration and velocity respectively, and $\left(J^T(JJ^T)^{-1}\right)$ is pseudo-inverse generalized (Siciliano *et al.*,

2009). The proposed joint-space based control in this paper does not need a Jacobian matrix or inversion of a Jacobian matrix, as for a Cartesian space-based controller. The role of the Jacobian matrix and its inverse here is the generation of the desired rehabilitation trajectory. Hence, the singularity is not an issue in this case (Rahman *et al.*, 2011b). Moreover, the singularities of the exoskeleton robot are known to us; they will appear when the ETS-MARSE is straight down ($\theta_2 = 0^\circ$, and/or $\theta_4 = 0^\circ$, and/or $\theta_2 = -90^\circ$). As well, a singularity will happen when the axes of rotation of joint-1 (Z1), and joint-3 (Z3), and/or joint-5 (Z5), and/or joint-7 (Z7) are aligned with each other (Rahman *et al.*, 2011b). By knowing these cases, we can easily define the trajectory by avoiding all kinematics singularities. More details about the singularities of ETS-MARSE can be found in (Rahman *et al.*, 2011b).

Table 5.1 Modified Denavit-Hartenberg parameters

joint (i)	α_{i-1}	a_{i-1}	d_i	θ_i
1	0	0	d_s	θ_1
2	$\frac{-\pi}{2}$	0	0	θ_2
3	$\frac{\pi}{2}$	0	d_e	θ_3
4	$\frac{-\pi}{2}$	0	0	θ_4
5	$\frac{\pi}{2}$	0	d_w	θ_5
6	$\frac{-\pi}{2}$	0	0	$\theta_6 - \frac{\pi}{2}$
7	$\frac{-\pi}{2}$	0	0	θ_7

The modified Denavit–Hartenberg (DH) parameters (Craig, 2005) are given in Table (5.1). These parameters are obtained from the reference frames shown in Figure 5.1 and are used to obtain the homogeneous transformation matrices. The workspace of the designed robot is given in Table (5.2). The details of the parameters and design of ETS- MARSE are given in (Rahman *et al.*, 2015).

Table 5.2 Workspace ETS-MARSE

joint (i)	Motion	Workspace
1	Shoulder joint horizontal flexion/extension	$0°/140°$
2	Shoulder joint vertical flexion/extension	$140°/0°$
3	Shoulder joint internal/external rotation	$-85°/75°$
4	Elbow joint flexion/extension	$120°/0°$
5	Forearm joint pronation/supination	$-85°/85°$
6	Wrist joint ulnar/radial deviation	$-30°/20°$
7	Wrist joint flexion/extension	$-50°/60°$

5.2.2.1 Dynamics of the ETS-MARSE Robot

The dynamics behavior of ETS-MARSE is given by the following expression using the Lagrangian approach (Craig, 2005):

$$M(\theta)\ddot{\theta} + C(\theta,\dot{\theta}) + G(\theta) + f_{dis} = \tau \tag{5.2}$$

where $\theta \in \mathbb{R}^7$, $\dot{\theta} \in \mathbb{R}^7$ and $\ddot{\theta} \in \mathbb{R}^7$ are, respectively, the joint's position, velocity, and acceleration vectors, $M(\theta) \in \mathbb{R}^{7\times7}$ is the symmetric and positive definite inertia matrix, $C(\theta,\dot{\theta}) \in \mathbb{R}^{7\times7}$ is the Coriolis and centrifugal vector, $G(\theta) \in \mathbb{R}^7$ is the gravitational vector, $\tau \in \mathbb{R}^7$ is the applied joint torque to the exoskeleton robot, and $f_{ex} \in \mathbb{R}^7$ is the external disturbances vector. Without loss of generality, the matrices of dynamic model (5.2) can be written as follows:

$$\begin{cases} M(\theta) = M_0(\theta) + \Delta M(\theta) \\ C\left(\theta,\dot{\theta}\right) = C_0\left(\theta,\dot{\theta}\right) + \Delta C\left(\theta,\dot{\theta}\right) \\ G(\theta) = G_0(\theta) + \Delta G(\theta) \end{cases} \tag{5.3}$$

where $M_0(\theta)$, $C_0\left(\theta,\dot{\theta}\right)$ and $G_0(\theta)$ are respectively the known inertia matrix, the Coriolis centrifugal matrix, and the gravity vector. $\Delta M(\theta)$, $\Delta C(\theta)$ and $\Delta G(\theta)$ are the uncertain parts.

Let us introduce a new variable such that: $\eta_1 = \theta$ and $\eta_2 = \dot{\theta}$; hence, the dynamic model expressed in (5.2) can be rewritten as follows:

$$\begin{cases} \dot{\eta}_1 = \eta_2 \\ \dot{\eta}_2 = U(t) + f(t) + H(t) \end{cases} \tag{5.4}$$

where, $U(t) = U(\eta_1)$, $H(t) = H(\eta_1, \eta_2, \dot{\eta}_2)$ and $f(t) = d\eta_1, \eta_2)$. This notation is used for easier handling the control scheme with:

- $U(t) = M_0^{-1}(\theta)\,\tau(t)$;
- $f(t) = M_0^{-1}(\theta)\left[-C_0\left(\theta, \dot{\theta}\right) - G_0(\theta)\right]$;
- $H(t) = H\left(\theta, \dot{\theta}, \ddot{\theta}\right) = M_0^{-1}(\theta)\left[-f_{ex} - \Delta M(\theta)\,\ddot{\theta} - \Delta C\left(\theta, \dot{\theta}\right)\dot{\theta} - \Delta G(\theta)\right]$.

5.2.2.2 Problem formulation

One of the main research objectives on this type of robots is to design a controller able to make the human-exoskeleton system achieve passive/active physical therapy movement. This should be performed without accurate information about the dynamics of the robotic system while ensuring a smooth movement similar to natural human motion. Therefore, the designed control scheme should ensure that the measured joint position $\eta_1 \in \mathbb{R}^7$ of the exoskeleton robot tracks the desired trajectory $\eta_d \in \mathbb{R}^7$. Before presenting the control design methodology, we state the properties and the assumptions used in this paper: $\eta_d \in \mathbb{R}^7$

Property 5.1: The known part of inertia matrix $M_0(\theta)$ is symmetric and positive definite for all $\theta \in \mathbb{R}^7$ and satisfying: $\gamma_{min}(M_0(\theta))\, I_{7\times7} \leq M_0(\theta) \leq \gamma_{max}(M_0(\theta))\, I_{7\times7}$, where γ_{min} and γ_{max} are minimum and maximum eigenvalues, respectively, of the known inertia matrix and $I_{7\times7}$ is identity matrix (Spong *et al.*, 2006b).

Assumption 5.1: The joint' positions are measured and the corresponding velocities are found from the filtered positions.

Assumption 5.2: The function $H(t)$ is globally Lipschitz function.

Assumption 5.3: The variation of the uncertainties parameters $H(t)$ in time is continuous and bounded with known delay t_d. It can be written as:

$$H(t) = H(t - t_d) + \varepsilon(t) \tag{5.5}$$

where $\varepsilon(t)$ is a vector of the delay error of uncertainties variation and t_d is the sampling time period.

Assumption 5.4: The desired trajectory is bounded.

Assumption 5.5: The Jacobian matrix $J(\eta_1)$ is known and non-singular in a finite workspace

Assumption 5.6: The external disturbance f_{ex} is supposed to be continuous, has finite energy and satisfies $\|f_{ex}\| \leq \vartheta$, with an unknown positive disturbance boundary ϑ.

5.3 Control design

In this section, we seek to design the control that is capable of performing both passive and active rehabilitation movements. Passive rehabilitation mode can be achieved by position control. In such case, the exoskeleton performs a predesigned task. On the other hand, the active assistive motion is achieved by the force exerted by the subject on the tip of the robot (wrist joint) and measured by a force sensor. This force is effective to produce some displacement. In our case, we estimate the desired motion intention of the subject from the measured force using Damped Least Square method (DLS).

5.3.1 Estimation of the Desired Motion Intention (DMI)

This section provides a summary of the estimation method of the Desired Movement Intention (DMI). Let us start with the definition of the desired trajectory in the active assistive motion.

In this protocol, the desired trajectory is updated as follows (Ochoa Luna *et al.*, 2015):

$$\eta_d = \eta_1 + \Delta\eta_d \tag{5.6}$$

where $\eta_1 \in \mathbb{R}^7$ is the measured joint position, and $\Delta\eta_d \in \mathbb{R}^7$ is the estimated of DMI where this quantity of movement is estimated from the measured user's force. If $\Delta\eta_d \longrightarrow 0$, this means that the exoskeleton's wearer stops exercising forces on the force sensor, making the exoskeleton to decrease its motion and progressively, and whenever $\eta_d = \eta_1$, the exoskeleton rests in its most recent position. With this mode, the exoskeleton is permitted to catch the user's DMI, while the adaptive tracking control ensures an accurate compensation of the robot dynamic uncertainties and the unexpected bounded disturbances submitted to the robot. Let us now estimate the desired movement intention $\Delta\eta_d$ from the user's force, we can use the following equation:

$$F_m = J(\eta_1) + \Delta\eta_d \tag{5.7}$$

where $F_m \in \Re^6$ is the measured user's force,. To solve the equation (5.7), we used Damped Least Squares (DLS) or Levenberg-Marquardt stabilization (Lawson and Hanson, 1995). This approach was originally employed for avoiding the singularity of inverse kinematics solution (Wampler, 1986; Nakamura and Hanafusa, 1986). Rather than merely obtaining the minimum vector $\Delta\eta_d$ that provides the best solution to equation (5.7), we determine the value of $\Delta\eta_d$ that minimizes the quantity

$$\min_{\Delta\eta_d} \|J(\eta)\Delta\eta_d - F_m\|^2 + \lambda^2 \|\Delta\theta_d\|^2 \tag{5.8}$$

where $0 < \lambda < 1$ is the damping factor and can be determined to be positive depending upon the accurate estimation specifications. Since the sum of equation (5.8) can be written as:

$$\left\| \begin{bmatrix} J(\theta) \\ \lambda I_{6\times 6} \end{bmatrix} \Delta\eta_d - \begin{bmatrix} F_m \\ 0 \end{bmatrix} \right\|^2 \tag{5.9}$$

Consequently, the DLS solution is:

$$\Delta\eta_d = J^T \left(JJ^T + \lambda^2 I_{6\times 6}\right)^{-1} F_m \tag{5.10}$$

Remark 5.1: The desired trajectory is the input of the proposed controller that will be detailed in the following subsection. Where, in active mode, the desired trajectory is updated by equation (5.6), while in passive mode, the desired trajectory is predefined by a therapist.

5.3.2 Control algorithm

This section presents the proposed tracking control based on the Backstepping integral control that can be expressed as follows: *Step 1*: Let us define the position error as follows:

$$e(t) = \eta_1 - \eta_d \tag{5.11}$$

where $\eta_d \in \mathbb{R}^7$ and $\eta_1 \in \mathbb{R}^7$ are the desired trajectory and measured trajectory, respectively. Now, we can choose the regulated errors variables as follows:

$$e_1 = \eta_1 - \eta_d + \Gamma \int_0^t e\, dt \tag{5.12}$$

$$e_2 = \eta_2 - \xi \tag{5.13}$$

where $\Gamma \in \mathbb{R}^{7\times 7}$ is a diagonal positive-definite matrix, and ξ is a virtual control input chosen as follows:

$$\xi = \dot{\eta}_d - \Gamma\, e - k_1 e_1 \tag{5.14}$$

where $k_1 \in \mathbb{R}^{7\times 7}$ is a diagonal positive-definite matrix. The derivative of the virtual control input (5.14) is: $\dot{\xi} = \ddot{\eta}_d - \Gamma\, \dot{e} - k_1 \dot{e}_1$.

The time derivative of equation (5.12) is given by:

$$\dot{e}_1 = \eta_2 - \dot{\eta}_d + \Gamma\, e \tag{5.15}$$

Substituting equation (5.13) into equation (5.15), we have:

$$\dot{e}_1 = e_2 + \xi - \dot{\eta}_d + \Gamma\, e \tag{5.16}$$

Consider the first Lyapunov function candidate as:

$$V_1 = \frac{1}{2} e_1^T e_1 \tag{5.17}$$

Taking time derivative of V_1 as follows:

$$\dot{V}_1 = e_1^T \dot{e}_1 = e_1^T \left(e_2 + \xi - \dot{\eta}_d + \Gamma\, e\right) \tag{5.18}$$

Substituting equation (5.14) into equation (5.18), we obtain:

$$\dot{V}_1 = -e_1^T k_1 e_1 + e_1^T e_2 \tag{5.19}$$

The first term of equation(5.19) is negative and the second term will be addressed in the next step.

Step 2: Differentiating (5.13) with respect to time yields:

$$\dot{e}_2 = U(t) + f(t) + H(t) - \dot{\xi} \tag{5.20}$$

Consider the second Lyapunov function candidate as:

$$V_2 = V_1 + \frac{1}{2} e_2^T e_2 \tag{5.21}$$

The time derivative of V_2 is given by:

$$\begin{aligned}\dot{V}_2 &= \dot{V}_1 + e_2^T \dot{e}_2 \\ &= \dot{V}_1 + e_2^T \left(U(t) + f(t) + H(t) - \dot{\xi} \right)\end{aligned} \tag{5.22}$$

Consider the control law $U(t)$ that stabilizes the robot system such that:

$$\begin{aligned}U(t) &= -k_2 e_2 - e_1 - f(t) - H(t) + \dot{\xi} \\ with \;\; \tau &= M_0(\theta)\, U(t)\end{aligned} \tag{5.23}$$

with $k_2 \in \mathbb{R}^{7\times 7}$ being a diagonal positive-definite matrix.

Substituting equation (5.23) into equation (5.22), we find:

$$\dot{V}_2 \leq -e_1^T k_1 e_1 - e_2^T k_2 e_2 \tag{5.24}$$

Relation (5.24) ensures the global stability of the system. However, $H(t)$ of relation (5.23) is uncertain and the control law of relation (5.23) becomes difficult to compute. To overcome this problem, the TDE approach (Youcef-Toumi and Ito, 1990) may be used to estimate the uncertainties of the nonlinear robot dynamics. So, if **Assumption 5.2** is verified, $H(t)$ can be estimated such that:

$$\hat{H}(t) \simeq H(t - t_d) = \dot{\eta}_2(t - t_d) - f(t - t_d) - U(t - t_d) \tag{5.25}$$

where, t_d is a very-small time delay constant. Practically, the smallest constant that can be achieved in real time is the sampling period. However, due to noisy measurements and non-linearity of signals along the sampling time, a time delay error (TDR) $\varepsilon(t)$ exists. This TDR would deteriorate the robustness and the accuracy of the robot. Unfortunately, the TDR is not available. In this case, let us apply an iterative estimator to estimate and reduce its effect and give more flexibility to the control system on dealing with parameters variation and unexpected

disturbances. The iterative estimator is given in scalar form as:

$$\hat{\varepsilon}_i(t) = \hat{\varepsilon}_i(t - t_d) - k_{3i} e_{2i}$$
$$\hat{\varepsilon}_i(t) = 0,\ \forall\, t \in [-t,\ 0];\ \ , i = 1, \ldots, 7 \tag{5.26}$$

where, k_{3i} is a positive constant. The proof of equation (5.26) is given in appendix II (1).

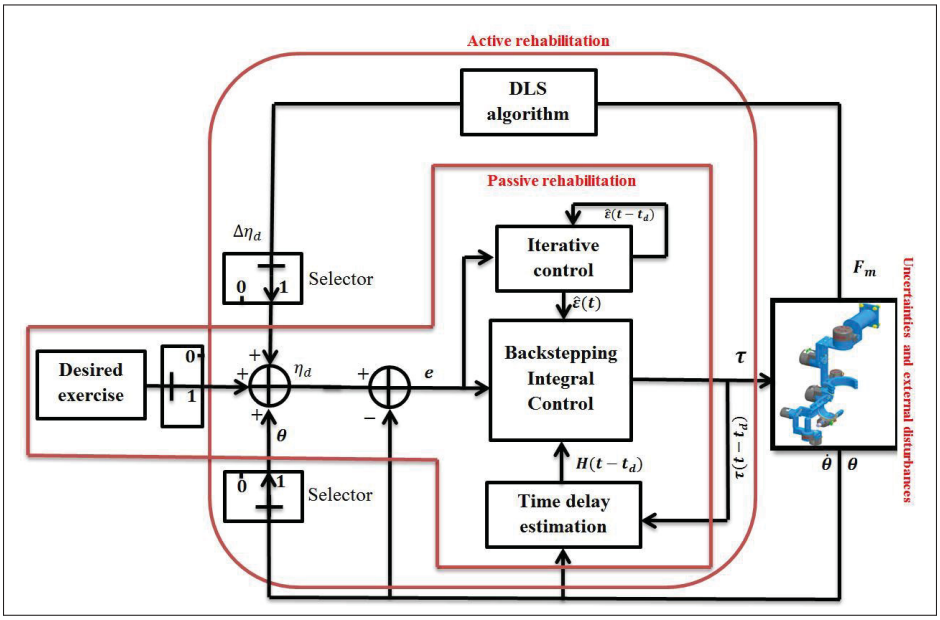

Figure 5.2 General schematic of proposed control (for Selector 1 is pass and 0 is stop)

We can now apply a feasible control input able to keep the stability of the system even if the dynamics of the robot is uncertain and the external disturbances exist. The proposed controller is given such that:

$$U(t) = -k_2 e_2 - e_1 - f(t) - \hat{H}(t) + \dot{\xi} - \hat{\varepsilon}(t) \tag{5.27}$$

with the desired torque:

$$\tau = M_0(\theta)\, U(t) \tag{5.28}$$

Before starting the proof of the stabilization of the system, let us define the estimation error of uncertainties using **Assumption 5.2** and **Assumption 5.3** such that:

$$\tilde{H}(t) = H(t) - \hat{H}(t) = H(t) - H(t - t_d) \qquad = \varepsilon(t) \tag{5.29}$$

We can now define the estimation error of time delay error $\varepsilon(t)$ as:

$$\tilde{\varepsilon}(t) = \hat{\varepsilon}(t) - \varepsilon(t) \tag{5.30}$$

To guarantee the asymptotic stability of the delayed system in the interval $[0,\infty)$, we propose the following Lyapunov–Krasovskii function:

$$V_3 = V_2 + \begin{cases} \sum_{i=1}^{n} \dfrac{1}{2k_{3i}} \int_0^t \tilde{\varepsilon}_i^2(s)ds,\ t \in [0, t_{d1}); \\ \dfrac{1}{2k_{3i}} \int_{t-t_{d1}}^t \tilde{\varepsilon}_i^2(s)ds + \sum_{i=2}^{n} \dfrac{1}{2k_{3i}} \int_0^t \tilde{\varepsilon}_i^2(s)ds,\ t \in [t_{d1}, t_{d2}); \\ \vdots \\ \sum_{i=1}^{n-1} \dfrac{1}{2k_{3i}} \int_{t-t_{di}}^t \tilde{\varepsilon}_i^2(s)ds + \dfrac{1}{2k_{3n}} \int_0^t \tilde{\varepsilon}_n^2(s)ds,\ t \in [t_{dn-1}, t_{dn}); \\ \sum_{i=1}^{n} \dfrac{1}{2k_{3i}} \int_{t-t_{di}}^t \tilde{\varepsilon}_i^2(s)ds,\ t \in [t_{dn}, \infty); \end{cases} \tag{5.31}$$

with:

$$V_2 = \frac{1}{2} e_1^T e_1 + \frac{1}{2} e_2^T e_2 \tag{5.32}$$

and $n = 7$. The derivative of the proposed Lyapunov–Krasovskii function with respect to time is obtained as follows:

$$\dot{V}_4 = -e_1^T k_1 e_1 - e_2^T k_2 e_2 - \frac{1}{2} \sum_{i=1}^{n} k_{3i} e_{2i}^2 \tag{5.33}$$

It is clear from (5.33) that $\dot{V}_4 \leq 0$, where all gains k_1, k_2, and k_3 are positive. The proof of the stability is detailed in Appendix II (2). The structure of the control scheme is shown in Figure 5.2.

5.4 Experimental and comparative study

5.4.1 Experiment Setup

Implementation was carried out on the ETS-MARSE system described below. The system consists of three processing units, the first is a PC where the top-level commands are sent to the robot using LabVIEW interface, i.e. the control scheme selection, joint or Cartesian space trajectory, gain adjustments, etc. This PC also receives the data after the robot task is executed to analyze its performance. The other two processing units are part of a National Instruments PXI platform. Firstly, a NI-PXI 8081 controller card with an Intel Core Duo processor; in this card, the main operating system of the robot and the top-level control scheme are executed. In our case, this is the integral backstepping based controller as well as the estimation based on TDE approach, at a sampling time of $500\mu\ s$. The inverse kinematics algorithm also runs inside this control loop. Finally, at input-output level, a NI PXI-7813R remote input–output card with an FPGA (field programmable gate array) executes the low-level control; i.e. a PI current control loop (sampling time of 50 $\mu\ s$) to maintain the current of the motors required by the main controller. Also, in this FPGA, the position feedback via Hall-sensors (joint position), and basic input-output tasks are executed. Force sensor feedback is important to accurately control the movement of the exoskeleton. A high linearity 6 axis force sensor [NANO17-R-1.8-M2-M1PCI, ATI industrial Automation] is so chosen to obtain accurate real-time force measurements. This sensor is mounted on the tip of the robot. The joint of the ETS-MARSE is powered by Brushless DC motors ((Maxon EC-45, EC-90) combined with harmonic drives (gear ratio 120:1 for motor-1, motor-2, and motor-4 and gear ratio 100:1 for motor-3 and motors 5–7) (Brahmi *et al.*, 2017c; Luna *et al.*, 2016).

The physical parameters of the ETS-MARSE relative to the base reference frame are given in Table (5.3). The diagram of the architecture and overview of the ETS-MARSE system with a human subject is shown in Figure 5.3.

Table 5.3 Physical parameters of ETS-MARSE

Joints (i)	Mass (kg)	Centre of mass (m)	Link length (m)
1	3.475	0.0984	0.145
2	3.737	0.1959	0
3	0	0	0.25
4	2.066	0.163	0
5	0	0	0.267
6	0.779	0.121	0
7	0.496	0.0622	0

The virtual environment HELIOS software was created using the open source ”Unity” platform. This interface consists of a set of functional movement tasks defined by a therapist. There are two types of communication with the ETS-MARSE system (LabVIEW). A User Datagram Protocol (UDP) for transferring position data, and a Transmission Control Protocol/Internet Protocol (TCP/IP) for transferring the operator's commands (e.g. start/stop the execution of the task). The choice of these protocols is based on the reliability and the speed of the transmission of data. Our platform contains two profiles: a user profile and an Admin profile. The user profile is under the supervision of a therapist and of a biomedical engineer. This latter is responsible for preparing the rehabilitation session (such as customizing the activities to the patient's needs). The Admin profile is responsible for managing the database of the patient (such Add/Edit/Delete a patient) and has access to the list of all patients and information concerning their rehabilitation sessions (Ferrer *et al.*, 2013).

A rehabilitation session was created to prove the effectiveness of the proposed control system. The physical therapy tasks are performed by three different healthy subjects (average age: 27 ± 4.6 years; average height: 170 ± 8.75 cm; average weight: 75 ± 18 kg). Each subject participated in a full session, under the supervision of a therapist and a control engineer. The role of the therapist is the definition of the range of motion of each subject and the attribution of the suitable exercise. Within the session, the subject was comfortably seated in a chair in front of the virtual interface as we show in Figure 5.3(a). The experimental session was divided into two scenarios. In passive rehabilitation, each subject performed the designed task of Figure 5.4(a). This task (Initial position $\rightarrow$ Target-A $\rightarrow$ Target-B $\rightarrow$ Target-C$\rightarrow$ Initial

position) is expressed in Cartesian space to evaluate the proposed control. The initial position of the robot is given where elbow joint position is at 90 degrees. This part is followed directly by a comparison study with conventional approaches to show the advantage of the proposed controller. In active rehabilitation, each subject has interacted with the virtual environment and tried to track the proposed trajectory.

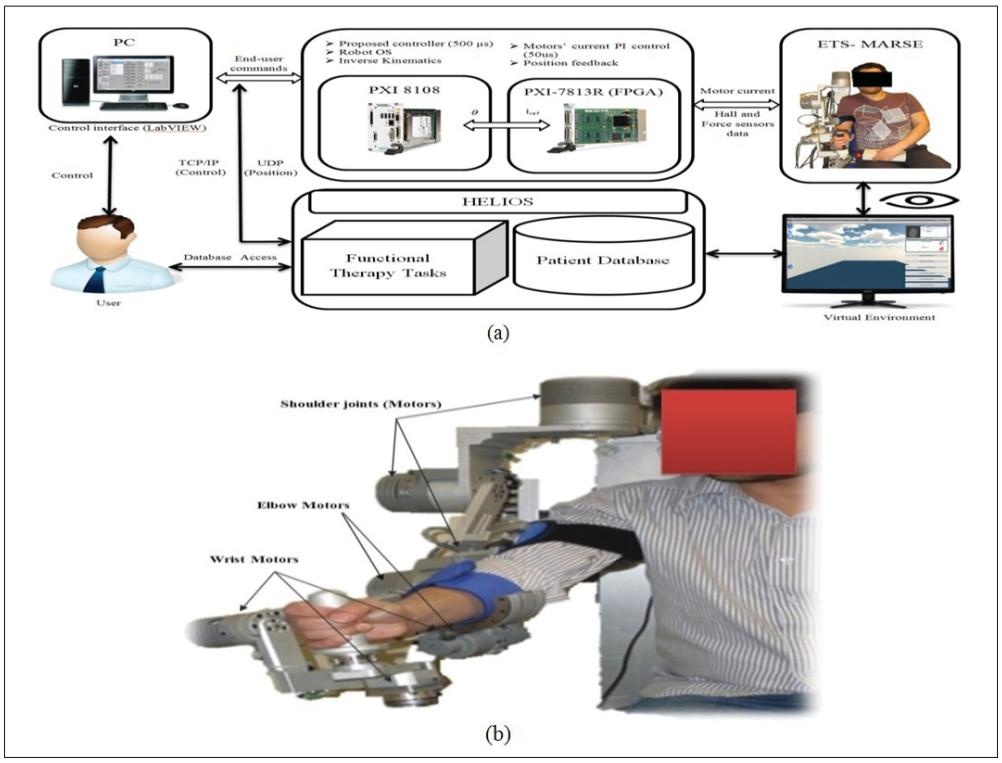

Figure 5.3 (a) General schematic of the experimental architecture.
(b) Overview of the ETS-MARSE with a human subject

It is important to notice that the external disturbances here are represented by different physiological conditions of the subjects, such as non-linear biomechanical characteristics of the musculoskeletal system and the different weights of the upper-limb for each subject. The control gains were tuned manually with a trial-and-error approach as shown in Table (5.4):

Table 5.4 Controller parameters

Gains	Value ($i = 1:7$)
k_{1i}	15
k_{2i}	55.5
k_{3i}	0.01
λ_i	0.6 for ($i = 6$)

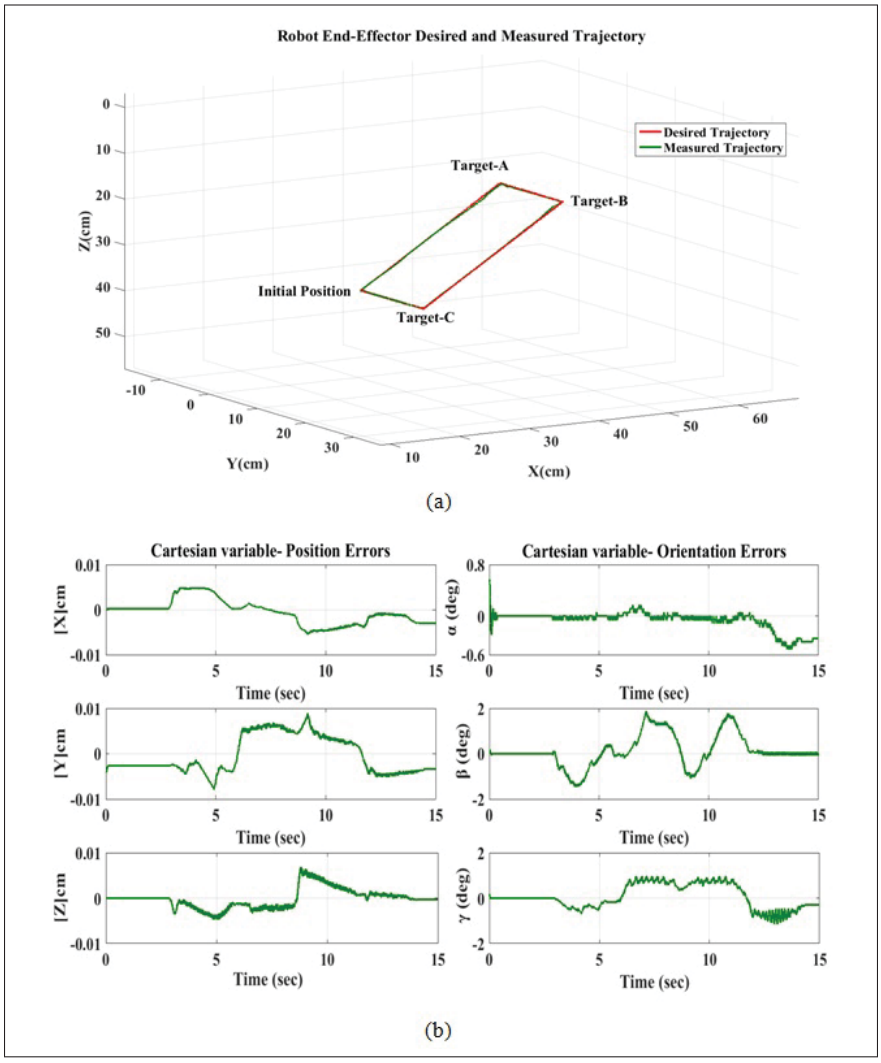

Figure 5.4 (a) Workspace trajectories of the robot in Cartesian space using the proposed controller, performed by Subject-1: (age: 28 years; height: 177 cm; weight: 83 kg). (b) Cartesian errors

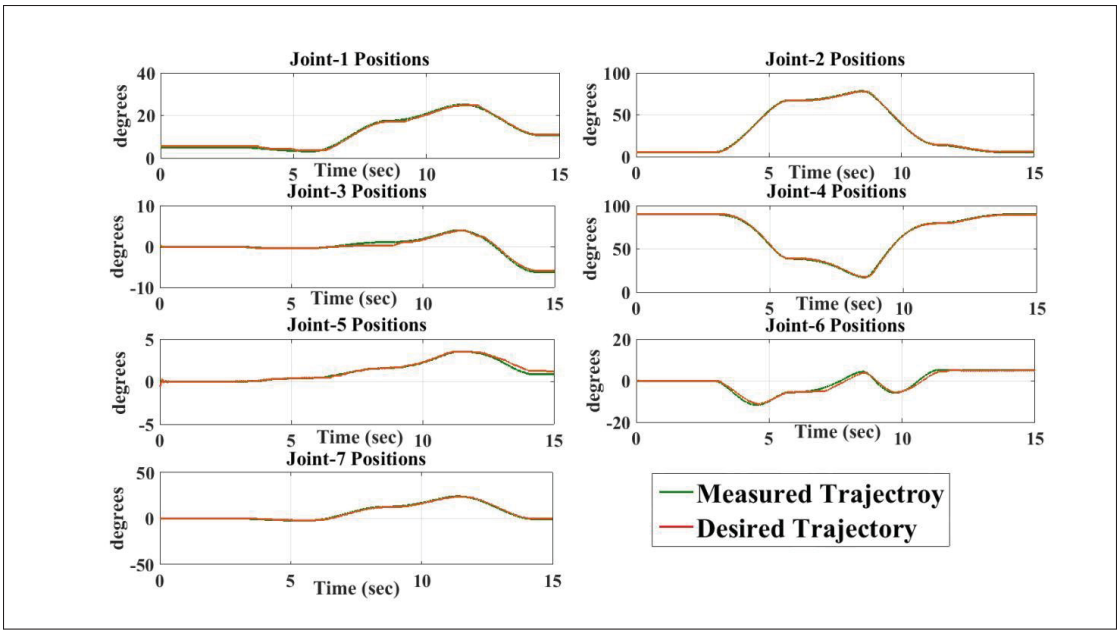

Figure 5.5 Position tracking of the robot in joint space corresponding to the movement performed by Subject-1(Fig. 4): (age: 28 years; height: 177 cm; weight: 83 kg)

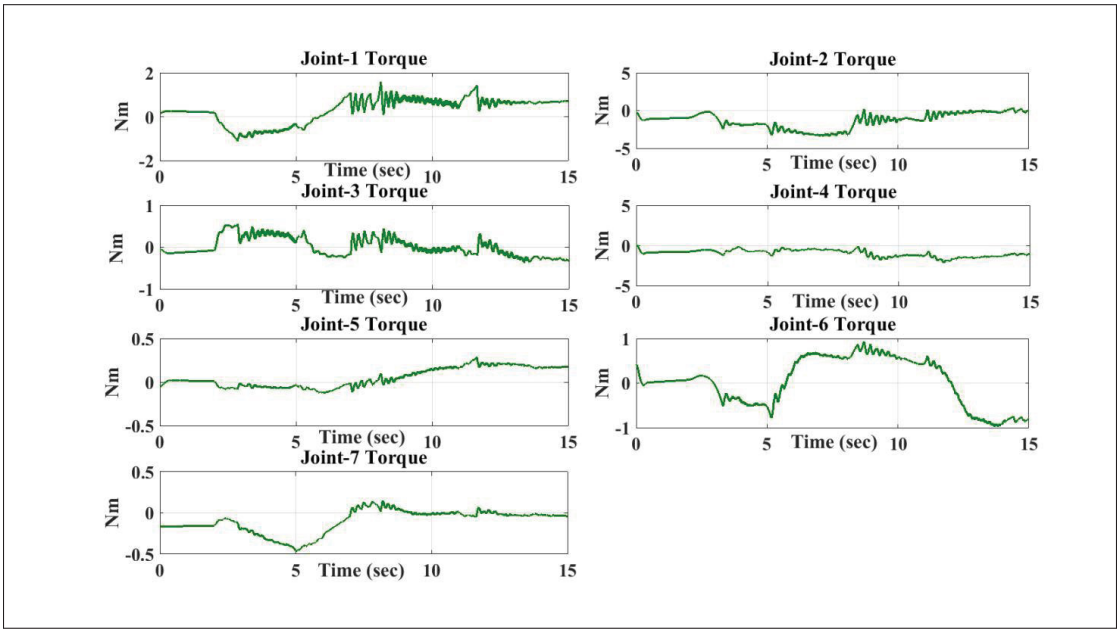

Figure 5.6 Control inputs of the proposed controller

5.4.2 Experimental results of passive rehabilitation

The experimental results with the ETS-MARSE robot in Cartesian space conducted by Subject-1: (age: 28 years; height: 177 cm; weight: 83 kg) using the proposed control strategy are shown in Figure 5.4 and Figure 5.5. From Figure 5.4(a) and Figure 5.5, we observe that the desired trajectory (red line) nearly overlapped with the measured trajectory (green line). In this case, we can say that these results are reasonably good. Figure 5.4(b) presents the Cartesian tracking errors as functions of time, where it is clear from this figure that the Cartesian errors are converging and smaller along the desired trajectory. Figure 5.6 shows that the control input is bounded without any noticeable chattering. So, these results confirm that the control strategy is suitable to perform the desired task even when the nonlinear dynamics of the robot are uncertain.

5.4.3 Comparative study

In order to prove the feasibility and efficiency of the proposed approach, we compared it experimentally with the conventional adaptive tracking control presented in (Kali *et al.*, 2016). In this latter, an integral backstepping control combined with TDE has been proposed without considering the effect of Time Delay Error (TDR). From this comparison, we can see clearly the impact of TDR on the robot's performance and the improvement that is provided by the approach proposed in this paper.

Figure 5.7(a) and Figure 5.8 present the Cartesian and joint trajectories tracking (red is the desired trajectory, green is real trajectory) performed by Subject-1: (age: 28 years; height: 177 cm; weight: 83 kg) using the conventional controller. In fact, we remark from figures (Figure 5.7(a and B) and Figure 5.8) that the conventional controller shows a good performance. Where, it is certain to ensure that the Cartesian error is getting smaller with time. However, the control inputs of the conventional controller presented in Figure 5.9 illustrate a noisy signal with chattering phenomenon, while the proposed controller provides a smooth control input Figure 5.6. It is important to remark that we used the same gains' values that employed in the

proposed approach. So, the TDR is the main cause of the noise in the control input, which may provoke damage in the motors. From the comparison of the two experimental results, we can conclude that the proposed strategy provides a high level of precision and robustness to the nonlinear uncertain dynamics and unknown disturbances without remarkable chattering, compared with the conventional controller.

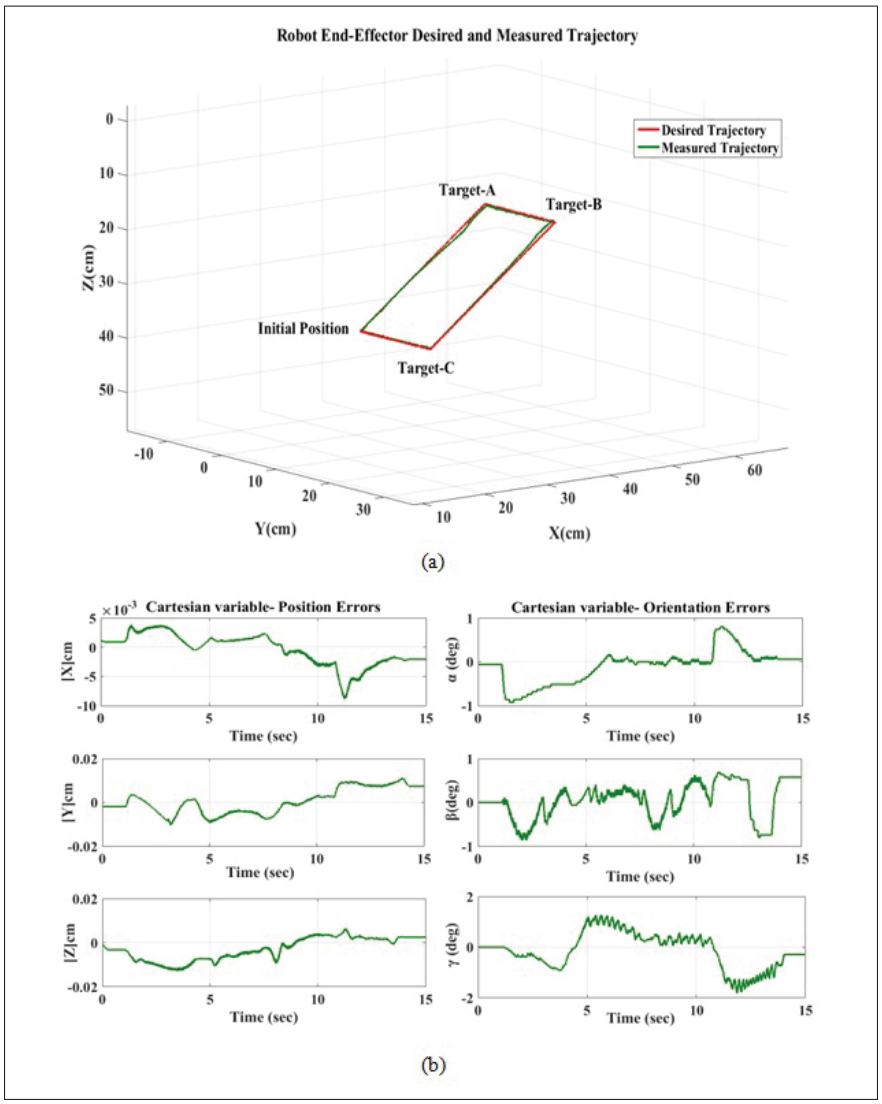

Figure 5.7 (a) Workspace tracking of the robot in Cartesian space using the conventional controller, performed by Subject-1: (age: 27 years; height: 177 cm; weight: 83 kg). (b) Cartesian errors

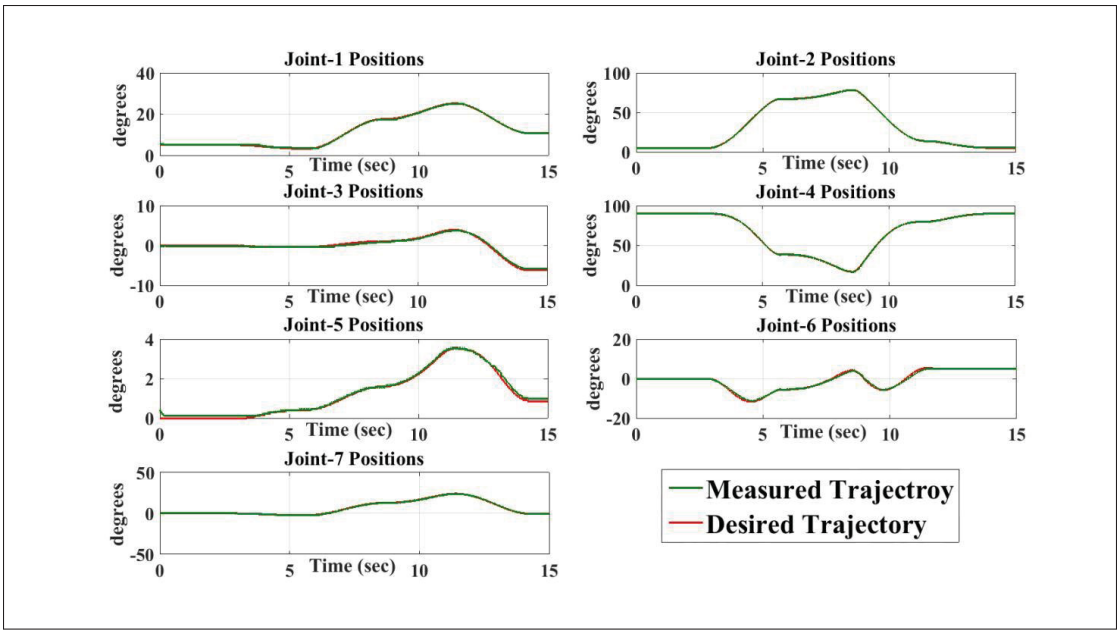

Figure 5.8 Position tracking of the robot in joint space corresponding to the movement performed by Subject-1: (age: 28 years; height: 177 cm; weight: 83 kg)

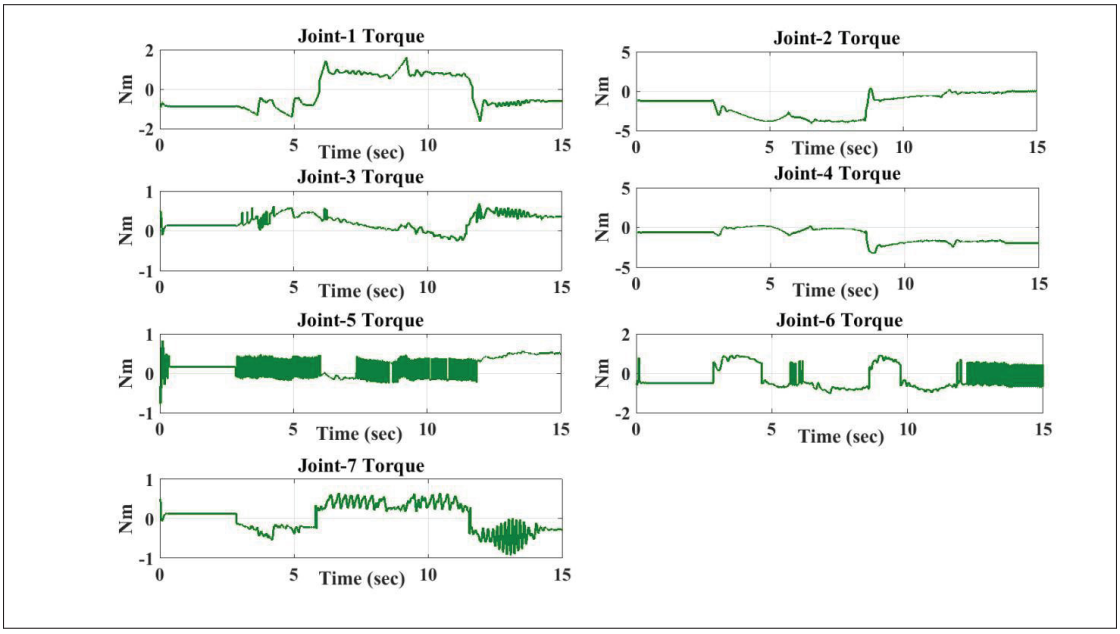

Figure 5.9 Control input of the conventional controller

To show more of the feasibility of the designed strategy, we propose a numerical comparison between the above controllers (conventional controller and proposed controller) by calculating the root mean square (RMS) of the error and the control input of each controller as follows:$\|e\|_{RMS} = \sqrt{\frac{1}{N}\sum_{i=1}^{N}\|e(i)\|^2}$ and $\|\tau\|_{RMS} = \sqrt{\frac{1}{N}\sum_{i=1}^{N}\|\tau(i)\|^2}$ where N is the number of samples of the signals, corresponding with the time steps of the trial. The evaluation of the controller is given in Table 5.5.

Table 5.5 Comparative study with conventional control

Subjects	**Root Mean Square (RMS)**			
	Proposed controller		***Conventional controller***	
	$\|e\|_{RMS\ error}$	$\|\tau\|_{RMS\ Torque}$	$\|e\|_{RMS\ error}$	$\|\tau\|_{RMS\ Torque}$
Subject-1	0.0149	2.9342	0.0408	3.4618
Subject-2	0.0191	2.9061	0.0416	3.4006
Subject-3	0.0165	2.9132	0.0410	4.4994

The results in Table 5.5 show that the proposed controller gives the robot system a high level of robustness to handle parameter variations, nonlinear uncertainties of the dynamics, and unknown disturbances (the different weight of the upper limb for each subject).

To prove the efficiency of the proposed controller, we provide another comparison study of the proposed controller with classical approaches that are previously applied on the ETS-MARSE robot. The subjects repeated the same tasks using conventional (Luna *et al.*, 2016) (PID controller and Computed Torque Control CTC) four consecutive times for each subject, giving a total of 12 experiments for each controller. Figure 5.10 presents the performance result of each controller with different subjects. It is clear from this figure (Figure 5.10) that the proposed control based on TDE presents an excellent performance, much better than PID and Computed Torque Control (CTC) and is not affected by parameters' variations. Meanwhile, the PID con-

troller exhibited a more variable behavior, while the CTC controller was the most influenced by variation in the subject's characteristics.

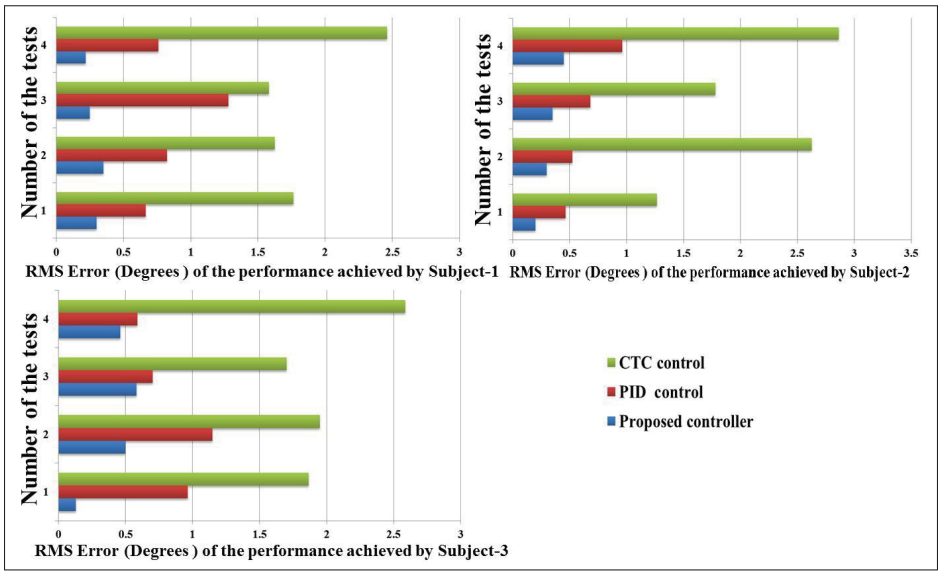

Figure 5.10 Comparison performance of the proposed controller with PID controller and CTC controller

The interpretation of these results is that the PID controller fundamentally does not need the dynamic parameters of the exoskeleton robot and its wearer to provide good results. On the other hand, the CTC controller needs these parameters to ensure a good performance, so, any variation on these parameters reflects negatively on its performance.

5.4.4 Experimental results of active rehabilitation

In this section, the subjects tried to follow the proposed triangle task (red line is the desired trajectory and green line is the actual trajectory) under a virtual interface with different values of damping factor λ. In this case, the exoskeleton robot is completely passive and the subject is completely active. The Damped Least Square (DLS) algorithm is used to provide the esti-

mation of the desired movement intention (DMI). Figures 5.11–5.13 present the results of this experiment.

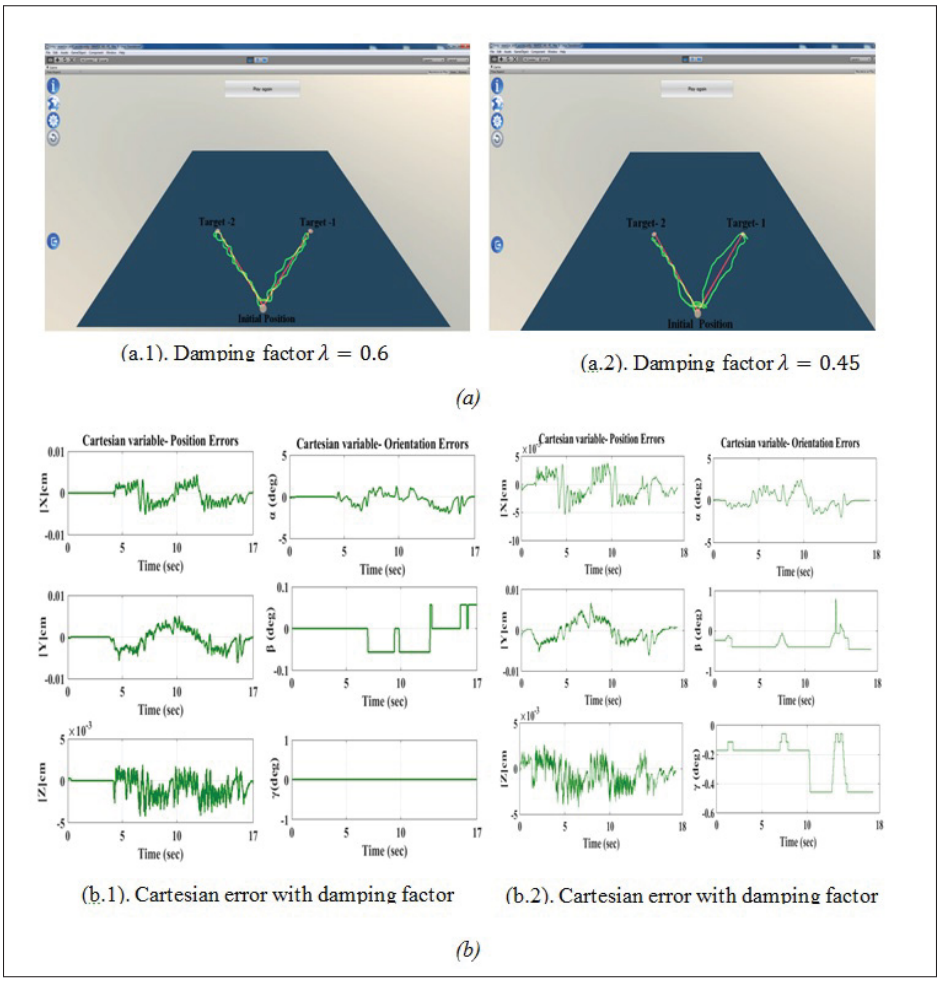

Figure 5.11 (a)Workspace tracking of the robot using DLS method performed by Subject-2: (age: 31 years; height: 183 cm; weight: 83.5 kg) (view on Unity platform). (b) Cartesian errors

Figures 5.11 presents the performance of subject-2 (age: 31 years; height: 183 cm; weight: 83.5 kg) in the virtual interface with help of the ETS-MARSE exoskeleton robot (red line is desired and the green line is the achieved trajectory) using different values of damping factor ($\lambda = 0.6$, $\lambda = 0.45$). Figures 5.11–5.13 present the workspace tracking of the robot in Cartesian space, the control input and the measured force exerted by the subject.

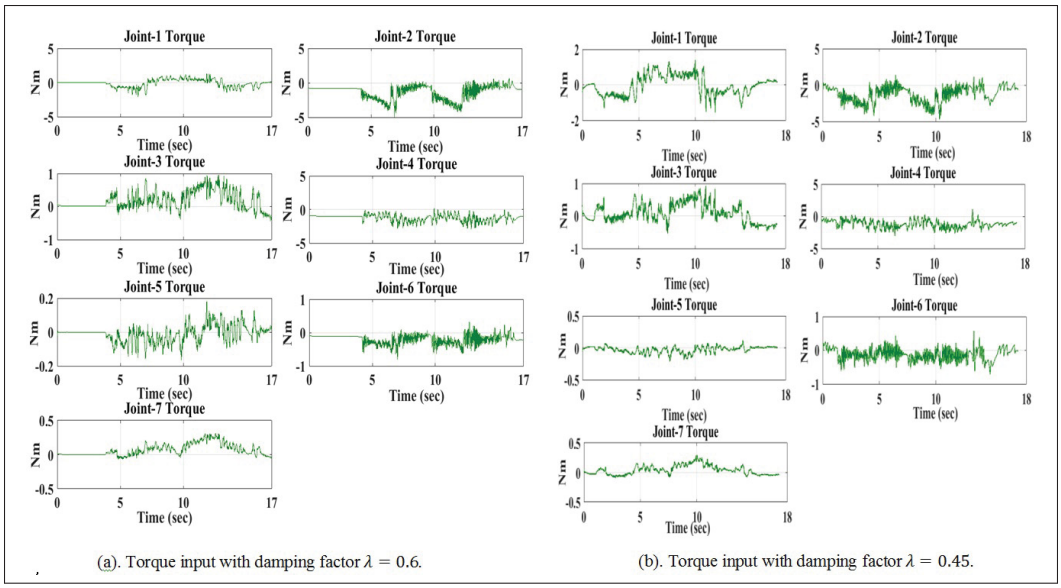

Figure 5.12 Torques input of active rehabilitation task.

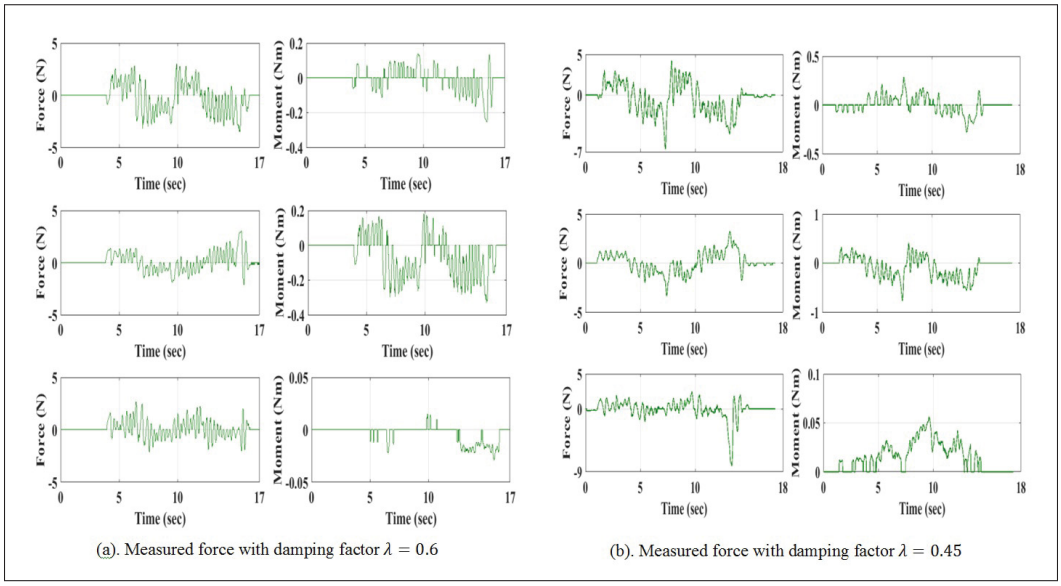

Figure 5.13 Torques input of active rehabilitation task.

It is clear from these plots (Figures 5.11–5.13) that the control strategy achieved the desired performance with small tracking errors and acceptable control input with different values of damping factor. From the good performance of the exoskeleton-subject-2 (Figure 5.11) with $\lambda = 0.6$), we can infer that the Damped Least Square (DLS) algorithm was qualified to estimate

accurately the desired movement intention $\Delta\eta_d$. During the experiment, we concluded that the damping factor λ acts as an influential role to realizing an accurate estimation of the user's intention, as shown in Figures 5.11 with $\lambda = 0.45$. Despite the controller having ensured a good tracking of the desired user's motion intention, the damping factor affects the estimation accuracy of the desired movement.

5.5 Conclusion

In this paper, we proposed an adaptive control of an exoskeleton robot with uncertain dynamics based on an integral backstepping controller and time delay estimation. Where, the TDR is taken into consideration. The TDE is used to estimate the robot's nonlinear uncertain dynamics and the unknown bounded perturbations exerted on the exoskeleton robot. To improve the accuracy of the robot performance, the TDR is estimated by a recursive control law to overcome the limitation of the time delay error inherent of the TDE approach. The proposed strategy is designed to provide a high-level of robustness and precision to compensate for nonlinear uncertainties of the dynamics and unknown disturbances, to make the exoskeleton robot achieve smooth motion similar to the natural human movement, and to give to the control system more flexibility to deal with the uncertainties and parameters variation. The Damped Least Square (DLS) method has been employed to estimate the Desired Movement Intention (DMI) of the subjects in order to provide active rehabilitation. The main benefit of the proposed adaptive control approach is that precise knowledge of the dynamic parameters of the robot is not required. Moreover, the proposed adaptive strategy is characterized by the easiness of real-time implementation. The stability analysis of the robot system and the convergence of its errors were proved based on Lyapunov–Krasovskii functional theory. The experimental results prove the effectiveness, facility of implementation, and accuracy of the proposed approach. As a future work, we will seek to overcome the limitations of this approach. In particular, the value of the delayed acceleration for the controller; where the estimation of this variable may deteriorate its accuracy. We are leaning to use this controller with a more complex scenario, such human-robot collaboration.

CHAPTER 6

ADAPTIVE CONTROL OF A 7-DOF EXOSKELETON ROBOT WITH UNCERTAINTIES ON KINEMATICS AND DYNAMICS

Brahim Brahmi[1], Maarouf Saad[1], Jacqueline Tu Anh Thu Lam[1], Cristobal Ochoa Luna [1]
Mohammad H. Rahman[2] and Philippe S. Archambault[3]

[1] Département of Electrical Engineering, École de Technologie Supérieure,
1100 Notre-Dame Ouest, Montréal, Québec, Canada H3C 1K3
[2] Mechanical/Biomedical Engineering Department,University of Wisconsin-Milwaukee,
3200 N. Cramer Street, Milwaukee, WI 53211,
[3] School of Physical and Occupational Therapy, McGill University; Centre for
Interdisciplinary Research in Rehabilitation of Greater Montreal,
Montréal, Québec, Canada,

Paper published in *European Journal of Control*, March 2018

Abstract

In this paper, we propose a new adaptive visual tracking control approach based on sliding mode control in Cartesian space applied to an exoskeleton robot with uncertain kinematics and dynamics, taking into account uncertainties in visual system (camera) parameters. The adaptation of kinematic uncertainties is based on a filtered regressor kinematic matrix, whereas, the adaptation of dynamic uncertainties is based on a Time Delay Estimation approach. This is performed considering the Time Delay Error (TDR) to provide a control action capable of following the designed functional therapy tasks. A new recursive controller is combined with TDE in order to estimate the TDR and limit its effect. The proposed strategy does not need the accurate dynamic and kinematic models of the exoskeleton. The update laws are designed using Lyapunov theory to solve the adaptation problem methodically and to show the stability of the robot system. Experimental results confirm the effectiveness and feasibility of the designed approach.

Keywords: Rehabilitation robots, Time delay control; Time delay error, Uncertainties, recursive control.

6.1 Introduction

Recently, stroke and neurological diseases have become among the most important health-related problems in the world. Stroke survivors bear with disabilities following an accident that affects their quality of life (Lundström *et al.*, 2008; Nichols-Larsen *et al.*, 2005). Annually, worldwide, six million people die and five million live with persistent weakness, from the 15 million people suffering a stroke (Sidney *et al.*, 2013). Physical therapy is the main treatment existing today. It is designed to relieve the patient from the impairment or/and injury and to improve his range of movement, functional capacity, and quality of life (De Morand, 2014). Thanks to robotics technology, modern rehabilitation treatment is supported by new devices named rehabilitation robots. This kind of robot is able to provide a wide range of physical therapy and overcome some of the limitations of conventional therapy. Many research teams participate in this field, among them, Assisted Rehabilitation and Measurement Guide (ARMin IV) (Philips *et al.*, 2017); Robotic Upper Extremity Repetitive Therapy (RUPERT) (Balasubramanian *et al.*, 2008); Saga University Exoskeleton For Upper Limb (SUEFUL-7) (de Santé, 2012). An important issue is that the design of these robots must be harmonious with the human anatomy configuration. To provide a modern physical therapy for the upper limb, we have developed an exoskeleton robot named ETS-MARSE. This robot is consistent with the human arm configuration and is capable of performing different rehabilitation movements (Brahim *et al.*, 2016b,a; Brahmi *et al.*, 2017c).

Generally, the dynamic parameters of an exoskeleton robot, for instance the ETS-MARSE, are hard to be modeled precisely because of the complexity of the mechanical design such as nonlinear friction forces, backlash, and the complexity of the actuators of the robot. In addition, the dynamic characteristics vary due to the different physiological conditions of the subjects, such as an external force caused by subject's muscular activity (Brahim *et al.*, 2016b). This kind of uncertain nonlinearities can be categorized as both parametric uncertainties and unknown nonlinear functions (Dawson *et al.*, 2003). Additionally, in most applications using rehabilitation robots, the therapeutic tasks are expressed in Cartesian space. In this case, the nonlinear transformation functions or Jacobian matrix that allows the mapping from joint space

to Cartesian space is assumed to be known, to ensure a perfect Cartesian control performance. However, when the feedback position of the robot's response is provided by a visual system, such as a camera or Kinect, the exoskeleton can be subject to uncertain kinematics. Due to firstly the uncertainties in camera parameters, secondly, when the human and exoskeleton carry/transfer an object with an unknown length and/or orientation (Arimoto, 1999). In this case, it is difficult to derive the solution of inverse kinematics using this standard approach. Moreover, to realize human motion via an exoskeleton robot, it is essential to determine accurately the lengths of links, the joints, and the dimension of the object carried by the robot. Unfortunately, it is difficult to define these physical parameters exactly. Various solutions have been proposed to estimate these parameters (Cheah, 2006; Cheah *et al.*, 1999; Bai *et al.*, 2017; Han, 2009; Tang and Li, 2014). However, almost none of these solutions consider the uncertainties of the camera parameters. This dilemma motivates us to set up a new control system capable of ensuring a sufficient performance in the presence of dynamic and kinematic uncertainties and unknown disturbances exist.

One of the research challenges on this class of robots is to develop a controller that can maneuver the human-exoskeleton system to mimic natural human upper extremity motion. It is remarkable from a natural human movement that the human does not need accurate information about kinematics and dynamics of the arm (or any object carried by upper extremity) to reach an object in space. Due to that, many control strategies have been designed to solve the problem of kinematic and dynamic uncertainties (Arimoto, 1999; Cheah, 2006; Yazarel and Cheah, 2002; Huang and Chien, 2010; Cheah *et al.*, 2005; Hutchinson *et al.*, 1996). The main innovative point of these controllers is that the adaptation of the both kinematic/dynamic uncertainties has been provided, which makes the exoskeleton robot perform the human-like motion and supplies to the control system more flexibility to handle the uncertainties and parameters variation. However, the above controllers are based on the classical regressor matrix. These types of controllers assume that the robot is linear in a set of physical parameters and find a control law able to ensure the stability of this linear system only around its operating points (Yao, 1996). In fact, the manipulator is highly nonlinear. So, the integration of this adaptation law may affect

the stability of the system in the presence of even small disturbances (Yao, 1996). Adaptive visual or image-based tracking control (Hutchinson *et al.*, 1996; Deng *et al.*, 2002; Espiau *et al.*, 1992; Gans *et al.*, 2003; Malis and Chaumette, 2002; Liu *et al.*, 2006) is one of the powerful approaches that has been developed to transact with the kinematic/dynamic uncertainties. This is due to their robustness practically to modeling and calibration errors (Deng *et al.*, 2002). However, these controllers are concentrated on uncertainties in nonlinear transformation functions or image Jacobian matrix but they ignored the uncertain kinematic/dynamic effects. Additionally, a few stability analyses are provided in the literature for visual tracking control with the uncertainties of kinematics/dynamics and in the presence of uncertainties in visual system (camera) parameters (Cheah *et al.*, 2006). A Time Delay Estimation (TDE) approach may be considered to compensate the uncertainties (Youcef-Toumi and Shortlidge, 1991; Efimov *et al.*, 2015; Rami *et al.*, 2013; **?**; Fridman, 2014; Zheng *et al.*, 2010; Brahmi *et al.*, 2017a,b). The TDE has been implemented in many robotic systems with consistently good performance (Jin *et al.*, 2015; Kim *et al.*, 2016). The TDE utilizes the previous response of the robot system, and the previous control input to provide new control actions able to provide an accurate approximation of uncertainty function. However, due to noisy measurements and nonlinearity of signals along the sampling time, a time delay error (TDR) exists, which would deteriorate the robustness and the accuracy of the robot. A through literature review revealed that no research work has proposed a systematic solution to eliminate the negative influence of this error.

A. Main contribution

All the papers that cited above, except TDE approach, are based on the conventional adaptive approaches (regressor function) and require a good knowledge of the robot system's parameters. Practically, it is impossible to define exactly the parameters of the robot system and the modelisation of the robot is typically uncertain. For these kinds of robots, the adaptation of the uncertainties function based on full dynamic is very complicated due to the high number of degrees of freedom (DOFs) of the robot. When the number of DOFs of the robot increases, it is not straightforward to find the parameters of the robot. Usually, the parameter vector of the robot can be greater than 100 if its DOFs are greater only than four (Brahmi *et al.*, 2017c).

To address the above problems, we propose a new adaptive visual tracking control for an exoskeleton robot with high number of degrees of freedom (7-DOFs) based on extension of sliding mode, TDE approach and Jacobian transpose taking into consideration the Cartesian and joint spaces. This controller is designed to be robust and more flexible to deal with the kinematic and dynamic uncertainties taking into consideration the uncertainties in the visual system parameters, and to be more robust to the parameter variations. The contribution of this paper can be summarized in three points:

- Considering the unknown kinematics and dynamics with unknown external disturbances (different weight of the arm of each subject), adaptive visual controller incorporating with recursive control is developed to estimate the nonlinear kinematic and dynamic uncertainties with unknown disturbances and to drive the robot to follow the desired functional therapy activity and provide a smooth exoskeleton-aided passive activity;
- The unknown dynamics and external disturbances of the robot system can estimate easily using Time Delay Estimation (TDE) approach. This strategy employs only time-delayed knowledge about the previous control input of the system and its response state to provide an accurate estimation of uncertainties. The main feature of this method is that not influenced by the high degree of freedom of the robot and the size of the estimated parameters;
- Using a new recursive control to reduce the effect of the Time Delay Error (TDR) and improve the robustness of the control system. Usually, this error limits the performance of TDE approach.

The proposed strategy is achieved based on the inner/outer loop structure of robotics system. This latter has some desirable characteristics such as the rapidity of the computation of the control system. In this case, the outer loop is designed to estimate the nonlinear kinematics parameters and uncertainties in the visual system (camera), and the Inner Loop is intended to provide a high-level of precision by compensating the unknown part of the dynamics using TDE approach and while considering the TDR. The recursive control here is designed to reduce the effect or TDR and improve the robustness of the TDE approach. The structure of the designed controller also aims to make the exoskeleton robot perform the human-like movement

using the predefined trajectories of physical therapy tasks (De Morand, 2014). The stability of the Inner/Outer system and the convergence of its errors are formulated and demonstrated based on Lyapunov function. Compared with conventional approach (Cheah, 2006; Cheah *et al.*, 1999, 2005; Liu *et al.*, 2006) that is applied on only 2-DOFs planar robot, the designed strategy is characterized by the ease of implementation and high precision and robustness to the kinematic/dynamic uncertainties, unforeseen disturbances and uncertainties of camera parameters. The efficiency and the robustness of the proposed approach are validated with Cartesian trajectory tracking corresponding to passive physical therapy tasks (De Morand, 2014).

The outline of the paper is organized as follows. The kinematics and dynamics of the robot are presented in the next section. The control scheme is described in section 6.3. Experimental and comparison results are shown in section 6.4; finally, the conclusion is presented in section 6.5.

6.2 Characterization of ETS-MARSE robot: kinematics and dynamics

6.2.1 Modeling of ETS-MARSE robot

The ETS-MARSE is a redundant robot with 7DOFs, as shown in Figure 6.1. It is designed to rehabilitate the impaired human upper limb. The design of the ETS-MARSE was originally inspired from the anatomy of the human arm. It was ergonomically designed to be comfortable for the subjects (robot users) during the rehabilitation sessions. The shoulder motion part (3-DOF) is consisted of three joints: the first two joints are responsible for shoulder joint's vertical and horizontal extension/flexion motion, while the third joint is aimed to conduct the internal and external rotation of the shoulder joint. The elbow motion part (1-DOF) is responsible for elbow joint flexion/extension motion. The wrist motion support part of the ETS-MARSE is consisted of three joints: the first joint is designed to achieve pronation and supination movement of the forearm, the second joint and the third joint are designed to perform ulnar/radial deviation, and flexion/extension of the wrist respectively. The design of the ETS-MARSE has special features compared with the existing exoskeleton robots (Rahman *et al.*, 2015). Among

them, it has a comparatively low weight, an excellent power/weight ratio, can be easily fitted or removed, and is capable of adequately compensating for gravity. A new power carrying mechanism was included for supporting the shoulder joint internal/external rotation and for forearm pronation/supination. This exoskeleton robot can be used with a wide range of subjects, due to its adjustable link mechanism. All the key characteristics and contribution features of the ETS-MARSE and comparison with similar existing exoskeleton robots are summarized in (Rahman *et al.*, 2015).

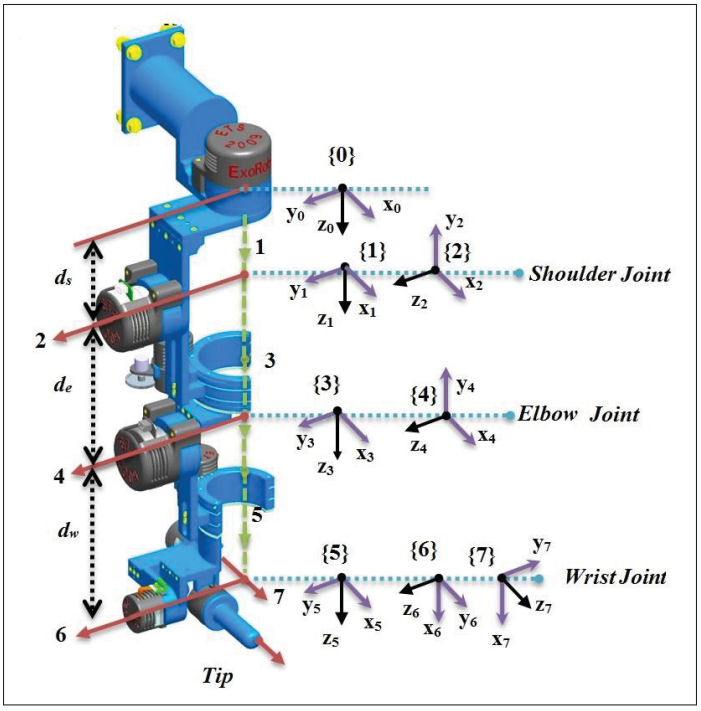

Figure 6.1 Reference frames of ETS-MARSE

6.2.1.1 Dynamics of the ETS-MARSE Robot

The dynamic behavior of ETS-MARSE manipulator is given by the following expression using the Lagrangian method (Dawson *et al.*, 2003):

$$M(\theta)\ddot{\theta} + C(\theta,\dot{\theta}) + G(\theta) = \tau + \tau_{ex} \tag{6.1}$$

where $\theta \in \mathbb{R}^7$, $\dot{\theta} \in \mathbb{R}^7$ and $\ddot{\theta} \in \mathbb{R}^7$ are, respectively, the joint's position, velocity, and acceleration vectors, $M(\theta) \in \mathbb{R}^{7\times7}$ is the symmetric and positive definite inertia matrix, $C(\theta,\dot{\theta}) \in \mathbb{R}^{7\times7}$ is the Coriolis and centrifugal vector, $G(\theta) \in \mathbb{R}^7$ is the gravitational vector, $\tau \in \mathbb{R}^7$ is the applied joint torque to the exoskeleton robot, and $\tau_{ex} \in \mathbb{R}^7$ is the external disturbances vector. Let us denote:

$$\begin{cases} M(\theta) = M_0(\theta) + \Delta M(\theta) \\ C\left(\theta,\dot{\theta}\right) = C_0\left(\theta,\dot{\theta}\right) + \Delta C\left(\theta,\dot{\theta}\right) \\ G(\theta) = G_0(\theta) + \Delta G(\theta) \end{cases} \tag{6.2}$$

where $M_0(\theta)$, $C_0\left(\theta,\dot{\theta}\right)$ and $G_0(\theta)$ are respectively the known inertia matrix, the Coriolis centrifugal matrix, and the gravity vector. $\Delta M(\theta)$, $\Delta C(\theta)$ and $\Delta G(\theta)$ are the uncertain parts.

Let us introduce a new variable such that: $\eta_1 = \theta$ and $\eta_2 = \dot{\theta}$; hence, the dynamic model expressed in (6.1) can be rewritten as follows:

$$\begin{cases} \dot{\eta}_1 = \eta_2 \\ \dot{\eta}_2 = U(t) + f(t) + H(t) \end{cases} \tag{6.3}$$

where, $U(t) = U(\eta_1)$, $H(t) = H(\eta_1,\eta_2,\dot{\eta}_2)$ and $f(t) = d\eta_1,\eta_2)$. This notation is used in order to handle easily later with the control scheme. Where:

- $U(t) = M_0^{-1}(\theta)\,\tau(t)$;
- $f(t) = M_0^{-1}(\theta)\left[-C_0\left(\theta,\dot{\theta}\right) - G_0(\theta)\right]$;
- $H(t) = H\left(\theta,\dot{\theta},\ddot{\theta}\right) = M_0^{-1}(\theta)\left[\tau_{ex} - \Delta M(\theta)\,\ddot{\theta} - \Delta C\left(\theta,\dot{\theta}\right)\dot{\theta} - \Delta G(\theta)\right]$.

6.2.1.2 Kinematics of ETS-MARSE robot

In most applications of rehabilitation robots, the desired trajectory is expressed in Cartesian space (De Morand, 2014). The transformation from Cartesian space to joint space is done by a non-linear function named the Jacobian matrix. If the position x of the end–effector of the

robot is provided by a visual system such a camera or Kinect, the standard relation between Cartesian velocity and joint velocity is given as follows:

$$\dot{x} = J(\eta_1)\eta_2 \tag{6.4}$$

where $J(\eta_1) = J_c(r)J_{RO}(\eta_1) \in \mathbb{R}^{6\times 7}$ is the total Jacobian matrix of the robot combined with the visual system. $J_c(r) \in \mathbb{R}^{6\times 6}$ is the image Jacobian matrix (Cheah *et al.*, 2005; Hutchinson *et al.*, 1996), $x \in \mathbb{R}^6$ is the Cartesian position of the end-effector of the robot, $r \in \mathbb{R}^6$ is the image feature parameters and $J_{RO}(\eta_1) \in \mathbb{R}^{6\times 6}$ is the Jacobian matrix of the manipulator.

6.2.1.3 Problem formulation

One of the main objectives of research on this kind of robots is to design a controller able to make the human-exoskeleton system achieve movement without exact information of the kinematics and dynamics of the robotic system and to provide a smooth movement, conforming to physical therapy exercise while the designed control scheme ensures that the measured Cartesian positions x of the robot tracks the desired Cartesian trajectory x_d. Before giving the control design methodology, we present the properties and the assumptions used in this paper.

Property 6.1: The known part of inertia matrix $M_0(\theta)$ is symmetric and positive definite for all $\theta \in \mathbb{R}^7$ (Dawson *et al.*, 2003).

Property 6.2: Equation (6.4) can be linear in a set of kinematics parameters like link lengths, which can be written as a linear combination of specified functions as given below (Liu *et al.*, 2006):

$$\dot{x} = J(\eta_1, \gamma_k)\eta_2 = Q(\eta_1, \eta_2)\gamma_k \tag{6.5}$$

where $Q(\eta_1, \eta_2) \in \mathbb{R}^{6\times 6}$ is the kinematic regressor matrix and $\gamma_k \in \mathbb{R}^6$ is the kinematics parameters vector

Assumption 6.1: The joint position and joint velocity are measured.

Assumption 6.2: All kinematic singularities are avoided.

Assumption 6.3: Since the dynamic model of the robot is continuous and bounded, we assume that the function $H(t)$ is locally Lipschitz function.

Assumption 6.4: The desired trajectory is bounded.

Assumption 6.5: The external disturbance τ_{ex} is supposed to be continuous, has finite energy and satisfies $\|\tau_{ex}\| \leq \vartheta$, with an unknown positive disturbance boundary ϑ.

6.3 Control design

The control of a robotic system always needs a precise input measurement to provide a good performance of this system. Particularly, in the case when we have a position feedback from visual devices, like a camera or Kinect. Since no sensor is available to measure the Cartesian velocity input, a linear filter can be used to obtain this variable such that:

$$\left(\frac{d}{dt}+\Lambda\right) z = \Lambda \dot{x} \tag{6.6}$$

The signal $z \in \mathbb{R}^6$ is obtained from the measured position $x \in \mathbb{R}^6$. Λ is a positive constant. Substituting equation (6.5) into (6.6), we can rewrite (6.6) such that:

$$\left(\frac{d}{dt}+\Lambda\right) z = \Lambda Q(\eta_1, \eta_2)\gamma_k \tag{6.7}$$

where:

$$z = \left(\frac{\Lambda}{\frac{d}{dt}+\Lambda}\right) Q(\eta_1, \eta_2)\gamma_k = \phi(t)\gamma_k \tag{6.8}$$

where $\phi(t) \in \mathbb{R}^{6\times6}$ is a filtered function of $Q(\eta_1, \eta_2)$. Usually the robot begins from the rest position, hence: $z(0) = 0$ and $\phi(t) = 0$ (Cheah *et al.*, 2005).

We can now determine the Cartesian position error, Cartesian velocity error, and estimated Cartesian velocity error as follows:

$$\begin{cases} e_x = x - x_d \\ \dot{e}_x = \dot{x} - \dot{x}_d \\ \dot{\hat{e}}_x = \dot{\hat{x}} - \dot{x}_d \end{cases} \tag{6.9}$$

where, $x_d \in \mathbb{R}^6$ is the desired Cartesian trajectory, $x \in \mathbb{R}^6$ is the measured position and $\dot{\hat{x}} \in \mathbb{R}^6$ is the estimated measured velocity.

Now, we define the vector of required Cartesian velocity as:

$$\dot{x}_r = \dot{x}_d - \beta e_x \tag{6.10}$$

where $\dot{x}_r \in \mathbb{R}^6$ and β is a positive constant. Differentiating equation (6.10) with respect to time yields:

$$\ddot{x}_r = \ddot{x}_d - \beta \dot{e}_x \tag{6.11}$$

Considering an uncertain kinematics, the Jacobian matrix is uncertain. In this case equation (6.5) is rewritten as follows:

$$\dot{\hat{x}} = \hat{J}(\eta_1, \hat{\gamma}_k)\eta_2 = Q(\eta_1, \eta_2)\hat{\gamma}_k \tag{6.12}$$

Using equation (6.12), we define the estimated sliding Cartesian surface vector as follows:

$$\hat{S}_x = \dot{\hat{x}} - \dot{x}_r = \hat{J}(\eta_1, \hat{\gamma}_k)\eta_2 - \dot{x}_r \tag{6.13}$$

Differentiating equation (6.13) with respect to time yields

$$\dot{\hat{S}}_x = \ddot{\hat{x}} - \ddot{x}_r = \hat{J}(\eta_1, \hat{\gamma}_k)\dot{\eta}_2 + \dot{\hat{J}}(\eta_1, \hat{\gamma}_k)\eta_2 - \ddot{x}_r \tag{6.14}$$

Now, we can define the required joint velocity vector as:

$$\dot{\eta}_r = \hat{J}^{+}(\eta_1, \hat{\gamma}_k)\dot{x}_r \tag{6.15}$$

where $\hat{J}^{+}(\eta_1, \hat{\gamma}_k) = \hat{J}^{T}(\eta_1, \hat{\gamma}_k)\left(\hat{J}^{T}(\eta_1, \hat{\gamma}_k)\hat{J}(\eta_1, \hat{\gamma}_k)\hat{J}^{T}(\eta_1, \hat{\gamma}_k)\right)^{-1}$ is the pseudo-Jacobian matrix. Differentiating equation (6.15) with respect to time:

$$\ddot{\eta}_r = \hat{J}^{+}(\eta_1, \hat{\gamma}_k)\ddot{x}_r + \dot{\hat{J}}^{+}(\eta_1, \hat{\gamma}_k)\dot{x}_r \tag{6.16}$$

It is important also to define the sliding joint surface vector. By using equation (6.10), equation (6.12) and equation (6.15) we have:

$$S = \eta_2 - \dot{\eta}_r = \hat{J}^{+}(\eta_1, \hat{\gamma}_k)\left[\left(\dot{\hat{x}} - \dot{x}_d\right) + \beta e_x\right] = \hat{J}^{+}(\eta_1, \hat{\gamma}_k)\hat{S}_x \tag{6.17}$$

The time derivative of relation equation (6.17) gives:

$$S = \eta_2 - \dot{\eta}_r = \hat{J}^{+}(\eta_1, \hat{\gamma}_k)\dot{\hat{S}}_x + \dot{\hat{J}}^{+}(\eta_1, \hat{\gamma}_k)\hat{S}_x \tag{6.18}$$

Substituting equation (6.18) into equation (6.3), the exoskeleton robot system equation (6.3) can be written as follows:

$$\begin{cases} S = \dot{\eta}_1 - \dot{\eta}_r \\ \dot{S} = U(t) + f(t) + H(t) - \ddot{\eta}_r \end{cases} \tag{6.19}$$

If all parameters of the robot system given in equation (6.19) are completely known, we can propose the following controller:

$$U(t) = -\hat{J}^T(\eta_1, \hat{\gamma}_k)\left(k_1 e_x + k_2 \dot{\hat{e}}_x + k_3 \hat{S}_x\right) - f(t) - H(t) + \ddot{\eta}_r - \varepsilon(t) \tag{6.20}$$

with:

$$\hat{S}_x = Q(\eta_1, \eta_2)\hat{\gamma}_k - \dot{x}_r \tag{6.21}$$

and k_1, k_2 and $k_3 \in \mathbb{R}^{6\times 6}$ being diagonal positive matrices. $\hat{J}^T(\eta_1, \hat{\gamma}_k)$ is the estimated Jacobian transpose based on feedback of Cartesian tracking. The adaptation laws are updated by:

$$\dot{\hat{\gamma}}_k = k_f^{-1}\phi^T(t)k_2\left(\phi(t)\hat{\gamma}_k - z\right) + k_f^{-1}Q^T(\eta_1, \eta_2)\left(k_1 + \beta k_2\right)e_x \tag{6.22}$$

where $k_f \in \mathbb{R}^{6\times 6}$ is a diagonal positive matrix. Since $H(t)$ is uncertain, that may influence the performance of robot tracking. So, if **Assumption 6.3** is verified, it is possible to use Time Delay Estimation (Youcef-Toumi and Shortlidge, 1991). In such case, the designed controller is given such that:

$$U(t) = -\hat{J}^T(\eta_1, \hat{\gamma}_k)\left(k_1 e_x + k_2 \dot{\hat{e}}_x + k_3 \hat{S}_x\right) - f(t) - \hat{H}(t) + \ddot{\eta}_r - \hat{\varepsilon}(t) \tag{6.23}$$

where $\hat{H}(t)$ is obtained using TDE (Youcef-Toumi and Shortlidge, 1991), using equation (6.3) to obtain:

$$\hat{H}(t) \simeq H(t - t_d) = \dot{\eta}_2(t - t_d) - f(t - t_d) - U(t - t_d) \tag{6.24}$$

where, t_d is a positive constant assumed to be very small. Practically, the smallest constant can be reached is the sampling time. However, due to noisy measurements and nonlinearity of signals along the sampling time, a time delay error (TDR) $\varepsilon(t)$ exists, which would deteriorate the robustness and the accuracy of the robot. Unfortunately, the TDR is not available. In

this case, let us apply an iterative estimator to estimate the TDR and to reduce its effect, and give to the control system more flexibility to deal with parameters' variation and unexpected disturbances. The iterative estimator is given as:

$$\begin{aligned}&\hat{\varepsilon}(t) = \hat{\varepsilon}(t-t_d) - k_4 S \\ &\hat{\varepsilon}(t) = 0,\ \forall\, t \in [-t,\ 0]\,;\ \ , k_4 = kI_{7\times 7}\end{aligned} \tag{6.25}$$

where, k is a positive constant. The proof of the above equation (6.25) is given in appendix III. The closed loop of the global system can be written using equation (6.19) and control input equation (6.23) as follows:

$$\begin{cases} S = \dot{\eta}_1 - \dot{\eta}_r \\ \dot{S} = -\hat{J}^T(\eta_1, \hat{\gamma}_k)\left(k_1 e_x + k_2 \dot{\hat{e}}_x + k_3 \hat{S}_x\right) - \tilde{\varepsilon}(t) \end{cases} \tag{6.26}$$

with: $\tilde{\varepsilon}(t) = \hat{\varepsilon}(t) - \varepsilon(t)$ and $\varepsilon(t) = H(t) - \hat{H}(t)$ are respectively Time Delay Error, and dynamic uncertainties. Let us know state the main result of the paper.

Theorem 6.1 The control law for sliding mode with time delay estimation (TDE) of uncertain robot dynamics determined in equation (6.23) ensures the asymptotic stability of the robot system. The desired torque input is given as:

$$\tau = M_0(\eta_1)U(t) \tag{6.27}$$

where $U(t)$ is given in equation (6.23).

Proof To facilitate the proof of stability, let us define the term of the iterative estimator. First, we can write $\frac{d}{dt}\int_{t-t_d}^{t} \tilde{\varepsilon}^T(w)\tilde{\varepsilon}(w)dw$ as follows:

$$\frac{d}{dt}\int_{t-t_d}^{t} \tilde{\varepsilon}^T(w)\tilde{\varepsilon}(w)dw = \tilde{\varepsilon}^T(t)\tilde{\varepsilon}(t) - \tilde{\varepsilon}^T(t-t_d)\tilde{\varepsilon}(t-t_d) \tag{6.28}$$

Additionally,

$$\frac{1}{2k}\tilde{\varepsilon}^T(t)\tilde{\varepsilon}(t)-\frac{1}{2k}\tilde{\varepsilon}^T(t-t_d)\tilde{\varepsilon}(t-t_d)=\tilde{\varepsilon}^T(t)S-S^T\frac{k_4^T}{2}S \tag{6.29}$$

The details of equation (6.28) and equation (6.29) are given in Appendix III. Consider the following Lyapunov function candidate:

$$V=\frac{1}{2}S^TS+\frac{1}{2}e_x^T\left(k_1+\beta k_2\right)e_x+\frac{1}{2}\Delta\gamma_k^Tk_f\Delta\gamma_k+\frac{1}{2k}\int_{t-t_d}^{t}\tilde{\varepsilon}^T(w)\tilde{\varepsilon}(w)dw \tag{6.30}$$

with: $\Delta\gamma_k=\gamma_k-\hat{\gamma}_k$, $\tilde{\varepsilon}(t)=\hat{\varepsilon}(t)-\varepsilon(t)$ and $\varepsilon(t)=H(t)-\hat{H}(t)$ are respectively the estimation errors of kinematic uncertainties, Time Delay Error, and dynamic uncertainties. The derivative of the proposed Lyapunov function with respect to time is obtained as:

$$\dot{V}=S^T\dot{S}+e_x^T\left(k_1+\beta k_2\right)\dot{e}_x-\Delta\gamma_k^Tk_f\dot{\hat{\gamma}}_k+\frac{1}{2k}\tilde{\varepsilon}^T(t)\tilde{\varepsilon}(t)-\frac{1}{2k}\tilde{\varepsilon}^T(t-t_d)\tilde{\varepsilon}(t-t_d) \tag{6.31}$$

Substituting $\dot{S}$ from equation (6.19) and using equation (6.29) into equation (6.31), we find:

$$\begin{aligned}\dot{V}&=-S^T\hat{f}^T(\eta_1,\hat{\gamma}_k)\left(k_1e_x+k_2\dot{\hat{e}}_x+k_3\hat{S}_x\right)+e_x^T\left(k_1+\beta k_2\right)\dot{e}_x-\Delta\gamma_k^Tk_f\dot{\hat{\gamma}}_k\\&\quad+S^T\varepsilon(t)-S^T\hat{\varepsilon}(t)+\tilde{\varepsilon}^T(t)S-S^T\frac{k_4^T}{2}S\\&=-S^T\hat{f}^T(\eta_1,\hat{\gamma}_k)\left(k_1e_x+k_2\dot{\hat{e}}_x+k_3\hat{S}_x\right)+e_x^T\left(k_1+\beta k_2\right)\dot{e}_x-\Delta\gamma_k^Tk_f\dot{\hat{\gamma}}_k\\&\quad-S^T\frac{k_4^T}{2}S\end{aligned} \tag{6.32}$$

Substituting equation (6.17) and equation (6.22) into equation (6.32), we find:

$$\begin{aligned}\dot{V}=&-\hat{S}_x^Tk_1e_x-\hat{S}_x^Tk_2\dot{\hat{e}}_x-\hat{S}_x^Tk_3\hat{S}_x-S^T\frac{k_4^T}{2}S+e_x^T\left(k_1+\beta k_2\right)\dot{e}_x-\Delta\gamma_k^T\phi^T(t)k_2\phi(t)\Delta\gamma_k\\&-\Delta\gamma_k^TQ^T(\eta_1,\eta_2)\left(k_1+\beta k_2\right)e_x\end{aligned} \tag{6.33}$$

We have from equation (6.5), equation (6.10) and equation (6.13):

$$\hat{S}_x = \dot{e}_x + \beta e_x - Q(\eta_1, \eta_2)\Delta\gamma_k = \dot{\hat{e}}_x + \beta e_x \tag{6.34}$$

with:

$$Q(\eta_1, \eta_2)\Delta\gamma_k = J(\eta_1)\eta_2 - \hat{J}(\eta_1, \hat{\gamma}_k)\eta_2 = \dot{x} - \dot{\hat{x}} \tag{6.35}$$

From equation (6.34) we have:

$$\dot{\hat{e}}_x = \dot{e}_x - Q(\eta_1, \eta_2)\Delta\gamma_k \tag{6.36}$$

Substituting equation (6.34) and equation (6.36) into equation (6.33), we find:

$$\begin{aligned}\dot{V} = -\dot{e}_x^T k_1 \dot{e}_x + 2\dot{e}_x^T k_2 Q(\eta_1, \eta_2)\Delta\gamma_k - \beta e_x^T k_1 e_x - \hat{S}_x^T k_3 \hat{S}_x - S^T \frac{k_4^T}{2} S - \Delta\gamma_k^T \phi^T(t) k_2 \phi(t) \Delta\gamma_k \\ -\Delta\gamma_k^T Q^T(\eta_1, \eta_2) k_2 Q(\eta_1, \eta_2)\Delta\gamma_k\end{aligned} \tag{6.37}$$

while $\dot{\hat{e}}_x = \dot{e}_x - Q(\eta_1, \eta_2)\Delta\gamma_k$, equation (6.34) can be reduced to:

$$\dot{V} = -\dot{\hat{e}}_x^T k_1 \dot{\hat{e}}_x - \beta e_x^T k_1 e_x - \hat{S}_x^T k_3 \hat{S}_x - S^T \frac{k_4^T}{2} S - \Delta\gamma_k^T \phi^T(t) k_2 \phi(t) \Delta\gamma_k \tag{6.38}$$

From equation (6.30), we can easily see that V is positive definite in S, $\dot{\hat{e}}$, $\Delta\gamma_k$, and $\tilde{\varepsilon}(t)$. Since $\dot{V}$ is negative definite from equation (6.38), and V is bounded, this implies that S, e, $\hat{\gamma}_k$, and $\hat{\varepsilon}(t)$ are bounded. From equation (6.17) $\hat{S}_x$ is bounded because S is bounded. x is bounded because x_d is assumed bounded (**Assumption 6.4**). While e_x is bounded and $\dot{x}_d$ is bounded (**Assumption 6.4**), this implies $\dot{x}_r$ in equation (6.10) is bounded. The pseudo-inverse of the Jacobian matrix in equation (6.15) is non singular and bounded (all joints of manipulator are revolute), this means that $\dot{\theta}_r$ is bounded. We observe from equation (6.17) that $\dot{\theta}$ is bounded, this implies $\dot{x}$ is bounded while the Jacobian matrix is bounded. We remark from equation (6.11) that $\ddot{x}_r$ is bounded because $\dot{e}_x$ and $\ddot{x}_d$ are bounded (**Assumption 6.4**). It is clear from equa-

tion (6.16) that $\ddot{\theta}_r$ is bounded. We see from equation (6.18) that $\dot{S}$ is bounded, that implies $\ddot{\theta}$ is bounded. We can conclude from equation (6.14) that $\dot{\hat{S}}_x$ is bounded. The derivative of equation (6.34) is expressed as follows:

$$\hat{S}_x = \ddot{\hat{e}}_x + \beta \dot{e}_x \tag{6.39}$$

where $\ddot{\hat{e}}_x = \ddot{\hat{e}} - \ddot{x}_d$ is bounded. Since V is bounded and $\dot{V}$ is continuous and negative semi-definite, we can utilize Barbalat's lemma by differentiating equation equation (6.38) such that:

$$\ddot{V} = -2\dot{\hat{e}}_x^T k_1 \ddot{\hat{e}}_x - 2\beta e_x^T k_1 \dot{e}_x - 2\hat{S}_x^T k_3 \dot{\hat{S}}_x - 2S^T \frac{k_4^T}{2} \dot{S} - \Delta\gamma_k^T \phi^T(t) k_2 \left(\dot{\phi}(t)\Delta\gamma_k - \phi(t)\hat{\gamma}_k\right) \tag{6.40}$$

Since $\dot{\theta}$ and $\ddot{\theta}$ are bounded, this means $\phi(t)$, $\dot{\phi}(t)$ are bounded. This proves that $\ddot{V}$ is bounded since e_x, $\dot{e}_x$, $\dot{\hat{e}}_x$, $\ddot{\hat{e}}_x$, $\dot{\hat{S}}_x$, and γ_k are all bounded. So, $\dot{V}$ is continuous and negative semi-definite; according to Barbalat's lemma. we have $e_x \to 0$, $\dot{e}_x \to 0$, $S \to 0$ and $\phi(t)\Delta\gamma_k \to 0$ as $t \to \infty$.

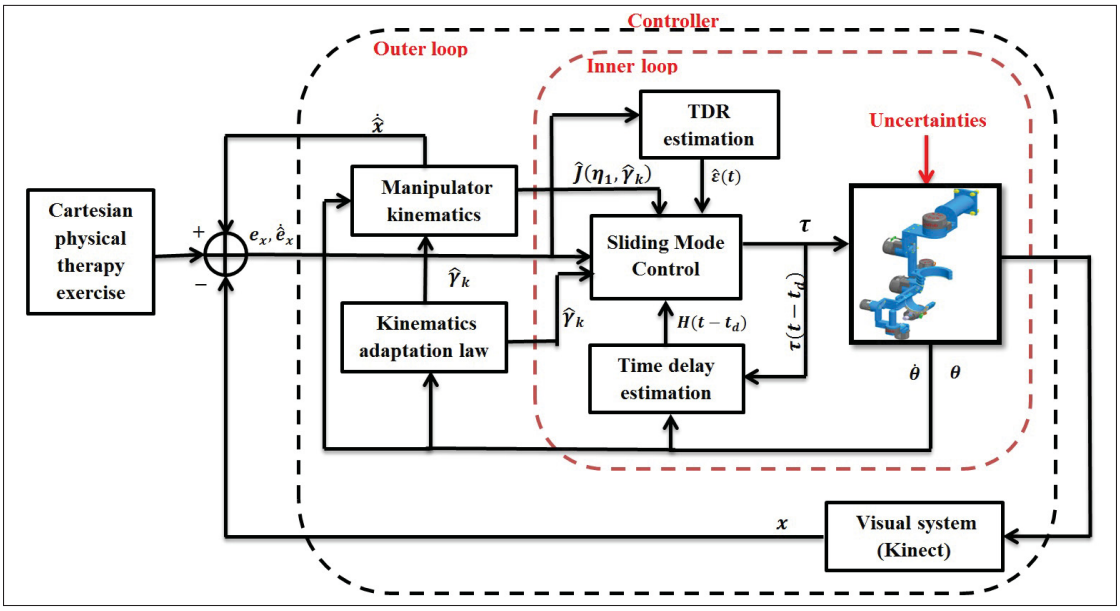

Figure 6.2 Block diagram of the proposed controller for exoskeleton robot with unknown kinematics/dynamics

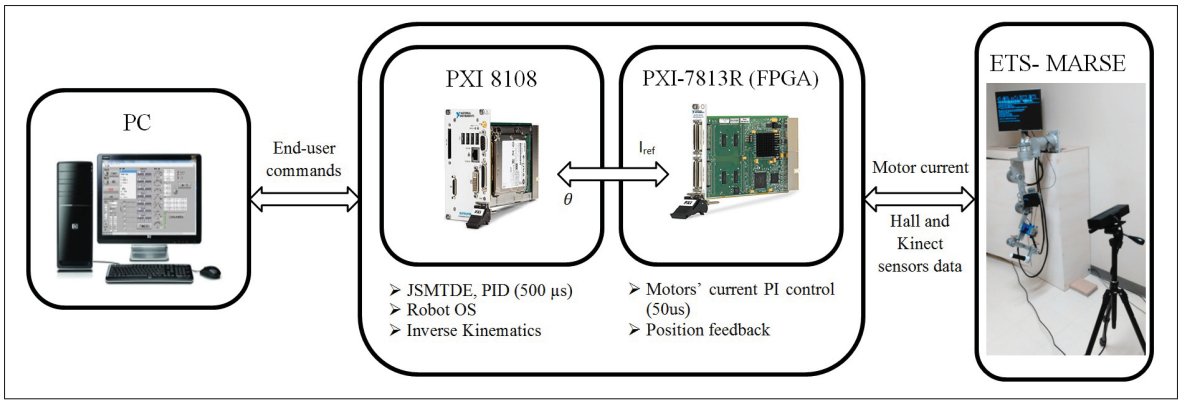

Figure 6.3 Experiments architecture

Now, the derivative of equation equation (6.34) with respect to time yields:

$$\ddot{e}_x + \beta \dot{e}_x = \dot{\hat{S}}_x + \dot{Q}(\eta_1, \eta_2)\Delta\gamma_k - Q(\eta_1, \eta_2)\dot{\hat{\gamma}}_k \tag{6.41}$$

That means $\ddot{e}_x$ is also bounded. In this case, we have $\dot{e}_x \to 0$ as $t \to \infty$ since $\ddot{e}_x$ and e_x are bounded. Hence, the proof is complete. The lock diagram of the proposed controller is given in Figure 6.2.

6.4 Experimental and comparative study

6.4.1 Experiment set-up

The experimental setup of the proposed system is shown in Figure 6.3. The system consists of three processing units. The first is a PC from where the top-level commands are sent to the robot using LabVIEW interface, i.e. the control scheme selection, joint or Cartesian space trajectory, gain adjustments, etc. This PC also receives the data after the robot task is executed to analyze its performance. The other two processing units are part of a National Instruments PXI platform. Firstly, a NI-PXI 8081 controller card with an Intel Core Duo processor; in this card, the main operating system of the robot and the top-level control scheme are executed. In our case, the sliding mode based controller as well as the estimation based on time delay approach, at a sampling time of 500 μs. The inverse kinematics algorithm also runs inside

this control loop. Finally, at input-output level, a NI PXI-7813R remote input–output card with an FPGA (field programmable gate array) executes the low-level control; i.e. a PI current control loop (sampling time of 50 μs) to maintain the current of the motors required by the main controller. Also, in this FPGA, the position feedback (Cartesian and joint) via Hall-sensors (joint position) and Kinect (Cartesian End-effector position), basic input-output tasks are executed.

Table 6.1 Modified Denavit-Hartenberg parameters

joint (i)	α_{i-1}	a_{i-1}	d_i	θ_i
1	0	0	d_s	θ_1
2	$\frac{-\pi}{2}$	0	0	θ_2
3	$\frac{\pi}{2}$	0	d_e	θ_3
4	$\frac{-\pi}{2}$	0	0	θ_4
5	$\frac{\pi}{2}$	0	d_w	θ_5
6	$\frac{-\pi}{2}$	0	0	$\theta_6 - \frac{\pi}{2}$
7	$\frac{-\pi}{2}$	0	0	θ_7

The modified Denavit-Hartenberg (DH) parameters are given in Table 6.1. These parameters are obtained from reference frames as shown in Figure 6.1, and are used to obtain the homogeneous transformation matrices.

Table 6.2 Workspace ETS-MARSE

joint (i)	Motion	Workspace
1	Shoulder joint horizontal flexion/extension	$0^\circ/140^\circ$
2	Shoulder joint vertical flexion/extension	$140^\circ/0^\circ$
3	Shoulder joint internal/external rotation	$-85^\circ/75^\circ$
4	Elbow joint flexion/extension	$120^\circ/0^\circ$
5	Forearm joint pronation/supination	$-85^\circ/85^\circ$
6	Wrist joint ulnar/radial deviation	$-30^\circ/20^\circ$
7	Wrist joint flexion/extension	$-50^\circ/60^\circ$

The workspace of the designed robot is given in Table 6.2 and the physical parameters of ETS-MARSE relative to the base reference frame are given in Table 6.3. The details of the parameters and design of ETS- MARSE are given in (Rahman *et al.*, 2015).

In the experiments, the desired Cartesian trajectory corresponds to a prescribed passive physical therapy task performed by three healthy subjects (age: 27 ± 4.6 years; height: 170 ± 8.75 cm; weight: 75 ± 18 kg). This trajectory (Initial position $\rightarrow$ Target-A $\rightarrow$Target-B $\rightarrow$ Target-C $\rightarrow$ Initial position) is expressed in Cartesian space to evaluate the proposed control. In this case, the position of the Cartesian End-Effector of the robot is provided by visual system (Kinect). For the carried object, the subject-robot system carried an object with unknown weight and dimensions during the desired trajectory. It is important to notice that the external disturbances here are represented by different physiological conditions of the subjects, such as non-linear biomechanical characteristics of the musculoskeletal system, the different weight of the upper-limb for each subject, the presence of spasticity in neurological patients, etc.

Table 6.3 Physical parameters of ETS-MARSE

Joints (i)	Mass (kg)	Centre of mass (m)	Link length (m)
1	3.475	0.0984	0.145
2	3.737	0.1959	0
3	0	0	0.25
4	2.066	0.163	0
5	0	0	0.267
6	0.779	0.121	0
7	0.496	0.0622	0

The experimental control gains are chosen by trial and error as follows: $k_1 = 20I_{6\times6}$, $k_2 = 70I_{6\times6}$, $k_3 = 18I_{6\times6}$, $k_f = 0.01I_{6\times6}$, $k_4 = 0.5I_{7\times7}$ and $\beta = 10$. The experimental results are given in Figure 6.4, Figure 6.5 and Figure 6.6.

6.4.2 Experimental results

6.4.2.1 The main results of the proposed controller with recursive control

The experimental results with ETS-MARSE robot in Cartesian space performed by Subject-1: (age: 27 years; height: 177 cm; weight: 83 kg) using the designed strategy are shown in Figure 6.4. As we see in this figure (Figure 6.4(a)), the desired trajectory (red line) nearly overlapped with the measured trajectory (green line). It can be noticed that these results are fairly good. Figure 6.4(b) presents the Cartesian errors as functions of time. From this figure, it is obvious that the Cartesian errors are getting smaller along the desired trajectory. Figure 6.5 shows that the control input is bounded without any noticeable control chattering. Finally, the convergence of the kinematic ($\hat{\gamma}_k$) and dynamic ($\hat{H}(t)$) parameters of the exoskeleton robot during the proposed control is shown in Figure 6.6 and Figure 6.7 respectively. These results confirm that the control strategy is able to achieve the desired robot's performance even if the nonlinear kinematics and dynamics of the exoskeleton robot are uncertain and the parameters of Kinect (camera) device are not completely known.

6.4.2.2 The results of the proposed controller without recursive control

Figure 6.8(a) presents the workspace performance of the robot in Cartesian space (red is the desired trajectory, green is real trajectory) performed with performed by Subject-1: (age: 28 years; height: 177 cm; weight: 83 kg) using the proposed controller without a recursive controller. In fact, we remark from figures (Figure 6.8)(a-b)) that the proposed controller without recursive controller shows a good performance. Where the Cartesian error (Figure 6.8)(b)) is getting smaller with time. However, the control inputs of the conventional approach, presented in Figure 6.9, illustrate a noisy control input with a small chattering phenomenon, meanwhile, noise and peaks appear also in the estimation parameters of the unknown dynamics parameters as we see in Figure 6.10.

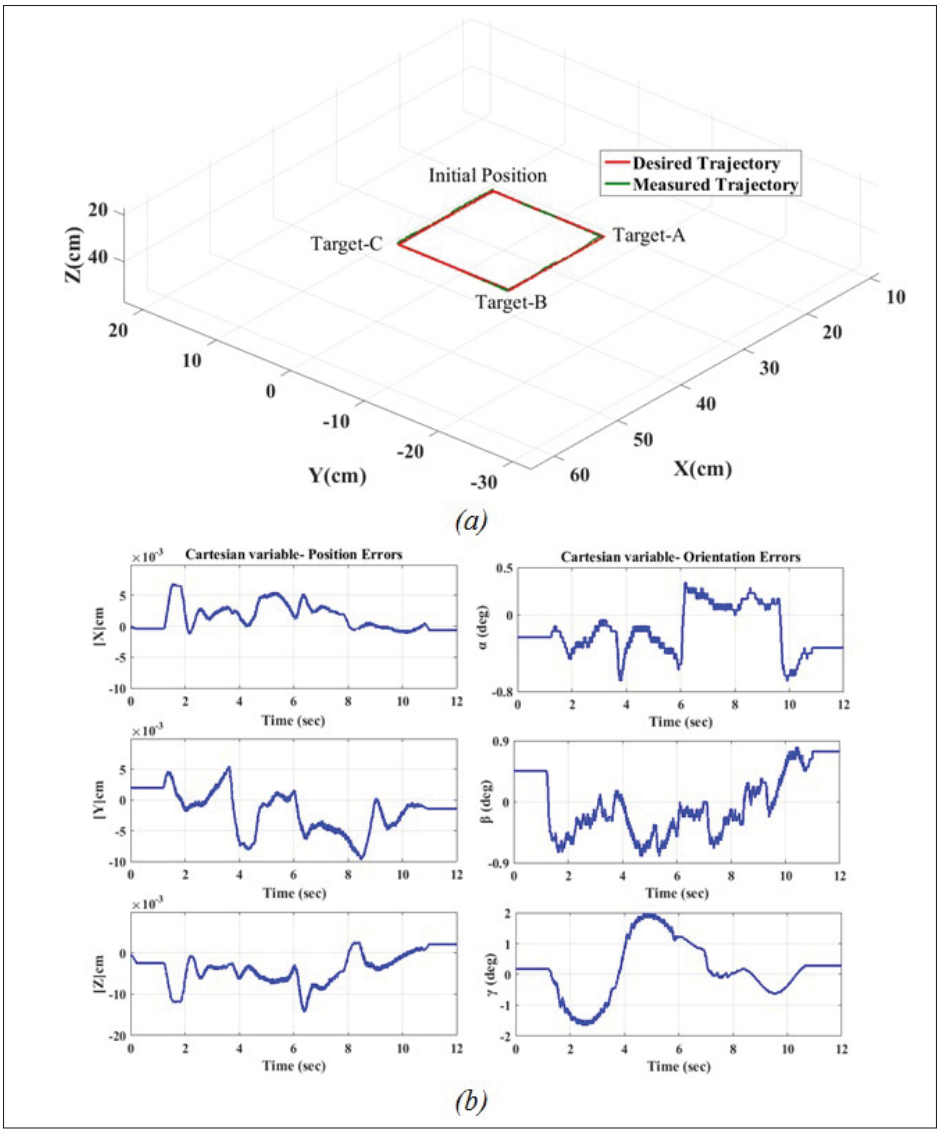

Figure 6.4 (a) Workspace performance of the robot in Cartesian space performed by Subject-1: (age: 27 years; height: 177 cm; weight: 83 kg). (b) Cartesian errors

On the other hand, the proposed controller with recursive control provides a smooth control input (Figure 6.5) and smooth estimation of unknown dynamics parameters (Figure 6.7). Therefore, we can say that the TDR is the main cause of the noise in the control input, which may damage the motors. From the comparison of the two experimental results, we can conclude that the proposed strategy with a recursive action provides a high level of precision and robustness against the nonlinear dynamic uncertainties and unknown disturbances.

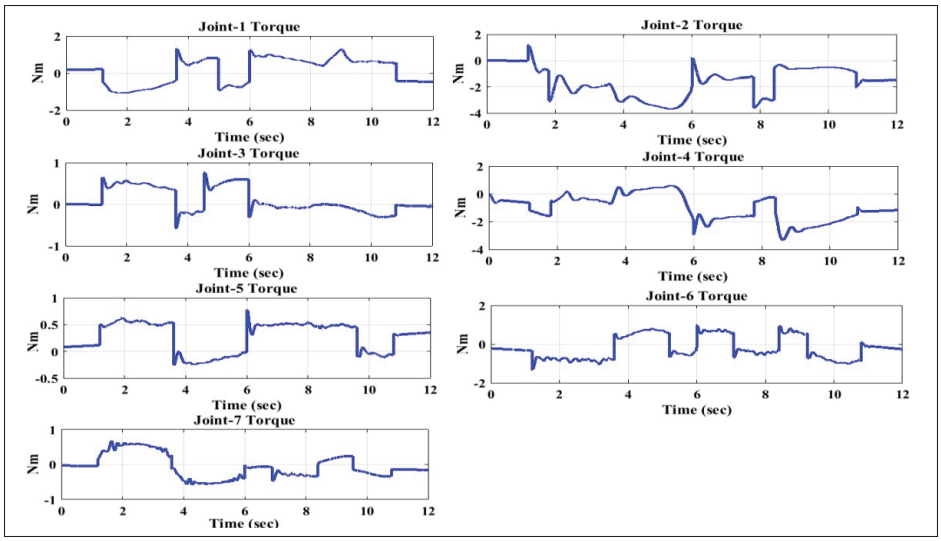

Figure 6.5 Control input of the proposed controller

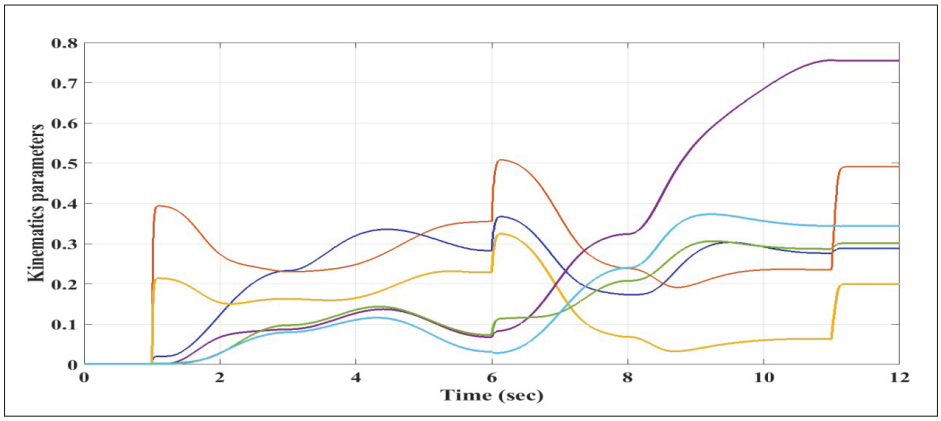

Figure 6.6 Kinematic ($\hat{\gamma}_k$) parameters convergence of the exoskeleton robot

6.4.3 Comparative study

In order to evaluate the efficiency and feasibility of the proposed control scheme, we compared it experimentally with the conventional adaptive visual tracking control presented in (Cheah, 2006). This latter is characterized by more complex implementation due to the complex regressor dynamic matrix, while the robot had a high degree of freedom (7-DOFs). To compute the regressor dynamic matrix of the robot, we use the virtual decomposition control (VDC) presented in (Luna *et al.*, 2016).

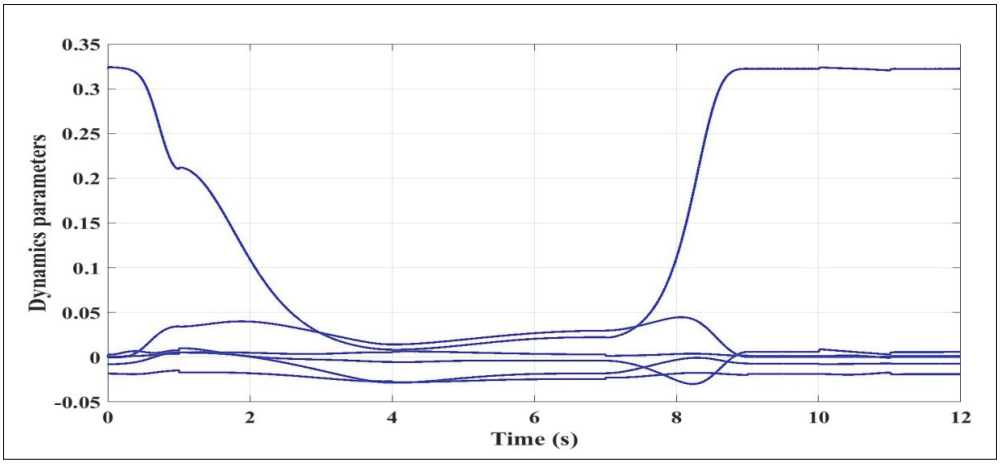

Figure 6.7 Unknown Dynamics ($\hat{H}(t)$) parameters convergence of the exoskeleton robot

Table 6.4 Comparative study of the controllers

Subjects	Root Mean Square (RMS)					
	The proposed controller with recursive action		*The proposed controller without recursive action*		*Conventional controller*	
	$\|e\|_{RMS\ error}$	$\|\tau\|_{RMS\ Torque}$	$\|e\|_{RMS\ error}$	$\|\tau\|_{RMS\ Torque}$	$\|e\|_{RMS\ error}$	$\|\tau\|_{RMS\ Torque}$
Subject-1	0.0317	2.0015	0.0487	2.6887	0.1987	4.8897
Subject-2	0.0299	1.8708	0.0417	2.1748	0.1478	4.1766
Subject-3	0.0281	1.9501	0.0335	2.8874	0.1797	4.7468

Figure 6.11(a) presents the Cartesian trajectory tracking in the 3D workspace (red is the desired trajectory, green is real trajectory) performed by the same subject (Subject-1: age: 27 years; height: 177 cm; weight: 83 kg) using the conventional controller. It is clear from (Figure 6.11 (a-b)) that the conventional controller provides a good tracking performance. Where, the error is converging along the desired trajectory as we show in Figure 6.11(b). Nevertheless, there is a presence of chattering phenomenon in the control inputs as shown in Figure 6.12, which may damage the motors of the robot. Compared with the smooth control input that is provided by the proposed strategy (Figure 6.5), we can conclude that the proposed strategy is easily implementable and provides a high precision and robustness to the kinematic/dynamic uncertainties, with unknown disturbances, and uncertainties of the camera parameters.

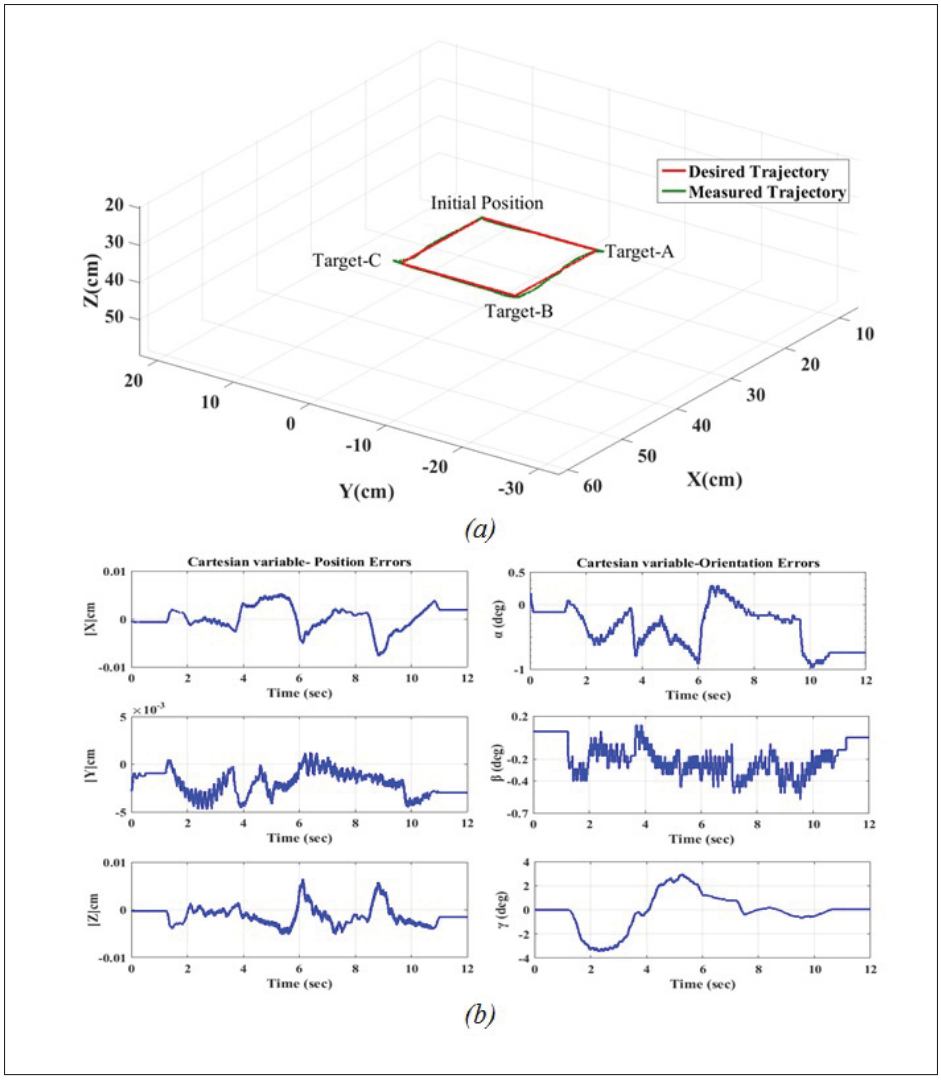

Figure 6.8 (a) Workspace performance of the robot in Cartesian space performed by Subject-1: (age: 27 years; height: 177 cm; weight: 83 kg). (b) Cartesian errors

To show more the feasibility of the designed strategy, we propose a numerical comparison between the above controller (conventional controller and proposed controller) by calculating the root mean square (RMS) of the error and the control input of each controller as follows: $\|e\|_{RMS} = \sqrt{\frac{1}{N}\sum_{i=1}^{N}\|e(i)\|^2}$ and $\|\tau\|_{RMS} = \sqrt{\frac{1}{N}\sum_{i=1}^{N}\|\tau(i)\|^2}$ where N is the number of the sampling time steps of the simulation. The evaluation of the controller is given Table 6.4.

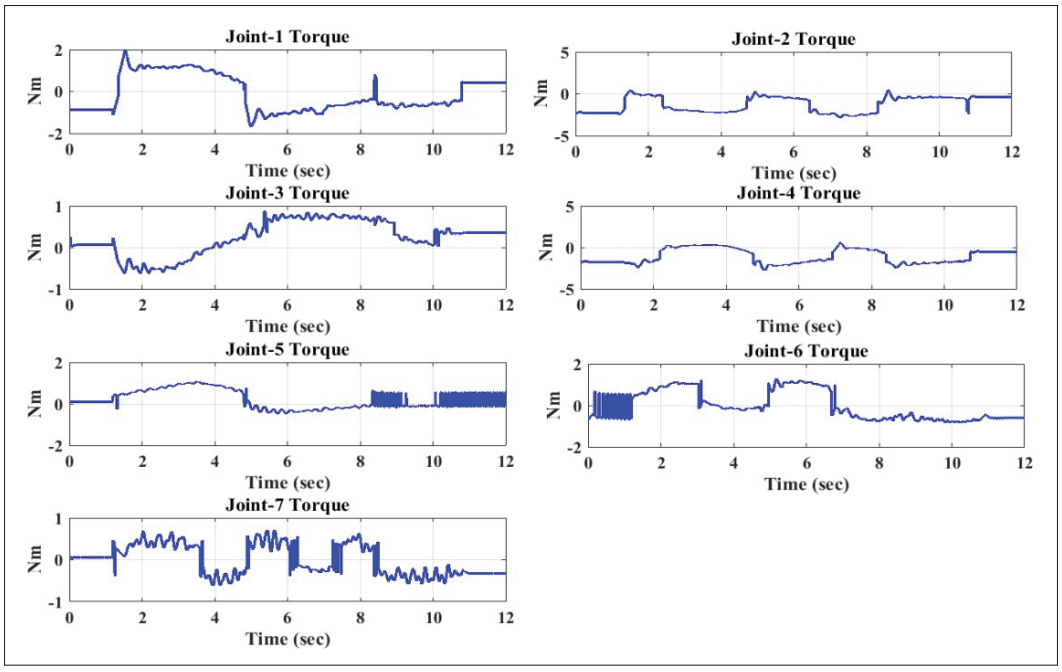

Figure 6.9 Control input.

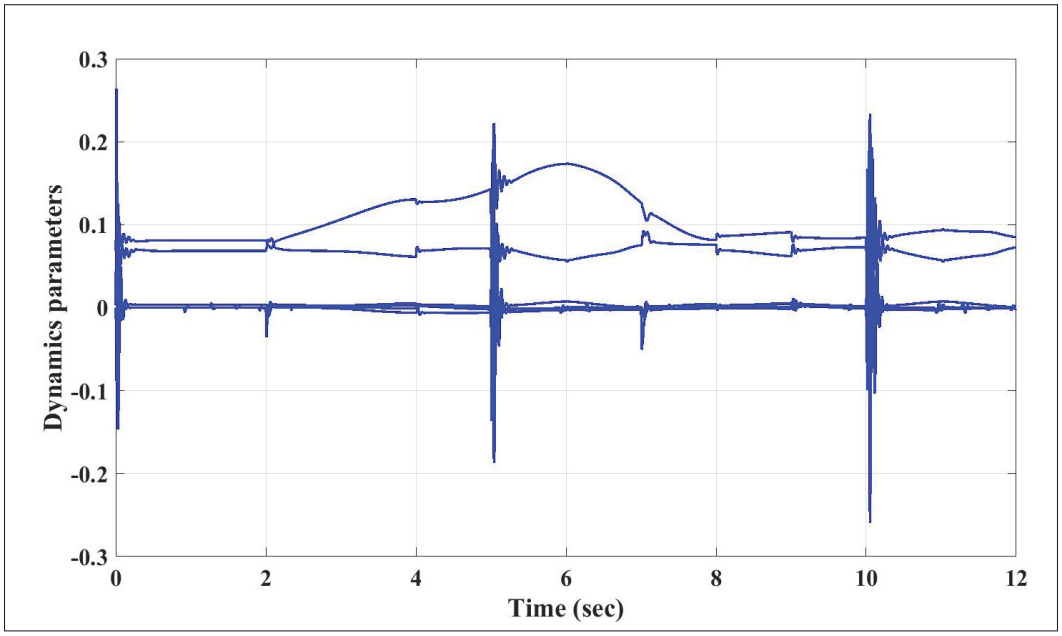

Figure 6.10 Unknown Dynamic parameters convergence of the exoskeleton robot

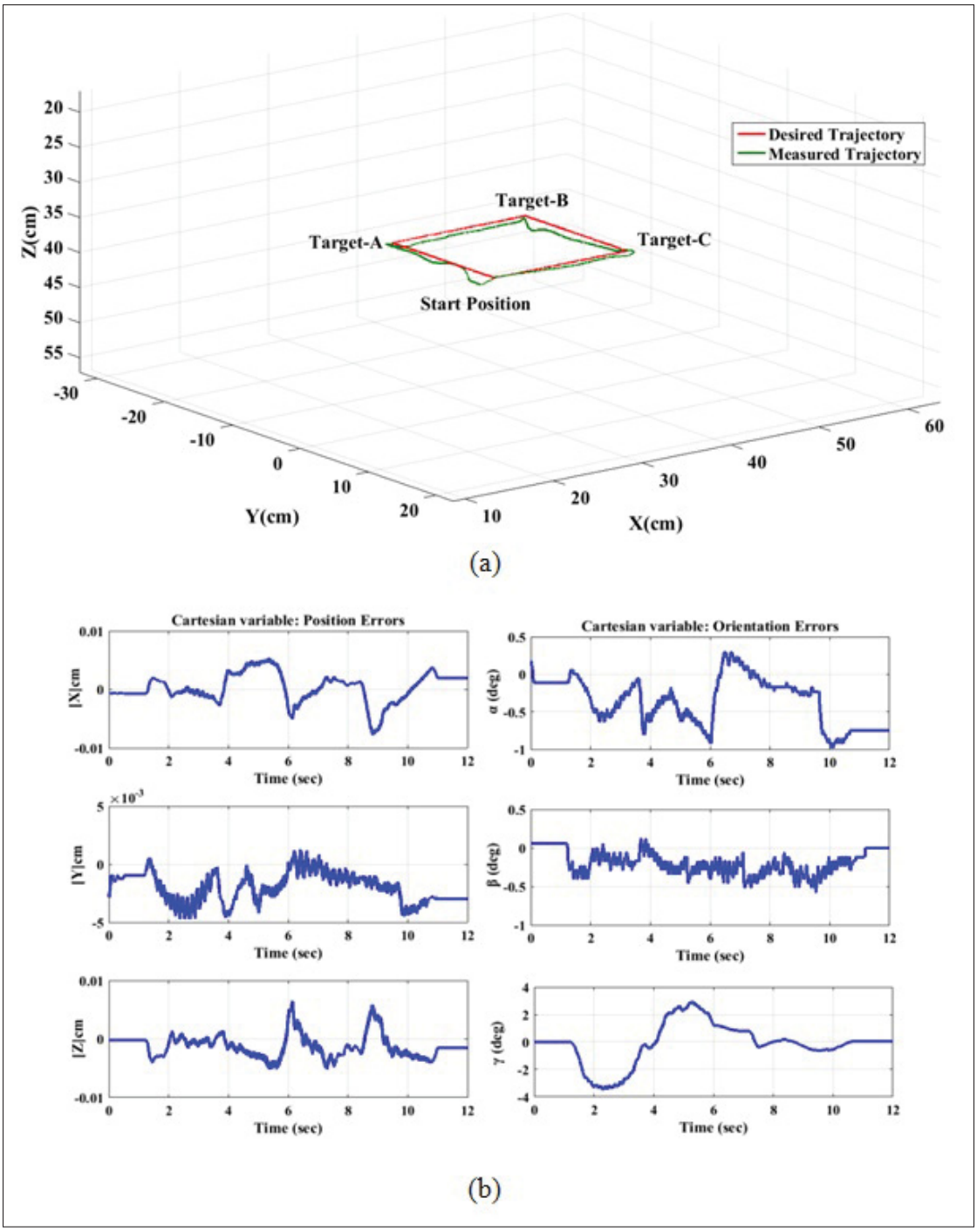

Figure 6.11 (a) Workspace performance of the robot in Cartesian space performed by Subject-1: (age: 27 years; height: 177 cm; weight: 83 kg). (b) Cartesian errors

It confirms that the proposed approach gives the robot a high degree of efficiency for dealing well with parameter variations and the nonlinear kinematic/dynamic uncertainties in presence of unknown disturbances (different subjects with different physiological conditions. These conditions include non-linear biomechanical characteristics of the musculoskeletal system, the different weight of the upper limb for each patient, the presence of spasticity/dystonia, muscle weakness in neurological patients,... etc) and parameters' uncertainties of the Kinect compared with the conventional adaptive controller. The proposed controller provides consistent performance with different subjects, keeping the RMS error and general torque input at a small value compared with the conventional controller. Compared with similar tests performed in a previous study with ETS-MARSE robot, the proposed control based on TDE presents an excellent performance as the Virtual Decomposition Control (Luna *et al.*, 2016), and better than PID and Computed Torque Control (CTC) (Luna *et al.*, 2016).

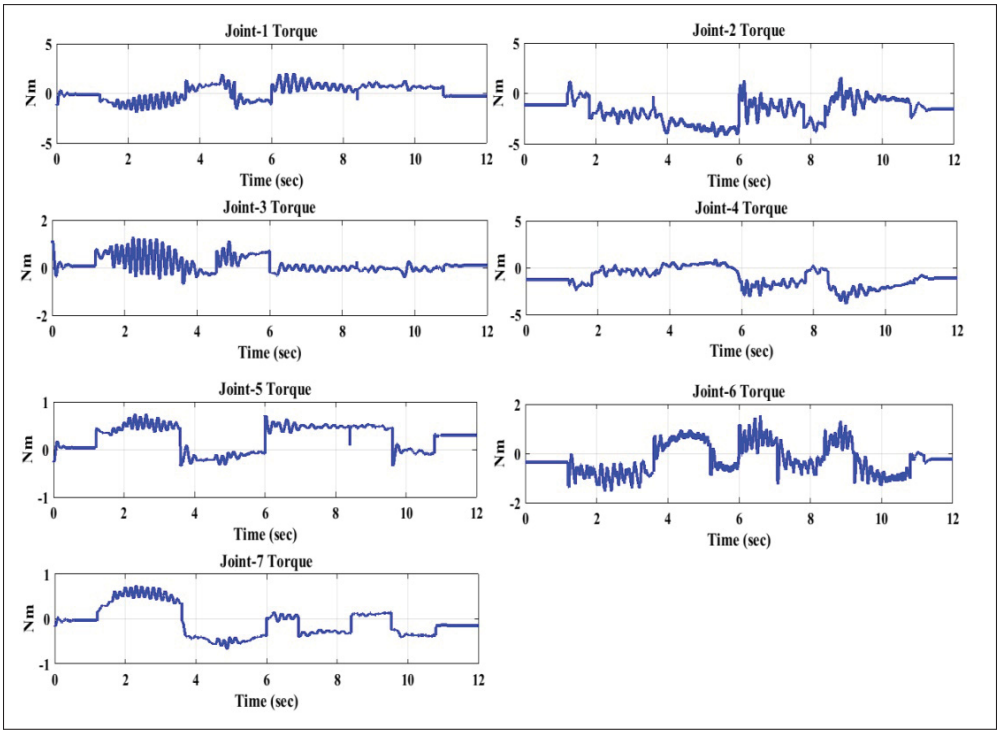

Figure 6.12 Control input

6.5 Conclusion

In this paper, we proposed an adaptive control of a 7DOFs exoskeleton robot with uncertain kinematics and dynamics based on sliding mode controller. Estimated Jacobian matrix is taken into consideration. The control strategy is achieved by inner/outer loops, where the outer loop is designed to estimate the nonlinear kinematic parameters and the Inner loop is designed to estimate the unknown dynamics of the robot using TDE approach and recursive control to limit the effect of its time delay error. The main benefit of the proposed adaptive control approach is that precise knowledge of the kinematic/dynamic parameters of the robot is not mandatory. Where, the proposed adaptive strategy is characterized by the ease of real-time implementation and provides a high precision and robustness to the kinematic/dynamic uncertainties, unknown perturbation, and uncertainties of the camera parameters. Additionally, the time delay error is taken into account to improve the accuracy of the robot performance. The stability analysis of inner/outer visual tracking control with kinematics/dynamics uncertainties taken into consideration the uncertainties in the camera device was proved by the Lyapunov function theorem. The robustness of the proposed control was proved with a Cartesian functional therapy task performed by the ETS-MARSE robot. The experimental results show the effectiveness, facility of implementation and accuracy of the proposed approach.

CONCLUSION AND RECOMMENDATIONS

This thesis focused on designing and developing a suitable control strategy for the ETS-MARSE exoskeleton robot (Motion Assistive Robotic-exoskeleton for Superior Extremity) located in the laboratory of GREPCI-ETS. Several adaptive approaches were validated experimentally with the ETS-MARSE and performed by healthy subjects in order to perform a smooth movement, similar to the natural human movement, and to provide different assistive motion: passive and active rehabilitation tasks. The main results in this project can be summarized as follows:

- A new solution of inverse kinematics for 7-DOFs exoskeleton robot has been proposed. It allowed to perform some rehabilitation trajectories in Cartesian space (chapter 2). In this work, we have proposed a new solution to the inverse kinematics problem, compatible with human upper limb movement and valid for human arm configuration. The main advantage of this approach is that it provides an optimal Cartesian solution resembling the human upper limb movement and always presents a valid human arm configuration. In addition, the proposed inverse kinematics algorithm provides a solution avoiding singularity problems and characterized by a high level of precision and rapidity of response.
- A new compliant control based on a second-order sliding mode with adaptive-gain incorporating time delay estimation was applied on ETS-MARSE performed with healthy subjects (chapter 3). In this work, the dynamics parameters of the system were considered uncertain and were estimated by modified time delay estimation. Additionally, the proposed inverse kinematics solution was used with the proposed controller to provide an appropriate compliance control that allows ETS-MARSE to interact perfectly with humans;
- Several adaptive approaches based on Backstepping controller (chapter 4 and 5) integrated with modified time-delay estimation (TDE) to provide an accurate estimation of unknown dynamics of the exoskeleton robot and to compensate for external bounded disturbances.

Unlike the conventional TDE approach, time delay error (TDR) is taken into consideration by estimating its value with a recursive estimator. This latter is designed to reduce the influence of this error on the accuracy of the uncertain estimation. The active rehabilitation tasks were achieved by catching the user's intention of movement using Damped Least Square method;

- A new adaptive visual tracking control approach based on sliding mode control applied to ETS-MARSE robot with uncertain kinematics and dynamics, taking into account uncertainties in visual system (camera) parameters (chapter 6). The update laws were designed and formulated based on Lyapunov function to solve the adaptation problem methodically and to show the stability of the robot system.

Finally, we conclude that the designed control approaches have ensured a good performance, compensate for the dynamic and kinematic uncertainties during the rehabilitation tasks and eliminated the effect of the bounded disturbances.

Some limitations and problems may be raised in this thesis and can be considered as future work. As a mandatory step, the proposed strategies in this work should validate in clinical trials with real rehabilitation patients. However, before starting this step a profound review of safety protocol and design correction are necessary.

Another significant step for active rehabilitation is mandatory using electromyographic signals. The EMGs signals can be combined with force sensor readings to detect and estimate the subject's motion intention. It can also be used to transform the stiffness and human force to the control system to allow to evaluate the spasticity of the patient's upper limb.

APPENDIX I

1. Proof of (4.18), (4.21), and (4.22)

In such case, considering:

$$\begin{cases} H_i(t) \in H(t) \\ \hat{H}_i(t) \in \hat{H}(t) \\ \tilde{H}_i(t) \in \tilde{H}(t) \\ g(t) \in \mathbb{R} \end{cases} \tag{AI-1}$$

where $i \in \{1,\ldots,7\}$, $g(t)$; it will be determined later. Now, let us propose the following equation:

$$\begin{cases} H_i(t) = H_i(t-t_d) + \varepsilon_i(t_d) \\ \tilde{H}_i(t) = H_i(t) - \hat{H}_i(t) \\ \hat{H}_i(t) = \hat{H}_i(t-t_d) + \varepsilon_i + g(t) \end{cases} \tag{AI-2}$$

Then: $\dfrac{d}{dt}\int_{t-t_d}^{t} \tilde{H}^T(w)\tilde{H}(w) = -2\tilde{H}^T(w)g(t) - g^T(t)g(t)$

Proof:

$\dfrac{d}{dt}\int_{t-t_d}^{t} \tilde{H}^T(w)\tilde{H}(w)dw = \tilde{H}^T(t)\tilde{H}(t) - \tilde{H}^T(t-t_d)\tilde{H}(t-t_d)$. Considering $\hat{H}_i(t) = \hat{H}_i(t-t_d) + \varepsilon_i(t) + g(t)$:

$$\begin{aligned} \tilde{H}_i^2(t-t_d) &= \left[H_i(t-t_d) - \hat{H}_i(t-t_d)\right]\left[H_i(t-t_d) - \hat{H}_i(t-t_d)\right] \\ &= \left[H_i(t) - \hat{H}_i(t) + g(t)\right]\left[H_i(t) - \hat{H}_i(t) + g(t)\right] \\ &= \tilde{H}_i^2(t) + 2\tilde{H}_i(t)g(t) + g^2(t) \end{aligned} \tag{AI-3}$$

Thus, we can obtain;

$$\tilde{H}_i^2(t) - \tilde{H}_i^2(t-t_d) = -2\tilde{H}_i(t)g(t) - g^2(t) \tag{AI-4}$$

Let us now define $g(t)$ function as:

$$g(t) = -k_{3i}e_{2i} \tag{AI-5}$$

Substituting equation (AI-5) in (AI-4), we obtain:

$$\tilde{H}_i^2(t) - \tilde{H}_i^2(t-t_d) = 2\tilde{H}_i(t)k_{3i}e_{2i} - (k_{3i}e_{2i})^2 \tag{AI-6}$$

Multiplying both sides of (AI-6) by $\dfrac{1}{2k_{3i}}$ to obtain:

$$\frac{1}{2k_{3i}}\tilde{H}_i^2(t) - \frac{1}{2k_{3i}}\tilde{H}_i^2(t-t_d) = \tilde{H}_i(t)e_{2i} - \frac{k_{3i}}{2}e_{2i}^2 \tag{AI-7}$$

2. Proof Stability of Functional Lyapunov–Krasovskii equation (4.27):

The proposed adaptive time-delay control law (4.17) makes the system converge asymptotically stable. Where $e_1 \to 0$ and $e_2 \to 0$ as $t \to \infty$. The proof is formed in three stages. Stage 1 proves the boundedness of $V_4(t)$ in the interval $[0,\ t_{dn})$. Stage 2 proves the negativeness of $V_4(t)$ and asymptotically convergence of tracking errors e_1 and e_2 in the interval $[t_{dn},\ \infty)$.

stage 1: Boundedness of $V_4(t)$ in the interval $[0,\ t_{dn})$. The derivative of equation (4.27) $V_4(t)$ with respect to time for$t \in [0,\ t_{dn})$ is given by:

$$\dot{V}_4(t) = \dot{V}_2(t) + \sum_{i=1}^{7} \frac{1}{2k_{3i}}\tilde{H}_i^2(t) \tag{AI-8}$$

Differentiating (4.28) $\dot{V}_2(t)$ with respect to time is given such that:

$$\dot{V}_2(t) = -e_1^T k_1 \dot{e}_1 + e_1^T e_2 + e_2^T \dot{e}_2 \tag{AI-9}$$

Substituting equation (4.8) and (4.12) into (AI-9) and applying the adaptive control law (4.17) to find:

$$\begin{aligned}\dot{V}_2(t) &= -e_1^T k_1 \dot{e}_1 + e_1^T e_2 + e_2^T \left(-k_2 e_2 - e_1 + \hat{H}(t) - H(t)\right) \\ &= -e_1^T k_1 e_1 + e_1^T e_2 + e_2^T \left(-k_2 e_2 - e_1 - \left(H(t) - \hat{H}(t)\right)\right)\end{aligned} \tag{AI-10}$$

One obtains:

$$\dot{V}_2(t) = -e_1^T k_1 e_1 - e_2^T k_2 e_2 - e_2^T \tilde{H}(t) \tag{AI-11}$$

For $t \in [0,\, t_{dn}]$, we have from equation (4.18): $\hat{H} = -k_3 e_2$. Hence:

$$\begin{aligned}\tilde{H}_i^2(t) &= \left(H_i(t) - \hat{H}_i(t)\right)^2 \\ &= H_i^2(t) - 2H_i(t)\hat{H}_i(t) + \hat{H}_i^2(t) \\ &= H_i^2(t) - 2\hat{H}_i(t)\left[\tilde{H}_i(t) + \hat{H}_i(t)\right] + \hat{H}_i^2(t) \\ &= H_i^2(t) + 2k_{3i}\tilde{H}_i(t)e_{2i} - \left(k_{3i}e_{2i}\right)^2(t)\end{aligned} \tag{AI-12}$$

Therefore, substituting (AI-11) and (AI-12) in (AI-8) the Lyapunov function $\dot{V}_4(t)$ is rewritten as follows:

$$\begin{aligned}\dot{V}_4(t) &= -e_1^T k_1 e_1 - e_2^T k_2 e_2 - e_2^T \tilde{H}(t) + \sum_{i=1}^{n} \frac{1}{2k_{3i}} H_i^2(t) + \sum_{i=1}^{n} \tilde{H}_i(t) e_{2i} - \sum_{i=1}^{n} \frac{1}{2k_{3i}} \left(k_{3i} e_{2i}\right)^2 \\ &= -e_1^T k_1 e_1 - e_2^T k_2 e_2 - \sum_{i=1}^{n} \frac{k_{3i}}{2} e_{2i}^2 + \sum_{i=1}^{n} \frac{1}{k_{3i}} H_i^2(t)\end{aligned} \tag{AI-13}$$

According to **Assumption 4.4**, $H_i(t)$, $i = 1, \ldots 7$ are bounded. This implies $\dot{V}_4(t)$ is bounded. Hence, $\dot{V}_4(t)$ is bounded in time interval $[0,\, t_{d1})$.

For $t \in [t_{dn-1},\, t_{dn})$, conforming to the derivative of $\dot{V}_4(t)$ with respect to time can be writing by

$$\begin{aligned}
\dot{V}_4(t) &= -e_1^T k_1 e_1 - e_2^T k_2 e_2 - e_2^T \tilde{H}(t) + \frac{1}{2k_{3n}} H_n^2(t) + \sum_{i=1}^{n-1} \frac{1}{2k_{3i}} \left(\tilde{H}_i^2(t) - \tilde{H}_i^2(t-t_d)\right) \\
&= -e_1^T k_1 e_1 - e_2^T k_2 e_2 - e_2^T \tilde{H}(t) + \frac{1}{2k_{3n}} H_n^2(t) + \tilde{H}_n(t) e_{2n} - \frac{k_{3n}}{2} e_{2n}^2 + \sum_{i=1}^{n-1} \tilde{H}_i(t) e_{2i} - \frac{1}{2} \sum_{i=1}^{n-1} k_{3i} e_2^2 \\
&= -e_1^T k_1 e_1 - e_2^T k_2 e_2 - e_2^T \tilde{H}(t) + \frac{1}{2k_{3n}} H_n^2(t) + \sum_{i=1}^{n} \tilde{H}_i(t) e_{2i} - \frac{1}{2} \sum_{i=1}^{n} k_{3i} e_2^2 \\
&= -e_1^T k_1 e_1 - e_2^T k_2 e_2 - \frac{1}{2} \sum_{i=1}^{n} k_{3i} e_2^2 + \frac{1}{2k_{3n}} H_n^2(t)
\end{aligned} \tag{AI-14}$$

It is clear from equation (AI-14) that $\dot{V}_4(t)$ is bounded for $t \in [t_{dn-1},\, t_{dn})$ because $H_i(t)$ is bounded. That means $\dot{V}_4(t)$ is bounded in time interval $[t_{dn-1},\, t_{dn})$.

stage 2: The negativeness of $\dot{V}_4(t)$ in the interval $[t_{dn},\, \infty)$. The derivative of $\dot{V}_4(t)$ with respect to time for $t \in [t_{dn},\, \infty)$ is given by:

$$\dot{V}_4(t) = -e_1^T k_1 e_1 - e_2^T k_2 e_2 - e_2^T \tilde{H}(t) + \sum_{i=1}^{n} \frac{1}{2k_{3i}} \left(\tilde{H}_i^2(t) - \tilde{H}_i^2(t-t_d)\right) \tag{AI-15}$$

We have from (AI-6): $\tilde{H}_i^2(t) - \tilde{H}_i^2(t-t_d) = 2\tilde{H}_i(t) k_{3i} e_{2i} - (k_{3i} e_{2i})^2$. So, (AI-15) can be rewritten as follows:

$$\begin{aligned}
\dot{V}_4(t) &= -e_1^T k_1 e_1 - e_2^T k_2 e_2 - e_2^T \tilde{H}(t) + \sum_{i=1}^{n} \tilde{H}_i e_{2i} - \frac{1}{2} \sum_{i=1}^{n} k_{3i} e_2^2 \\
&= -e_1^T k_1 e_1 - e_2^T k_2 e_2 - \frac{1}{2} \sum_{i=1}^{n} k_{3i} e_2^2
\end{aligned} \tag{AI-16}$$

It is clear from (AI-16) that $\dot{V}_4(t) \leq 0$ for $t \in [t_{dn},\, \infty)$, where all gains k_1, k_2, and k_{3i} are positive, which means that the robot system is stable. Hence, the signals e_1, e_2 and $\tilde{H}(t)$ are bounded.

APPENDIX II

1. Proof of the equation 5.26 (Li *et al.*, 2015a):

For very small sampling time period, it is acceptable to assume that the previous time delay error equals the current time delay error. In this case, considering:

$$\begin{cases} \varepsilon_i(t) \in \varepsilon(t) \\ \hat{\varepsilon}_i(t) \in \hat{\varepsilon}(t) \\ \tilde{\varepsilon}_i(t) \in \tilde{\varepsilon}(t) \\ g(t) \in \mathbb{R} \end{cases} \tag{AII-1}$$

where $i \in \{1,\ldots,7\}$, $g(t)$; it will be determined later. Now, let us propose the following equation:

$$\begin{cases} \varepsilon_i(t) = \varepsilon_i(t-t_d) + \varepsilon_i(t_d) \\ \tilde{\varepsilon}_i(t) = \varepsilon_i(t) - \hat{\varepsilon}_i(t) \\ \hat{\varepsilon}_i(t) = \hat{\varepsilon}_i(t-t_d) + g(t) \end{cases} \tag{AII-2}$$

Then: $\dfrac{d}{dt}\int_{t-t_d}^{t} \tilde{\varepsilon}^T(s)\tilde{\varepsilon}(s)ds = -2\tilde{\varepsilon}^T(t)g(t) - g^T(t)g(t)$

Proof:

$\dfrac{d}{dt}\int_{t-t_d}^{t} \tilde{\varepsilon}^T(s)\tilde{\varepsilon}(s)ds = \tilde{\varepsilon}^T(t)\tilde{\varepsilon}(t) - \tilde{\varepsilon}^T(t-t_d)\tilde{\varepsilon}(t-t_d)$. Considering $\hat{\varepsilon}_i(t) = \hat{\varepsilon}_i(t-t_d) + g(t)$:

$$\begin{aligned} \tilde{\varepsilon}_i^2(t-t_d) &= [\varepsilon_i(t-t_d) - \hat{\varepsilon}_i(t-t_d)]\,[\varepsilon_i(t-t_d) - \hat{\varepsilon}_i(t-t_d)] \\ &= [\varepsilon_i(t) - \hat{\varepsilon}_i(t) + g(t)]\,[\varepsilon_i(t) - \hat{\varepsilon}_i(t) + g(t)] \\ &= \tilde{\varepsilon}_i^2(t) + 2\tilde{\varepsilon}_i(t)g(t) + g^2(t) \end{aligned} \tag{AII-3}$$

Thus, we can obtain;

$$\tilde{\varepsilon}_i^2(t) - \tilde{\varepsilon}_i^2(t-t_d) = -2\tilde{\varepsilon}_i(t)g(t) - g^2(t) \tag{AII-4}$$

Let us now define $g(t)$ function as:

$$g(t) = -k_{3i}e_{2i} \tag{AII-5}$$

Substituting equation (AII-5) in (AII-4), we obtain:

$$\tilde{\varepsilon}_i^2(t) - \tilde{\varepsilon}_i^2(t-t_d) = 2\tilde{\varepsilon}_i(t)k_{3i}e_{2i} - (k_{3i}e_{2i})^2 \tag{AII-6}$$

Multiplying both sides of (AII-6) by $\dfrac{1}{2k_{3i}}$ to obtain:

$$\frac{1}{2k_{3i}}\tilde{\varepsilon}_i^2(t) - \frac{1}{2k_{3i}}\tilde{\varepsilon}_i^2(t-t_d) = \tilde{\varepsilon}_i(t)e_{2i} - \frac{k_{3i}}{2}e_{2i}^2 \tag{AII-7}$$

2. Stability proof of functional Lyapunov-Krasovskii equation (5.33):

The proposed adaptive time-delay control law (5.27) ensures the asymptotic stability of the system. Where $e_1 \to 0$ and $e_2 \to 0$ as $t \to \infty$. The proof is done in three stages. Stage 1 proves the boundedness of $V_3(t)$ in the interval $[0,\ t_{dn})$. Stage 2 proves the negativeness of $V_3(t)$ and asymptotically convergence of tracking errors e_1 and e_2 in the interval $[t_{dn},\ \infty)$.Stage 3 concludes the asymptotical convergence of tracking errors e_1 and e_2 .

stage 1: Boundedness of $V_3(t)$ in the interval $[0,\ t_{dn})$. The derivative of equation (5.31) $V_3(t)$ with respect to time for$t \in [0,\ t_{d1})$ is given by:

$$\dot{V}_3(t) = \dot{V}_2(t) + \sum_{i=1}^{7} \frac{1}{2k_{3i}}\tilde{\varepsilon}_i^2(t) \tag{AII-8}$$

Differentiating (5.32) $\dot{V}_2(t)$ with respect to time is given such that:

$$\dot{V}_2(t) = -e_1^T k_1 \dot{e}_1 + e_1^T e_2 + e_2^T \dot{e}_2 \tag{AII-9}$$

Substituting equation (5.14), (5.16) and (5.20) into (AII-9) and applying the adaptive control law (5.27) to find:

$$\begin{aligned}\dot{V}_2(t) &= -e_1^T k_1 \dot{e}_1 + e_1^T e_2 + e_2^T \left(-k_2 e_2 - e_1 - \hat{H}(t) + H(t) - \hat{\varepsilon}(t)\right) \\ &= -e_1^T k_1 e_1 + e_1^T e_2 + e_2^T \left(-k_2 e_2 - e_1 - \left(H(t) - \hat{H}(t)\right) - \hat{\varepsilon}(t)\right)\end{aligned} \tag{AII-10}$$

From equation (5.29) and equation (5.30), we find:

$$\dot{V}_2(t) = -e_1^T k_1 e_1 - e_2^T k_2 e_2 - e_2^T \tilde{\varepsilon}(t) \tag{AII-11}$$

For $t \in [0,\, t_{d1}]$, we have from equation (5.26): $\hat{\varepsilon} = -k_3 e_2$. Hence:

$$\begin{aligned}\tilde{\varepsilon}_i^2(t) &= \left(\varepsilon_i(t) - \hat{\varepsilon}_i(t)\right)^2 \\ &= \varepsilon_i^2(t) - 2\varepsilon_i(t)\hat{\varepsilon}_i(t) + \hat{\varepsilon}_i^2(t) \\ &= \varepsilon_i^2(t) - 2\hat{\varepsilon}_i(t)\left[\tilde{\varepsilon}_i(t) + \hat{\varepsilon}_i(t)\right] + \hat{\varepsilon}_i^2(t) \\ &= \varepsilon_i^2(t) + 2k_{3i}\tilde{\varepsilon}_i(t)e_{2i} - \left(k_{3i}e_{2i}\right)^2(t)\end{aligned} \tag{AII-12}$$

Therefore, substituting (AII-11) and (AII-12) in (AII-8) the Lyapunov function $\dot{V}_3(t)$ is rewritten as follows:

$$\begin{aligned}\dot{V}_3(t) &= -e_1^T k_1 e_1 - e_2^T k_2 e_2 - e_2^T \tilde{\varepsilon}(t) + \sum_{i=1}^{n} \frac{1}{2k_{3i}} \varepsilon_i^2(t) + \sum_{i=1}^{n} \tilde{\varepsilon}_i(t) e_{2i} - \sum_{i=1}^{n} \frac{1}{2k_{3i}} \left(k_{3i} e_{2i}\right)^2 \\ &= -e_1^T k_1 e_1 - e_2^T k_2 e_2 - \sum_{i=1}^{n} \frac{k_{3i}}{2} e_{2i}^2 + \sum_{i=1}^{n} \frac{1}{k_{3i}} \varepsilon_i^2(t)\end{aligned} \tag{AII-13}$$

According to **Assumption 5.2** and **Assumption 5.3**, $\varepsilon_i(t)$, $i = 1, \ldots 7$ are bounded. This implies $\dot{V}_3(t)$ is bounded. Hence, $\dot{V}_3(t)$ is bounded in time interval $[0,\, t_{d1})$.

For $t \in [t_{dn-1},\, t_{dn})$, conforming to the derivative of $\dot{V}_3(t)$ with respect to time can be writing by

$$\begin{aligned}
\dot{V}_4(t) &= -e_1^T k_1 e_1 - e_2^T k_2 e_2 - e_2^T \tilde{\varepsilon}(t) + \frac{1}{2k_{3n}}\varepsilon_n^2(t) + \sum_{i=1}^{n-1} \frac{1}{2k_{3i}} \left(\tilde{\varepsilon}_i^2(t) - \tilde{\varepsilon}_i^2(t-t_d)\right) \\
&= -e_1^T k_1 e_1 - e_2^T k_2 e_2 - e_2^T \tilde{\varepsilon}(t) + \frac{1}{2k_{3n}}\varepsilon_n^2(t) + \tilde{\varepsilon}_n(t) e_{2n} - \frac{k_{3n}}{2} e_{2n}^2 + \sum_{i=1}^{n-1} \tilde{\varepsilon}_i(t) e_{2i} - \frac{1}{2}\sum_{i=1}^{n-1} k_{3i} e_2^2 \\
&= -e_1^T k_1 e_1 - e_2^T k_2 e_2 - e_2^T \tilde{\varepsilon}(t) + \frac{1}{2k_{3n}}\varepsilon_n^2(t) + \sum_{i=1}^{n} \tilde{\varepsilon}_i(t) e_{2i} - \frac{1}{2}\sum_{i=1}^{n} k_{3i} e_2^2 \\
&= -e_1^T k_1 e_1 - e_2^T k_2 e_2 - \frac{1}{2}\sum_{i=1}^{n} k_{3i} e_2^2 + \frac{1}{2k_{3n}}\varepsilon_n^2(t)
\end{aligned} \tag{AII-14}$$

It is clear from equation (AII-14) that $\dot{V}_3(t)$ for $t \in [t_{dn-1},\, t_{dn})$ because $\varepsilon_i(t)$ is bounded. That means $\dot{V}_3(t)$ is bounded in time interval $[t_{dn-1},\, t_{dn})$.

stage 2: The negativeness of $\dot{V}_3(t)$ in the interval $[t_{dn},\, \infty)$. The derivative of $\dot{V}_3(t)$ with respect to time for $t \in [t_{dn},\, \infty)$ is given by:

$$\dot{V}_4(t) = -e_1^T k_1 e_1 - e_2^T k_2 e_2 - e_2^T \tilde{\varepsilon}(t) + \sum_{i=1}^{n} \frac{1}{2k_{3i}} \left(\tilde{\varepsilon}_i^2(t) - \tilde{\varepsilon}_i^2(t-t_d)\right) \tag{AII-15}$$

We have from (AII-6): $\tilde{\varepsilon}_i^2(t) - \tilde{\varepsilon}_i^2(t-t_d) = 2\tilde{\varepsilon}_i(t) k_{3i} e_{2i} - (k_{3i} e_{2i})^2$. So, (AII-15) can be rewritten as follows:

$$\begin{aligned}
\dot{V}_4(t) &= -e_1^T k_1 e_1 - e_2^T k_2 e_2 - e_2^T \tilde{\varepsilon}(t) + \sum_{i=1}^{n} \tilde{\varepsilon}_i e_{2i} - \frac{1}{2}\sum_{i=1}^{n} k_{3i} e_2^2 \\
&= -e_1^T k_1 e_1 - e_2^T k_2 e_2 - \frac{1}{2}\sum_{i=1}^{n} k_{3i} e_2^2
\end{aligned} \tag{AII-16}$$

It is clear from (AII-16) that $\dot{V}_3(t) \leq 0$ for $t \in [t_{dn},\, \infty)$.

stage 3: It is clear from equation (5.31) that $V_3(t)$ is positive definite in e_1, e_2, $\tilde{\varepsilon}(t)$ and $\tilde{H}(t)$. Since $\dot{V}_3(t)$ is semi-negative definite, and $V_3(t)$ is bounded, this implies that e_1, e_2, $\tilde{\varepsilon}(t)$ and $\tilde{H}(t)$ are bounded. In this case, we can utilize Barbalat's lemma to complete the stability proof. From **Assumption 5.3** and the boundedness ofe_1 and e_2, and from the boundedness of ξ in equation (5.14), and boundedness of $\dot{\theta}$ in equation (5.13), we conclude that $\dot{e}_1$ is bounded in

equation (5.14). $\dot{\theta}$ is bounded from equation (5.2) and $\dot{\theta}_d$ is bounded (**Assumption 5.4**), this means that $\dot{e}_2$ is bounded. $\dot{e}_1$ and $\dot{e}_2$ are bounded imply that e_1 and e_2 are uniformly continuous. According to Barbalat's theorem $e_1 \to 0$ and $e_2 \to 0$ as $t \to \infty$ and the proof is completed.

APPENDIX III

1. Proof of equations (6.18) and 6.19 (Brahim *et al.*, 2016b,a)

for very small sampling time period, it is acceptable to assume that the previous time delay error equals the current time delay error. In this case, considering:

$$\begin{cases} \varepsilon(t) = \varepsilon(t-t_d) \\ \tilde{\varepsilon}(t) = \varepsilon(t) - \hat{\varepsilon}(t) \\ \hat{\varepsilon}(t) = \hat{\varepsilon}_i(t-t_d) + g(t) \end{cases} \tag{AIII-1}$$

where $g(t) \in \mathbb{R}^7$; it will be determined later. Then:

$$\frac{d}{dt}\int_{t-t_d}^{t} \tilde{\varepsilon}^T(w)\tilde{\varepsilon}(w)dw = -2\tilde{\varepsilon}^T(t)g(t) - g^T(t)g(t) \tag{AIII-2}$$

Proof:

It is easy to conclude that:

$$\frac{d}{dt}\int_{t-t_d}^{t} \tilde{\varepsilon}^T(w)\tilde{\varepsilon}(w)dw = \tilde{\varepsilon}^T(t)\tilde{\varepsilon}(t) - \tilde{\varepsilon}^T(t-t_d)\tilde{\varepsilon}(t-t_d) \tag{AIII-3}$$

Considering the following equation: $\hat{\varepsilon}(t) = \hat{\varepsilon}(t-t_d) + g(t)$:

$$\begin{aligned} \tilde{\varepsilon}^T(t-t_d)\tilde{\varepsilon}(t-t_d) &= \left[\varepsilon^T(t-t_d) - \hat{\varepsilon}^T(t-t_d)\right]\left[\varepsilon(t-t_d) - \hat{\varepsilon}(t-t_d)\right] \\ &= \left[\varepsilon^T(t) - \hat{\varepsilon}^T(t) + g^T(t)\right]\left[\varepsilon(t) - \hat{\varepsilon}(t) + g(t)\right] \\ &= \tilde{\varepsilon}^T(t)\tilde{\varepsilon}(t) + 2\tilde{\varepsilon}^T(t)g(t) - g^T(t)g(t) \end{aligned} \tag{AIII-4}$$

Thus, we can obtain;

$$\tilde{\varepsilon}^T(t)\tilde{\varepsilon}(t) - \tilde{\varepsilon}^T(t-t_d)\tilde{\varepsilon}(t-t_d) = -2\tilde{\varepsilon}^T(t)g(t) - g^T(t)g(t) \tag{AIII-5}$$

Let us now define $g(t)$ function as:

$$g(t) = -k_4 S \tag{AIII-6}$$

Substituting equation (AIII-6) in (AIII-5), we obtain:

$$\tilde{\varepsilon}^T(t)\tilde{\varepsilon}(t) - \tilde{\varepsilon}^T(t-t_d)\tilde{\varepsilon}(t-t_d) = 2\tilde{\varepsilon}^T(t)k_4 S - (k_4 S)^T(k_4 S) \tag{AIII-7}$$

Hence, we have:

$$\frac{1}{2k}\tilde{\varepsilon}^T(t)\tilde{\varepsilon}(t) - \frac{1}{2k}\tilde{\varepsilon}^T(t-t_d)\tilde{\varepsilon}(t-t_d) = \tilde{\varepsilon}^T(t)S - S^T\frac{k_4^T}{2}S \tag{AIII-8}$$

BIBLIOGRAPHY

Adams, Richard J and Blake Hannaford. 1999. "Stable haptic interaction with virtual environments". *IEEE Transactions on robotics and Automation*, vol. 15, n° 3, p. 465–474.

Arimoto, Suguru. 1999. "Robotics research toward explication of everyday physics". *The International Journal of Robotics Research*, vol. 18, n° 11, p. 1056–1063.

Asfour, Tamim and Rüdiger Dillmann. 2003. "Human-like motion of a humanoid robot arm based on a closed-form solution of the inverse kinematics problem". In *Intelligent Robots and Systems, 2003.(IROS 2003). Proceedings. 2003 IEEE/RSJ International Conference on*. p. 1407–1412. IEEE.

Atkeson, Christopher G, PW Babu Benzun, Nandan Banerjee, Dmitry Berenson, Christoper P Bove, Xiongyi Cui, Mathew DeDonato, Ruixiang Du, Siyuan Feng, Perry Franklin et al. 2018. "What happened at the DARPA Robotics Challenge finals". In *The DARPA Robotics Challenge Finals: Humanoid Robots To The Rescue*, p. 667–684. Springer.

Aviles, Luis Adrian Zuñiga, Jesus Carlos Pedraza Ortega and Efren Gorrostieta Hurtado. 2012. "Experimental Study of the Methodology for the Modelling and Simulation of Mobile Manipulators". *International Journal of Advanced Robotic Systems*, vol. 9, n° 5, p. 192.

Bai, Yuliang, James D Biggs, Franco Bernelli Zazzera and Naigang Cui. 2017. "Adaptive attitude tracking with active uncertainty rejection". *Journal of Guidance, Control, and Dynamics*, vol. 41, n° 2, p. 550–558.

Balasubramanian, Sivakumar, Ruihua Wei, Mike Perez, Ben Shepard, Edward Koeneman, James Koeneman and Jiping He. 2008. "RUPERT: An exoskeleton robot for assisting rehabilitation of arm functions". In *Virtual Rehabilitation, 2008*. p. 163–167. IEEE.

Bartolini, Giorgio, Antonella Ferrara and Elio Usai. 1998. "Chattering avoidance by second-order sliding mode control". *IEEE Transactions on automatic control*, vol. 43, n° 2, p. 241–246.

Bartolini, Giorgio, Alessandro Pisano and Elio Usai. 2001. "Digital second-order sliding mode control for uncertain nonlinear systems". *Automatica*, vol. 37, n° 9, p. 1371–1377.

Bautista, Anthony James and Samuel Oliver Wane. 2018. "ATLAS Robot: A Teaching Tool for Autonomous Agricultural Mobile Robotics". In *2018 International Conference on Control, Automation and Information Sciences (ICCAIS)*. p. 264–269. IEEE.

Bin, Zhang, Xiong Rong and Wu Jun. 2011. "Kinematics analysis of a novel 7-DOF humanoid manipulator for table tennis". In *Electronics, Communications and Control (ICECC), 2011 International Conference on*. p. 1524–1528. IEEE.

Brahim, B, S Maarouf, C Ochoa Luna, B Abdelkrim and MH Rahman. 2016a. "Adaptive iterative observer based on integral backstepping control for upper extremity exoskeleton robot". In *Modelling, Identification and Control (ICMIC), 2016 8th International Conference on*. p. 886–891. IEEE.

Brahim, Brahmi, Mohammad Habibur Rahman, Maarouf Saad and C Ochoa Luna. 2016b. "Iterative estimator-based nonlinear backstepping control of a robotic exoskeleton". *World Academy of Science, Engineering and Technology, International Journal of Mechanical, Aerospace, Industrial, Mechatronic and Manufacturing Engineering*, vol. 10, n° 8, p. 1313–1319.

Brahim, Brahmi, Cristóbal Ochoa-Luna, Maarouf Saad, Md Assad-Uz-Zaman, Md Rasedul Islam and Mohammad Habibur Rahman. 2017. "A new adaptive super-twisting control for an exoskeleton robot with dynamic uncertainties". In *Biomedical Conference (GLBC), 2017 IEEE Great Lakes*. p. 1–1. IEEE.

Brahmi, A, M Saad, G Gauthier, B Brahmi, W-H Zhu and J Ghommam. 2016. "Adaptive backstepping control of mobile manipulator robot based on virtual decomposition approach". In *Modelling, Identification and Control (ICMIC), 2016 8th International Conference on*. p. 707–712. IEEE.

Brahmi, B, M Saad, C Ochoa Luna, PS Archambault and MH Rahman. 2017a. "Sliding mode control of an exoskeleton robot based on time delay estimation". In *Virtual Rehabilitation (ICVR), 2017 International Conference on*. p. 1–2. IEEE.

Brahmi, Brahim, Maarouf Saad, Cristobal Ochoa-Luna and Mohammad H Rahman. 2017b. "Adaptive control of an exoskeleton robot with uncertainties on kinematics and dynamics". In *Rehabilitation Robotics (ICORR), 2017 International Conference on*. p. 1369–1374. IEEE.

Brahmi, Brahim, Maarouf Saad, Mohammad H Rahman and Cristobal Ochoa-Luna. 2017c. "Cartesian trajectory tracking of a 7-DOF exoskeleton robot based on human inverse kinematics". *IEEE Transactions on Systems, Man, and Cybernetics: Systems*, , p. 1–12.

Brahmi, Brahim, Maarouf Saad, Abdelkrim Brahmi, Cristobal Ochoa Luna and Mohammad Habibur Rahman. 2018a. "Compliant control for wearable exoskeleton robot based on human inverse kinematics". *International Journal of Advanced Robotic Systems*, vol. 15, n° 6, p. 1729881418812133.

Brahmi, Brahim, Maarouf Saad, Jacqueline Tu Anh Thu Lam, Cristobal Ochoa Luna, Philippe S Archambault and Mohammad H Rahman. 2018b. "Adaptive control of a 7-DOF exoskeleton robot with uncertainties on kinematics and dynamics". *European Journal of Control*.

Brahmi, Brahim, Maarouf Saad, Cristobal Ochoa Luna, Philippe S Archambault and Mohammad H Rahman. 2018c. "Passive and active rehabilitation control of human upper-limb exoskeleton robot with dynamic uncertainties". *Robotica*, vol. 36, n° 11, p. 1757–1779.

Brahmi, Brahim, Maarouf Saad, Cristobal Ochoa-Luna, Mohammad Habibur Rahman and Abdelkrim Brahmi. 2018d. "Adaptive tracking control of an exoskeleton robot with uncertain dynamics based on estimated time-delay control". *IEEE/ASME Transactions on Mechatronics*, vol. 23, n° 2, p. 575–585.

Calanca, Andrea, Riccardo Muradore and Paolo Fiorini. 2016. "A review of algorithms for compliant control of stiff and fixed-compliance robots". *IEEE/ASME Transactions on Mechatronics*, vol. 21, n° 2, p. 613–624.

Carignan, Craig, Jonathan Tang, Stephen Roderick and Michael Naylor. 2007. "A configuration-space approach to controlling a rehabilitation arm exoskeleton". In *Rehabilitation Robotics, 2007. ICORR 2007. IEEE 10th International Conference on*. p. 179–187. IEEE.

Chan, Kai-Chi, Cheng-Kok Koh and CS George Lee. 2014. "A 3-D-Point-Cloud System for Human-Pose Estimation.". *IEEE Trans. Systems, Man, and Cybernetics: Systems*, vol. 44, n° 11, p. 1486–1497.

Cheah, Chien Chern. 2006. "Approximate Jacobian control for robot manipulators". In *Advances in Robot Control*, p. 35–53. Springer.

Cheah, Chien Chern, Sadao Kawamura and Suguru Arimoto. 1999. "Feedback control for robotic manipulator with an uncertain Jacobian matrix". *Journal of Robotic Systems*, vol. 16, n° 2, p. 119–134.

Cheah, Chien-Chern, Chao Liu and Jean-Jacques E Slotine. 2005. "Adaptive Jacobian tracking control of robots based on visual task-space information". In *Robotics and Automation, 2005. ICRA 2005. Proceedings of the 2005 IEEE International Conference on*. p. 3498–3503. IEEE.

Cheah, Chien-Chern, Chao Liu and Jean-Jacques E Slotine. 2006. "Adaptive tracking control for robots with unknown kinematic and dynamic properties". *The International Journal of Robotics Research*, vol. 25, n° 3, p. 283–296.

Chen, Shan, Zheng Chen, Bin Yao, Xiaocong Zhu, Shiqiang Zhu, Qingfeng Wang and Yang Song. 2017. "Adaptive robust cascade force control of 1-dof hydraulic exoskeleton for human performance augmentation". *IEEE/ASME Transactions on Mechatronics*, vol. 22, n° 2, p. 589–600.

Chen, Weisheng, Shuzhi Sam Ge, Jian Wu and Maoguo Gong. 2015. "Globally stable adaptive backstepping neural network control for uncertain strict-feedback systems with tracking accuracy known a priori". *IEEE transactions on neural networks and learning systems*, vol. 26, n° 9, p. 1842–1854.

Chen, Zheng, Ya-Jun Pan and Jason Gu. 2016. "Integrated adaptive robust control for multilateral teleoperation systems under arbitrary time delays". *International Journal of Robust and Nonlinear Control*, vol. 26, n° 12, p. 2708–2728.

Choi, Younggeun, James Gordon, Duckho Kim and Nicolas Schweighofer. 2009. "An adaptive automated robotic task-practice system for rehabilitation of arm functions after stroke". *IEEE Transactions on Robotics*, vol. 25, n° 3, p. 556–568.

Chua, Yuanwei, Keng Peng Tee and Rui Yan. 2013. "Robust Optimal inverse kinematics with Self-Collision avoidance for a Humanoid robot". In *RO-MAN, 2013 IEEE*. p. 496–502. IEEE.

Ciliz, M Kemal. 2005. "Adaptive control of robot manipulators with neural network based compensation of frictional uncertainties". *Robotica*, vol. 23, n° 2, p. 159–167.

Clancy, Gearóid, Daniël Peeters, Vincenzo Oliveri, David Jones, Ronan M O'Higgins and Paul M Weaver. 2018. "A study of the influence of processing parameters on steering of carbon Fibre/PEEK tapes using laser-assisted tape placement". *Composites Part B: Engineering*.

Craig, John J. 2005. *Introduction to robotics: mechanics and control*. Pearson/Prentice Hall Upper Saddle River, NJ, USA:.

Crocher, Vincent. 2012. "Commande d'un exosquelette du membre supérieur à des fins de rééducation neuromotrice". PhD thesis, UPMC, Paris Sorbonne.

Culmer, Peter R, Andrew E Jackson, Sophie Makower, Robert Richardson, J Alastair Cozens, Martin C Levesley and Bipin B Bhakta. 2010. "A control strategy for upper limb robotic rehabilitation with a dual robot system". *IEEE/ASME Transactions on Mechatronics*, vol. 15, n° 4, p. 575–585.

Dawson, Darren M, Chaouki T Abdallah and Frank L Lewis. 2003. *Robot manipulator control: theory and practice*. CRC Press.

De Morand, Anne. 2014. *Pratique de la rééducation neurologique*. Elsevier Masson, 1–61 p.

de Santé, Haute Autorité. 2012. "Accident vasculaire cérébral: méthodes de rééducation de la fonction motrice chez l'adulte".

Deng, Lingfeng, Farrokh Janabi-Sharifi and William J Wilson. 2002. "Stability and robustness of visual servoing methods". In *Robotics and Automation, 2002. Proceedings. ICRA'02. IEEE International Conference on*. p. 1604–1609. IEEE.

Du, Guanglong and Ping Zhang. 2015. "A Markerless Human-Robot Interface Using Particle Filter and Kalman Filter for Dual Robots.". *IEEE Trans. Industrial Electronics*, vol. 62, n° 4, p. 2257–2264.

Efimov, Denis, Andrey Polyakov and Jean-Pierre Richard. 2015. "Interval observer design for estimation and control of time-delay descriptor systems". *European Journal of Control*, vol. 23, p. 26–35.

Espiau, Bernard, François Chaumette and Patrick Rives. 1992. "A new approach to visual servoing in robotics". *ieee Transactions on Robotics and Automation*, vol. 8, n° 3, p. 313–326.

Ferguson, James M, Leon Y Cai, Alexander Reed, Michael Siebold, Smita De, S Duke Herrell and Robert J Webster. 2018. "Toward image-guided partial nephrectomy with the da Vinci robot: exploring surface acquisition methods for intraoperative re-registration". In *Medical Imaging 2018: Image-Guided Procedures, Robotic Interventions, and Modeling*. p. 1057609. International Society for Optics and Photonics.

Ferrer, SB, Cristóbal Ochoa-Luna, MH Rahman, Maarouf Saad and Philippe S Archambault. 2013. "HELIOS: The human machine interface for MARSE robot". In *2013 6th International Conference on Human System Interactions (HSI)*. p. 117–122. IEEE.

Fridman, Emilia. 2014. "Tutorial on Lyapunov-based methods for time-delay systems". *European Journal of Control*, vol. 20, n° 6, p. 271–283.

Fridman, L. 1999. "The problem of chattering: an averaging approach". In *Variable structure systems, sliding mode and nonlinear control*, p. 363–386. Springer.

Gans, Nicholas R, Seth A Hutchinson and Peter I Corke. 2003. "Performance tests for visual servo control systems, with application to partitioned approaches to visual servo control". *The International Journal of Robotics Research*, vol. 22, n° 10-11, p. 955–981.

Gauthier, P-A, C Camier, F-A Lebel, Y Pasco, A Berry, J Langlois, C Verron and C Guastavino. 2016. "Experiments of multichannel least-square methods for sound field reproduction inside aircraft mock-up: Objective evaluations". *Journal of Sound and Vibration*, vol. 376, p. 194–216.

Gopura, Ranathunga Arachchilage Ruwan Chandra, Kazuo Kiguchi and Yang Li. 2009. "SUEFUL-7: A 7DOF upper-limb exoskeleton robot with muscle-model-oriented EMG-based control". In *Intelligent Robots and Systems, 2009. IROS 2009. IEEE/RSJ International Conference on*. p. 1126–1131. IEEE.

Guidali, Marco, Alexander Duschau-Wicke, Simon Broggi, Verena Klamroth-Marganska, Tobias Nef and Robert Riener. 2011. "A robotic system to train activities of daily living in a virtual environment". *Medical & biological engineering & computing*, vol. 49, n° 10, p. 1213.

Han, Jingqing. 2009. "From PID to active disturbance rejection control". *IEEE transactions on Industrial Electronics*, vol. 56, n° 3, p. 900–906.

Hogan, Neville, Hermano Igo Krebs, J Charnnarong, P Srikrishna and Andre Sharon. 1992. "MIT-MANUS: a workstation for manual therapy and training. I". In *Robot and Human Communication, 1992. Proceedings., IEEE International Workshop on*. p. 161–165. IEEE.

Hogan, Neville, Hermano Igo Krebs, J Charnnarong, P Srikrishna and Andre Sharon. 1993. "MIT-MANUS: a workstation for manual therapy and training II". In *Telemanipulator Technology*. p. 28–35. International Society for Optics and Photonics.

Huang, An-Chyau and Ming-Chih Chien. 2010. *Adaptive control of robot manipulators: a unified regressor-free approach*. World Scientific.

Huang, Jian, Weiguang Huo, Wenxia Xu, Samer Mohammed and Yacine Amirat. 2015. "Control of upper-limb power-assist exoskeleton using a human-robot interface based on motion intention recognition". *IEEE transactions on automation science and engineering*, vol. 12, n° 4, p. 1257–1270.

Huang, Jian, Xikai Tu and Jiping He. 2016. "Design and evaluation of the RUPERT wearable upper extremity exoskeleton robot for clinical and in-home therapies". *IEEE Transactions on Systems, Man, and Cybernetics: Systems*, vol. 46, n° 7, p. 926–935.

Hughes, Ann-Marie, Sofia Barbosa Bouças, Jane H Burridge, Margit Alt Murphy, Jaap Buurke, Peter Feys, Verena Klamroth-Marganska, Ilse Lamers, Gerdienke Prange-Lasonder, Annick Timmermans et al. 2016. "Evaluation of upper extremity neurorehabilitation using technology: a European Delphi consensus study within the EU COST Action Network on Robotics for Neurorehabilitation". *Journal of neuroengineering and rehabilitation*, vol. 13, n° 1, p. 86.

Hutchinson, Seth, Gregory D Hager and Peter I Corke. 1996. "A tutorial on visual servo control". *IEEE transactions on robotics and automation*, vol. 12, n° 5, p. 651–670.

Jamwal, Prashant K, Shahid Hussain, Mergen H Ghayesh and Svetlana V Rogozina. 2016. "Impedance control of an intrinsically compliant parallel ankle rehabilitation robot". *IEEE Transactions on Industrial Electronics*, vol. 63, n° 6, p. 3638–3647.

Jiang, Hairong, Bradley S Duerstock and Juan P Wachs. 2014. "A machine vision-based gestural interface for people with upper extremity physical impairments". *IEEE Transactions on Systems, Man, and Cybernetics: Systems*, vol. 44, n° 5, p. 630–641.

Jin, Maolin, Jinoh Lee and Kyung Kwan Ahn. 2015. "Continuous nonsingular terminal sliding-mode control of shape memory alloy actuators using time delay estimation". *IEEE/ASME Transactions on Mechatronics*, vol. 20, n° 2, p. 899–909.

Jin, Xu and Jian-Xin Xu. 2013. "Iterative learning control for output-constrained systems with both parametric and nonparametric uncertainties". *Automatica*, vol. 49, n° 8, p. 2508–2516.

Kahn, LE, ML Zygman, WZ Rymer and DJ Reinkensmeyer. 2001. *Effect of robot-assisted and unassisted exercise on functional reaching in chronic hemiparesis*. Technical report.

Kali, Yassine, Maarouf Saad, Khalid Benjelloun and Mohammed Benbrahim. 2016. "Control of Uncertain Robot Manipulators using Integral Backstepping and Time Delay Estimation.". In *ICINCO (2)*. p. 145–151.

Karafyllis, Iasson, Michael Malisoff, Frederic Mazenc and Pierdomenico Pepe. 2016. *Recent results on nonlinear delay control systems*. Springer.

Keller, Urs, Sabine Schölch, Urs Albisser, Claudia Rudhe, Armin Curt, Robert Riener and Verena Klamroth-Marganska. 2015. "Robot-assisted arm assessments in spinal cord injured patients: A consideration of concept study". *PloS one*, vol. 10, n° 5, p. e0126948.

Keller, Urs, Hubertus JA van Hedel, Verena Klamroth-Marganska and Robert Riener. 2016. "ChARMin: The first actuated exoskeleton robot for pediatric arm rehabilitation". *IEEE/ASME Transactions on Mechatronics*, vol. 21, n° 5, p. 2201–2213.

Kelly, Rafael, Victor Santibáñez Davila and Julio Antonio Loría Perez. 2006. *Control of robot manipulators in joint space*. Springer Science & Business Media.

Khalil, HK and J Grizzle. 1996. "Nonlinear systems. vol. 3 Prentice hall". *New Jersey*.

Khan, Abdul Manan, Muhammad Usman, Ahmad Ali, Fatima Khan, Sheraz Yaqub and Changsoo Han. 2016a. "Muscle circumference sensor and model reference-based adaptive impedance control for upper limb assist exoskeleton robot". *Advanced Robotics*, vol. 30, n° 24, p. 1515–1529.

Khan, Abdul Manan, Deok-won Yun, Mian Ashfaq Ali, Khalil Muhammad Zuhaib, Chao Yuan, Junaid Iqbal, Jungsoo Han, Kyoosik Shin and Changsoo Han. 2016b. "Passivity based adaptive control for upper extremity assist exoskeleton". *International Journal of Control, Automation and Systems*, vol. 14, n° 1, p. 291–300.

Khan, Abdul Manan, Deok-won Yun, Khalil Muhammad Zuhaib, Junaid Iqbal, Rui-Jun Yan, Fatima Khan and Changsoo Han. 2017. "Estimation of Desired Motion Intention and compliance control for upper limb assist exoskeleton". *International Journal of Control, Automation and Systems*, vol. 15, n° 2, p. 802–814.

Khoogar, Ahmad Reza, Alireza K Tehrani and Mehdi Tajdari. 2011. "A dual neural network for kinematic control of redundant manipulators using input pattern switching". *Journal of Intelligent & Robotic Systems*, vol. 63, n° 1, p. 101–113.

Kim, Hyunchul, Levi Makaio Miller, Aimen Al-Refai, Moshe Brand and Jacob Rosen. 2011a. "Redundancy resolution of a human arm for controlling a seven dof wearable robotic system". In *Engineering in Medicine and Biology Society, EMBC, 2011 Annual International Conference of the IEEE*. p. 3471–3474. IEEE.

Kim, Hyunchul, Levi Makaio Miller, Aimen Al-Refai, Moshe Brand and Jacob Rosen. 2011b. "Redundancy resolution of a human arm for controlling a seven dof wearable robotic system". In *Engineering in Medicine and Biology Society, EMBC, 2011 Annual International Conference of the IEEE*. p. 3471–3474. IEEE.

Kim, Jongkyoo, Hangil Joe, Son-cheol Yu, Jin S Lee and Minsung Kim. 2016. "Time-delay controller design for position control of autonomous underwater vehicle under disturbances". *IEEE Transactions on Industrial Electronics*, vol. 63, n° 2, p. 1052–1061.

Klein, Charles A and Ching-Hsiang Huang. 1983. "Review of pseudoinverse control for use with kinematically redundant manipulators". *IEEE Transactions on Systems, Man, and Cybernetics*, , p. 245–250.

Krstic, Miroslav, Ioannis Kanellakopoulos, Petar V Kokotovic et al. 1995. *Nonlinear and adaptive control design*. Wiley New York.

Lawson, Charles L and Richard J Hanson. 1995. *Solving least squares problems*. Society for Industrial and Applied Mathematics, US.

Lee, Byeong-Kyu, Hee-Don Lee, Ji-yeong Lee, Kyoosik Shin, Jung-Soo Han and Chang-Soo Han. 2012. "Development of dynamic model-based controller for upper limb exoskeleton robot". In *Robotics and Automation (ICRA), 2012 IEEE International Conference on*. p. 3173–3178. IEEE.

Letier, Pierre and André Preumont. 2010. "Bras exosquelette haptique: conception et contrôle". PhD thesis, Université libre de Bruxelles.

Levant, Arie. 2003. "Higher-order sliding modes, differentiation and output-feedback control". *International journal of Control*, vol. 76, n° 9-10, p. 924–941.

Li, Yongming, Shaocheng Tong, Yan-Jun Liu and Tieshan Li. 2014. "Adaptive fuzzy robust output feedback control of nonlinear systems with unknown dead zones based on a small-gain approach.". *IEEE Trans. Fuzzy Systems*, vol. 22, n° 1, p. 164–176.

Li, Zhijun, Chun-Yi Su, Guanglin Li and Hang Su. 2015a. "Fuzzy Approximation-Based Adaptive Backstepping Control of an Exoskeleton for Human Upper Limbs.". *IEEE Trans. Fuzzy Systems*, vol. 23, n° 3, p. 555–566.

Li, Zhijun, Chun-Yi Su, Liangyong Wang, Ziting Chen and Tianyou Chai. 2015b. "Nonlinear disturbance observer-based control design for a robotic exoskeleton incorporating fuzzy approximation". *IEEE Transactions on Industrial Electronics*, vol. 62, n° 9, p. 5763–5775.

Li, Zhijun, Shengtao Xiao, Shuzhi Sam Ge and Hang Su. 2016. "Constrained multilegged robot system modeling and fuzzy control with uncertain kinematics and dynamics incorporating foot force optimization". *IEEE Transactions on Systems, Man, and Cybernetics: Systems*, vol. 46, n° 1, p. 1–15.

Li, Zhijun, Zhicong Huang, Wei He and Chun-Yi Su. 2017a. "Adaptive impedance control for an upper limb robotic exoskeleton using biological signals". *IEEE Transactions on Industrial Electronics*, vol. 64, n° 2, p. 1664–1674.

Li, Zhijun, Yu Kang, Zhiye Xiao and Weiguo Song. 2017b. "Human–robot coordination control of robotic exoskeletons by skill transfers". *IEEE Transactions on Industrial Electronics*, vol. 64, n° 6, p. 5171–5181.

Ling, Rui, Meirong Wu, Yan Dong and Yi Chai. 2012. "High order sliding-mode control for uncertain nonlinear systems with relative degree three". *Communications in Nonlinear Science and Numerical Simulation*, vol. 17, n° 8, p. 3406–3416.

Liu, Cai, Chao Song, Qi Lu, Yang Liu, Xuan Feng and Yue Gao. 2015. "Impedance inversion based on L1 norm regularization". *Journal of Applied Geophysics*, vol. 120, p. 7–13.

Liu, Chao, Chien Chern Cheah and Jean-Jacques E Slotine. 2006. "Adaptive Jacobian tracking control of rigid-link electrically driven robots based on visual task-space information". *Automatica*, vol. 42, n° 9, p. 1491–1501.

Liu, Dexin, Mingming Sun and Dianwei Qian. 2018. "Structural Design and Gait Simulation of Bionic Quadruped Robot". In *2018 International Conference on Advanced Mechatronic Systems (ICAMechS)*. p. 16–20. IEEE.

Loh, Byoung Gook and Jacob Rosen. 2013. "Kinematic analysis of 7 degrees of freedom upper-limb exoskeleton robot with tilted shoulder abduction". *International Journal of Precision Engineering and Manufacturing*, vol. 14, n° 1, p. 69–76.

Luna, Cristobal Ochoa, Mohammad Habibur Rahman, Maarouf Saad, Philippe Archambault and Wen-Hong Zhu. 2016. "Virtual decomposition control of an exoskeleton robot arm". *Robotica*, vol. 34, n° 7, p. 1587–1609.

Lundström, Erik, Andreas Terént and Jörgen Borg. 2008. "Prevalence of disabling spasticity 1 year after first-ever stroke". *European journal of neurology*, vol. 15, n° 6, p. 533–539.

Luo, Youxin, Qiyuan Liu, Xiaoyi Che and Lingfang Li. 2013. "Damped least-square method based on chaos anti-control for solving forward displacement of general 6-6-type parallel mechanism". *International Journal of Advanced Robotic Systems*, vol. 10, n° 4, p. 186.

Malis, Ezio and François Chaumette. 2002. "Theoretical improvements in the stability analysis of a new class of model-free visual servoing methods". *IEEE Transactions on robotics and automation*, vol. 18, n° 2, p. 176–186.

Nakamura, Yoshihiko and Hideo Hanafusa. 1986. "Inverse kinematic solutions with singularity robustness for robot manipulator control". *Journal of dynamic systems, measurement, and control*, vol. 108, n° 3, p. 163–171.

Nef, Tobias, Matjaz Mihelj, Gabriela Kiefer, Christina Perndl, Roland Muller and Robert Riener. 2007. "ARMin-Exoskeleton for arm therapy in stroke patients". In *Rehabilitation Robotics, 2007. ICORR 2007. IEEE 10th International Conference on*. p. 68–74. IEEE.

Nichols-Larsen, Deborah S, PC Clark, Angelique Zeringue, Arlene Greenspan and Sarah Blanton. 2005. "Factors influencing stroke survivors' quality of life during subacute recovery". *Stroke*, vol. 36, n° 7, p. 1480–1484.

Ochoa Luna, Cristóbal. 2016. "Nonlinear control of a seven degrees-of-freedom exoskeleton robot arm". PhD thesis, École de technologie supérieure.

Ochoa Luna, Cristóbal, Mohammad Habibur Rahman, Maarouf Saad, Philippe S Archambault and Steven Bruce Ferrer. 2015. "Admittance-based upper limb robotic active and active-assistive movements". *International Journal of Advanced Robotic Systems*, vol. 12, n° 9, p. 117.

Ozkul, Fatih and Duygun Erol Barkana. 2013. "Upper-extremity rehabilitation robot RehabRoby: methodology, design, usability and validation". *International Journal of Advanced Robotic Systems*, vol. 10, n° 12, p. 401.

Philips, Gavin R, Janis J Daly and José C Príncipe. 2017. "Topographical measures of functional connectivity as biomarkers for post-stroke motor recovery". *Journal of neuroengineering and rehabilitation*, vol. 14, n° 1, p. 67.

Rahman, MH, Maarouf Saad, C Ochoa-Luna, Jean-Pierre Kenné and PS Archambault. 2012a. "Cartesian trajectory tracking of an upper limb exoskeleton robot". In *IECON 2012-38th Annual Conference on IEEE Industrial Electronics Society*. p. 2668–2673. IEEE.

Rahman, Mohammad H, T K-Ouimet, Maarouf Saad, Jean P Kenné and Philippe S Archambault. 2011a. "Tele-operation of a robotic exoskeleton for rehabilitation and passive arm movement assistance". In *Robotics and Biomimetics (ROBIO), 2011 IEEE International Conference on*. p. 443–448. IEEE.

Rahman, Mohammad H, Maarouf Saad, Jean-Pierre Kenné and Philippe S Archambault. 2013. "Control of an exoskeleton robot arm with sliding mode exponential reaching law". *International Journal of Control, Automation and Systems*, vol. 11, n° 1, p. 92–104.

Rahman, Mohammad Habibur. 2012. "Development of an exoskeleton robot for upper-limb rehabilitation". PhD thesis, École de technologie supérieure.

Rahman, Mohammad Habibur, Thierry Kittel-Ouimet, Maarouf Saad, Jean-Pierre Kenné and Philippe S Archambault. 2011b. "Dynamic modeling and evaluation of a robotic exoskeleton for upper-limb rehabilitation". *International Journal of Information Acquisition*, vol. 8, n° 01, p. 83–102.

Rahman, Mohammad Habibur, Thierry Kittel-Ouimet, Maarouf Saad, Jean-Pierre Kenné and Philippe S Archambault. 2012b. "Development and control of a robotic exoskeleton for shoulder, elbow and forearm movement assistance". *Applied Bionics and Biomechanics*, vol. 9, n° 3, p. 275–292.

Rahman, Mohammad Habibur, Maarouf Saad, Jean Pierre Kenné and Philippe S Archambault. 2012c. "Nonlinear sliding mode control implementation of an upper limb exoskeleton robot to provide passive rehabilitation therapy". In *International Conference on Intelligent Robotics and Applications*. p. 52–62. Springer.

Rahman, Mohammad Habibur, Cristóbal Ochoa-Luna, Md Jahidur Rahman, Maarouf Saad and Philippe Archambault. 2014. "Force-position control of a robotic exoskeleton to provide upper extremity movement assistance". *International Journal of Modelling, Identification and Control*, vol. 21, n° 4, p. 390–400.

Rahman, Mohammad Habibur, Md Jahidur Rahman, OL Cristobal, Maarouf Saad, Jean-Pierre Kenné and Philippe S Archambault. 2015. "Development of a whole arm wearable robotic exoskeleton for rehabilitation and to assist upper limb movements". *Robotica*, vol. 33, n° 1, p. 19–39.

Rami, Mustapha Ait, Michael Schönlein and Jens Jordan. 2013. "Estimation of linear positive systems with unknown time-varying delays". *European Journal of Control*, vol. 19, n° 3, p. 179–187.

Rigatos, Gerasimos, Pierluigi Siano and Masoud Abbaszadeh. 2018. "Nonlinear H-infinity control for 4-DOF underactuated overhead cranes". *Transactions of the Institute of Measurement and Control*, vol. 40, n° 7, p. 2364–2377.

Siciliano, Bruno, Lorenzo Sciavicco, Luigi Villani and Giuseppe Oriolo. 2009. "Kinematics". *Robotics: Modelling, Planning and Control*, p. 39–103.

Sidney, Stephen, Wayne D Rosamond, Virginia J Howard and Russell V Luepker. 2013. "The "heart disease and stroke statistics—2013 update" and the need for a national cardiovascular surveillance system".

Skjetne, Roger and Thor I Fossen. 2004. "On integral control in backstepping: Analysis of different techniques". In *American Control Conference, 2004. Proceedings of the 2004*. p. 1899–1904. IEEE.

Slotine, Jean-Jacques E, Weiping Li et al. 1991. *Applied nonlinear control*. Prentice hall Englewood Cliffs, NJ.

Spong, Mark W, Seth Hutchinson, Mathukumalli Vidyasagar et al. 2006a. *Robot modeling and control*. Wiley New York.

Spong, Mark W, Seth Hutchinson, Mathukumalli Vidyasagar et al. 2006b. *Robot modeling and control*. Wiley New York.

Sun, FC, ZQ Sun and Gang Feng. 1999. "An adaptive fuzzy controller based on sliding mode for robot manipulators". *IEEE Transactions on Systems, Man, and Cybernetics, Part B (Cybernetics)*, vol. 29, n° 5, p. 661–667.

Tan, Yaolong, Jie Chang, Hualin Tan and Jun Hu. 2000. "Integral backstepping control and experimental implementation for motion system". In *Control Applications, 2000. Proceedings of the 2000 IEEE International Conference on*. p. 367–372. IEEE.

Tang, Hui and Yangmin Li. 2014. "Development and active disturbance rejection control of a compliant micro-/nanopositioning piezostage with dual mode". *IEEE Transactions on Industrial Electronics*, vol. 61, n° 3, p. 1475–1492.

Tolani, Deepak and Norman I Badler. 1996. "Real-time inverse kinematics of the human arm". *Presence: Teleoperators & Virtual Environments*, vol. 5, n° 4, p. 393–401.

Tolani, Deepak, Ambarish Goswami and Norman I Badler. 2000. "Real-time inverse kinematics techniques for anthropomorphic limbs". *Graphical models*, vol. 62, n° 5, p. 353–388.

Ueda, Jun, Ding Ming, Vijaya Krishnamoorthy, Minoru Shinohara and Tsukasa Ogasawara. 2010. "Individual muscle control using an exoskeleton robot for muscle function testing". *IEEE Transactions on Neural Systems and Rehabilitation Engineering*, vol. 18, n° 4, p. 339–350.

Utkin, Vadim, Jürgen Guldner and Jingxin Shi. 2009. *Sliding mode control in electromechanical systems*. CRC press.

Volpini, Mariana, Volker Bartenbach, Marcos Pinotti and Robert Riener. 2017. "Clinical Evaluation of a low-cost robot for use in physiotherapy and gait training". *Journal of Rehabilitation and Assistive Technologies Engineering*, vol. 4, p. 2055668316688410.

Wampler, Charles W. 1986. "Manipulator inverse kinematic solutions based on vector formulations and damped least-squares methods". *IEEE Transactions on Systems, Man, and Cybernetics*, vol. 16, n° 1, p. 93–101.

Weiss, Patrice L, Emanuel Tirosh and Darcy Fehlings. 2014. "Role of virtual reality for cerebral palsy management". *Journal of child neurology*, vol. 29, n° 8, p. 1119–1124.

Xia, Youshen and Jun Wang. 2001. "A dual neural network for kinematic control of redundant robot manipulators". *IEEE Transactions on Systems, Man, and Cybernetics, Part B (Cybernetics)*, vol. 31, n° 1, p. 147–154.

Xie, Shane et al. 2016. "Advanced Robotics for Medical Rehabilitation". *Springer Tracts in Advanced Robotics*, vol. 108, p. 1–41.

Xu, Li Da, Eric L Xu and Ling Li. 2018. "Industry 4.0: state of the art and future trends". *International Journal of Production Research*, vol. 56, n° 8, p. 2941–2962.

Yao, Bin. 1996. "Adaptive robust control of nonlinear systems with application to control of mechanical systems". PhD thesis, University of California, Berkeley.

Yazarel, Hakan and Chien-Chern Cheah. 2002. "Task-space adaptive control of robotic manipulators with uncertainties in gravity regressor matrix and kinematics". *IEEE Transactions on Automatic Control*, vol. 47, n° 9, p. 1580–1585.

Yoo, Byung Kook and Woon Chul Ham. 2000. "Adaptive control of robot manipulator using fuzzy compensator". *IEEE Transactions on fuzzy systems*, vol. 8, n° 2, p. 186–199.

Youcef-Toumi, K and CC Shortlidge. 1991. "Control of robot manipulators using time delay". In *Robotics and Automation, 1991. Proceedings., 1991 IEEE International Conference on*. p. 2391–2398. IEEE.

Youcef-Toumi, Kamal and Osamu Ito. 1990. "A time delay controller for systems with unknown dynamics". *Journal of dynamic systems, measurement, and control*, vol. 112, n° 1, p. 133–142.

Young, K. D., V. I. Utkin and U. Ozguner. May 1999. "A control engineer's guide to sliding mode control". *IEEE Transactions on Control Systems Technology*, vol. 7, n° 3, p. 328-342.

Yu, Wen and Jacob Rosen. 2010. "A novel linear PID controller for an upper limb exoskeleton". In *Decision and Control (CDC), 2010 49th IEEE Conference on*. p. 3548–3553. IEEE.

Yu, Wen and Jacob Rosen. 2013. "Neural PID control of robot manipulators with application to an upper limb exoskeleton". *IEEE Transactions on cybernetics*, vol. 43, n° 2, p. 673–684.

Zanchettin, Andrea Maria, Nicola Maria Ceriani, Paolo Rocco, Hao Ding and Björn Matthias. 2016. "Safety in human-robot collaborative manufacturing environments: Metrics and control". *IEEE Transactions on Automation Science and Engineering*, vol. 13, n° 2, p. 882–893.

Zhang, Xiaoqin, Changcheng Li, Weiming Hu, Xiaofeng Tong, Steve Maybank and Yimin Zhang. 2014. "Human pose estimation and tracking via parsing a tree structure based human model". *IEEE Transactions On Systems, Man, And Cybernetics: Systems*, vol. 44, n° 5, p. 580–592.

Zhao, Yi Min, Yu Lin, Fengfeng Xi and Shuai Guo. 2015. "Calibration-based iterative learning control for path tracking of industrial robots". *IEEE Transactions on industrial electronics*, vol. 62, n° 5, p. 2921–2929.

Zheng, Da, Zhengyun Ren and Jian'an Fang. 2010. "Stability analysis of time delayed system with coefficient uncertainty and time delay uncertainty". *European Journal of Control*, vol. 16, n° 1, p. 5–13.

Zhou, Jing and Changyun Wen. 2008. *Adaptive backstepping control of uncertain systems: Nonsmooth nonlinearities, interactions or time-variations*. Springer.